INVESTIGATION OF WATER, AIR, AND HYBRID COOLING FOR SUPERCRITICAL CARBON DIOXIDE BRAYTON CYCLES

by

Doug J. Gavic

A thesis submitted in partial fulfillment of

the requirements for the degree of

Master of Science

(Mechanical Engineering)

at the

UNIVERSITY OF WISCONSIN-MADISON

2012

This thesis has been approved by

_____

Professor Sanford A. Klein

_____

Professor Gregory F. Nellis

_____

Professor Douglas T. Reindl

Date: _____

Abstract

There is renewed interest in the closed Brayton cycle, using carbon dioxide as the working fluid, for utility-scale power production. The Brayton cycle rejects heat to the ambient environment using air, water, or a hybrid arrangement that employs both fluids. Cooling with water, from a cooling tower, provides higher and more consistent Brayton cycle thermal efficiencies year-round, while also having lower capital costs for the heat exchanger equipment when compared to air-cooling. However, a major concern with water-cooling, especially for solar thermal applications, is the large amount of water required for the heat rejection coincident in plant locations where there is limited availability of water.

To address water limitations, air-cooling has become a major topic among researchers in the field of CSP technologies. It has been found that while air-cooling will eliminate the majority of the water usage, it causes reduced thermal efficiencies year-round and higher capital costs due to the substantial size of the air-coolers.

The alternative to direct water-cooling or direct air-cooling is a hybrid configuration that combines both water and air-cooling processes. The hybrid configuration strives to maintain the advantages of each process, but can also potentially mitigate the disadvantages. In the Brayton cycle using carbon dioxide, the precooler can be configured to take advantage of the high CO_2 temperatures by arranging the heat rejection system into two heat exchangers, a water and air-cooler, each set in series.

The size of the air-cooler can be significantly reduced by increasing the approach temperature. The size of the air-cooler has been found to be more sensitive to the approach temperature, when compared to the more physically compact water-cooler. The water-cooler operates at a lower heat sink temperature (i.e. wet bulb temperature) and completes the heat rejection from CO_2. It is sized and operated to reduce the CO_2 temperature to the desired condition for the compressor inlet.

In comparing the three different configurations using an LCC analysis, it was found that there is an advantage to the hybrid configuration as a cooling solution for the Brayton cycle. The hybrid configuration advantage lies with the ability to design the system at the optimal point and constantly operate at a fraction of air cooling that minimizes cost per hour. On a cost stand point, hybrid cooling makes sense because of the flexibility of the system. It also creates a best of both worlds situation where water use, capital costs, and energy use can be reduced.

NREL's interest in the "precooler" heat exchanger is to reduce water use by using air or a combination of air and water. The LCC is a good representation of the design concern for NREL. It shows that on a LCC basis, there is an advantage to designing for a hybrid configuration. Using the hybrid configuration with air cooling as the primary means of cooling allows for reduced water usage. The water cooling is used when the load cannot be met by the air cooling alone. This means that the cooling process is very flexible and can be optimized to reduce water use and cost. Hybrid cooling should be considered a viable cooling solution for NREL's 10 MW CSP plant.

Acknowledgements

I would first like to thank the National Renewable Energy Laboratory (NREL) for their sponsoring of this research.

I owe a lot of thank-yous to many people that have contributed to my work as well as all the people that motivated and supported me. First, I have to thank Greg Nellis, who I attribute as being the first person that got me interested into the fields of heat transfer and thermodynamics. Without the many classes I took with him, I know I would not have the same interest and understanding that I now have. Greg was also the person who motivated me to pursue my master's degree by offering me a position in the Solar Energy Lab. Coming from one of the most knowledgeable persons in his field and being one of my favorite professors, it made the decision simple. I cannot thank you enough for the opportunity you gave me and it was a true honor to work with you the last year and a half.

I am thankful for the time and effort invested by my advisors, Sanford Klein, Greg Nellis, and Doug Reindl. Sandy, Greg and Doug have provided me with more knowledge and guidance than they will ever know. The classes I took with Sandy taught me more than just theory, but an understanding that forced you to look deeper into problems than just the surface. The meetings I had with three of the most knowledgeable people in their fields showed me that there was always something more or a different way of looking at data that brought out much more understanding than I originally had thought satisfying. Sandy, Greg, and Doug you're instructive criticism was sometimes hard to hear, but always led to more understanding and satisfaction with the results. I truly thank you for your time and effort in working with me.

Dad and Mom, I am indebted to your encouragements in the pursuit of my master's degree. I could not have gotten here without everything you guys have done for me and provided for me. I plan on taking this master's degree and using it to repay everything you have ever given me. Your support and life lessons made me who I am today, thank you.

A large thank you has to be said to my patient and supportive girlfriend, Olivia. Without you I would not have been able to manage myself during the last months of my research. Thank you for your encouragement, love, and support. I'm glad to finally be home to see you every day.

In the end, I would like to thank John E., Matt, John D., Wenjie, Mohamed, Kendra, Russell, Rogelio, Brad, Eric, Nevzat, and the rest of the SEL group for their friendship and support. Thanks for spending your days with me, both at the SEL and at Union South. I will certainly miss you all and I know I will be seeing you guys in the future.

Table of Contents

Table of Figures

List of Tables

Nomenclature

Abbreviations

PCHE	Printed Circuit Heat Exchanger
ACHE	Air Cooled Heat Exchanger
SCO2	Supercritical Carbon Dioxide
CSP	Concentrating Solar Power
EES	Engineering Equation Solver (Software)
T-S	Diagram Temperature-Entropy Diagram
NREL	National Renewable Energy Lab
HX	Heat Exchanger
GUI	Graphical user interface
DOE	Department of energy

Variables

UA	Conductance
T	Temperature
ε	Heat exchanger effectiveness
Q	Heat transfer rate
i	Enthalpy
m	Mass flow rate
N	Number of sub-HX's
C	Capacitance rate
NTU	Number of transfer units
C_r	Ratio of minimum capacitance rate to maximum capacitance rate
s	Entropy
P	Pressure
cp	Specific heat
Nu	Nusselt Number
D	Diameter
Dh	Hydraulic diameter
th_p	Thickness of plate
th_H	Hot fluid channel height
th_C	Cold fluid channel height
th_f	Thickness of fins
W_f	Width between fins
N_{fins}	Number of fins
N_{ch}	Number of channel pairs
N_{tot}	Total number of channel pairs
A_c	Cross sectional area
Per	Perimeter of channel
H	Height

W	Width
L	Length
U	Fluid velocity
μ	Fluid viscosity
ρ	Fluid density
Re	Reynolds number
f	Friction factor
R_{conv}	Convection resistance
R_{cond}	Conduction resistance
R_{fin}	Fin resistance
η_{fin}	Fin efficiency
η_o	Overall fin efficiency
η	Efficiency
X	Distance
V	Shear force
M	Moment
σ	Bending stress
τ	Shear stress
ω	Humidity ratio
s_v	Vertical spacing
s_h	Horizontal spacing
N_{loops}	Number of air cooler tube passes
$N_{t,col}$	Number of tube columns
$N_{t,row}$	Number of tube rows
TH,B	Hot side bulk temperature
TH,W	Hot side wall temperature
TC,B	Cold side bulk temperature
TC,W	Cold side wall temperature
h	Heat transfer coefficient
k	Thermal conductivity
f_{AC}	Fraction of air cooling
req	Required

Subscripts

H	Hot
C	Cold
WF	Working fluid
CF	Cooling fluid
i	Node i
max	Maximum
min	Minimum
in	Inlet
out	Outlet

col	Columns
row	Rows
AC	Air cooler
WC	Water cooler
CT	Cooling tower
W	Water
A	Air

1 INTRODUCTION

The goal of this project is to prepare a detailed design study of the cooling process in a supercritical carbon dioxide (S-CO_2) Brayton power cycle. There are three heat exchangers required in the Brayton cycle. The "primary" heat exchanger transfers energy from the heat transfer fluid (molten salt) at approximately 600°C and near ambient pressure to supercritical carbon dioxide operating at a pressure of approximately 25 MPa. The "recuperator" heat exchanger transfers energy between low pressure and high pressure carbon dioxide streams at approximately 8 MPa and 25 MPa, respectively. The "precooler" heat exchanger rejects heat from carbon dioxide at approximately 8 MPa leaving the recuperator to the ambient environment using either air, water, or a series of heat exchangers that employ both fluids as a terminal means of cycle heat rejection.

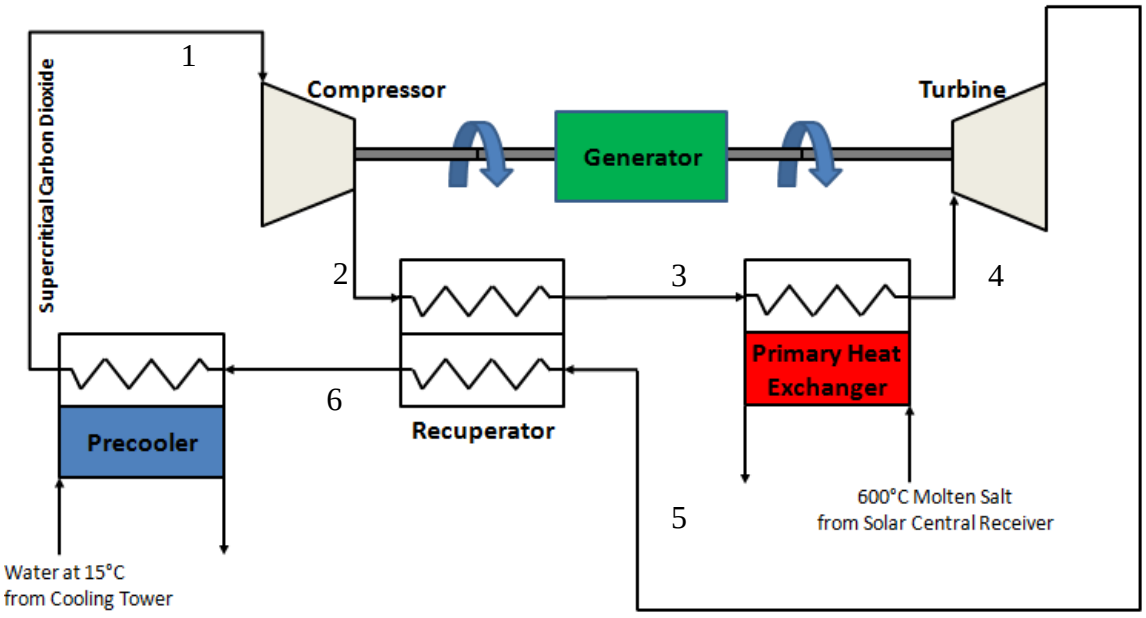

Figure 1: Simple Brayton cycle showing the three heat exchangers and turbo-machinery

The objective of the present design study is to investigate precooler heat exchanger configurations that can meet the cycle's on-design performance specifications. This project is in collaboration with John Dyreby, from the UW Solar Energy Lab, who is focusing his modeling efforts and analysis on developing a system-level model of the supercritical carbon dioxide Brayton cycle.

The precooler model was analyzed at three design points determined from the system-level modeling of John Dyreby (Dyreby, 2012). Figure 2 illustrates where these design points lie on a plot of total cycle thermal efficiency as a function of recuperator conductance. The three design points are labeled as *simple high*, *simple low*, and *recompression*. The *simple high* and *low* are points that lie on the *simple* cycle curve and have either a high or low thermal efficiency, respectively. The *recompression* point lies on the *recompression* curve and is the optimal design point where increasing recuperator size will not further increase thermal efficiency. All design points have a net cycle power output of 10 MW, as well as a precooler CO_2 outlet temperature of 48ºC. The boxes in Figure 2 show the conditions that would be experienced by the precooler for each design point. Table 1 summarizes these conditions.

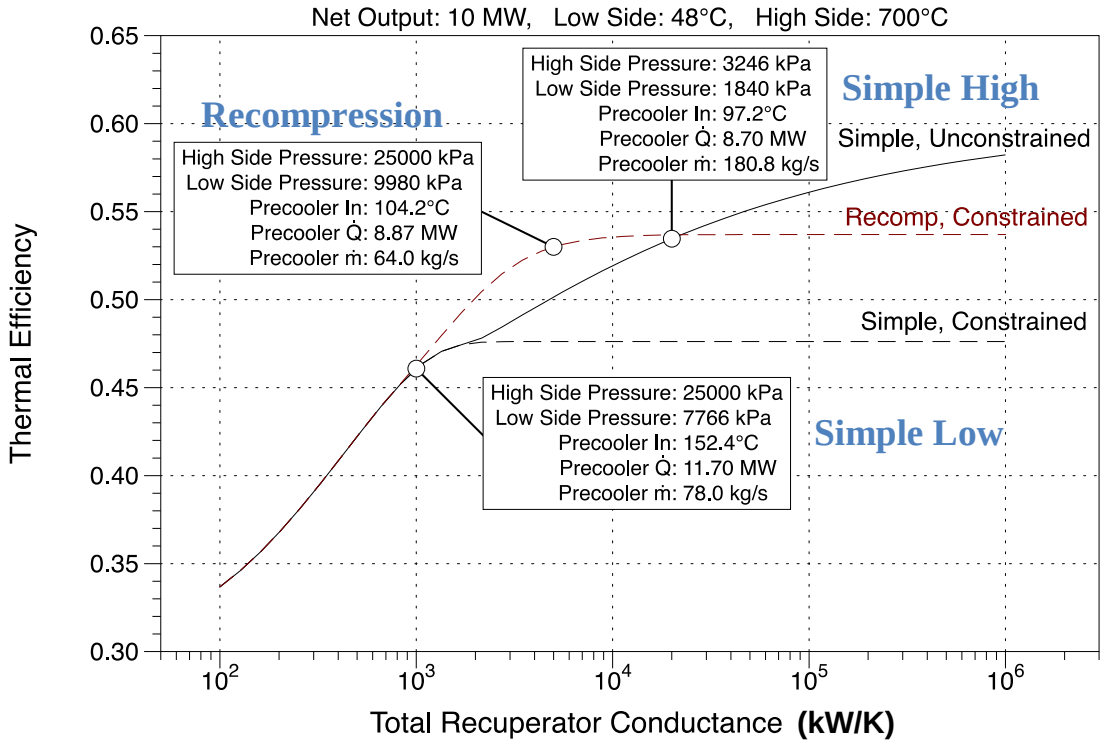

Figure 2: Plot showing three design points on cycle thermal efficiency as a function of recuperator conductance (Dyreby, 2012)

	Simple Low	Recompression	Simple High
Inlet CO_2 Temperature [C]	152.4	104.2	97.2
Outlet CO_2 Temperature [C]	48	48	48
Outlet CO_2 Pressure [MPa]	7.766	9.98	1.84
Heat Input Rate [MW]	11.7	8.87	8.7

Table 1: Precooler conditions and constraints for three design points

This thesis will investigate different methods of heat rejection specifically for supercritical carbon dioxide Brayton cycles. This investigation includes model development, done in Engineering Equation Solver (EES) (Klein, 2011), for various cooling configurations including a water cooler, cooling tower, air cooler (indirect and direct), and hybrid cooler. These models will later be used to compare the cooling configurations in terms of heat exchanger cost/size, water usage, and energy consumption. With the comparison results, it is critical to prioritize key criteria for the system (e.g., water use, energy use, and cost) before designing the heat rejection system configuration. Designing for reduced water use will likely be different than designing for pure economic viability. The goal is to provide the means of making this decision and selecting the most feasible option for the specific cooling process.

2 WATER COOLER

There is a wide array of options and configurations that can be used for the precooler, which makes this heat exchanger one of the more challenging to design. These options can include shell and tube and parallel plate configurations, as well as compact heat exchangers similar to those manufactured by Heatric (Southall, 2009). The options can also extend into using water, air, or both by employing a single heat exchanger with a cooling tower or multiple heat exchangers. The precooler is responsible for rejecting heat from the Brayton cycle to the ambient environment. It is situated between the outlet of the recuperator and the compressor inlet, as shown in Figure 1 from Chapter 1.

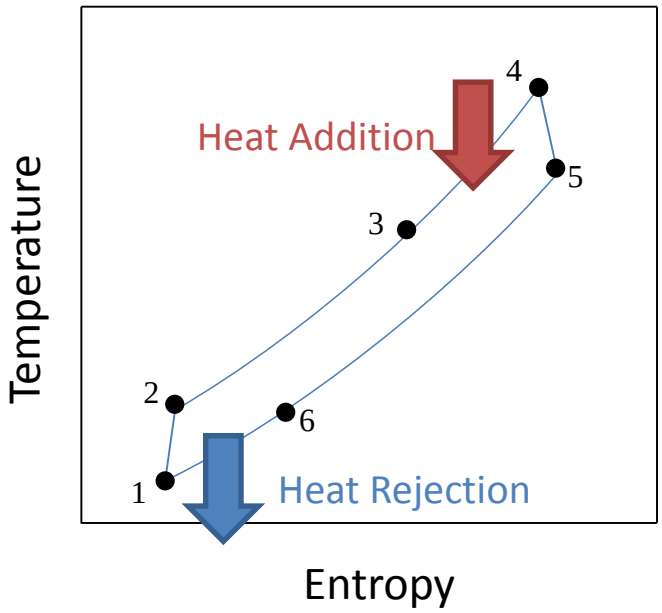

Figure 3: T-s diagram for the simple Brayton cycle in Figure 1. The state points in Figure 1 correspond to the states in the T-s diagram. Image from Seidel (2010) (Revised)

Within the precooler, the carbon dioxide has the potential to transition through the pseudocritical temperature, from gas-like to liquid-like state. Figure 3 shows the state points for the entire Brayton cycle corresponding to the numbered locations on Figure 1 from Chapter 1. State point 6 is the precooler inlet and state point 1 is the outlet. The exiting state of carbon dioxide allows the compressor to operate with a very dense fluid inlet; thereby, reducing the compressor work input.

2.1 Model Development

Due to the potential to transition through the pseudocritical point, the carbon dioxide can experience major property variations within the precooler. These property variations call into question the applicability of using the *ε-NTU* method to directly analyze the entire heat exchanger. A simple but accurate alternative is to divide the heat exchanger into small "sub-heat exchangers", found in section 8.6.3 (Nellis & Klein, 2009). The size of each sub-heat exchanger is chosen to limit the property variations so that the *ε-NTU* method becomes valid within each sub-heat exchanger. The required sub-heat exchanger size is found by plotting a significant output parameter, like outlet CO_2 temperature, as a function of the number of sub-heat exchangers used in the analysis. The plot will asymptotically approach a constant value, establishing the number of sub-heat exchangers needed to obtain an accurate result.

2.1.1 Parallel-plate, counter-flow configurations

The geometry of the precooler analyzed in this section is a parallel plate arranged in a counter flow configuration. Carbon dioxide flows through one side of the heat exchanger and the other uses either water or air. The required heat exchanger capacity is achieved by arranging alternating channels of carbon dioxide and air/water in a stacked configuration. Fins are added within each channel to provide mechanical support needed to accommodate the high carbon dioxide working pressure and also to increase the heat exchanger surface area. Figure 4 and Figure 5 illustrate the geometry of the heat exchanger.

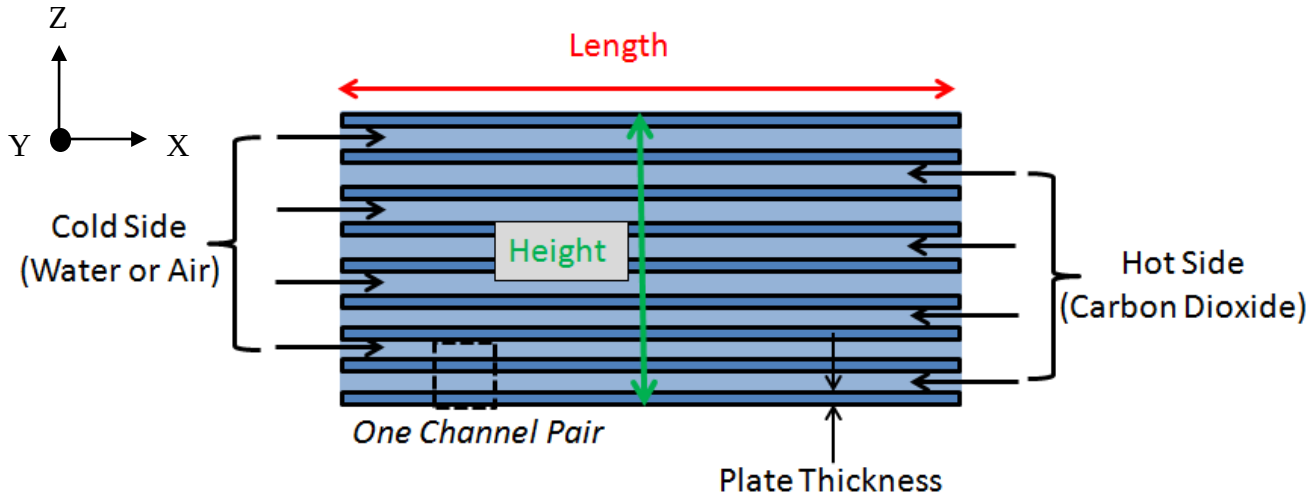

Figure 4: Diagram illustrates a side view of the heat exchanger

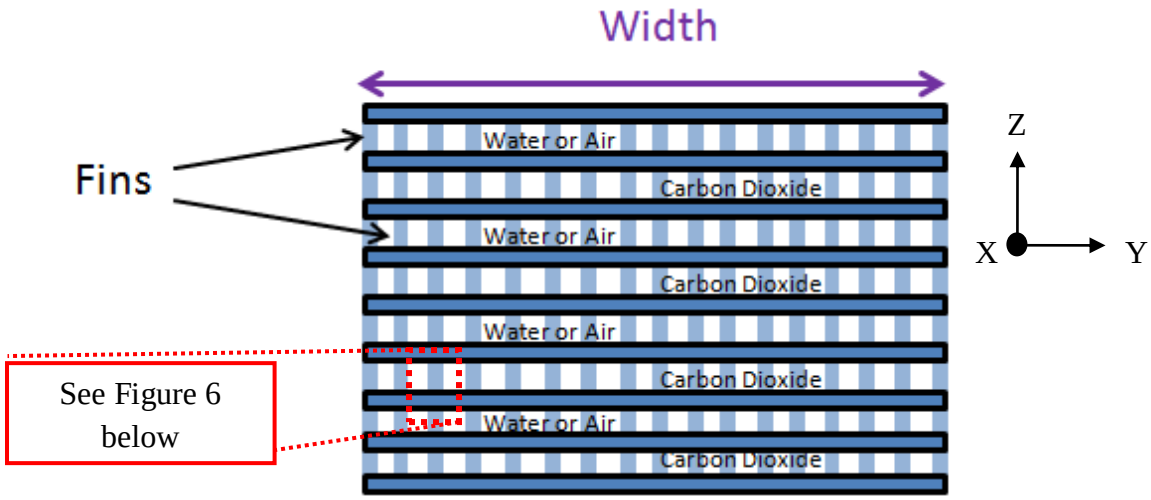

Figure 5: Diagram illustrates an elevation of the heat exchanger including the fins

The first step in the precooler heat exchanger model development is to specify the required inputs and parameters to implement the sub-heat exchanger model. The parameters include the width, length, height, fluid channel thickness (th_H, th_C), thickness of the plates (th_p) and fins (th_f), distance between fins (W_f), and the number of sub-heat exchangers (N), while the inputs include inlet pressures and temperatures, fluid mass flow rates, fluid/material specifications and properties. Refer to Figure 6 for a detailed schematic of the flow channels.

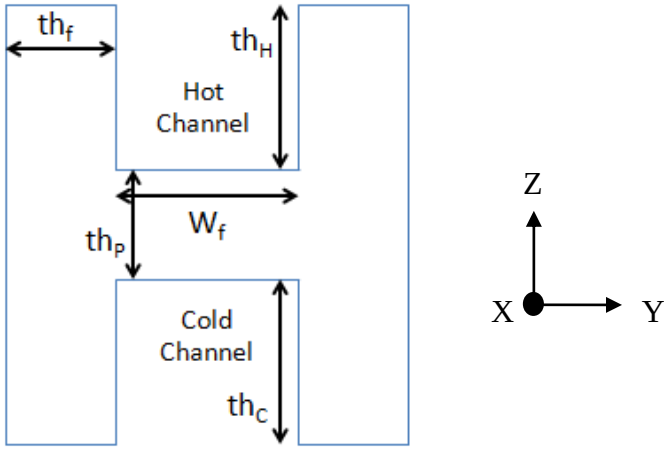

Figure 6: Zoomed in view from Figure 5 (red dashed rectangle) to illustrate dimensions

The inputs and parameters for the model are:

```
"Inputs"
P_H_in=8[MPa]*convert(MPa,Pa)                "Pressure at inlet, hot side"
P_C_in=1[atm]*convert(atm,Pa)                "Pressure at inlet, cold side"
T_H_in=ConvertTemp(C,K,60[C])                "Temperature at inlet, hot side"
T_C_in= ConvertTemp(C,K,15[C])               "Temperature at inlet, cold side"
m_dot_H=80[kg/s]                             "Mass flow rate, hot side"
m_dot_C=300[kg/s]                            "Mass flow rate, cold side"
Metal$='Titanium'                            "HX metal material"
H$='CarbonDioxide'                           "Hot side fluid"
C$='Water'                                   "Cold side fluid"

“Parameters”
W=1[m]                                       "Width of HX"
H=1[m]                                       "Height of HX"
th_p=2[mm]*convert(mm,m)                     "Plate thickness"
th_f=2[mm]*convert(mm,m)                     "Fin thickness"
th_H=10[mm]*convert(mm,m)                    "Channel height, hot side"
th_C=10[mm]*convert(mm,m)                    "Channel height, cold side"
W_f=10[mm]*convert(mm,m)                     "Distance between fins"
N=10[-]                                      "Number of sub-HX"
```

The number of fins (N_{fins}) and channel pairs (N_{ch}) are calculated using equations 2.1 and 2.2:

$$W = W_f\left(N_{fins} + 1\right) + th_f N_{fins} + 2th_f \qquad 2.1$$

$$H = N_{ch}\left[2th_p + th_C + th_H\right] + th_p \qquad 2.2$$

The total number of channels is obtained by:

$$N_{tot} = N_{ch}(N_{fins} + 1) \qquad 2.3$$

```
W=(W_f*(N_fins+1))+(th_f*N_fins)+(2*th_f)        "Calculate # of fins"
H=(((2*th_p)+th_C+th_H)*N_ch)+th_p               "Calculate # of channel pairs"
N_tot=N_ch*(N_fins+1)                            "Total number of channels"
```

First, the overall heat transfer rate is found by assuming a hot-side (i.e. carbon dioxide side) outlet temperature,

```
T_H_out=ConvertTemp(C,K,40[C])                   "Assumed outlet hot temperature"
```

where the heat transfer rate is calculated as follows:

$$\dot{Q} = \dot{m}_H(i_{H,in} - i_{H,out}) \qquad 2.4$$

The specific enthalpies are found using internal property data in EES:

```
"Hot side analysis"
i_H_in=Enthalpy(H$,T=T_H_in,P=P_H_in)            "Enthalpy at inlet, hot side"
i_H_out=Enthalpy(H$,T=T_H_out,P=P_H_out)         "Enthalpy at outlet, hot side"
q_dot=m_dot_H*(i_H_in-i_H_out)                   "Total heat transfer rate"
```

The inlet temperature and pressure are specified in the inputs, the outlet temperature was assigned a guess value, and the outlet pressure is calculated after finding the pressure drop using the local pressure gradient and differential length of each sub-heat exchanger. This will be discussed in more detail later in this section.

```
DELTAPC=-SUM((DELTAx[i]*dPCdx[i]), i=1,N)        "Pressure drop on cold-side"
DELTAPH=-SUM((DELTAx[i]*dPHdx[i]), i=1,N)        "Pressure drop on hot-side"
P_H_out=P_H_in-DELTAPH                           "Pressure at outlet, hot side"
P_C_out=P_C_in-DELTAPC                           "Pressure at outlet, cold side"
```

The outlet specific enthalpy of the cold-side (air or water) is computed from an energy balance on the cold-side of the heat exchanger:

$$i_{C,out} = i_{C,in} + \frac{\dot{Q}}{\dot{m}_C} \qquad 2.5$$

The inlet specific enthalpy is computed using EES based on the inlet pressure and temperature. The cold-side outlet temperature is obtained using EES, evaluated with outlet pressure and specific enthalpy:

```
"Cold side analysis"
i_C_in=Enthalpy(C$,T=T_C_in,P=P_C_in)                "Enthalpy at inlet, cold side"
i_C_out=i_C_in+(q_dot/m_dot_C)                       "Enthalpy at outlet, cold side"
T_C_out=Temperature(C$,h=i_C_out,P=P_C_out)          "Temperature at outlet, cold side"
```

The inlet temperature and pressure are specified in the inputs and the outlet pressure is calculated as indicated above.

2.1.2 Discretization into sub-heat exchangers

The total heat transfer rate increases along the length of the heat exchanger (including more sub-heat exchangers), moving from left-to-right shown in Figure 7 below. It is assumed that each sub-heat exchanger experiences the same rate of heat transfer.

$$\dot{Q}_i = \left(\frac{\dot{Q}}{N}\right) i \;\; for\; i = 1 \ldots N \qquad 2.6$$

This variable is used to track the heat transfer rate throughout the length of the heat exchanger.

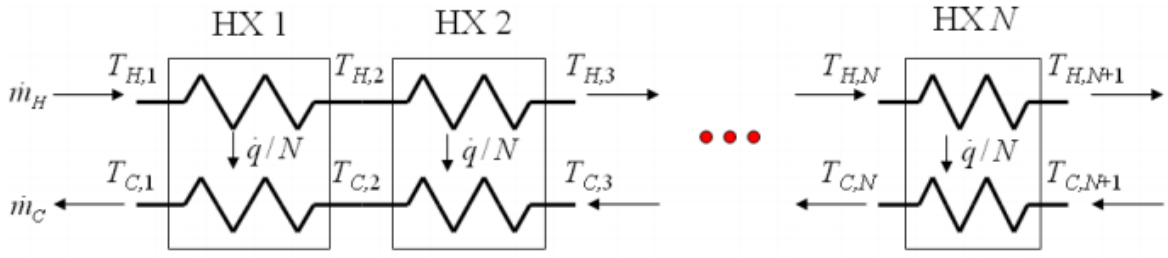

Figure 7: Sub-heat exchanger model with a counter-flow configuration (Nellis & Klein, 2009)

```
"Sub heat exchanger analysis(Left to right)"
duplicate i=1,N
    q_dot[i]=i*q_dot/N                               "Total heat transfer rate(sub)"
end
```

The temperatures of the fluids at node 1, for the hot-side and cold-side, are the hot inlet and cold outlet fluid temperatures, respectively. The specific enthalpies of these fluids have been calculated.

```
"Temperature distribution"
T_H[1]=T_H_in                                        "Inlet temperature, hot side"
T_C[1]=T_C_out                                       "Outlet temperature, cold side"
i_H[1]=i_H_in                                        "Inlet enthalpy, hot side"
i_C[1]=i_C_out                                       "Outlet enthalpy, cold side"
```

Doing an energy balance on the hot-side for each sub-heat exchanger leads to:

$$i_{H,i} = i_{H,i-1} - \frac{\dot{Q}}{N\dot{m}_H} \; for \; i = 2 \ldots (N+1) \qquad 2.7$$

which provides the outlet specific enthalpies for each sub-heat exchanger. The temperatures leaving each of the sub-heat exchangers are obtained using EES based on the specific enthalpies and pressures leaving each sub-heat exchanger:

```
"Hot side analysis"
duplicate i=2,(N+1)
    i_H[i]=i_H[i-1]-q_dot/(N*m_dot_H)                "Energy balance on hot side of each sub-HX"
    T_H[i]=Temperature(H$,h=i_H[i],P=P_H_in[i]) "Temperature leaving hot side of each sub-HX"
end
```

The inlet pressures for each sub-heat exchanger are found later in the program, with the differential length of each sub-heat exchanger and the local pressure gradient.

```
"Inlet pressure for each sub HX"
P_H_in[1]=P_H_in
P_C_in[1]=P_C_in
duplicate i=1,N
    P_H_in[i+1]=P_H_in[i]+(DELTAx[i]*dPHdx[i])
    P_C_in[i+1]=P_C_in[i]+(DELTAx[i]*dPCdx[i])
end
```

An energy balance on the cold-side for each sub-heat exchanger determines the specific enthalpies leaving each sub-heat exchanger:

$$i_{C,i} = i_{C,i-1} - \frac{\dot{Q}}{N\dot{m}_C} \; for \; i = 2 \ldots (N+1) \qquad 2.8$$

The temperatures are obtained based on the specific enthalpies and pressures leaving each sub-heat exchanger:

```
"Cold side analysis"
duplicate i=2,(N+1)
    i_C[i]=i_C[i-1]-q_dot/(N*m_dot_C)                "Energy balance on cold side of each sub-HX"
    T_C[i]=Temperature(C$,h=i_C[i],P=P_C_in[i])  "Temperature leaving cold side of each sub-HX"
End
```

The ε-*NTU* method is applied to each of the sub-heat exchangers. To start, the hot and cold side capacitance rates are found for each of the sub-heat exchangers:

$$\dot{C}_{H,i} = \dot{m}_H \frac{(i_{H,i} - i_{H,i+1})}{(T_{H,i} - T_{H,i+1})} \; for \; i = 1 \ldots N \qquad 2.9$$

$$\dot{C}_{C,i} = \dot{m}_C \frac{(i_{C,i} - i_{C,i+1})}{(T_{C,i} - T_{C,i+1})} \; for \; i = 1 \ldots N \qquad 2.10$$

The capacitance rates, calculated above, are based on average specific heat capacity defined as the ratio of the difference in enthalpies over the difference in temperatures.

```
"Effectiveness-NTU Method"
duplicate i=1,N
    C_dot_H[i]=m_dot_H*((i_H[i]-i_H[i+1])/(T_H[i]-T_H[i+1])          "Capacitance rate, hot side"
    C_dot_C[i]=m_dot_C*((i_C[i]-i_C[i+1])/(T_C[i]-T_C[i+1]))        "Capacitance rate, cold side"
end
```

The effectiveness of each sub-heat exchanger is computed:

$$\dot{C}_{min,i} = MIN\left(\dot{C}_{C,i}, \dot{C}_{H,i}\right) \; for \; i = 1 \ldots N \qquad 2.11$$

$$\varepsilon_i = \frac{\dot{Q}}{N\dot{C}_{min,i}(T_{H,i} - T_{C,i+1})} \; for \; i = 1 \ldots N \qquad 2.12$$

The number of transfer units is found using the counter-flow heat exchanger function in EES. The conductance for each sub-heat exchanger is computed based on the number of transfer units:

$$UA_i = NTU_i \dot{C}_{min} \; for \; i = 1 \ldots N \qquad 2.13$$

```
duplicate i=1,N
    C_dot_min[i]=MIN(C_dot_C[i],C_dot_H[i])                          "Minimum capacitance rate"
    Epsilon[i]=q_dot/(N*C_dot_min[i]*(T_H[i]-T_C[i+1]))              "Effectiveness for each sub-HX"
    NTU[i]=HX('counterflow', Epsilon[i], C_dot_C[i], C_dot_H[i], 'NTU') "NTU for each sub-HX"
    UA[i]=NTU[i]*C_dot_min[i]                                        "Conductance of each sub-HX"
end
```

Flow characteristics for each channel are found by obtaining the cross sectional area, perimeter, and the hydraulic diameter:

$$A_C = H_{channel} W_{channel} \qquad 2.14$$

$$per = 2(H_{channel} + W_{channel}) \quad 2.15$$

The hydraulic diameter is defined as:

$$D_h = \frac{4A_C}{per} \quad 2.16$$

```
"Flow Properties"
A_c_H=th_H*W_f                    "Cross sectional area, hot-side"
per_H=2*(th_H+W_f)                "Perimeter, hot-side"
A_c_C=th_C*W_f                    "Cross sectional area, cold-side"
per_C=2*(th_C+W_f)                "Perimeter, cold-side"
D_h_H=(4*A_c_H)/per_H             "Hydraulic diameter, hot-side"
D_h_C=(4*A_c_C)/per_C             "Hydraulic diameter, cold-side"
```

The channel width, W_f, is the distance between the fins and is constrained to be the same on both hot and cold sides, simplifying the resistance network. The channel heights, th_H and th_C, are the hot and cold channel heights, respectively. Figure 6 illustrates these dimensions.

The properties of the cold and hot-side fluids within the heat exchanger are evaluated within each sub-heat exchanger using the average of the inlet temperature, $T_H[1]$ and $T_C[N+1]$, and the temperature at the outlet of each sub-heat exchanger. Dashed lines in Figure 8 represent the center temperature. The inlet pressure of each sub-heat exchanger is used.

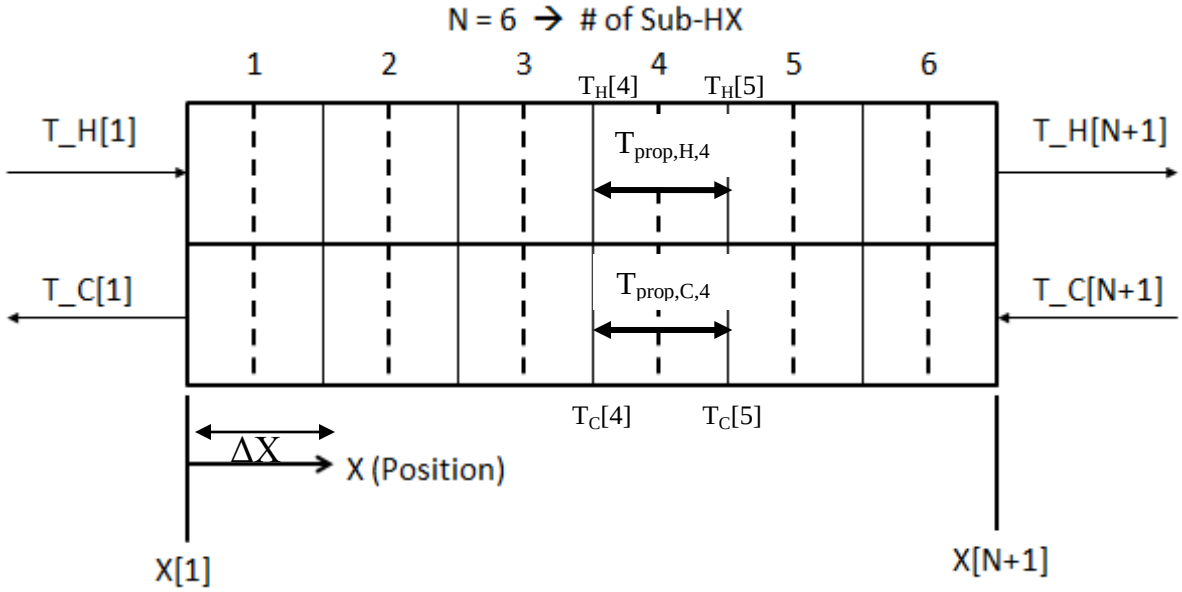

Figure 8: Schematic of the sub-heat exchanger model showing where the properties are evaluated for the cold and hot-side fluids. Example is shown for finding property temperature for sub-HX #4

Equations 2.17 and 2.18 show the temperatures used to find the density, specific heat, viscosity, conductivity, and Prandtl number for each sub-heat exchanger and each fluid:

$$T_{prop,H,i} = \frac{T_{H,i} + T_{H,i+1}}{2} \; for \; i = 1 \ldots N \qquad 2.17$$

$$T_{prop,C,i} = \frac{T_{C,i} + T_{C,i+1}}{2} \; for \; i = 1 \ldots N \qquad 2.18$$

Refer to Figure 8 for an example of calculating bulk temperature for sub-heat exchanger # 4.

```
duplicate i=1,N
    T_prop_H[i]= (T_H[i]+T_H[i+1])/2                    "Temperature for properties, hot-side"
    T_prop_C[i]=(T_C[i]+T_C[i+1])/2                     "Temperature for properties, cold side"
end
duplicate i=1,N
    rho_H[i]=Density(H$,T=T_prop_H[i],P=P_H_in[i])      "Density, hot-side"
    rho_C[i]=Density(C$,T=T_prop_C[i],P=P_C_in[i])      "Density, cold-side"
    cp_H[i]=cp(H$,T=T_prop_H[i],P=P_H_in[i])            "Specific heat, hot-side"
    cp_C[i]=cp(C$,T=T_prop_C[i],P=P_C_in[i])            "Specific heat, cold-side"
    mu_H[i]=Viscosity(H$,T=T_prop_H[i],P=P_H_in[i])     "Viscosity, hot-side"
    mu_C[i]=Viscosity(C$,T=T_prop_C[i],P=P_C_in[i])     "Viscosity, cold-side"
    k_H[i]=Conductivity(H$,T=T_prop_H[i],P=P_H_in[i])   "Conductivity, hot-side"
    k_C[i]=Conductivity(C$,T=T_prop_C[i],P=P_C_in[i])   "Conductivity, cold-side"
    Pr_H[i]=Prandtl(H$,T=T_prop_H[i],P=P_H_in[i])       "Prandtl #, hot-side"
    Pr_C[i]=Prandtl(C$,T=T_prop_C[i],P=P_C_in[i])       "Prandtl #, cold-side"
end
```

The velocity and Reynolds number for each channel and sub-heat exchanger can now be evaluated:

$$u_{H,i} = \frac{\dot{m}_{H,i}}{N_{tot}\rho_{H,i}A_{c,H}} \; for \; i = 1 \ldots N \qquad 2.19$$

$$u_{C,i} = \frac{\dot{m}_{C,i}}{N_{tot}\rho_{C,i}A_{c,C}} \; for \; i = 1 \ldots N \qquad 2.20$$

$$Re_{H,i} = \frac{\rho_{H,i}u_{H,i}D_{h,H}}{\mu_{H,i}} \; for \; i = 1 \ldots N \qquad 2.21$$

$$Re_{C,i} = \frac{\rho_{C,i} u_{C,i} D_{h,C}}{\mu_{C,i}} \; for \; i = 1 \ldots N \qquad 2.22$$

```
duplicate i=1,N
    u_H[i]=m_dot_H/(N_tot*rho_H[i]*A_c_H)          "Mean velocity, hot-side"
    u_C[i]=m_dot_C/(N_tot*rho_C[i]*A_c_C)          "Mean velocity, cold-side"
    Re_H[i]=(rho_H[i]*D_h_H*u_H[i])/mu_H[i]        "Reynold's number, hot-side"
    Re_C[i]=(rho_C[i]*D_h_C*u_C[i])/mu_C[i]        "Reynold's number, cold-side"
end
```

The local Nusselt number and friction factor are found using the DuctFlow_N_local procedure in EES, which uses the Gnielinski turbulent flow correlation:

```
duplicate i=1,N
"Finding Nusselt number and friction factor"
call
DuctFlow_N_local(Re_H[i],Pr_H[i],99999,th_H/W_f,0:Nusselt_T_x_H[i],Nusselt_H_x_H[i],f_x_H[i])
call DuctFlow_N_local(Re_C[i],Pr_C[i],99999,th_C/W_f,0: Nusselt_T_x_C[i], Nusselt_H_x_C[i],&
f_x_C[i])
end
```

The value for x/D is set to a very high number when determining the heat transfer coefficient in order to simulate fully developed flow within each section. The relative roughness is set to zero, which assumes that the channel surface is smooth. The procedure generates two values for the Nusselt number, assuming constant wall temperature or constant heat flux. When flow is turbulent, both values of Nusselt number are equal and because both flows are turbulent, there is no need to distinguish which one to use.

The local heat transfer coefficient and pressure drop can be found using Equations 2.23 through 2.26:

$$Nu_{H,i} = \frac{h_{H,i} D_{h,H}}{k_{H,i}} \qquad 2.23$$

$$Nu_{C,i} = \frac{h_{C,i} D_{h,C}}{k_{C,i}} \qquad 2.24$$

where $k_{C,i}$, $k_{H,i}$ and $h_{C,i}$, $h_{H,i}$ are the conductivities and heat transfer coefficients of the cold and hot fluids, respectively.

$$f_{H,i} = \frac{2\left[\frac{dP}{dx}\right]_{H,i} D_{h,H}}{\rho_{H,i} {u_{H,i}}^2} \qquad 2.25$$

$$f_{C,i} = \frac{2\left[\frac{dP}{dx}\right]_{C,i} D_{h,C}}{\rho_{C,i} {u_{C,i}}^2} \qquad 2.26$$

where $f_{H,i}$, $f_{C,i}$ and $dP/dx_{H,i}$, $dP/dx_{C,i}$ are the friction factor and local pressure gradient for the hot and cold fluids, respectively.

```
duplicate i=1,N
"Finding heat transfer coefficient"
    Nusselt_H_x_H[i]=(h_H[i]*D_h_H)/k_H[i]
    Nusselt_H_x_C[i]=(h_C[i]*D_h_C)/k_C[i]
"Finding pressure drop"
    f_x_H[i]=(-dPHdx[i]*2*D_h_H)/(rho_H[i]*u_H[i]^2)
    f_x_C[i]=(-dPCdx[i]*2*D_h_C)/(rho_C[i]*u_C[i]^2)
end
```

Next the differential length associated with each segment that is required to achieve the conductance associated with that sub-heat exchanger is computed. By summing the differential lengths, the value for the overall length of the heat exchanger is computed.

The unit cell and resistance network are shown in Figure 9.

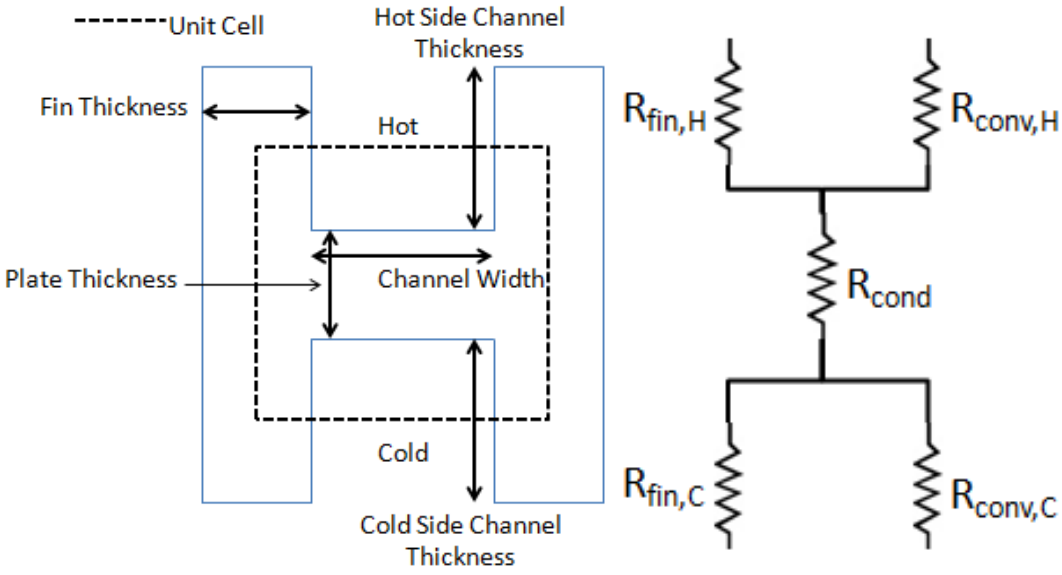

Figure 9: Diagram on left shows the unit cell of the heat exchanger including the fins, refer to Figure 4 and Figure 5. Diagram on the right shows the resistance network that can be repeated for the whole heat exchanger.

The resistances associated with the heat exchanger are evaluated as follows:

$$R_{conv,H,i} = \frac{1}{h_{H,i}\Delta X_i W_f} \; for \; i = 1 \ldots N \qquad 2.27$$

$$R_{conv,C,i} = \frac{1}{h_{C,i}\Delta X_i W_f} \; for \; i = 1 \ldots N \qquad 2.28$$

$$R_{cond,i} = \frac{th_p}{k_{p,i}\Delta X_i (W_f + th_f)} \; for \; i = 1 \ldots N \qquad 2.29$$

$$R_{fin,H,i} = \frac{1}{2\eta_{H,i} h_{H,i} \left(\frac{th_H}{2}\right) \Delta X_i} \; for \; i = 1 \ldots N \qquad 2.30$$

$$R_{fin,C,i} = \frac{1}{2\eta_{C,i} h_{C,i} \left(\frac{th_C}{2}\right) \Delta X_i} \; for \; i = 1 \ldots N \qquad 2.31$$

where ΔX is the length of each sub-heat exchanger (refer to Figure 8), W_f is the channel width, th_f is the thickness of the fins, k_p is the conductivity of the metal, η_H and η_C are the fin efficiencies for the hot and cold-side, respectively, and th_H and th_C represent the hot and cold-side channel thickness, respectively. Refer to Figure 6 for a schematic and terminology.

The fin efficiencies are calculated using the solution for a constant cross-sectional area fin with an adiabatic tip. The length of the fin is taken to be half of the channel thickness due to symmetry. The conductivity of the plate is evaluated at the average of the hot and cold fluid temperatures, at various positions in the heat exchanger. The function eta_fin_straight_rect in EES is used for this calculation.

```
duplicate i=1,N
eta_fin_H[i]=eta_fin_straight_rect(th_f,th_H/2,h_H[i],k_p[i])     "Fin efficiency, hot-side"
eta_fin_C[i]=eta_fin_straight_rect(th_f,th_C/2,h_C[i],k_p[i])     "Fin efficiency, cold-side"
k_p[i]=k_(Metal$, (T_H[i]+T_C[i])/2)                              "Metal conductivity at average
temperature"
end
```

The total resistance is evaluated according to:

$$R_{total,i} = \frac{1}{\left[\frac{1}{R_{conv,H,i}} + \frac{1}{R_{fin,H,i}}\right]} + R_{cond,i} + \frac{1}{\left[\frac{1}{R_{conv,C,i}} + \frac{1}{R_{fin,C,i}}\right]} for\ i = 1 \ldots N \qquad 2.32$$

```
duplicate i=1,N
"Length of each sub-HX"
    R_conv_H[i]=1/(h_H[i]*DELTAx[i]*W_f)                    "Convection resistance, hot-side"
    R_conv_C[i]=1/(h_C[i]*DELTAx[i]*W_f)                    "Convection resistance, cold-side"
    R_cond[i]=th_p/(k_p[i]*DELTAx[i]*(W_f+th_f))            "Conduction resistance"
    R_fin_H[i]=1/(eta_fin_H[i]*h_H[i]*(th_H/2)*DELTAx[i]*2) "Fin resistance, hot-side"
    R_fin_C[i]=1/(eta_fin_C[i]*h_C[i]*(th_C/2)*DELTAx[i]*2) "Fin resistance, cold-side"
"Total thermal resistance"
    R_total[i]=(1/((1/R_conv_H[i])+(1/R_fin_H[i])))+R_cond[i]+(1/((1/R_conv_C[i])+(1/R_fin_C[i])))
end
```

The total conductance is:

$$UA_i = \frac{2N_{tot}}{R_{total,i}} \qquad 2.33$$

Note that the total conductance is multiplied by two because the unit cell (Figure 9) includes half of a channel pair and multiplied by the total number of channels, so that it represents the entire heat exchanger.

```
duplicate i=1,N
UA[i]=(2*N_tot)/R_total[i]                                  "Total conductance"
end
```

The length is found by adding up the differential lengths of the sub-heat exchangers:

```
x[1]=0[m]                                                   "Starting position of 1st sub-HX"
duplicate i=1,N
x[i+1]=x[i]+DELTAx[i]                                       "Length of the HX"
end
```

The last step, is to comment out the assumed outlet temperature,

```
{T_H_outlet=40[C]        "Assumed outlet hot temperature"
```

and replace it with an equation that equates the specified overall heat exchanger length with the length calculated by summing up the differential lengths of each sub-heat exchanger. The model can now calculate the hot outlet temperature, if an overall length of the heat exchanger

is specified. This is most simply done with an error function and minimizing the error to zero:

$$err = \frac{|x[n+1] - L|}{L} \qquad 2.34$$

$$err = 0 \qquad 2.35$$

```
err=abs(x[N+1]-L)/L        "To get length of HX"
err=0                      "Error, to make sure lengths are equal"
```

2.2 Graphical user interface (GUI)

A graphical user interface has been developed to make the design study more efficient and intuitive. See Figure 10 for a snapshot of the GUI.

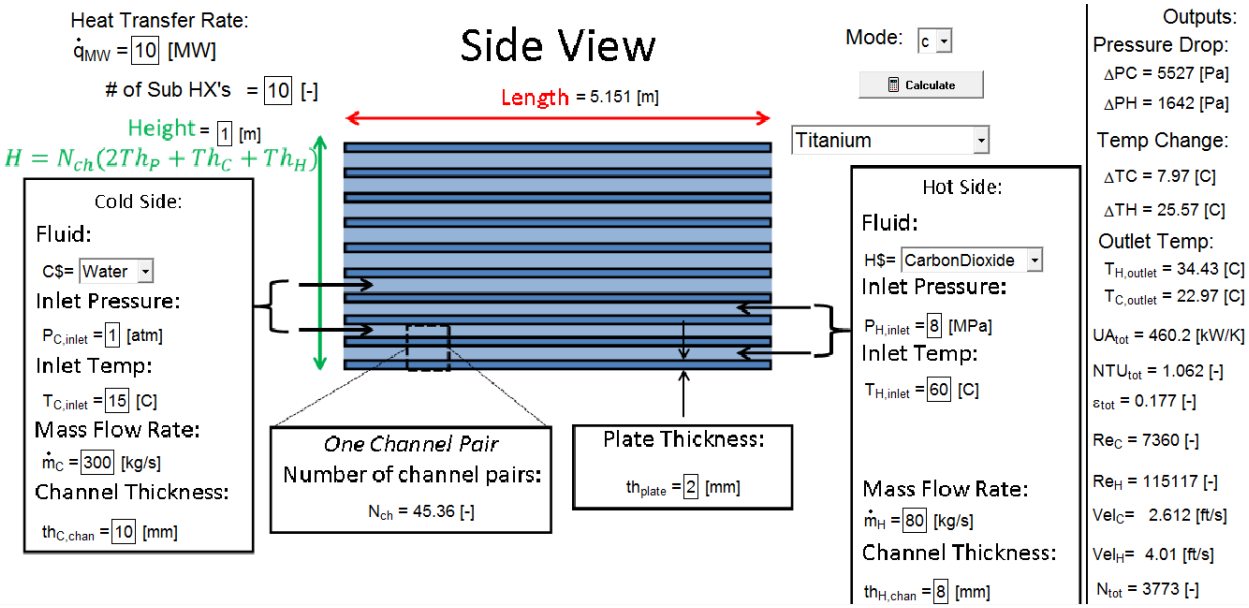

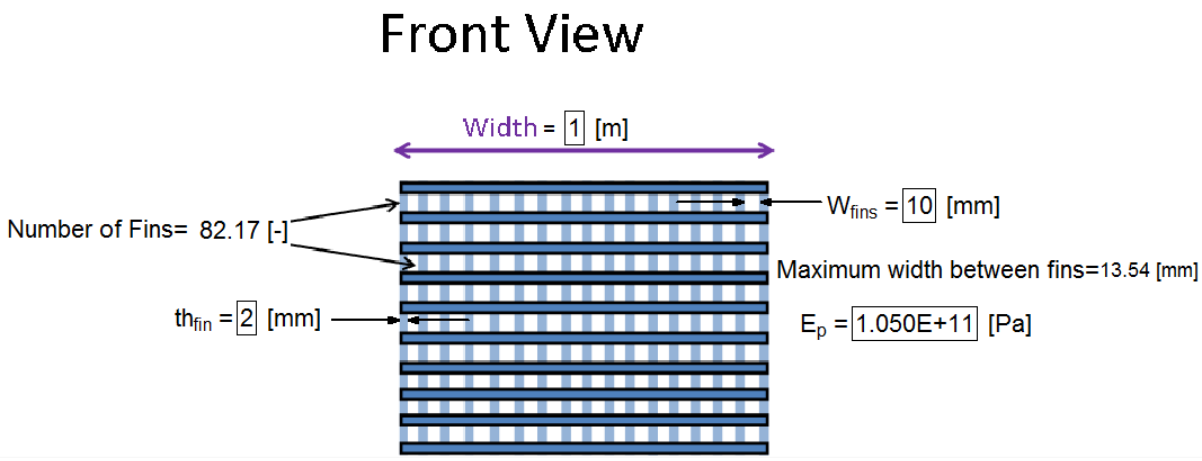

Figure 10: Graphical user interface built into EES code to make design study more efficient

The parameters with boxes around the numbers represent inputs to the model, while texts with no boxes represent outputs. These inputs and outputs can be easily interchanged and solved simultaneously. There are also three drop down menus that allow for the working fluids and the material of the plate and fins to be changed.

2.3 Model verification

Now that the model has been developed, it is important to verify some of the major components of the model. Two major components of the model are the sub-heat exchangers and the fins (i.e., structural members) can be tested to either verify it is working properly or confirm the result is correct after imposing it with certain conditions. The following section will go through this process of model verification.

2.3.1 Sub-heat exchanger model

To confirm that the sub-heat exchanger model was producing internally-consistent results, the model was compared with a simple counter flow heat exchanger model with constant properties. In the comparison case, the sub-heat exchanger model uses water for both channels in order to minimize the effects of property variations. The simple heat exchanger model was developed using the ε-*NTU* method that only used inlet and outlet conditions. It was based on Example 8.3-1, page 858 (Nellis & Klein, 2009). This model was then tested

against the sub-heat exchanger model, both running water through the channels. Each model had the same properties and inputs which are shown in Table 2.

Inputs	Parameters
Hot Fluid=Water	Width=1[m]
Cold fluid=Water	Height=1[m]
P_C_in=1[atm]	th_C=500[mm]
P_H_in=8[MPa]	th_H=500[mm]
T_C_in=15[C]	th_p=2[mm]
T_H_in=60[C]	Length=1-200[m]
m_dot_H=80[kg/s]	N_ch=1-10[-]
m_dot_C=300[kg/s]	N=1-10[-]

Table 2: Inputs and parameters for both simple and sub-heat exchanger models

The two models were tested against one another for different conditions, generating the results in Table 3 through Table 6.

Property	Sub-HX Model Results	Simple Model Results
T_C_out [K]	290.4	290.5
T_H_out [K]	324.5	324.4
UA [W/K]	72836	74208
NTU [-]	.2186	.2227
Effectiveness [-]	.1917	.1948

Table 3: Results for: Length=10[m], Number of Channels=10[-], Number of sub-HX's=1[-]

Property	Sub-HX Model Results	Simple Model Results
T_C_out [K]	291.3	291.3
T_H_out [K]	321.3	321.2
UA [W/K]	106157	107135
NTU [-]	.3187	.3216
Effectiveness [-]	.2642	.2662

Table 4: Results for: Length=200[m], Number of Channels=1[-],Number of sub-HX's=1[-]

Property	Sub-HX Model Results	Simple Model Results
T_C_out [K]	290.5	290.5
T_H_out [K]	324.5	324.4
UA [W/K]	73413	74208
NTU [-]	.2203	.2227
Effectiveness [-]	.193	.1948

Table 5: Results for: Length=10[m], Number of Channels=10[-],Number of sub-HX's=10[-]

Property	Sub-HX Model Results	Simple Model Results
T_C_out [K]	291.3	291.3
T_H_out [K]	321.2	321.2
UA [W/K]	106433	107135
NTU [-]	.3195	.3216
Effectiveness [-]	.2648	.2662

Table 6: Results for: Length=200[m], Number of Channels=1[-],Number of sub-HX's=10[-]

With a length of 10 meters and 10 channel pairs, the results are nearly identical. As the length is increased, the results start to vary slightly. This is most likely due to the larger temperature change within the heat exchanger. The simple model evaluates all properties at the inlet and outlet temperatures and pressures, while the sub-heat exchanger model evaluates all the properties at the bulk temperatures and pressures for each sub-heat exchanger. As the sub-heat exchanger length increases there is a larger temperature difference and therefore more variation in properties. This means that the simple model becomes less and less accurate, but even with the length and channel pair variation, the temperatures are very consistent.

2.3.2 Fin Model

One issue that the precooler heat exchanger needs to deal with is containing the high pressures on the carbon dioxide, 8 MPa side. Without adequate structural support, the plates

used to form the channels of the heat exchanger may break or deflect significantly. To address this issue, supports (i.e., fins) were added to make the channel structure, as shown in Figure 5, more rigid. The fins also served to increase the heat transfer surface area. The addition of these supports changes the resistance network for the heat exchanger. Figure 9 illustrates the unit cell and resistance network.

The fins add convection surface area that will increase the effectiveness of the heat exchanger in addition to providing support. By setting the conductivity of the metal, fin and plate, to a very large number, approaching infinity; the fin efficiency goes to the limit of unity. This causes the plate temperature to become uniform throughout the heat exchanger, which eliminates the fin and conduction resistances and leaves only convection from the entire surface area of each channel. The resistance network in this limit includes only convection from the hot side and convection on the cold side in series. The total resistance is then:

$$R_{total,i} = \frac{1}{h_{H,i}A_{c,H,infin}} + \frac{1}{h_{C,i}A_{c,C,infin}} \quad 2.36$$

$$A_{c,H,infin} = 2(th_H + W_f)L \quad 2.37$$

$$A_{c,C,infin} = 2(th_C + W_f)L \quad 2.38$$

$$UA_i = \frac{1}{R_{total,i}} \quad 2.39$$

Length [m]	# Channel Pairs	UA_test [W/K]	UA_model [W/K]
10	**10**	831039	831039
20	**5**	301489	301489
40	**1**	348064	348064

Table 7: Results from fin testing

Knowing the total resistance, the total conductance can be calculated as the inverse of the total resistance. If the heat transfer coefficients are set to constants, the conductance from the model can be compared to the conductance found using the simple resistance network. The two conductances should be exactly the same, if they are not, then the model has an error. The results from this test showed that the two conductances were exactly the same. Refer to Table 7 for results from the test.

2.4 Performance plots

Now that the model has been developed, a design study using the heat exchanger model can be prepared. The design study aims to produce optimal or limited geometries that can be later used in place of performance constraints. This will allow the heat exchanger performance to be evaluated on a larger scale, to quantify auxiliary power consumption and water use.

This design study will determine optimal or limited geometry constraints that meet performance requirements while also being as small as possible. The list below illustrates performance constraints on this particular heat exchanger, the set dimensions and parameters, and finally the free parameters that are varied in the design study.

Performance constraints:

1. Q_dot: Heat transfer rate → 10 MW (Minimum)
2. DELTAP_H: Pressure drop on hot-side → 40 kPa (Limit)
3. DELTAP_C: Pressure drop on cold-side → 5 kPa (Limit)

The required heating load for the precooler heat exchanger was set to 10 MW, which sets the overall length of the heat exchanger. The CO_2 and water side pressure drops were set to 0.5% and 5% of the inlet pressures, respectively. These performance constraints were used to set the CO_2 and water channel heights, accordingly.

Set Parameters:

1. P_H_inlet: Inlet pressure CO2 side= 8 MPa
2. P_C_inlet: Inlet pressure Water side = 1 atm

3. T_H_inlet: Inlet temperature CO2 side = 60 C
4. T_C_inlet: Inlet temperature Water side = 15 C
5. m_dot_H: Mass flow rate CO2 side = 80 kg/s
6. m_dot_C: Mass flow rate water side = 300 kg/s
7. N: Number of sub-HX's = 10[-]
8. th_H: Height of hot side channel-> Set by DELTAP_H
9. th_C: Height of cold side channel-> Set by DELTAP_C
10. L: Length of HX-> Set by Heat transfer rate

Set parameters 1-7, listed above, were given values that were thought to represent actual operating conditions. Set parameters 8-10 are given values predicted by the model for the given performance constraints.

Free Parameters:

1. W and H: Width and Height of HX = 1 m
2. th_plate: Thickness of plates = 2 mm
3. th_fin: Thickness of fins = 2 mm
4. W_fins: Width between fins = 5 mm

After all above constraints were set, there are only four free geometric parameters left to be studied. The overall width and height of the heat exchanger are set equal at 1 m, making the frontal heat exchanger area square. The plate and fin thicknesses, which are illustrated in Figure 6 as th_p and th_f, respectively, are set to 2 mm. Lastly, the width between the fins, illustrated in Figure 6 as W_f, is set at 5 mm.

The free parameters were varied one at a time while tracking multiple variables, with the most important one being the overall mass of the heat exchanger. Figure 11 through Figure 14 show the results of the study.

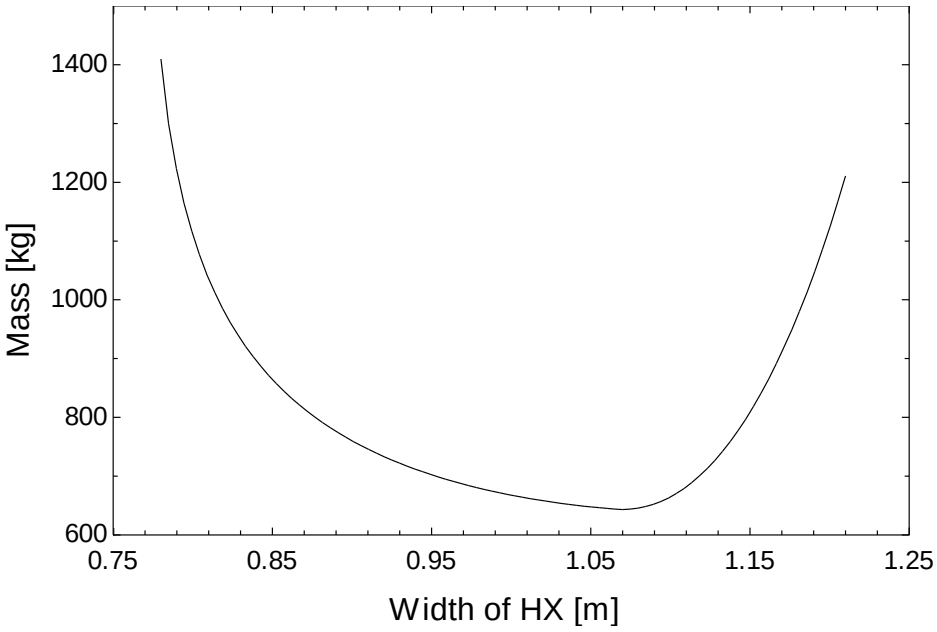

Figure 11: Mass as a function of width and height of heat exchanger

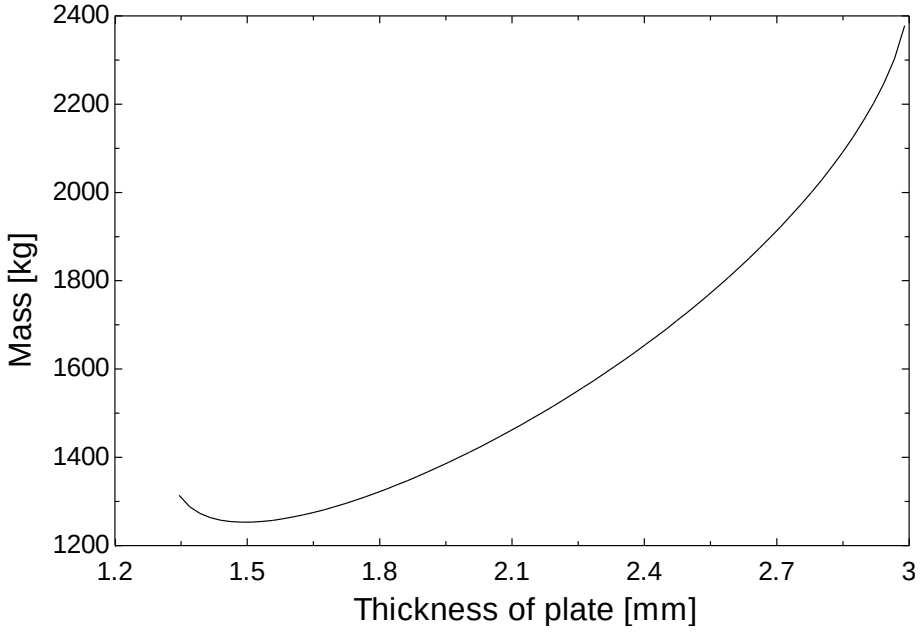

Figure 12: Mass as a function of plate thickness

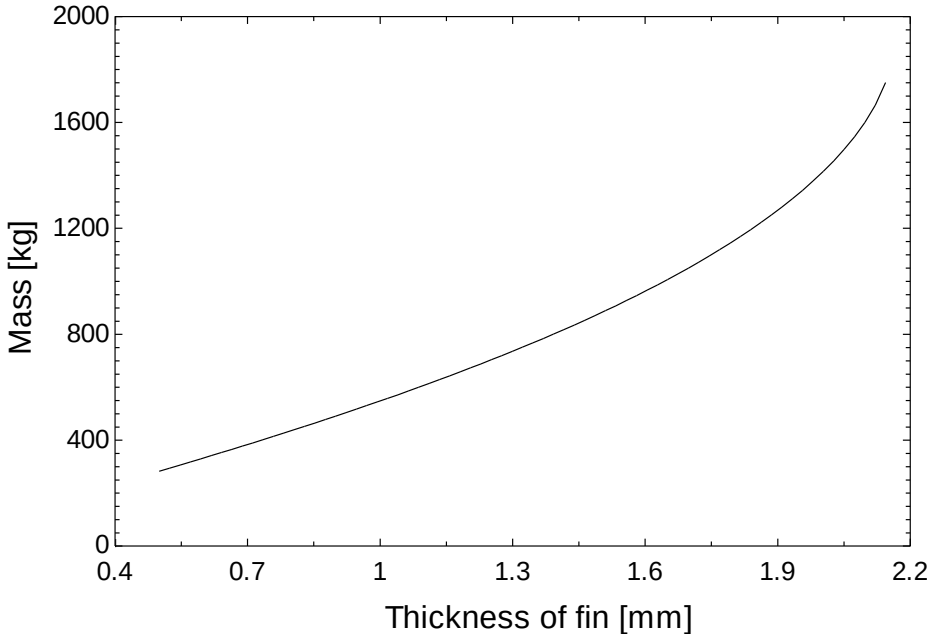

Figure 13: Mass as a function of fin thickness

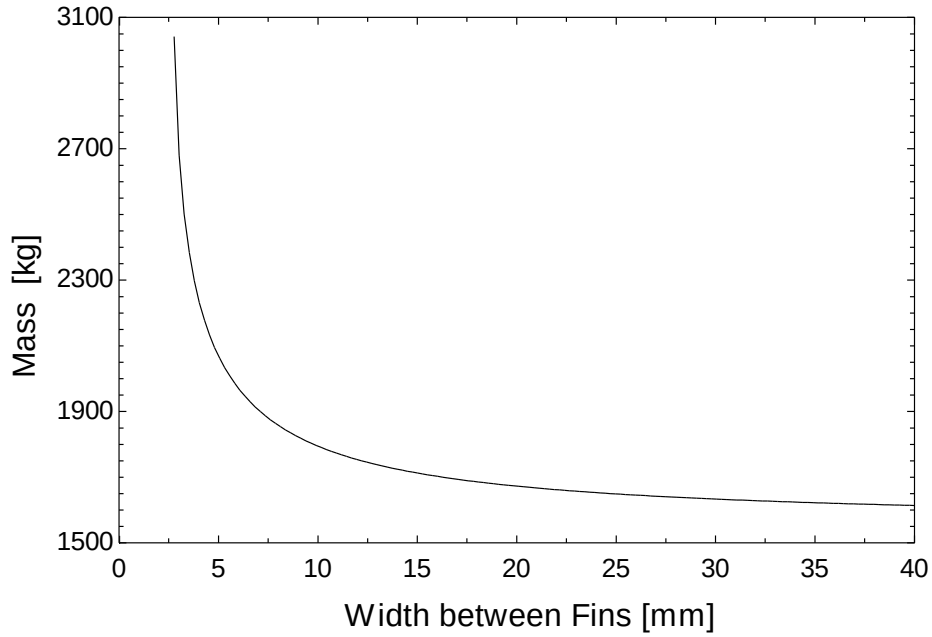

Figure 14: Mass as a function of width between fins

Reviewing the plots, a minimum heat exchanger mass occurs when varying the width/height of heat exchanger and plate thickness. For the fin thickness, it appears that the smallest possible thickness, which will certainly be constrained by manufacturability and strength, is

desirable. Varying the width between the fins shows that it would be advantageous to make the fin-to-fin distance as wide as possible, constrained by strength and deflection limitations.

This initial design study shows that the width between the fins and fin thickness design parameters can be set to the strength/deflection and manufacturability/strength limit, respectively. The width/height of heat exchanger and the plate thickness can then be set using a two degree of freedom optimization.

To obtain reasonable values for the width between the fins and fin thickness, a simple stress and deflection analysis was done. Figure 15 shows a drawing of the section that will be analyzed. The direction of flow is into the page.

The plate separating the high pressure CO2 and low pressure water is of concern for deflection and failure. The pressure difference acting on the plate results in a downward force, per unit length into the page, on the beam. A beam deflection analysis can be done to obtain a value for the width between the fins given a value for plate thickness and maximum deflection from pg. 817 (Juvinall, 2006).

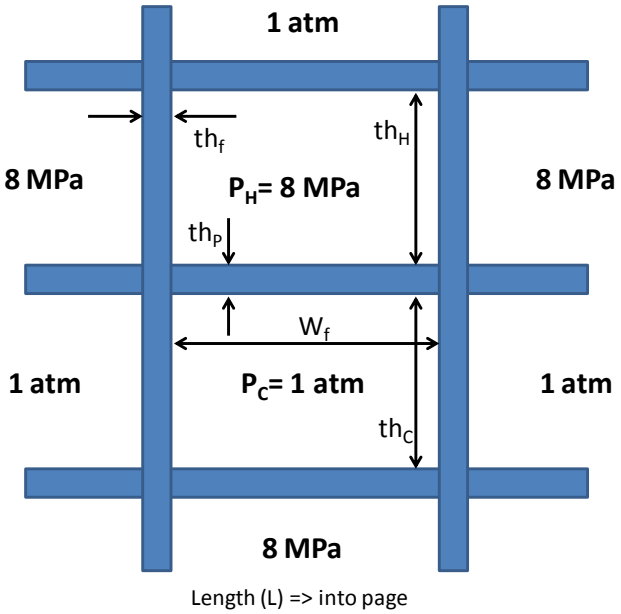

Figure 15: Drawing of stress/deflection section of heat exchanger

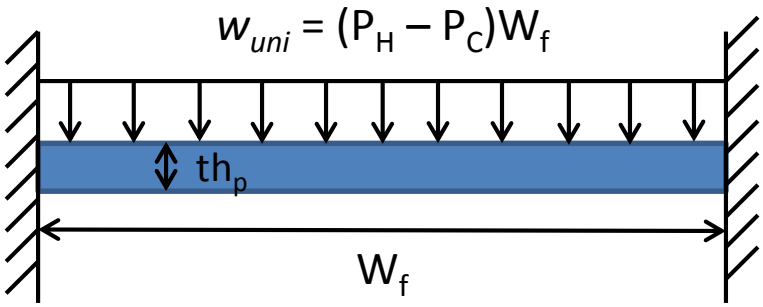

Figure 16: Free body diagram of beam

$$F = (P_H - P_C)\, W_f\, L \tag{2.40}$$

$$w_{uni} = \frac{F}{L} \tag{2.41}$$

$$I_p = \frac{L\, th_p^3}{12} \quad for\ a\ rectangular\ cross\ section \tag{2.42}$$

$$\delta_{max} = \frac{w_{uni}\, W_f^4}{384\, E\, I_p} \tag{2.43}$$

Simplifying these equations gives an explicit equation for W_f:

$$W_f = \left(\frac{32\, \delta_{max}\, th_p^3\, E\, L}{P_H - P_C}\right)^{\frac{1}{5}} \tag{2.44}$$

```
W_s=((32*Delta_max*th_p^3*E_p*L)/(P_H_in-P_C_out))^(1/5)
```

The width between the fins is set to half of the value found through the analysis for a factor of safety of two.

To ensure that failure will not occur, the maximum bending stress and maximum shear stress are found and compared to the yield stress. Maximum shear force occurs on the ends of the beam where the reactions supporting the downward force occur. The maximum bending moment also occurs on the ends where the greatest moment arm occurs. Figure 17 illustrates this. Note the force is not applied directly in the middle span of the beam in the figure.

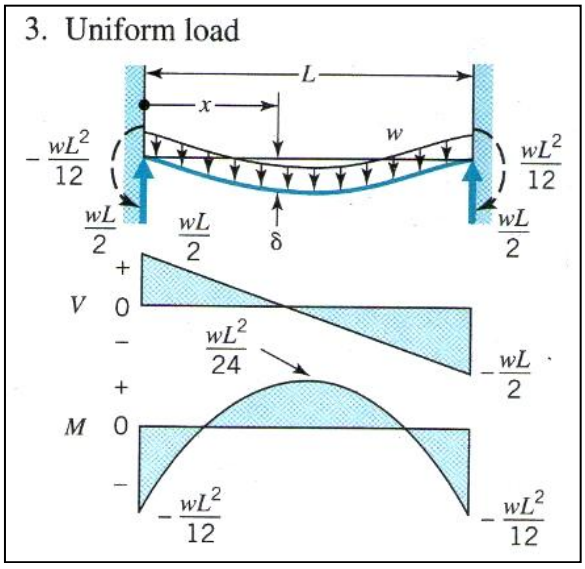

Figure 17: Uniform load, fixed ends beam analysis (Image from Juvinall)

$$V_{max} = \frac{w_{uni} W_f}{2} \qquad 2.45$$

$$M_{max} = \frac{w_{uni} W_f^2}{12} \qquad 2.46$$

Pure Bending (Juvinall, pg. 123):

$$\sigma_{max} = \frac{M_{max}}{Z} \qquad 2.47$$

$$Z = \frac{I_p}{c} \; where \; c = \frac{th_p}{2} \qquad 2.48$$

Traverse Shear (Juvinall, pg. 133):

$$\tau_{max} = \left(\frac{3}{2}\right)\frac{V_{max}}{A}\ where\ A = th_p\ L \qquad 2.49$$

```
V_max=(w_uni*W_f)/2                                  "Shear force"
M_max=(w_uni*W_f^2)/12                               "Moment arm"
tau_max=((3/2)*(V_max/(1[m]*th_p)))*convert(Pa,MPa)  "Shear stress"
Z=I_p/(th_p/2)                                       "Section modulus"
sigma_max=(M_max/Z)*convert(Pa,MPa)                  "Normal stress"
```

When setting the plate thickness to 1 mm and then comparing the values for the bending and shear stresses with the yield stress of the steel, the values are almost a factor of five from the yield stress. This means that the plate thickness has a lower bound constrained by the manufacturability. From this analysis, it can also be determined that the fin thickness has a lower bound based on the manufacturability as well. The fin thickness does not experience a pressure difference and therefore does not have a net force acting on it. As a result, it does not need the strength that the horizontal plate needs. Therefore, to set the fin thickness a value of 1[mm] was selected based on manufacturability.

Once the fin thickness and width between the fins have been set, the plate thickness and width/height of the heat exchanger must be obtained using a two degree of freedom optimization that minimizes mass. The results of the optimization are shown below in Figure 18.

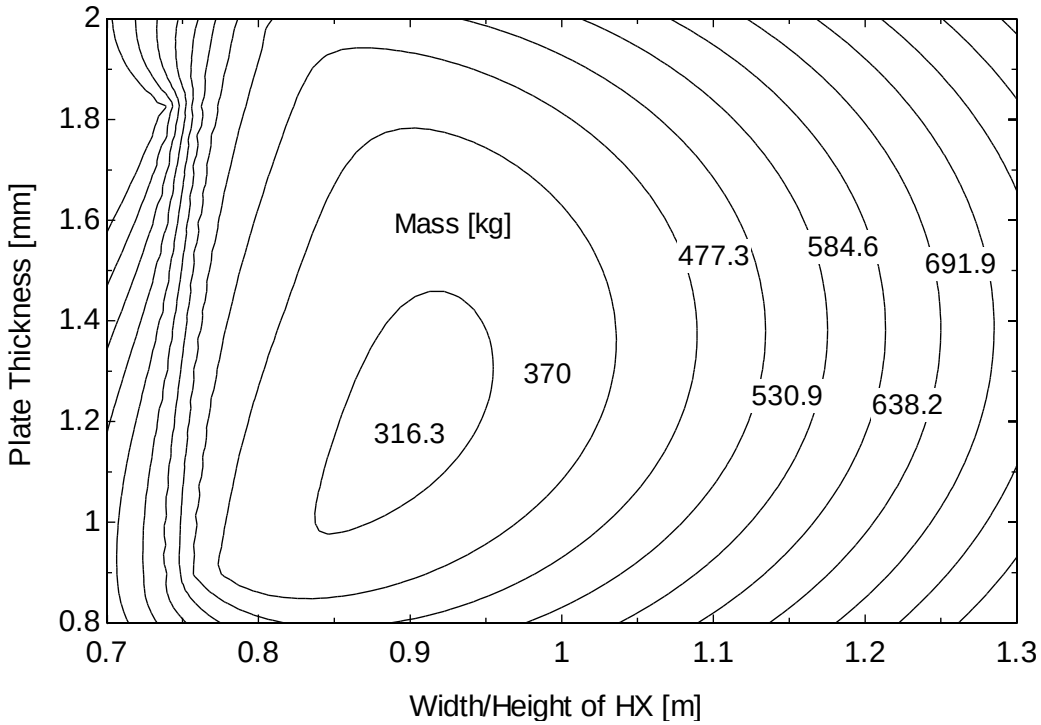

Figure 18: Two degree of freedom optimization minimizing mass of HX

With the results of the optimization, the width/height and plate thickness minimize the mass at approximately 0.9 m and 1.2 mm. This means that the size of the heat exchanger is 1.0 m by 1.0 m by 0.5 m and the mass is around 300 kg or 660 lbs for a heat exchanger that provides 1000 kW of cooling.

3 COOLING TOWER

Cooling towers have been proven to provide cost-effective cooling for a wide range of processes. The issue with water cooling is the consumption of water that occurs during the cooling process. Not only is water expensive but it is also a scarce resource especially in desert/arid regions where solar generation plants are strategically placed. During operation of a cooling tower, the process water (i.e. used in cooling working fluid) flows over the heat transfer surface (i.e. fill) of the cooling tower, which can vary depending on type of cooling tower. Air is introduced into the tower, which evaporates a fraction of this process water to cool the remaining water down to the required temperature or to satisfy a required load (Baltimore Aircoil Company, 2011). The two configurations that are typically used in cooling towers are cross-flow and counter-flow. Schematics of the fill surfaces for each configuration are shown in Figure 19 and Figure 20.

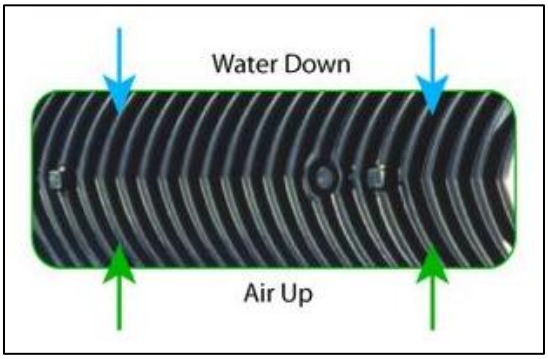

Figure 19: Schematic of a counter-flow fill for a cooling tower

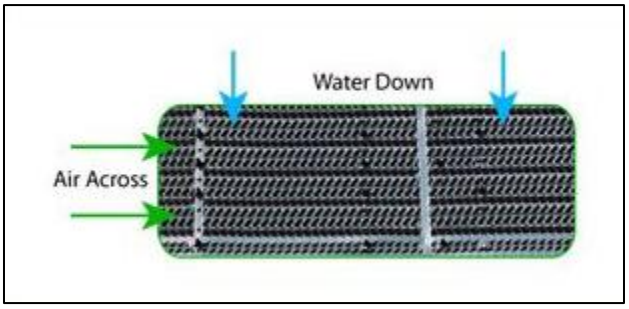

Figure 20: Schematic of a cross-flow fill for a cooling tower

In the counter-flow configuration, the water flows vertically down the fill as the air flows vertically up. In the cross-flow configuration, the water flows vertically down the fill as the

air flows horizontally across. Towers with cross-flow fills typically have lower pumping head, lower noise, and allow for easier maintenance when compared to the counter-flow configuration (Baltimore Aircoil Company, 2011). Counter-flow configurations are used when icing and space requirements are major concerns. In the case for the Brayton cycle, the cross-flow configuration seems to fit the requirements better than the counter-flow configuration.

Most cooling tower fans are either centrifugal or axial fans. Axial fans typically require about half the amount of fan power required by the load when compared to a similarly sized centrifugal fan (Baltimore Aircoil Company, 2011). However, centrifugal fans can be placed in more robust ambient conditions (e.g. high static pressures, outdoor installations). Being that the cooling tower would be located in a desert area, the power savings are more of a concern than overcoming tough ambient conditions, so axial fans were selected for the following analysis.

There are two ways to push the air through the towers, either induced or forced draft. Forced draft is the most typical way due the equipment being located at the base of the towers for ease of access and maintenance. Induced draft equipment is located at the top of the tower, providing reduced noise and protection from icing in sub-freezing conditions (Baltimore Aircoil Company, 2011). A forced draft tower was selected to be modeled in the following section.

3.1 Model development

Knowing the type of cooling tower and major components, developing the model of representing the performance of a cooling tower is the next step. The model represented in the following section uses the enthalpy-effectiveness method and actual cooling tower performance data from the Baltimore Aircoil Company.

3.1.1 Enthalpy-effectiveness method

The cooling tower model uses the enthalpy-effectiveness approach proposed by Braun et al. (1989). The model utilizes the mass/energy transfer effectiveness's to determine the tower effectiveness and makeup water mass flow rate.

Energy transfer effectiveness:

$$\varepsilon_{ct} = \frac{h_{a,o} - h_{a,i}}{h_{a,s,o} - h_{a,i}} \tag{3.1}$$

Mass transfer effectiveness:

$$\varepsilon_{ct} = \frac{\omega_{a,o} - \omega_{a,i}}{\omega_{a,s,o} - \omega_{a,i}} \tag{3.2}$$

Makeup water mass flow rate:

$$\dot{m}_{muw} = \dot{m}_a(\omega_{a,o} - \omega_{a,o}) \tag{3.3}$$

Energy balance:

$$\dot{m}_w h_{w,i} + \dot{m}_{muw} h_{muw} + \dot{m}_a h_{a,i} = \dot{m}_w h_{w,o} + \dot{m}_{a,o} h_{a,o} \tag{3.4}$$

Heat transfer rate:

$$\dot{Q}_{ct} = \dot{m}_w(h_{w,i} - h_{w,o}) \tag{3.5}$$

Effectiveness/ NTU relationship, based on the dry counter-flow heat exchanger relationship:

$$\varepsilon_{ct} = \frac{1 - \exp\left(-NTU(1 - m^*)\right)}{1 - m^* \exp\left(-NTU(1 - m^*)\right)} \tag{3.6}$$

Where,

$$m^* = \frac{\dot{m}_a}{\dot{m}_{w,i}\left(\frac{Cp_w}{C_s}\right)} \tag{3.7}$$

The effective specific heat capacity is defined as:

$$C_s = \frac{h_{s,w,i} - h_{s,w,o}}{T_{w,i} - T_{w,o}} \qquad 3.8$$

$h_{s,w,i}$ and $h_{s,w,o}$ are the saturated air enthalpies evaluated at the inlet and outlet water temperatures.

Applying equations 3.1 through 3.8, allows for the calculation of cooling tower effectiveness and makeup water mass flow rate given five inputs such as inlet and outlet water temperatures, inlet wet bulb temperature, water flow rate, and air flow rate.

3.1.2 Manufacturers data (BAC)

In addition to the enthalpy-effectiveness method, actual performance data from a cooling tower is used to establish a relationship between variables within the model. The Baltimore Aircoil Company has a cooling tower selection program that provides performance and technical data for their entire selection of cooling towers (Baltimore Aircoil Company, 2011). All data is certified by the Cooling Technology Institute (CTI). CTI guarantees that a CTI certified model "will perform thermally in accordance with the Manufacturer's published ratings" (Cooling Technology Institute, 2012). By selecting a model and inputting design conditions, performance capability and performance curves can be generated. The program also provides tower dimensions, weight, motor horsepower, and pumping head. BAC has six model lines that can provide varying loads as well as different configurations and components. The six different lines can be seen in Figure 21 and Figure 22.

VT0/VT1	LOW PROFILE VTL	FXT	
			Model
Counterflow, Forced Draft, Centrifugal Fan	Counterflow, Forced Draft, Centrifugal Fan	Crossflow, Forced Draft, Axial Fan	Flow and Fan System
12 - 1,335 Nominal Tons*	16 - 272 Nominal Tons*	58 - 268 Nominal Tons*	Catalogued Capacity Range
• Indoor applications • High temperature industrial applications • Suitable for sound sensitive applications • Redundancy using the BALTIGUARD™ Fan System • Split fan housing eases replacement of fan or fan shaft • Easy maintenance with motors and drives located outside of discharge air stream	• Installations with low height requirements • Indoor applications • High temperature industrial applications • Redundancy using the BALTIGUARD™ Fan System • Suitable for sound sensitive applications • Single piece shipping and rigging	• Easy motor access • High efficiency, low horsepower axial fans • Single piece shipping and rigging • No sheaves to align and no belts to install • Long service life • Easy maintenance	UNIQUE FEATURES

Figure 21: Three lines of cooling tower models that use force draft

	SERIES 3000	SERIES 1500	PT2
Model			
Flow and Fan System	Crossflow, Induced Draft, Axial Fan	Crossflow, Induced Draft, Axial Fan	Counterflow, Induced Draft, Axial Fan
Cataloged Capacity Range	220 - 1,350 Nominal Tons*	128 - 428 Nominal Tons*	99 - 787 Nominal Tons*
UNIQUE FEATURES	• Shake table tested up to a S_{DS} of 3.50g at grade • Meets wind and seismic requirements for the 2009 International Building Code (IBC) • IBC compliant for critical buildings • Piping flexibility • Redundancy using the BALTIGUARD™ Fan System • TriArmor® Corrosion Protection System • EVERTOUGH™ Construction • Reliable year-round operation • Low sound options	• Ideal replacement unit • Ideal for tight enclosures • Standard internal walkway • Redundancy using the BALTIGUARD™ Fan System • Independent fan operation • TriArmor® Corrosion Protection System • Reliable year-round operation • Single water inlet with integral strainer • Low sound options	• Shake table tested up to a S_{DS} of 2.93g at grade • Meets wind and seismic requirements for the 2009 International Building Code (IBC) • IBC compliant for critical buildings • Reduced footprint for low tonnage applications • TriArmor® Corrosion Protection System • EVERTOUGH™ Construction • New PT2-1218 box with standard two fan mechanical provides redundancy and larger capacity

Figure 22: Three lines of cooling towers that use induced draft

Knowing that the cooling tower should have an axial fan, cross-flow configuration, and use forced draft; series 3000 was selected from the BAC line of towers. The series 3000 line was selected because of the large capacity some of the larger towers can handle. The recompression cycle, which has one of the largest heat load requirements of the three design points discussed in Chapter 1, needs 8.87 MW of cooling. For a cooling tower, a nominal ton is defined as:

$$1\ Nominal\ Ton = 15{,}000\,\frac{BTU}{hr} \qquad 3.9$$

The largest capacity in the 3000 series lines has the capacity of 1,350 nominal tons, which is 20,250,000 BTU/hr or 5.94 MW. This means that if all water cooling is done, two cooling towers will be required to handle the cooling load for a recompression design point. With this

in mind, model 31301C, which had the listed 1350 nominal ton capacity, was used to provide a performance relationship which can be used in the enthalpy-effectiveness method.

Knowing the model, the tower selection program provided the nominal fan motor power, nominal air flow rate, and required pumping head for the water, which are 100 HP, 302,580 CFM, and 9 psi, respectively. The nominal fan power and flow rate are based on standard conditions of 78 F wet bulb, 95/85 F inlet and outlet water temperatures, and 3 GPM/ton of cooling. It also provided the size, weight and approximate purchase price of one unit. Table 8 and Figure 23 summarize the dimensions and weights of the cooling tower. The unit purchase price of model 31301C is quoted at approximately $98,000 (Baltimore Aircoil Company, 2011).

Weights [lbs]			Dimensions			
Operating	Shipping	Heaviest Section	L	W	H	A
47,680	23,450	13,230	14’-0”	24’-1”	22’-9”	20’-10”

Table 8: Summary of weights and dimensions of model 31301C (refer to Figure 23)

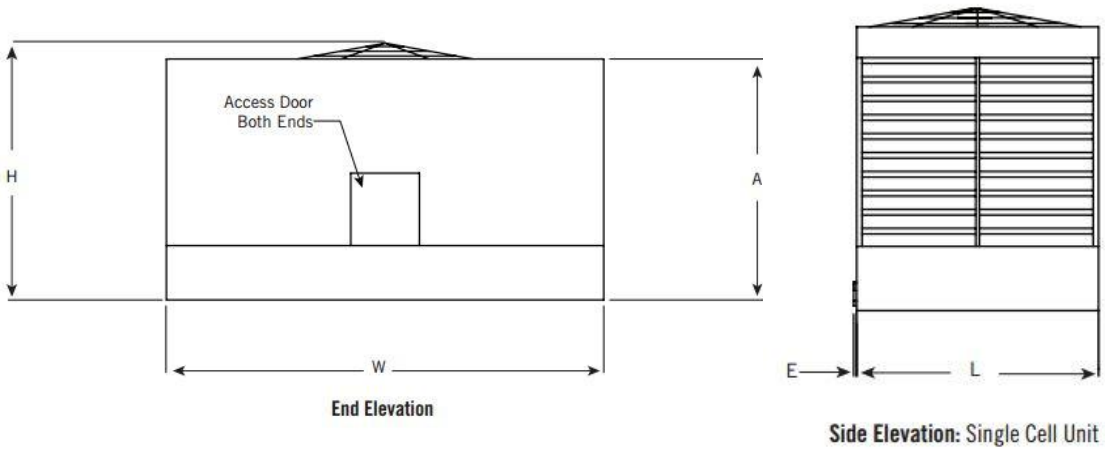

Figure 23: Schematic of cooling tower with labeled dimensions

The cooling tower selection program provides the rest of the required information to obtain a part load performance relationship. The program allows a user to specify design conditions for a specific model and, in turn, will produce the maximum capability of the tower. It also

gives the user the option to vary the fan speed by simulating a variable frequency drive (VFD) controller. A VFD controller allows for the control of motor speed and torque by varying the motor input frequency and voltage (Campbell, 1987). With the option of varying the fan speed, the tower's performance can be tested at multiple part-load situations. The first fan law states that the fan speed is proportional to the air flow rate (e.g., reducing the fan speed by 10% means the air flow rate is reduced by 10%) (U.S. EPA, 2010). Knowing the flow rate at 100% of the maximum fan speed, (i.e., 302,580 CFM) allows for calculation of part-load air flow rates by knowing the percentage of the max fan speed.

The model was tested at various wet bulb temperatures, inlet and outlet water temperatures, and fan speeds (i.e., air flow rate) with the cooling tower selection program. The program provided the maximum water flow rate the tower could handle at those specific operating conditions. These data points were then supplied to the enthalpy-effectiveness model to give makeup water, cooling tower effectiveness, and number of transfer units (NTU). The NTU value and air flow rate provide the calculation of the total conductance (UA) with the definition of UA:

$$UA_{CoolingTower} = NTU * \dot{C}_{air} \qquad 3.10$$

where $\dot{C}_{air}$ is the capacitance rate, defined as:

$$\dot{C}_{air} = c_{p,air} * \dot{m}_{air} \qquad 3.11$$

Mass flow rate and volumetric flow rate are related by the density of the air. Seeing this relationship, the UA value was plotted as a function of the air flow rate, shown in Figure 24.

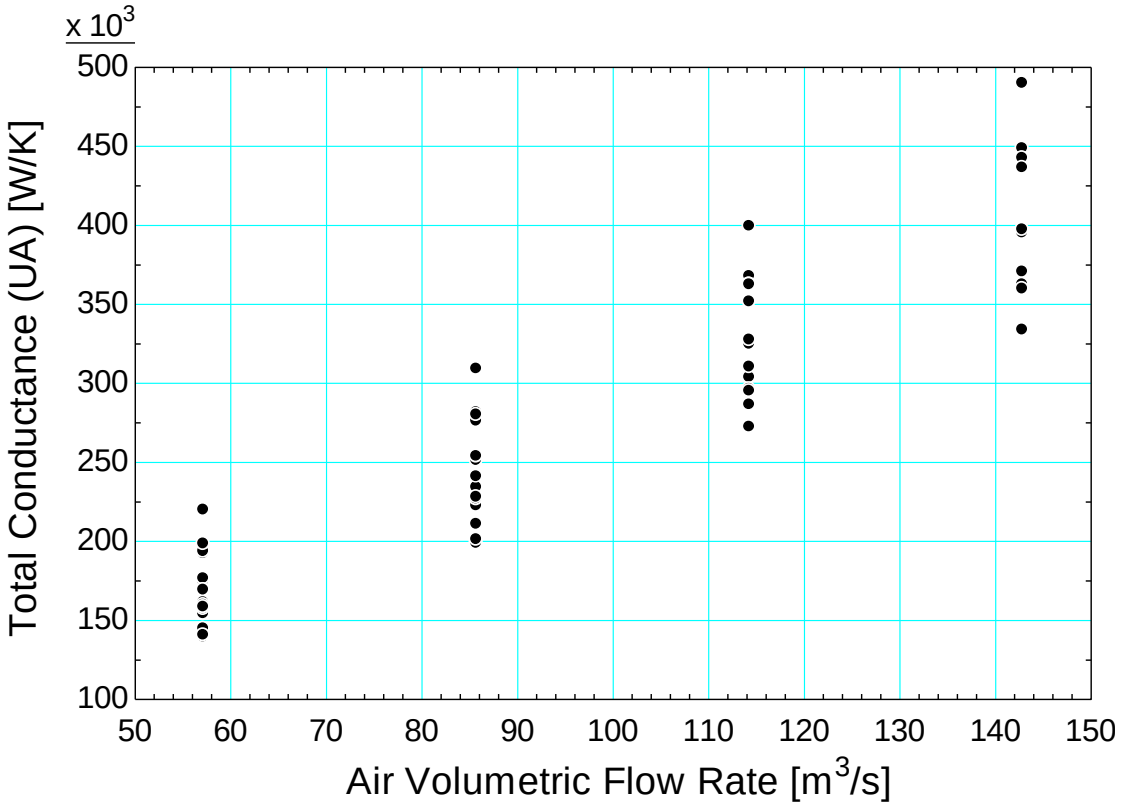

Figure 24: Total cooling tower conductance as a function of air volumetric flow rate

Figure 24 shows that the UA has a linear relationship to air flow, as it should, but is also a function of NTU which is dependent on water mass flow rate and inlet and outlet water temperatures. Multiple linear regressions were done with UA as the dependent variable and various independent variables. Air flow rate was the primary independent variable, but water flow rate and inlet and outlet water temperatures were also tested as independent variables. A linear relationship between UA and air flow rate was judged to be sufficient for this study. It was found that the other variables did not significantly improve the accuracy of predicting UA. Figure 25 shows the result of the linear regression with the relationship equation used to predict the UA value shown in equation 3.12.

$$UA = 13887.5\left[\frac{W}{K}\right] + 2733.28\left[\frac{W\ s}{K\ m^3}\right] * \dot{V}_{air} \qquad 3.12$$

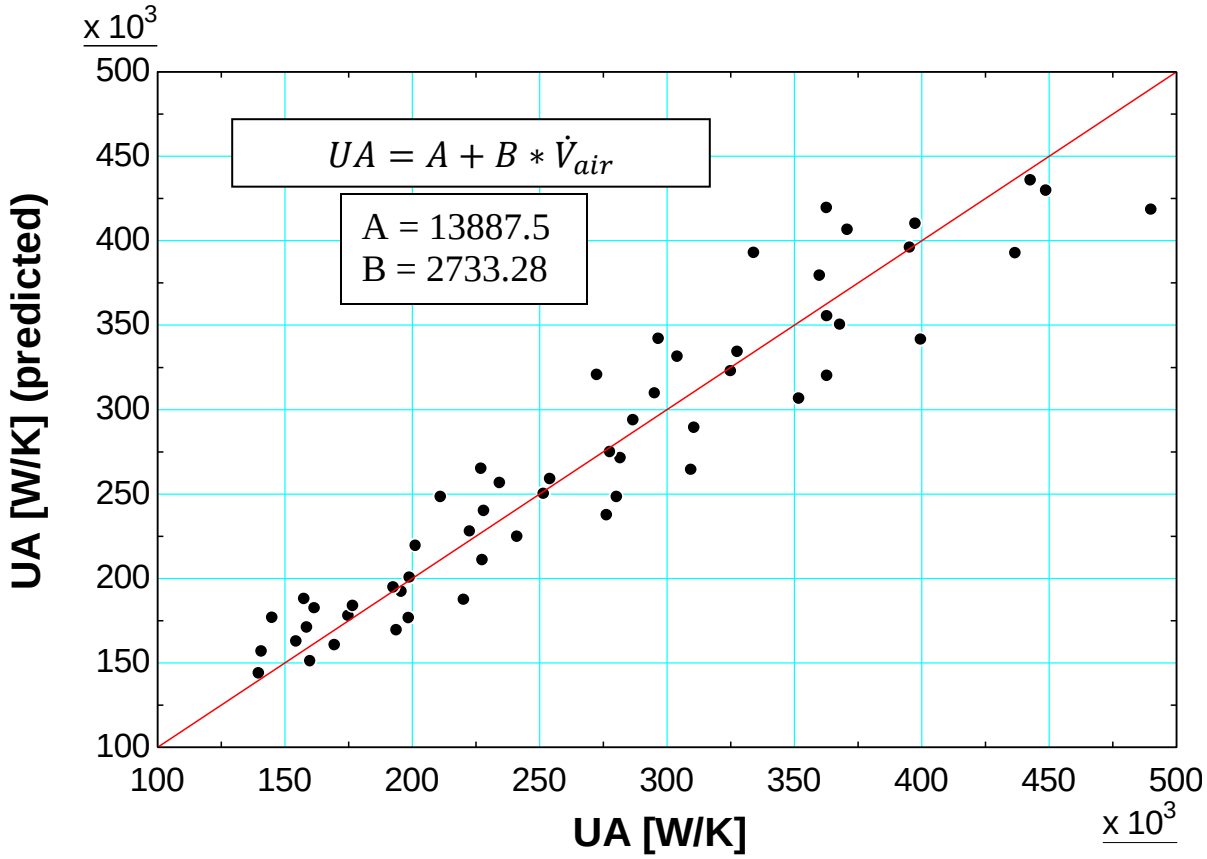

Figure 25: Predicted total conductance as a function of actual conductance

The model now predicts the performance of the specific model (i.e. 31301C) given various operating conditions. The last thing required for the model to output, that has not yet been implemented, is calculating the part load fan power required at specific operating conditions. Braun provides an equation for part load fan power as a function of the actual and nominal flow rates and nominal fan power (Braun, 1989):

$$\dot{P}_{fan} = \gamma^3 \dot{P}_{fan,nominal} \qquad 3.13$$

Where,

$$\gamma = \frac{\dot{V}_{air}}{\dot{V}_{air,nominal}} \qquad 3.14$$

As stated previously in this section, the nominal fan power and air flow rate for this model is 100 HP and 302,580 CFM, respectively.

3.2 Model verification

Verification was first conducted to confirm the enthalpy-effectiveness method was correctly predicting cooling tower performance. Braun provides two plots that show how the model should be performing given inputs of NTU, water to air mass flow rate ratios, wet bulb, dry bulb, and inlet water temperatures. The results of this verification are shown in Figure 26 and Figure 27 that show the air heat transfer effectiveness and water temperature effectiveness as a function of NTU at various mass flow rate ratios. Data points have been extrapolated from plots in Braun's thesis with the tower model overlaid on the extrapolated points. The plots verify that the tower performs exactly to Braun's model, as it should.

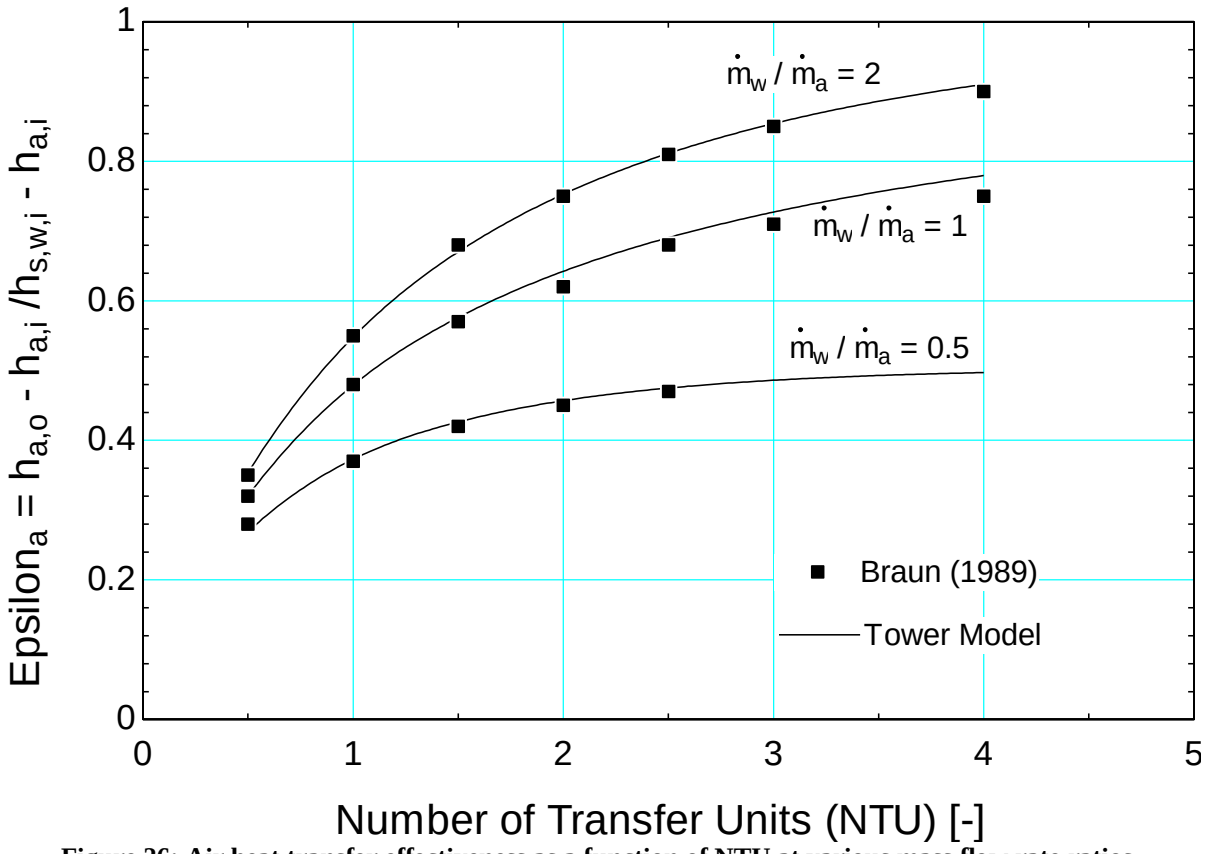

Figure 26: Air heat transfer effectiveness as a function of NTU at various mass flow rate ratios. Comparing results from developed cooling tower model to results from a thesis written by Braun (1989). (Dry Bulb, Wet Bulb, and Water Inlet Temperatures of 70 F, 60 F and 90 F)

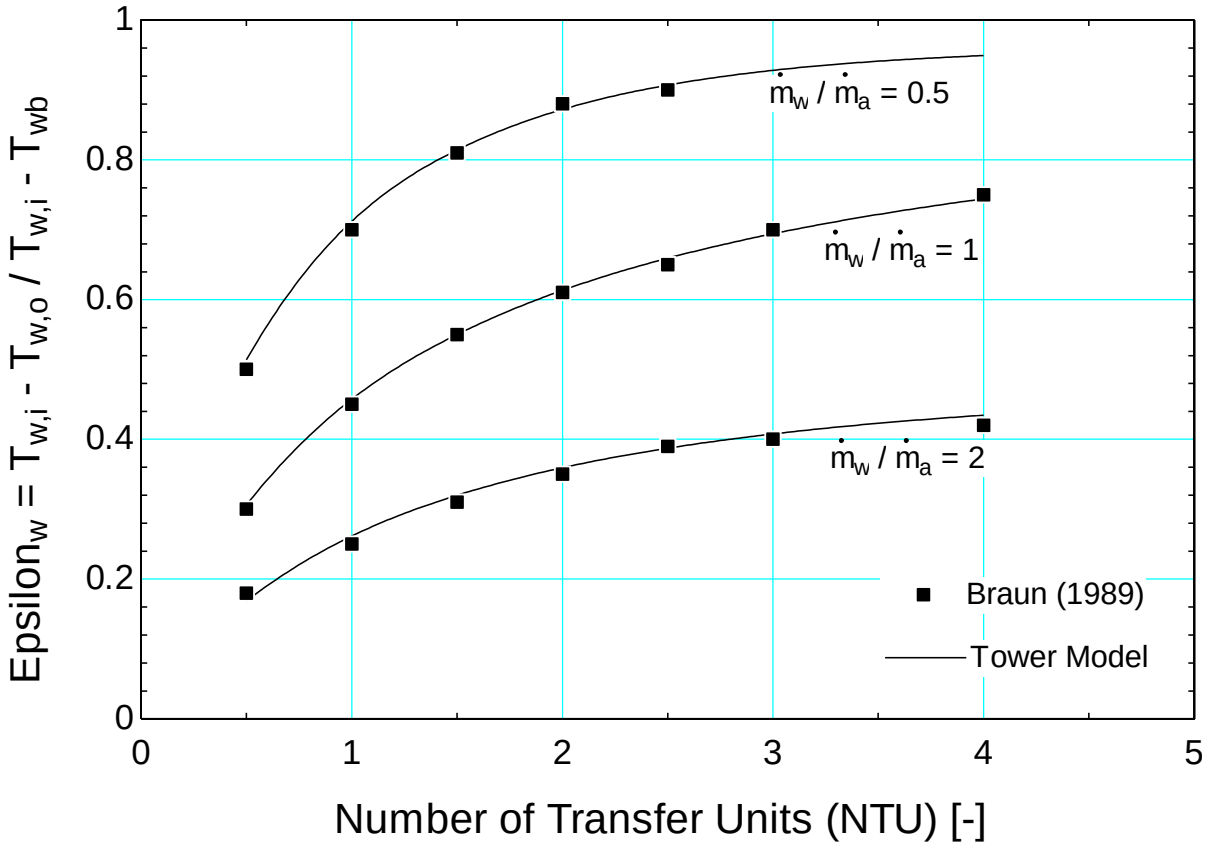

Figure 27: Water temperature effectiveness as a function of NTU at various mass flow rate ratios. Comparing results from developed cooling tower model to model results from a thesis written by Braun (1989). (Dry Bulb, Wet Bulb, and Water Inlet Temperatures of 70 F, 60 F and 90 F)

The final test is to verify that the predicted model performance is consistent with the actual performance provided by BAC.

Figure 28 shows outlet water temperature as a function of the wet bulb temperature at various fan powers, water flow rates, and water temperature ranges for both the tower model and BAC data. It shows that the model is very consistent with what BAC provides as the tower's performance.

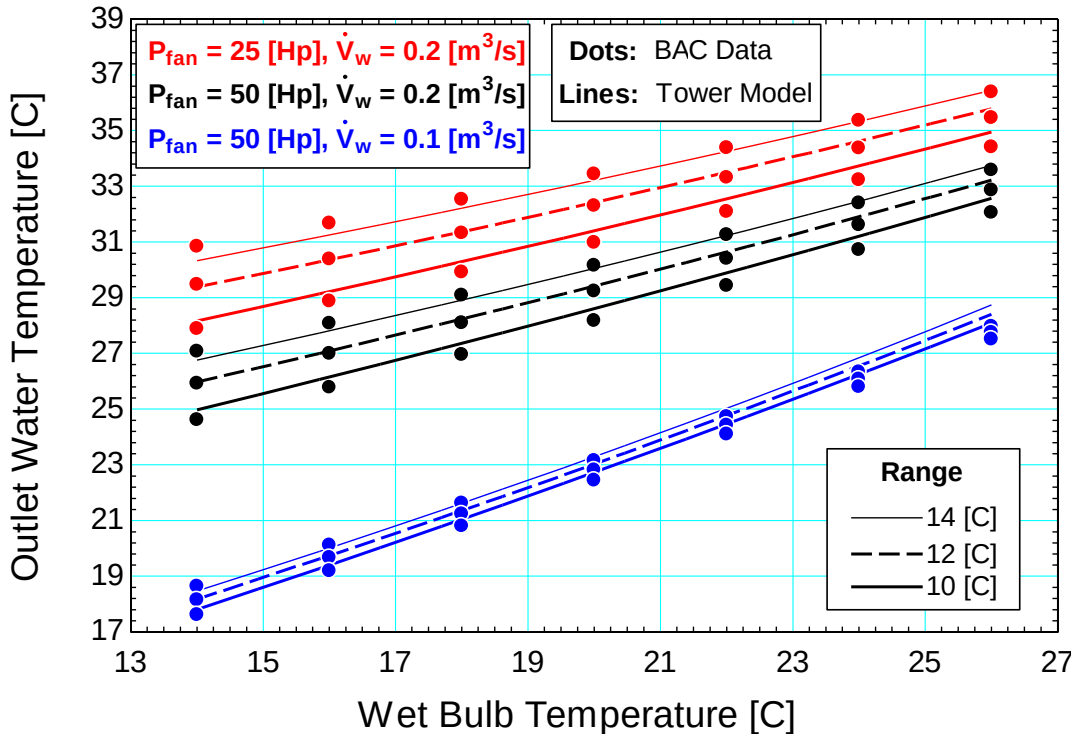

Figure 28: Outlet water temperature from cooling tower as a function of the wet bulb temperature for various fan power, water flow rates, and cooling tower range. Lines represent the model, Dots represent actual cooling tower performance data.

Figure 29 shows the fan power as a function of wet bulb temperature for two water temperature ranges. The model provides results that are consistent with the BAC performance data for that cooling tower.

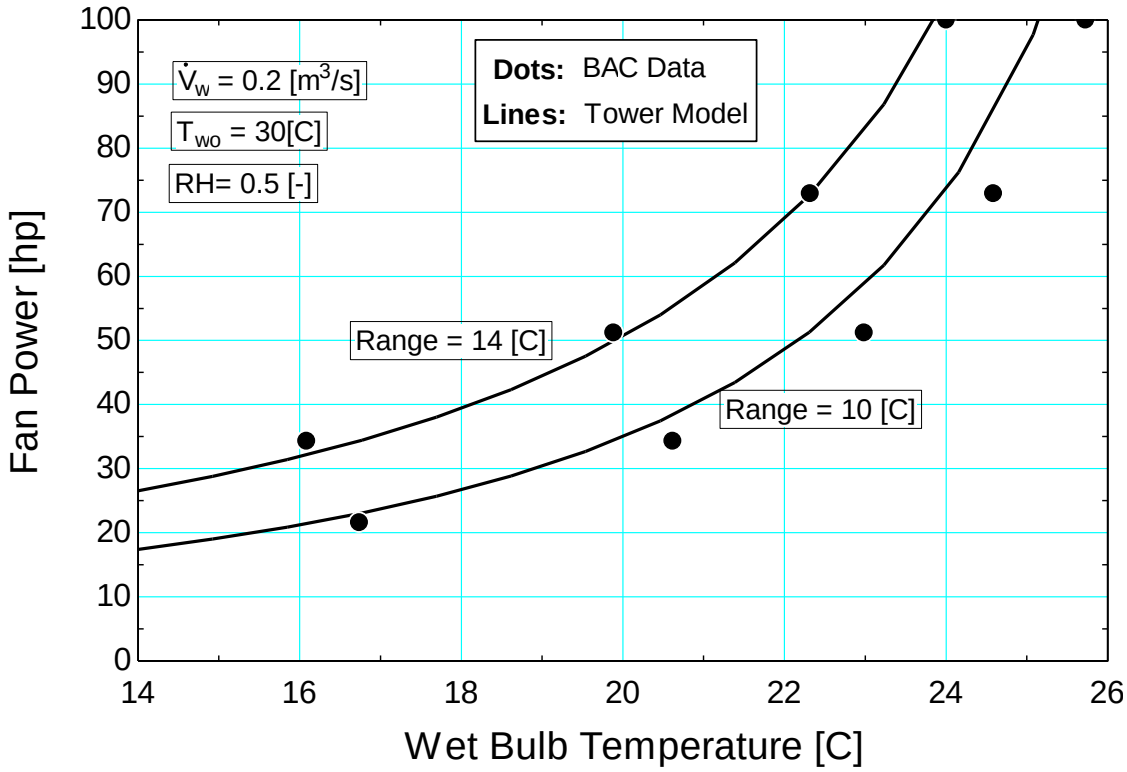

Figure 29: Cooling tower fan power as a function of wet bulb temperature for two different ranges. The lines are the model results and dots are actual cooling tower performance data.

The cooling tower model can now be confidently used for further analysis on the cooling process for supercritical carbon dioxide Brayton cycles.

4 INDIRECT AIR COOLER

The precooler is a counter-flow heat exchanger that can reject heat from the CO_2 cycle to a closed water loop. Heat from the water loop is rejected to the ambient air through a cross-flow heat exchanger. The schematic of this setup, including a possible set of inlet and outlet temperatures, is shown in Figure 30. The CO_2-to-water compact heat exchanger model was previously discussed in Chapter 2. Therefore, it was necessary to develop the cross-flow heat exchanger model and couple the two models using a closed water loop.

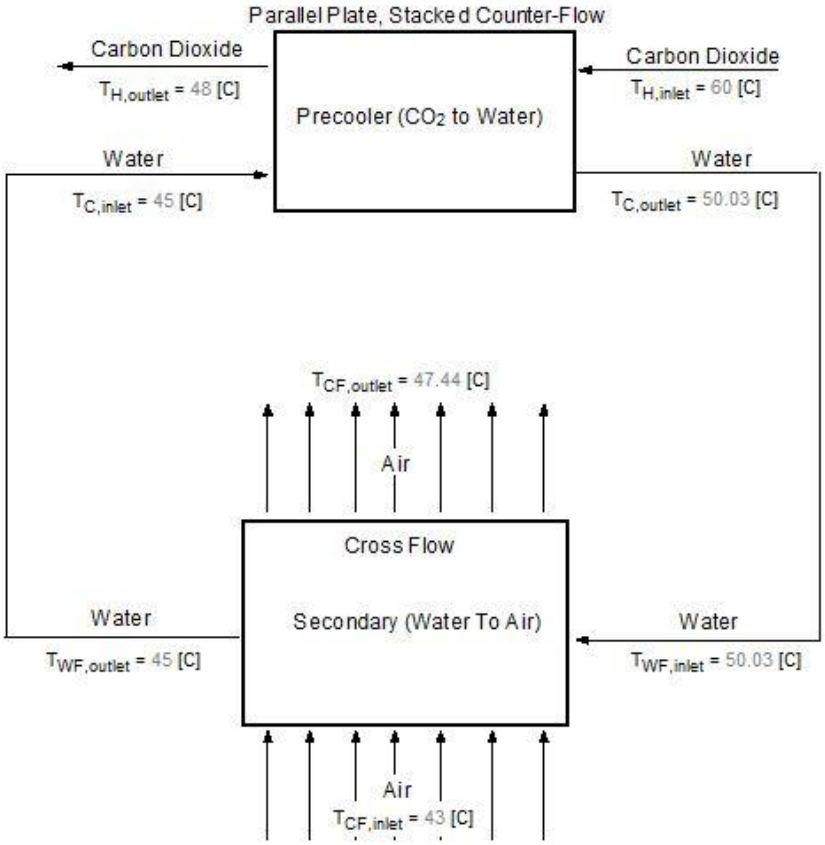

Figure 30: Precooler setup showing counter-flow and cross-flow heat exchangers

Due to the absence of major property variations within the heat exchanger, the water-to-air heat exchanger model is slightly less complicated than the precooler heat exchanger. The properties of water and air vary only slightly over the range of temperatures and pressures

being considered. Therefore, the *ε-NTU* method can be directly used to model the water-to-air cross-flow heat exchanger.

4.1 Model development

For cross-flow heat exchangers, the air-side resistance typically dominates the heat exchanger performance. For this reason, it is important to accurately calculate the overall heat transfer coefficient on the air-side. EES has an extensive library of compact cross-flow heat exchanger correlations that includes several heat exchanger configurations. The procedures in this library are based on the experimental data presented in Kays and London (Kays & London, 1984). Given the desired heat exchanger configuration, the procedures in EES will output all the geometric parameters needed for an analysis of the heat exchanger. The procedure will also predict the air-side pressure drop and heat transfer coefficient given the configuration, mass flow rate, frontal area, length (i.e., the distance in the air-flow direction), and bulk temperature and pressure. The water-to-air heat exchanger model uses this library to calculate the air-side pressure drop and heat transfer coefficient. The actual heat exchanger configuration may differ slightly from a pure cross-flow heat exchanger, but this approach is expected to provide a good representation of the expected performance.

4.1.1 Cross-flow configuration

There are several liquid-to-air cross-flow heat exchanger configurations built into the compact heat exchanger library. Figure 31 shows the different configurations that are considered in this model; all of the configurations are of the circular-finned tube type.

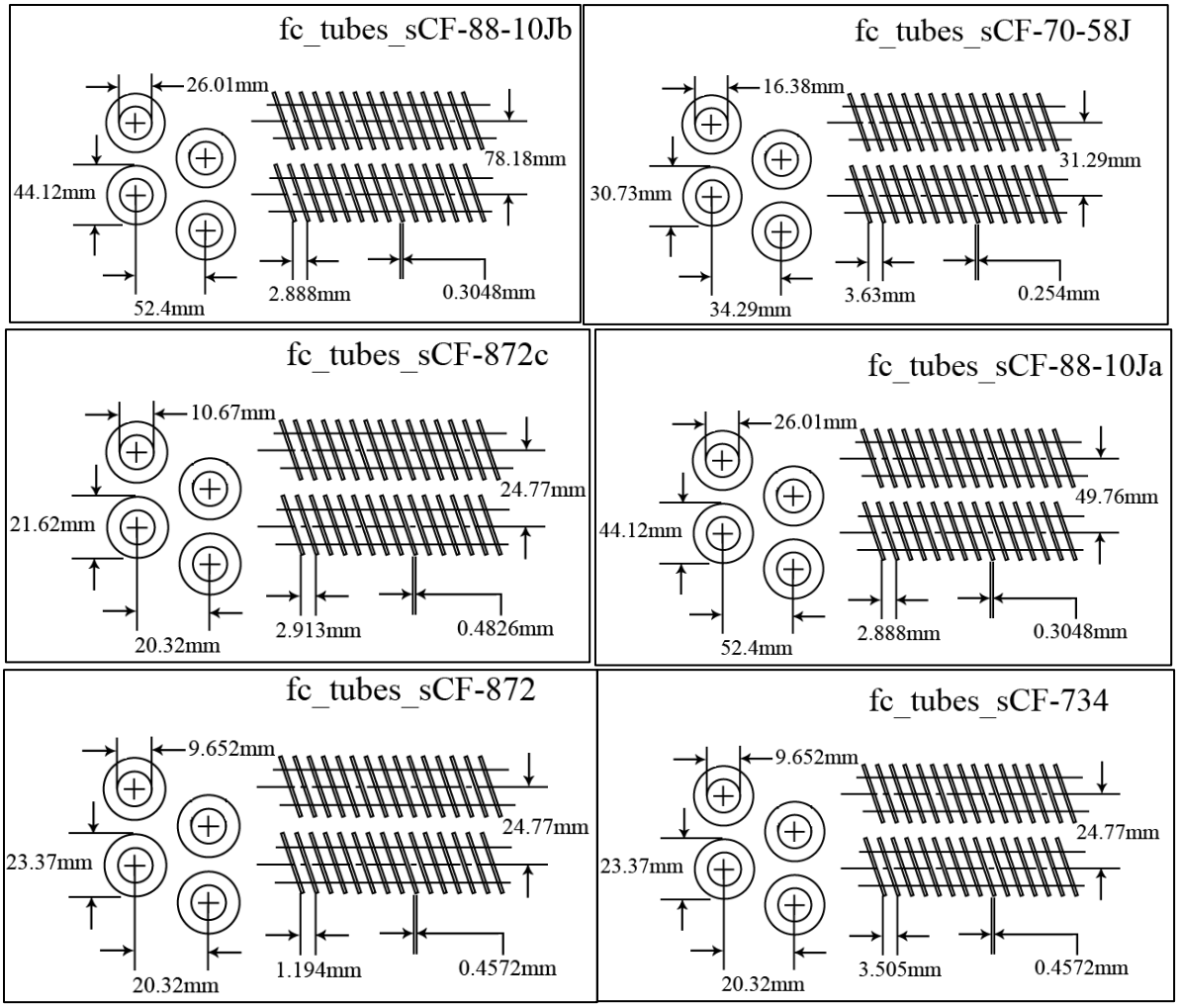

Figure 31: Six different compact cross-flow configurations

The modeling process starts by selecting one of the configurations shown in Figure 31. The geometric parameters associated with that specific heat exchanger core are obtained using the CHX_geom_finned_tube procedure.

```
Config$='fc_tubes_sCF-775-58T'                    "Compact HX configuration"
CoolingFluid$='Air_ha'                                "Cooling Fluid"
WorkingFluid$='Water'                                 "Working Fluid"
Metal_WA$='Stainless_AISI302'                         "Metal"
"Geometry"
Call CHX_geom_finned_tube(Config$: D_o, fin_pitch, D_h_CF, fin_thk, sigma, alpha, A_fin\A)
```

This procedure outputs the outer tube diameter (D_O), fin pitch, hydraulic diameter ($D_{h,CF}$), thickness of each fin (fin_{thk}), ratio of free-flow to frontal area (σ), ratio of gas-side heat

transfer area to core volume (i.e., Length*Width*Height) (α), and finally the ratio of finned to total surface area on the gas-side ($A_{fin}\backslash A$).

The inlet pressures and temperatures are known, as well as the water mass flow rate and heat transfer rate. The mass flow rate is the flow rate required by the primary precooler and the heat transfer rate will be the same as the primary precooler, which is set to 10 MW.

The operating conditions are set as follows:

```
"Conditions"
"!Pressure"
P_CF_in=1[atm]*convert(atm,Pa)                    "Air inlet pressure"
P_WF_in=2[atm]*convert(atm,Pa)                    "Water inlet pressure"
"!Temperature"
T_CF_in=converttemp(C,K,43[C])                    "Air inlet temperature"
T_WF_in=converttemp(C,K,53[C])                    "Water inlet temperature"

"!Mass flow rates"
m_dot_WF=590[kg/s]                                "Mass flow rate of water"
m_dot_CF=V_dot_CF*rho_CF                          "Mass flow rate of air"
"!Heat rate"
Q_dot_MW_WA=10[MW]                                "Heat rate"
```

All the properties are evaluated using average of the inlet and outlet bulk temperatures and pressures:

```
T_WF_b=(T_WF_in+T_WF_out)/2                       "Water bulk temperature"
T_CF_b=(T_CF_in+T_CF_out)/2                       "Air bulk temperature"
P_WF_b=(P_WF_in+P_WF_out)/2                       "Water pressure"
P_CF_b=(P_CF_in+P_CF_out)/2                       "Air pressure"

"Air"
rho_CF=Density(CoolingFluid$,T=T_CF_b,P=P_CF_b)   "Density, Air-side"
Pr_CF=Prandtl(CoolingFluid$,T=T_CF_b,P=P_CF_b)    "Prandtl number, Air-side"
cp_CF=Cp(CoolingFluid$,T=T_CF_b,P=P_CF_b)         "Specific Heat, Air-side"
mu_CF=Viscosity(CoolingFluid$,T=T_CF_b,P=P_CF_b)  "Viscosity, Air-side"
k_CF=Conductivity(CoolingFluid$,T=T_CF_b,P=P_CF_b) "Conductivity, Air-side"
"Water"
cp_WF=Cp(WorkingFluid$,T=T_WF_b,P=P_WF_b)         "Specific Heat, Water-side"
mu_WF=Viscosity(WorkingFluid$,T=T_WF_b,P=P_WF_b)  "Viscosity, Water-side"
k_WF=Conductivity(WorkingFluid$,T=T_WF_b,P=P_WF_b) "Conductivity, Water-side"
rho_WF=Density(WorkingFluid$,T=T_WF_b,P=P_WF_b)   "Density, Water-side"
Pr_WF=Prandtl(WorkingFluid$,T=T_WF_b,P=P_WF_b)    "Prandtl number, Water-side"
```

The model has the capability to evaluate the properties using known inlet temperatures and pressures, instead of the average inlet and outlet temperature and pressures (which are

calculated through the model) in order to aid in convergence. This capability provides guess values for all variables in the problem and enhances convergence when properties are evaluated at the mean temperature.

4.1.2 ε-NTU method for uniform properties

The *ε-NTU* method is implemented with equations 4.1 to 4.6:

$$\dot{C}_{CF} = \dot{m}_{Cf} cp_{CF} \quad 4.1$$

$$\dot{C}_{WF} = \dot{m}_{Wf} cp_{WF} \quad 4.2$$

$$\dot{C}_{min} = MIN(\dot{C}_{CF}, \dot{C}_{WF}) \quad 4.3$$

$$\dot{Q}_{max} = \dot{C}_{min}(T_{WF,in} - T_{CF,in}) \quad 4.4$$

$$\varepsilon = \dot{Q}/\dot{Q}_{max} \quad 4.5$$

The number of transfer units is found as the ratio of the conductance to the minimum capacitance rate.

$$NTU = UA/\dot{C}_{min} \quad 4.6$$

Energy balances on the air and water-sides, determine the outlet temperatures of the water-to-air heat exchanger.

$$\dot{C}_{CF}T_{CF,in} + \dot{Q} = \dot{C}_{CF}T_{CF,out} \quad 4.7$$

$$\dot{C}_{WF}T_{WF,in} = \dot{Q} + \dot{C}_{WF}T_{WF,out} \quad 4.8$$

```
"Effectiveness-NTU method"
C_dot_CF=m_dot_CF*cp_CF                                  "Capacitance rate air-side"
C_dot_WF=m_dot_WF*cp_WF                                  "Capacitance rate water-side"
C_dot_min=MIN(C_dot_CF,C_dot_WF)                         "Minimum capacitance rate"
NTU=UA/C_dot_min                                         "Finding overall conductance"

"Effectiveness for an unmixed cross flow heat exchanger"
epsilon=HX('crossflow_both_unmixed', NTU, C_dot_CF, C_dot_WF, 'epsilon')

q_dot_max=C_dot_min*(T_WF_in-T_CF_in)                    "Max heat rate"
```

```
Epsilon=q_dot/q_dot_max                                   "Heat rate"
C_dot_CF*T_CF_in+q_dot=C_dot_CF*T_CF_out                  "Energy balance on air-side"
C_dot_WF*T_WF_out+q_dot=C_dot_WF*T_WF_in                  "Energy balance on water-side"
```

Instead of specifying a volumetric flow rate of the air, the maximum amount of fan power that is allowed is specified and used to solve for the volumetric air flow rate. This was done because it was felt that a reasonable value for maximum fan power (i.e., some acceptable fraction of the plant output power) is easier to estimate than a reasonable amount of volumetric air flow.

$$\dot{W}_{fan} = \frac{\Delta P_{CF} \dot{V}_{CF}}{\eta_{fan}} \qquad 4.9$$

```
eta_fan=0.5[-]                                            "Fan efficiency"
W_dot_fan=((DELTAP_CF*V_dot_CF)/eta_fan)*convert(W,MW)    "Fan power"
W_dot_fan=1[MW]                                           "Setting fan power"
```

The pressure drop on the air side is found using the compact heat exchanger library pressure drop procedure:

```
A_fr=W*H                                                  "HX frontal area"
"Pressure drop"
Call CHX_DELTAp_finned_tube(Config$, m_dot_CF, A_fr,L,CoolingFluid$, T_CF_in, T_CF_out,
P_CF_in: DELTAP_CF)
```

Since the goal of this model is to determine the heat exchanger geometric parameters, the pressure drop is specified as a design parameter in place of specifying the length of the heat exchanger. The length required to achieve the specified pressure drop is calculated.

```
"Determine overall length"
DELTAP_CF=160[Pa]
```

The width and height of the heat exchanger are set equal, making the frontal area square. The width is therefore the only remaining, unspecified geometric parameter. To determine the width, a resistance network analysis is used to find the overall conductance (UA) as shown in Figure 32.

Figure 32: Resistance network for cross-flow heat exchanger

The air-side heat transfer coefficient is calculated using the heat transfer coefficient procedure in the compact heat exchanger library:

```
"Air side heat transfer coefficient"
Call CHX_h_finned_tube(Config$, m_dot_CF, A_fr, CoolingFluid$,(T_CF_in+T_CF_out)/2,
P_CF_in:h_CF)
```

The total outside surface area, fin efficiency, and overall surface efficiency are required for the air-side resistance.

The total air-side surface area is found by multiplying α (ratio of total air-side surface area to core volume) by the overall volume of the heat exchanger.

```
A_s_out_tot=alpha*(L*W*H)                                    "Total outside surface area"
```

The fin efficiency is found using the EES fin efficiency procedure in terms of the fin thickness, outer tube diameter, diameter of the fin, air-side heat transfer coefficient, and thermal conductivity of the metal.

```
eta_fin=eta_fin_annular_rect(th_fin, D_out/2, D_fin/2, h_CF, k_m_tube)      "Fin efficiency"
```

The overall surface efficiency is found according to Nellis and Klein (Nellis & Klein, 2009), which uses the ratio of fin area to total area and fin efficiency. The fin area to total area is one of the geometric parameters returned by the compact heat exchanger library call for the specified heat exchanger.

$$\eta_o = 1 - \left(\frac{A_{fin}}{A_{tot}}\left(1 - \eta_{fin}\right)\right) \qquad 4.10$$

```
eta_o=1-(A_fin\A*(1-eta_fin))                                "Overall surface efficiency"
```

Finally, the outer surface resistance is found using the heat transfer coefficient, overall surface efficiency, and total air-side surface area.

$$R_{out} = \frac{1}{\eta_o h_{CF} A_{s,tot}} \quad 4.11$$

```
R_out=1/(eta_o*h_CF*A_s_out_tot)                    "Outer surface resistance"
```

To determine the water-side resistance, the tube wall thickness needs to be specified to find the inner diameter. Currently, the tube wall thickness is set to a reasonable value; this value is better defined in Chapter 6, when the hybrid configuration is analyzed.

```
th_tube=1[mm]*convert(mm,m)                         "Tube thickness"
D_in=D_out-2*th_tube                                "Inner diameter of tube"
```

The water-side flow was constrained by setting a possible range of fluid velocities. Typically when water-side velocities are too low (e.g., 1 ft/s), the heat exchanger is susceptible to deposition fouling and when velocities are too high (e.g., 15 ft/s), the heat exchanger tubes are susceptible to erosion. Presently, the fluid velocity is fixed to 10 ft/s to allow for easy calculation of Reynolds number and mass flow rate through each tube. With Reynolds number specified, the heat transfer coefficient and pressure drop can be found using standard heat transfer and pressure drop correlations for flow in a tube.

$$Re_{WF} = \frac{\rho_{WF} U_{WF} D_{in}}{\mu_{WF}} \quad 4.12$$

$$A_c = \left(\frac{PI}{4}\right) D_{in}^4 \quad 4.13$$

$$\dot{V}_{WF} = U_{WF} A_c \quad 4.14$$

$$\dot{m}_{tube} = \dot{V}_{WF} \rho_{WF} \quad 4.15$$

```
Re_WF=rho_WF*U_WF*D_in/mu_WF                        "Reynolds number"
A_c=(PI/4)*D_in^2                                   "Cross sectional area of tube"
V_dot_WF=U_WF*A_c                                   "Volumetric flow rate through each tube"
m_dot_tube=V_dot_C*rho_WF                           "Mass flow rate through each tube"
```

The PipeFlow_N procedure in EES calculates the Nusselt number and friction factor, given Reynolds number and Prandtl number:

```
"Pipe flow correlation"
call PipeFlow_N(Re_WF,Pr_WF,9999,0: Nusselt_T_WF,Nusselt_H_WF,f_WF)
```

The heat transfer coefficient and pressure drop are then calculated using the following equations:

$$Nusselt_{WF} = \frac{h_{WF} D_{in}}{k_{WF}} \quad 4.16$$

$$f_{WF} = \frac{2\Delta P_{WF} D_{in}}{W \rho_{WF} U_{WF}^2} \quad 4.17$$

```
Nusselt_T_WF=(h_WF*D_in)/k_WF                    "Heat transfer coefficient"
f_WF=(2*DELTAP_WF*D_in)/(L_WF_tube*rho_WF*U_WF^2)    "Pressure drop"
```

The water-side resistance is found using:

$$R_{in} = \frac{1}{h_{WF} \pi D_{in} N_{tubes} W} \quad 4.18$$

The area in the denominator of Equation 4.18 is the total inner surface area of the tubes. The number of tubes is found using the height and length of the heat exchanger, as well as vertical (S_v) and horizontal (S_h) distances between each tube, which are known from the geometry procedure.

$$N_{col} = L/s_h \quad 4.19$$

$$N_{row} = H/s_v \quad 4.20$$

$$N_{tubes} = N_{row} N_{col} \quad 4.21$$

```
R_in=1/(h_WF*PI*D_in*N_tubes*W)    "Water-side convection resistance"
```

The fouling resistance is calculated by finding the fouling factor, which is found using the FoulingFactor procedure in EES using ‘Closed-loop treated water’.

```
R``_f_in=FoulingFactor('Closed-loop treated water')    "Fouling factor on inner surface of tube"
```

The fouling resistance is calculated using the following equation:

$$R_{f,in} = \frac{R''_{f,in}}{\pi D_{in} N_{tubes} W} \quad 4.22$$

```
R_f_in=R``_f_in/(PI*D_in*N_tubes*W)          "Fouling resistance on inner surface of tube"
```

Finally, the conduction resistance through the tube wall is found using the cylinder conduction resistance definition (Nellis and Klein, 2009):

$$R_{cond} = \frac{\ln\left(\frac{D_{out}}{D_{in}}\right)}{2k_{m,tube}\pi N_{tubes} W} \quad 4.23$$

```
k_m_tube=k_(Metal_WA$,(T_CF_in+T_WF_in)/2)          "Thermal conductivity of the metal"
R_cond=ln(D_out/D_in)/(2*k_m_tube*PI*N_total*W)     "Conduction resistance"
```

The total resistance is the sum of the four resistances, which is the inverse of the total conductance.

$$R_{tot} = R_{out} + R_{in} + R_{f,in} + R_{cond} \quad 4.24$$

$$UA = \frac{1}{R_{tot}} \quad 4.25$$

```
R_tot=R_out+R_in+R_f_in+R_cond          "Total resistance"
UA=1/R_tot                              "Total conductance"
```

By setting the UA calculated using the ε-*NTU* method equal to the UA calculated using the resistance network, the final geometric parameter, width and height, can be determined.

4.2 Coupling the CO_2-to-water (counter-flow) and water-to-air (cross-flow)

The next step is to couple the CO_2-to-water and water-to-air heat exchanger models so that it is not necessary to input the two water inlet temperatures for each heat exchanger. The two codes were combined into one EES file. Once they were in the same model, they needed to be coupled by eliminating the inlet water temperature specifications. These inputs were replaced with the following equations:

$$T_{C,in} = T_{WF,out} \quad 4.26$$

$$T_{C,out} = T_{WF,in} \quad 4.27$$

where $T_{C,in}$ and $T_{C,out}$ are the water temperatures entering and exiting the CO_2 to water heat exchanger, respectively, and $T_{WF,in}$ and $T_{WF,out}$ are the water temperatures entering and exiting the water to air heat exchanger, respectively. Equations 4.26 and 4.27 reflect the fact that the heat exchangers are connected by a closed water loop where the pipe heat losses can be assumed to be negligible. See the schematic in Figure 30 for reference.

4.3 Graphical user interface (GUI)

A GUI has been developed that incorporates inputs and outputs for both heat exchangers. This interface allows for a user to easily and intuitively run the program for multiple configurations, conditions, and material selection. The parameters with boxes around the numbers represent inputs to the model, while texts with no boxes represent outputs. These inputs and outputs can be easily interchanged and solved simultaneously. Figure 33 shows the parent window where all the outputs and overall precooler schematic is shown. Clicking on the drawings for the primary and secondary heat exchanger brings up child windows where inputs, conditions, and configurations can be set for each heat exchanger. See Figure 34 and Figure 35.

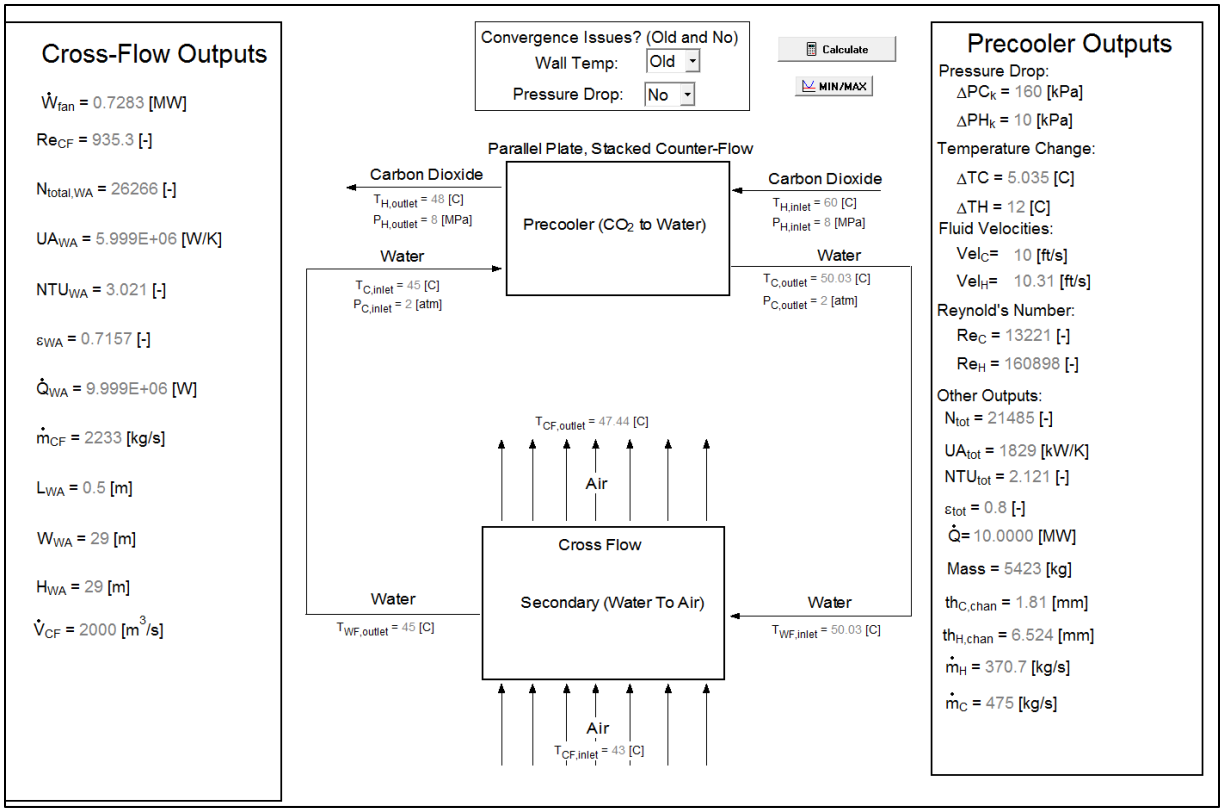

Figure 33: Parent window showing the overall schematic of the precooler

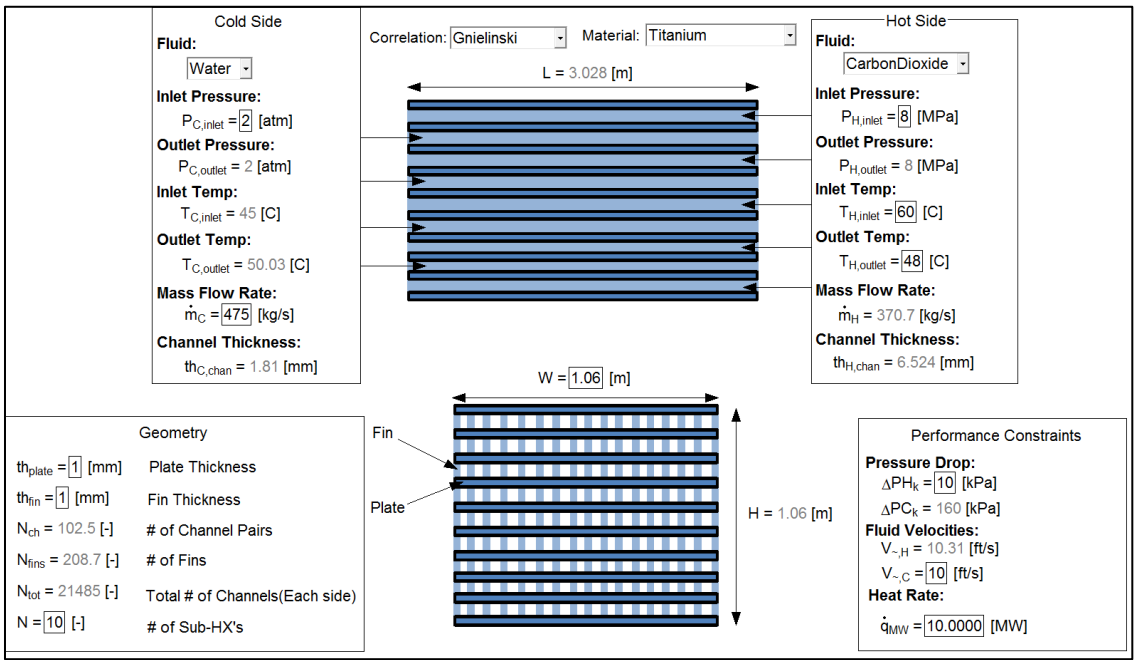

Figure 34: Child window showing the primary precooler (CO2 to water). Opened by clicking the precooler drawing.

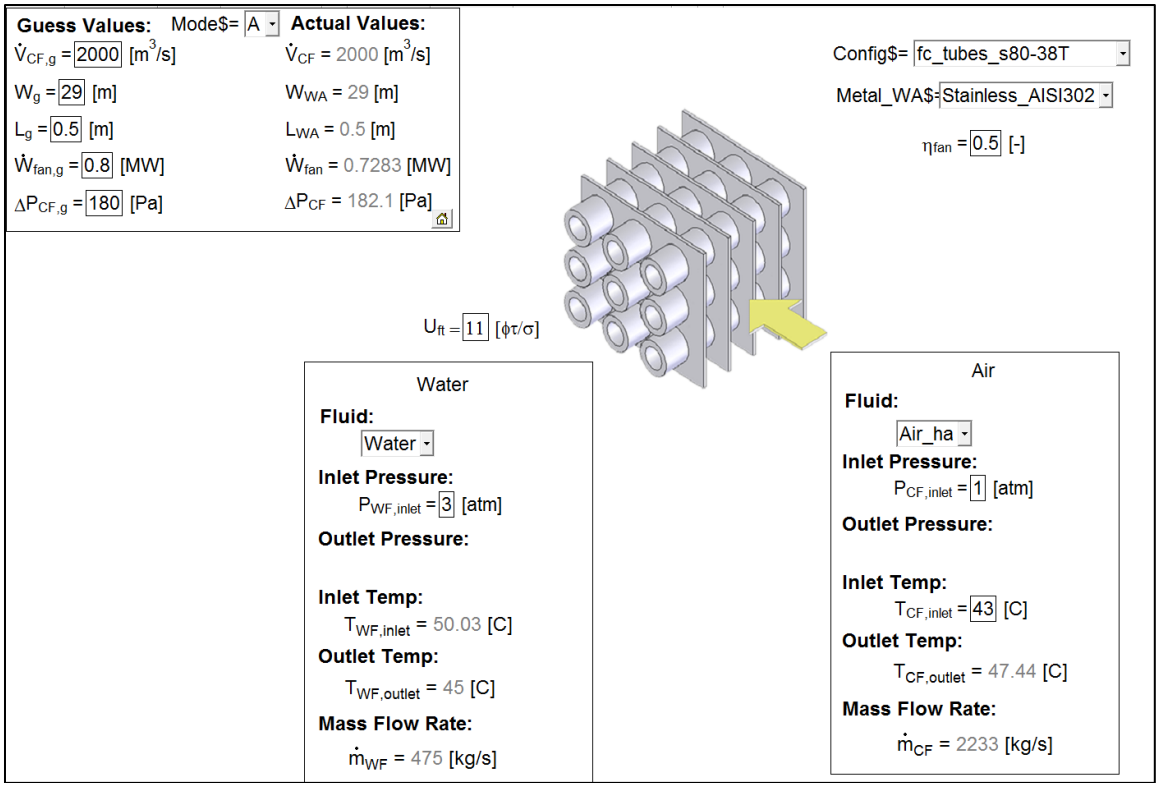

Figure 35: Child window showing the secondary precooler (air to water). Opened by clicking the cross-flow drawing.

4.4 Performance plots

The precooler model that has been developed is a counter-flow heat exchanger that rejects heat from the S-CO_2 cycle to a closed water loop. Heat from the water loop is then rejected to the ambient air through a cross-flow heat exchanger. A schematic of this setup, including a possible set of conditions, is shown in Figure 36.

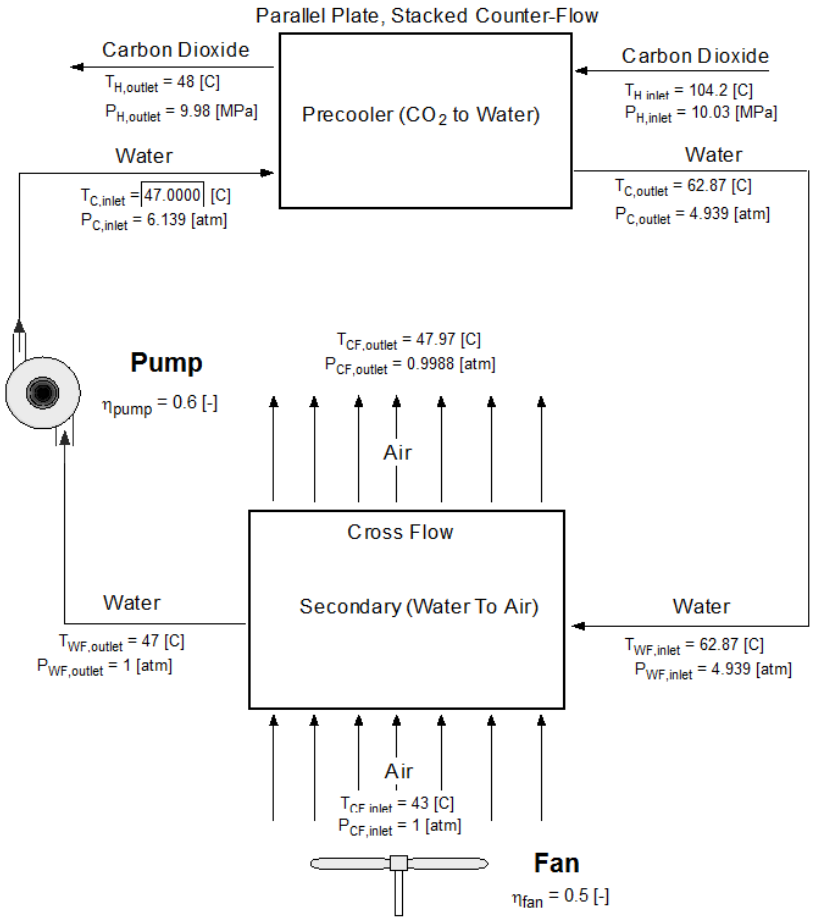

Figure 36: Precooler setup showing counter-flow and cross-flow heat exchangers

Table 9 and Table 10 summarize the inputs, parameters and performance constraints for both the counter-flow (CO_2-water) and cross-flow (water-air) heat exchangers, respectively.

Inputs	Parameters	Performance Constraints
Cold Fluid: Water	**Water Channel Height** = 3 [mm]	**Water Velocity** = 6 [ft/s]
Hot Fluid: Carbon Dioxide	**CO_2 Channel Height** = 3 [mm]	**Pressure Drop Ratio:** 0.1% to 20%
Water Inlet Temperature: 43°C to 48°C	**Plate Thickness** = 1 [mm]	**Heat Input Rate:** Varied per design point
CO_2 Inlet Temperature: Varied per design point	**Fin Thickness** = 1 [mm]	
CO_2 Outlet Temperature = 48°C	**# of Sub HX's** = 20 [-]	
CO_2 Outlet Pressure: Varied per design point		

Table 9: Inputs, Parameters, and Performance Constraints for the counter-flow heat exchanger

Inputs	Parameters	Performance Constraints
Cold Fluid: Air	**Pipe Wall Thickness** = 1[mm]	**Water Velocity** = 6 [ft/s]
Hot Fluid: Water	**Configuration:** CF-872c	**Air Side Pressure Drop** = 160 [Pa]
Air Inlet Pressure = 1 [atm]		**Fan Power:** Varied
Air Inlet Temperature = 43°C		
Water Outlet Pressure = 1 [atm]		

Table 10: Inputs, Parameters, and Performance Constraints for the cross-flow heat exchanger

Fixing the variables identified in Table 9 and Table 10 allows the calculation of the overall dimensions and mass of each heat exchanger as well as the required auxiliary power input to the precooler.

The five variables that will be considered in detail include the pressure drop ratio for the CO_2 (defined in Equation 4.28), water velocity, water temperature entering the counter-flow or exiting the cross-flow heat exchanger, the pressure drop on the air-side, and the fan power (defined in Equation 4.29).

The *pressure drop ratio* is defined as:

$$PressureDropRatio = \frac{Pressure\ Drop}{Inlet\ Pressure} * 100\% \qquad 4.28$$

The pressure drop ratio is varied from 0.1% to 20% to assess its impact on the major outputs of the model. This is an important constraint for the CO_2 side as it affects the compressor power and thus the overall cycle efficiency.

The water temperature entering the counter-flow or exiting the cross-flow heat exchanger (assuming negligible thermal losses in the connecting piping) is an input that was required to complete the energy balances performed on both heat exchangers. Looking at the schematic in Figure 36, this temperature was selected because of the limited range of temperatures that are physically possible. The lower bound is found by considering the performance of the cross-flow heat exchanger. A perfect cross-flow heat exchanger would cool the water to the ambient dry bulb temperature, 43ºC. The upper limit on the water temperature is found by looking at the performance of the counter-flow heat exchanger.

Since the outlet CO_2 temperature is set at 48ºC, the highest possible cooling water temperature entering the counter-flow heat exchanger, assuming a perfect heat exchanger, is 48ºC. Therefore, the temperature is now bounded between 43ºC and 48ºC. A parametric study in this section will show how the optimal value of this temperature was selected.

The last two variables used to constrain the cross-flow heat exchanger are the fan power and air-side pressure drop across the cross-flow heat exchanger. Fan power is computed according to:

$$Fan\ Power = \dot{W}_{fan} = \frac{\Delta P_{air}\dot{V}_{air}}{\eta_{fan}} \qquad 4.29$$

By setting the fan power and air-side pressure drop, the air-side volumetric flow rate and mass flow rate can be found. This information completes the energy balances on the cross-flow heat exchanger. The results that follow use an assumed value of 160 Pa for the air-side pressure drop, which is a typical value for air-side pressure drop (GEA Heat Exchangers, 2011).

Figure 31 shows six compact heat exchanger designs using circular finned tubes that are being considered for the water-to-air heat exchanger. The heat exchangers are identified by a name at the upper right corner of each figure.

The model requires the specification of the Brayton cycle design point, which establishes the CO_2 operating conditions for the heat exchanger. The CO_2 operating conditions for each design point are summarized in Table 1 from Chapter 1.

The model was run for each of the different configurations, holding fan power constant at 0.5 MW, the pressure drop ratio at 0.5%, and the inlet water temperature at 47ºC for each of the three conditions, while letting pump power vary. Figure 37 through Figure 39 show the key results for the cross-flow heat exchanger using each of the core configurations.

Recompression:

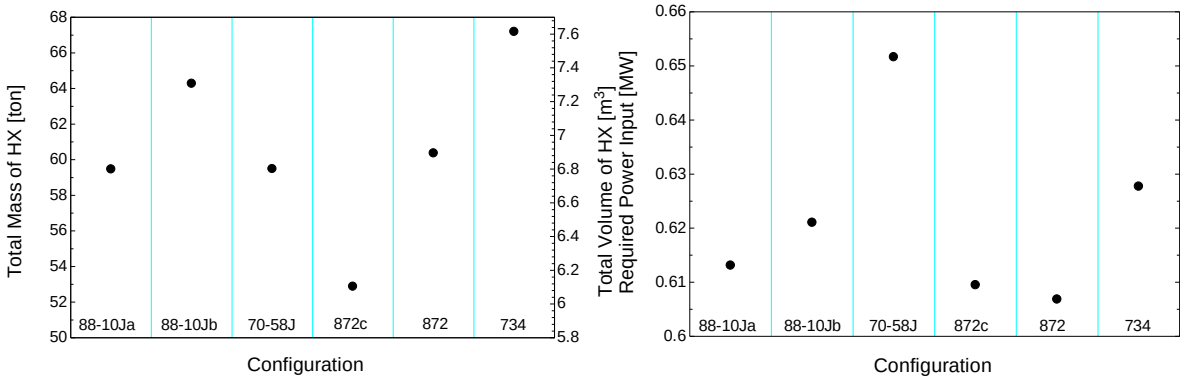

Figure 37: Total mass/volume and required power input as a function of cross-flow HX configuration for the recompression cycle

Simple, High Efficiency:

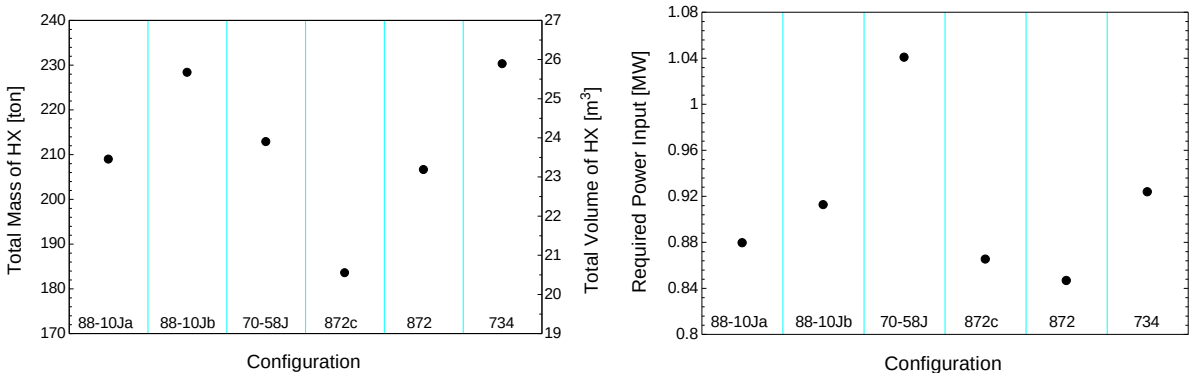

Figure 38: Total mass/volume and required power input as a function of cross-flow HX configuration for the simple, high efficiency cycle

Simple, Low Efficiency:

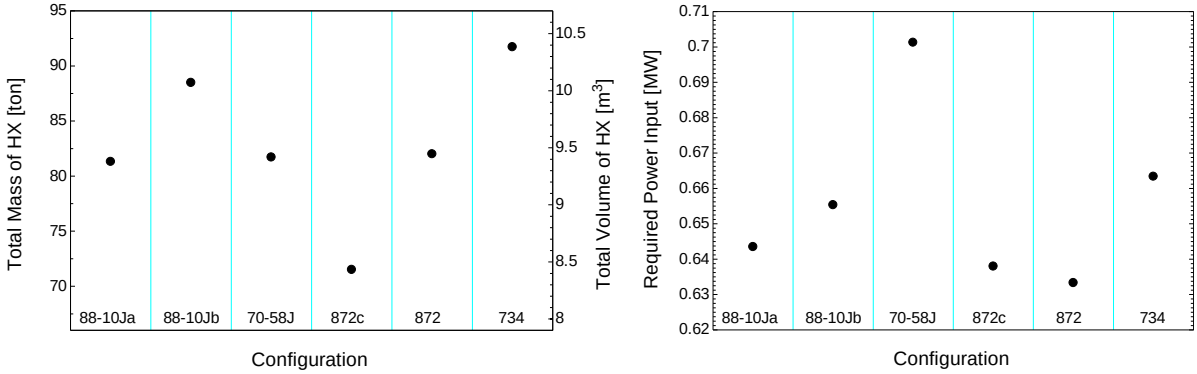

Figure 39: Total mass/volume and required power input as a function of cross-flow HX configuration for the simple, low efficiency cycle

For all three conditions, the core configuration labeled CF-872c provided the lowest mass and 2nd to lowest auxiliary power input. Looking at the schematics of each of the six configurations, in Figure 31, gives some insight into why this core geometry provided the best results. For the mass, CF-872c has the smallest fin diameter, while also being more compact compared to the other configurations, meaning a higher air-side surface area to core volume. This provides less material and a higher air-side heat transfer rate. The auxiliary power input is smaller than most of the other configurations due to the fact that it has a comparatively small tube diameter. Smaller tube diameters lead to higher heat transfer coefficients on CO_2 side but not necessarily on the air-side. This causes the pressure drop across the width of the heat exchanger to be significantly reduced, which leads to less pump

work. The cross-flow configuration CF-872c is used throughout the rest of the analysis in this section.

The water temperature entering the counter-flow or exiting the cross-flow heat exchangers is bounded between 43ºC and 48ºC and was varied to find an optimum value. The results of this parametric study are shown below in Figure 40 through Figure 42. The plots represent the total mass/volume of both heat exchangers (left) and the mass of each heat exchanger (right), both in I.P. short ton, as a function of the temperature.

Recompression:

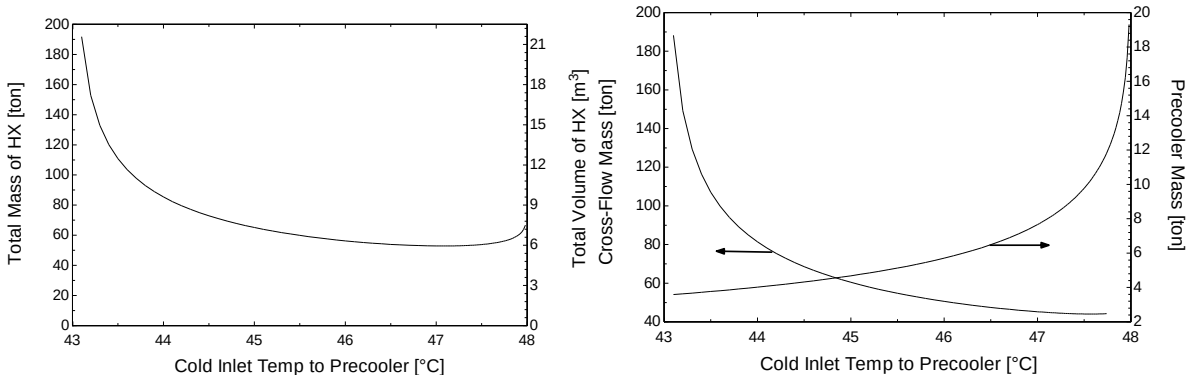

Figure 40: Total mass and cross-flow/counter-flow masses as a function of water temperature entering precooler for the recompression cycle

Simple, High Efficiency:

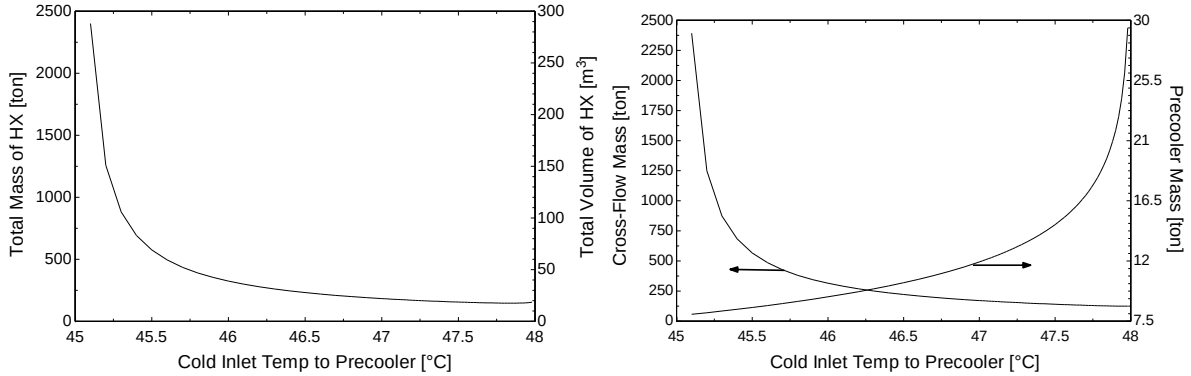

Figure 41: Total mass and cross-flow/counter-flow masses as a function of water temperature entering precooler for the simple, high efficiency cycle

Simple, Low Efficiency:

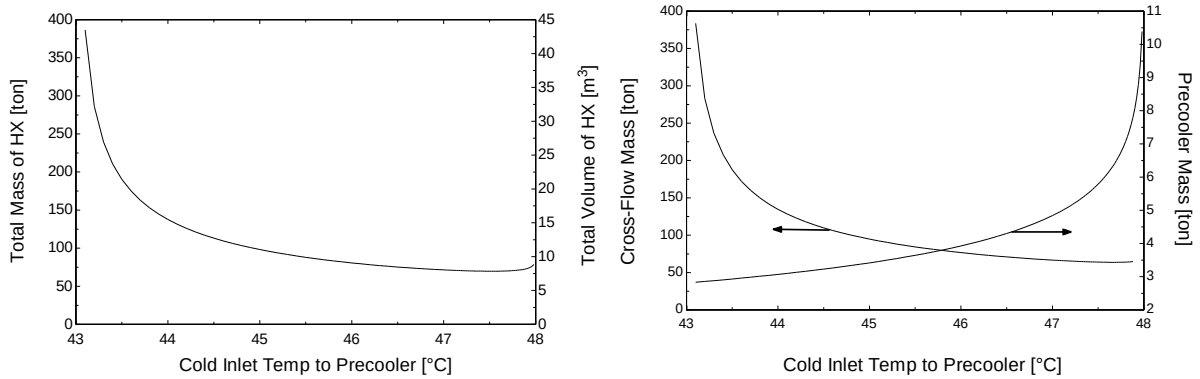

Figure 42: Total mass and cross-flow/counter-flow masses as a function of water temperature entering precooler for the simple, low efficiency cycle

The plots show the expected behavior as the temperature moves toward each of the bounds. As the temperature moves closer to lower limit of 43ºC, the cross-flow heat exchanger effectiveness starts to approach unity and the required surface area approaches infinity. As the temperature approaches the upper limit of 48ºC, the same behavior occurs for the counter-flow heat exchanger; the counter-flow heat exchanger effectiveness approaches unity and as a result the heat exchanger becomes very large. The total mass of the heat exchanger than should be represented by a U-shape as seen in the plots above. If simulations were run with the temperature even closer to 48ºC, using more significant figures, the curves would show a much more distinct U-shape. This parametric study also provided an optimal value of the temperature for each of the conditions which is associated to the point where the lowest mass occurred. The recompression, simple-high, and simple-low temperatures were set to 47.0ºC, 47.8ºC, and 47.4ºC, respectively for the rest of the analysis. This optimal value is pushed towards the 48°C because the mass of the cross-flow heat exchanger is much larger compared to the counter-flow heat exchanger. Pushing the temperature as close to 48°C increases the approach temperature of the cross-flow heat exchanger.

With the configuration and water temperature constrained, the only variable left to vary was the input fan power. The input fan power is varied for each of the design points at different pressure drop ratios, heat exchanger materials, and assuming both mixed and unmixed behavior for the cross-flow heat exchanger; the actual heat exchanger behavior is expected to

lie somewhere between these two limits. The results of these parametric studies are shown below as performance plots. The required power input is the sum of the pump power required for the water loop and the fan power required by the cross-flow heat exchanger.

Recompression:

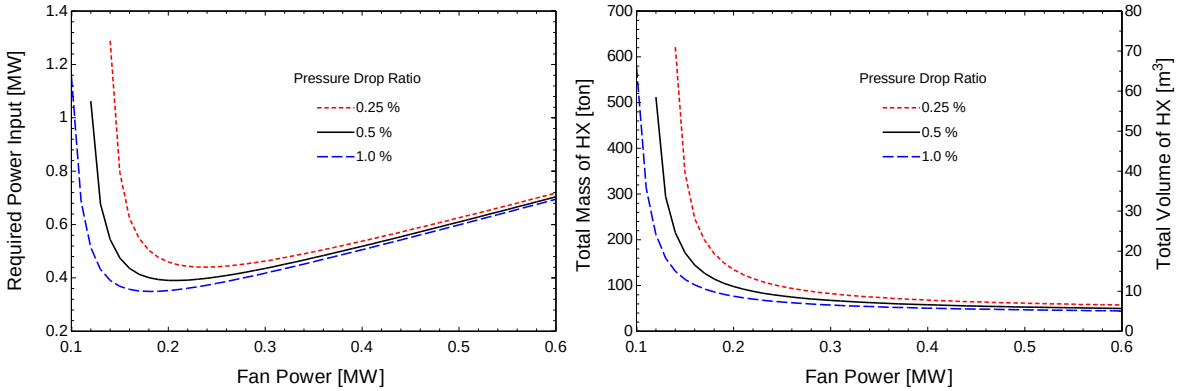

Figure 43: Required power input and total mass/volume as a function of input fan power at varying pressure drop ratios for the recompression cycle

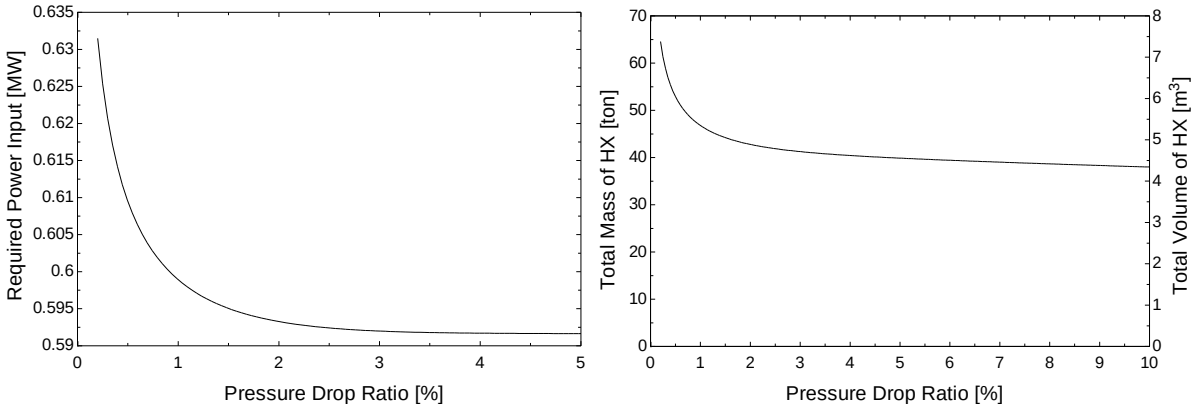

Figure 44: Required power input and total mass/volume as a function of pressure drop ratio for the recompression cycle

Simple, High Efficiency:

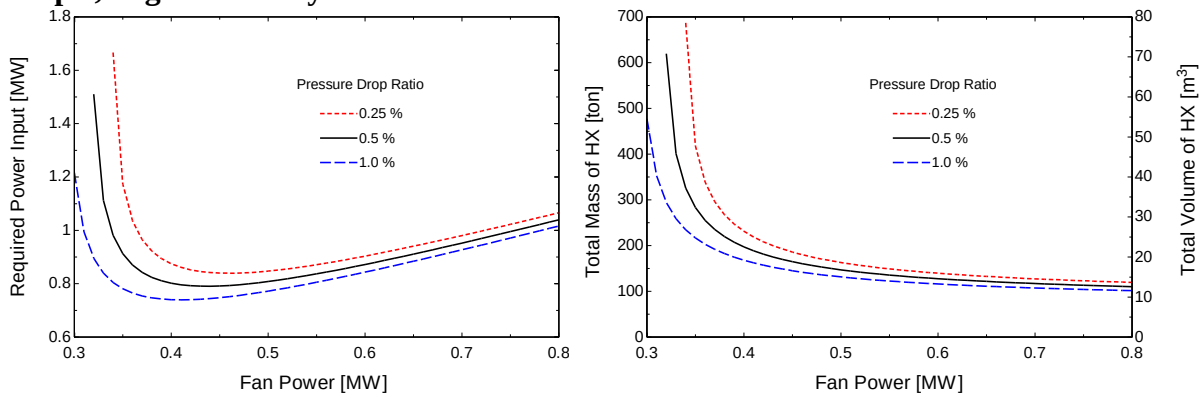

Figure 45: Required power input and total mass/volume as a function of input fan power at varying pressure drop ratios for the simple, high efficiency cycle

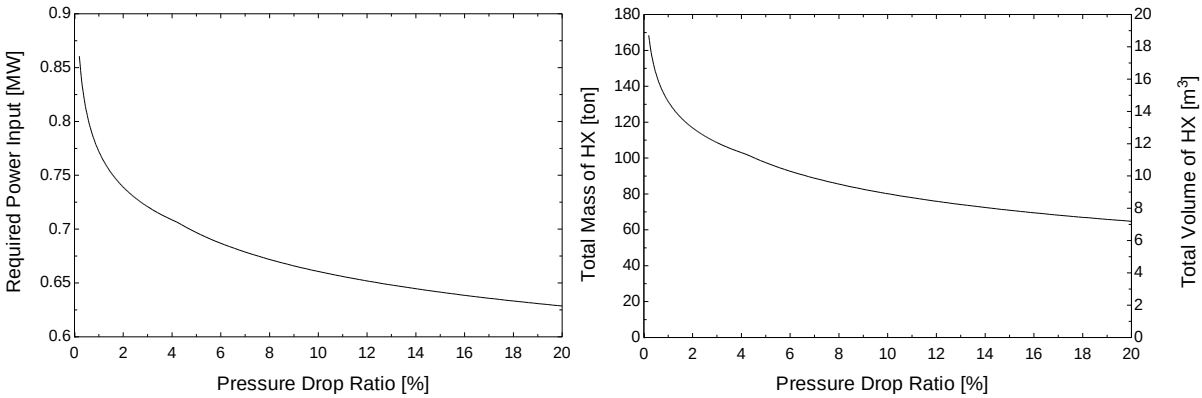

Figure 46: Required power input and total mass/volume as a function of pressure drop ratio for the simple, high efficiency cycle

Simple, Low Efficiency:

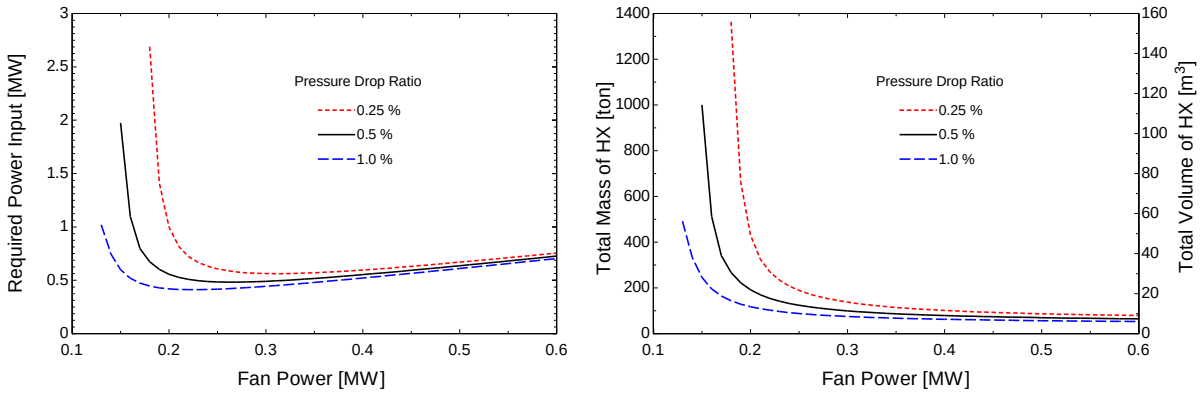

Figure 47: Required power input and total mass/volume as a function of input fan power at varying pressure drop ratios for the simple, low efficiency cycle

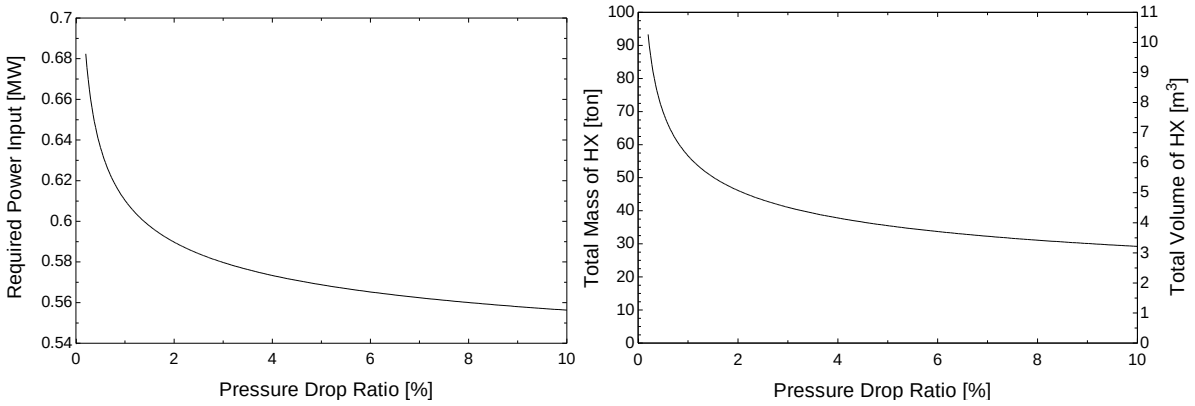

Figure 48: Required power input and total mass/volume as a function of pressure drop ratio for the simple, low efficiency cycle

The performance plots in Figure 43, Figure 45, and Figure 47 show that as fan power is decreased beyond the minimum, the pump power drastically increases. As the fan power decreases, the volumetric air flow rate decreases (for a constant pressure drop). As flow rate decreases, the length in the air-flow direction increases to maintain that pressure drop. With more length, the configuration must change by adding more tubes. More tubes means longer tubing the water has to pass through and with constant velocity through the tubes, pressure drop increases and as a result so does the pump power. Another way to think about this is as one power input decreases, the other has to increase in order to maintain the performance constraints of the heat exchanger. The U-shape that is observed represents the inverse relationship between pump power and fan power.

Figure 44, Figure 46, and Figure 48 show how the pressure drop ratio affects the mass and auxiliary power input. As the pressure drop ratio increases, the length of the counter-flow heat exchanger increases to maintain the pressure drop. With an increase in length and a fixed effectiveness, the energy balance forces the mass flow rate/capacitance rate of the water to decrease. With decreased water mass flow rate, the pressure drops on the water sides of the heat exchangers drop, decreasing the input pump work and auxiliary power input. The mass also decreases due to the cross-flow heat exchanger being more effective, which is the heat exchanger that has the majority of the mass.

Increasing the pressure drop ratio, decreases mass and required power input, but only to a certain point. There is a point where increasing does not change the outputs as significantly.

These plots show that there are optimal points for the auxiliary power input, but these points are not necessarily the optimal points for the mass of the heat exchanger. The selection of the operating point is selected by weighing the economics of increased capital investment for the heat exchanger against the power to run the precooler.

Figure 49 through Figure 54 show the sensitivity of the model to different considerations such as the material selection and modeling the cross-flow heat exchanger as mixed or unmixed for the three design conditions.

Recompression:

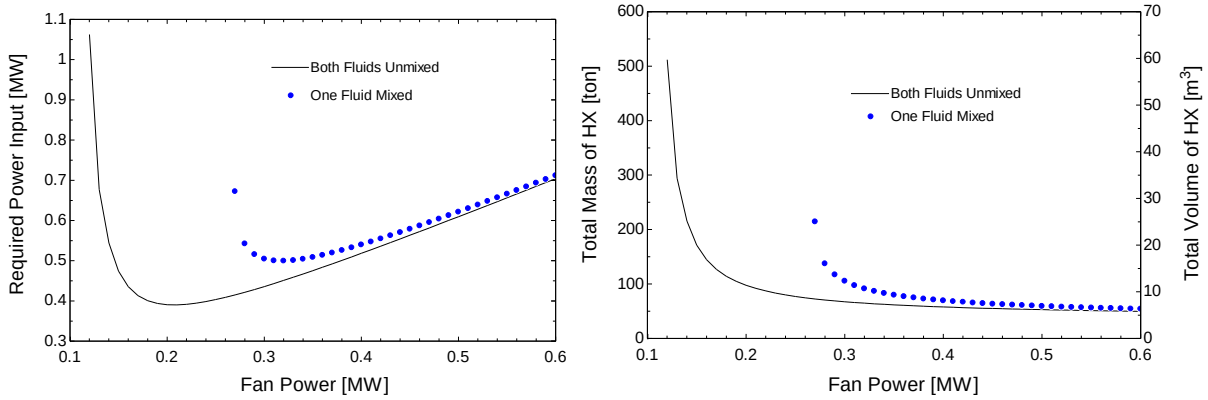

Figure 49: Required power input and total mass/volume as a function of input fan power, at different cross-flow heat exchanger behaviors for the recompression cycle

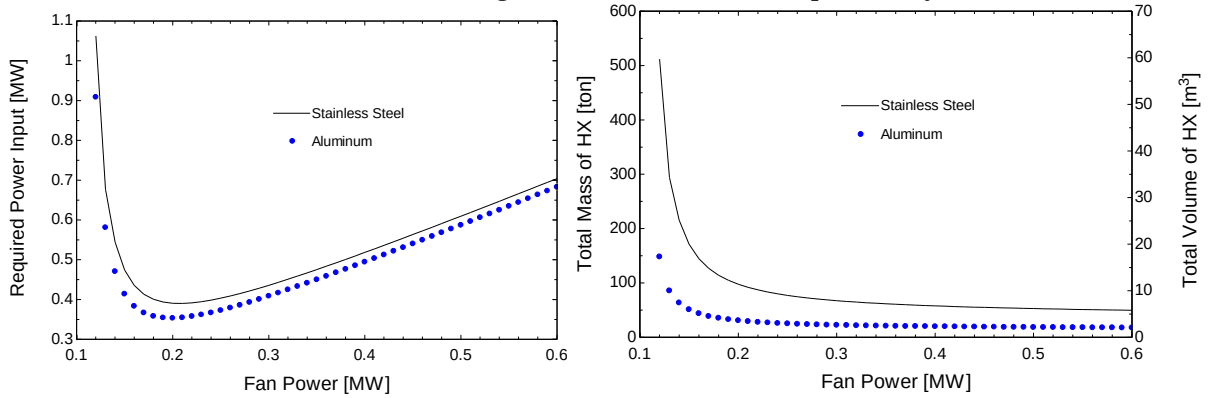

Figure 50: Required power input and total mass/volume as a function of input fan power, using different materials for the recompression cycle

Simple, High Efficiency:

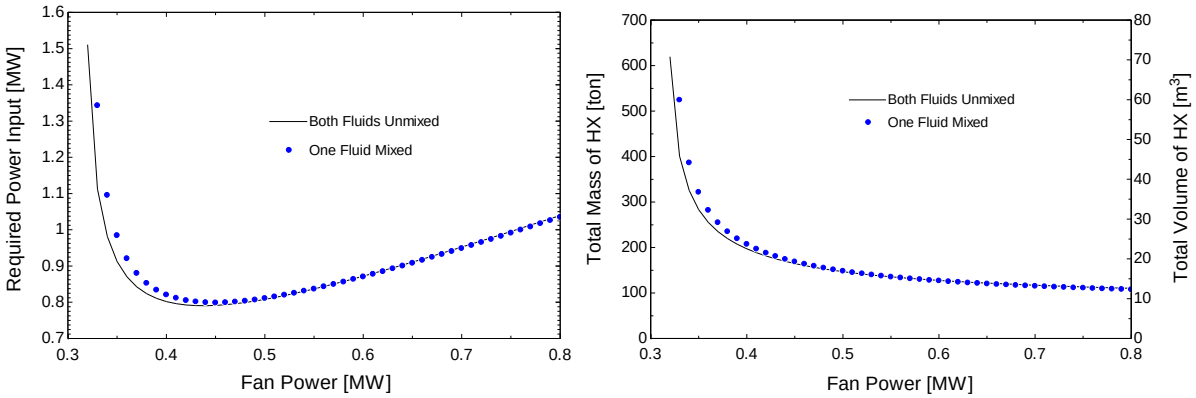

Figure 51: Required power input and total mass/volume as a function of input fan power, at different cross-flow heat exchanger behaviors for the simple, high efficiency cycle

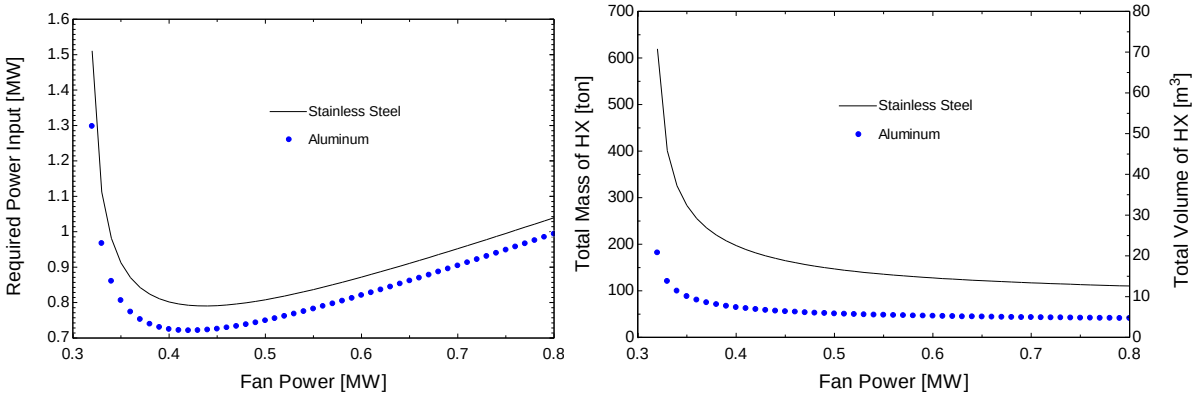

Figure 52: Required power input and total mass/volume as a function of input fan power, using different materials for the simple, high efficiency cycle

Simple, Low Efficiency:

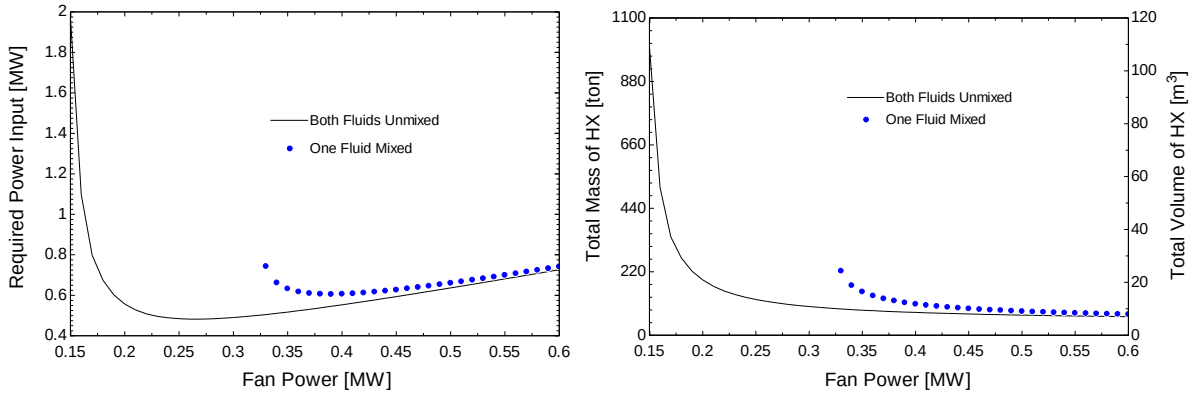

Figure 53: Required power input and total mass/volume as a function of input fan power, at different cross-flow heat exchanger behaviors for the simple, low efficiency cycle

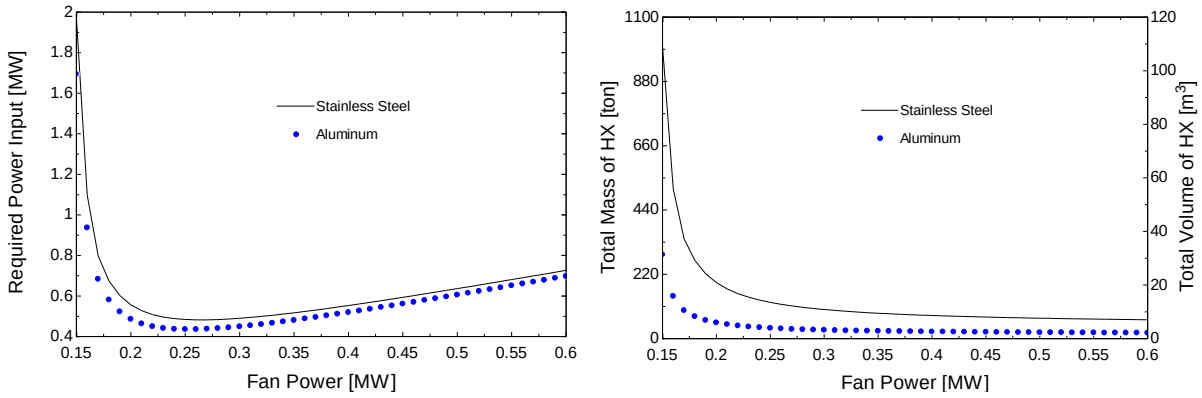

Figure 54: Required power input and total mass/volume as a function of input fan power, using different materials for the simple, low efficiency cycle

All of the cases show that the unmixed cross-flow heat exchanger performs better than the mixed, as expected. The unmixed behavior allows for temperature gradients across the heat exchanger, while the mixed does not.

The change in material from stainless steel to aluminum is accounted in the model by adjusting the fin efficiency calculation, metal density, and stress and deflection analysis that goes into calculating the width between fins in the counter-flow heat exchanger, discussed in Chapter 2. Steel has a significantly higher density compared to aluminum, which is represented in the mass plots for the two heat exchangers. Aluminum also has higher thermal conductivity which enables it to achieve a higher heat exchanger effectiveness compared to the stainless steel option.

4.5 Comparison with simple air-to-CO_2

A simple CO_2-to-air cross-flow heat exchanger model was developed. This simple model is very similar to the water-to-air cross-flow heat exchanger previously developed in this section. In Chapter 5, a more sophisticated model is developed in order to account for the significant property variation of the carbon dioxide.

This simple model was developed so that a rough comparison between the previous model with a water loop and a direct air cooling model with no water loop can be prepared. The

results are found by evaluating the CO_2 properties with the average of the inlet and outlet temperatures of the CO_2. This comparison was done in order to get an initial idea of the potential advantages of a direct CO_2-to-air heat exchanger.

A comparison of the air-to-CO_2 model, with water as the working fluid instead of CO_2, and the air-to-water heat exchanger model built into the water loop code, was done to confirm both produced similar results. The results are shown in Table 11. The results confirmed that the two configuration models could be compared to see the advantages of direct air cooling.

Property	Air to CO_2 Model	Water loop Model
Mass of cross-flow HX [ton]	50.18	50.16
Capacitance Rate (Air) [MW/K]	1.786	1.786
Capacitance Rate (CO_2) [W/K]	559962	560049
Fan Power [MW]	0.4	0.4
Pressure Drop Air-Side [Pa]	125	125
Pressure Drop Water-Side [atm]	3.939	3.939

Table 11: Confirming model produced similar results to the water loop model

Two scenarios were considered to test the simple CO_2-to-air model. The first scenario set the capacitance rates of the air and CO_2 equal for both models, and then compared the size and power inputs. The second scenario set the fan power in the CO_2 to air model equal to the total auxiliary power input required by the water loop model. The results of these tests are shown below for each of the three design points in Table 12 through Table 17.

Recompression:

Equal Capacitance Rates

Property	Air to CO_2	CO_2 to Water, Water to Air
Mass [ton]	20.62	57.82
Capacitance Rate (Air) [MW/K]	1.786	1.786
Capacitance Rate (CO_2) [W/K]	157829	157829
Width=Height [m]	17.27	20.26
Length [m]	0.0516	0.09117
Volume [m^3]	2.328	6.521
Required Power Input [MW]	0.4	0.52

Table 12: Comparison of direct air cooling model and water loop model with equal capacitance rates, recompression cycle

Equal Required Power Input

Property	Air to CO_2	CO_2 to Water, Water to Air
Mass [ton]	19.41	57.82
Capacitance Rate (Air) [MW/K]	2.34	1.786
Capacitance Rate (CO_2) [W/K]	157829	157829
Width=Height [m]	18.58	20.26
Length [m]	0.04198	0.09117
Volume [m^3]	2.191	6.521
Required Power Input [MW]	0.52	0.52

Table 13: Comparison of direct air cooling model and water loop model with equal required input power, recompression cycle

Simple, High Efficiency:

Equal Capacitance Rates

Property	Air to CO_2	CO_2 to Water, Water to Air
Mass [ton]	37.98	127.6
Capacitance Rate (Air) [MW/K]	2.686	2.686
Capacitance Rate (CO_2) [W/K]	176829	176829
Width=Height [m]	21.96	26.53
Length [m]	0.05881	0.1155
Volume [m^3]	4.287	14.39
Required Power Input [MW]	0.6	0.87

Table 14: Comparison of direct air cooling model and water loop model with equal capacitance rates, simple-high efficiency cycle

Equal Required Power Input

Property	Air to CO_2	CO_2 to Water, Water to Air
Mass [ton]	35.94	127.6
Capacitance Rate (Air) [MW/K]	3.90	2.686
Capacitance Rate (CO_2) [W/K]	176829	176829
Width=Height [m]	24.49	26.53
Length [m]	0.04473	0.1155
Volume [m^3]	4.056	14.39
Required Power Input [MW]	0.87	0.87

Table 15: Comparison of direct air cooling model and water loop model with equal required power input, simple-high efficiency cycle

Simple, Low Efficiency:

Equal Capacitance Rates

Property	Air to CO_2	CO_2 to Water, Water to Air
Mass [ton]	19.07	79.1
Capacitance Rate (Air) [MW/K]	1.781	1.781
Capacitance Rate (CO_2) [W/K]	112069	112069
Width=Height [m]	17.06	21.71
Length [m]	0.04898	0.1164
Volume [m^3]	2.155	8.921
Required Power Input [MW]	0.4	0.553

Table 16: Comparison of direct air cooling model and water loop model with equal capacitance rates, simple-low efficiency cycle

Equal Required Power Input

Property	Air to CO_2	CO_2 to Water, Water to Air
Mass [ton]	17.87	79.1
Capacitance Rate (Air) [MW/K]	2.456	1.781
Capacitance Rate (CO_2) [W/K]	112069	112069
Width=Height [m]	18.67	21.71
Length [m]	0.0383	0.1164
Volume [m^3]	2.019	8.921
Required Power Input [MW]	0.553	0.553

Table 17: Comparison of direct air cooling model and water loop model with equal required power input, simple-low efficiency cycle

The results of the comparison show the expected advantages to the direct air cooling. Without the water loop there is no need for a second heat exchanger and the pump power is

eliminated, reducing mass and auxiliary power input required by the precooler. The mass of the CO_2-air cross-flow heat exchanger is also far less than the water-air cross-flow heat exchanger. These observations motivate the development of a more sophisticated model of a direct air-cooled model in Chapter 5.

5 DIRECT AIR COOLER

Air-cooling has become a major topic among researchers in the field of CSP technologies. CSP plants are effective in areas with high direct insolation, which often occurs in arid regions of the world where there is limited availability of water. Currently, water-cooling is more economical than air-cooling because it allows for lower heat sink temperatures and more consistent efficiencies year-round. Water cooling also has lower capital costs and achieves higher plant thermal efficiencies. Air-cooling causes reduced average thermal efficiency when higher air temperatures occur, especially in desert areas where most CSP plants are strategically placed (U.S. Department of Energy, 2011).

Models of air-cooling heat exchangers are required to evaluate use of air-cooling for S-CO_2 Brayton cycles. The remainder of this section will focus on the development of a CO_2-to-air compact heat exchanger model using EES.

5.1 Model development

Refer to the introduction of Section 4.1 for a discussion on how the heat exchanger configurations are selected.

Figure 55 shows the graphical user interface utilized by the CO_2-to-air model. Figure 55 shows that the CO_2 is plumbed in a way that provides a counter-flow interaction with the air. The schematic of the piping shown in the GUI is a top view of the heat exchanger and utilizes the assumption that the same conditions are seen by the array of pipes at every location along the height of the heat exchanger. A 3-D view, shown in Figure 56, illustrates the array of pipes.

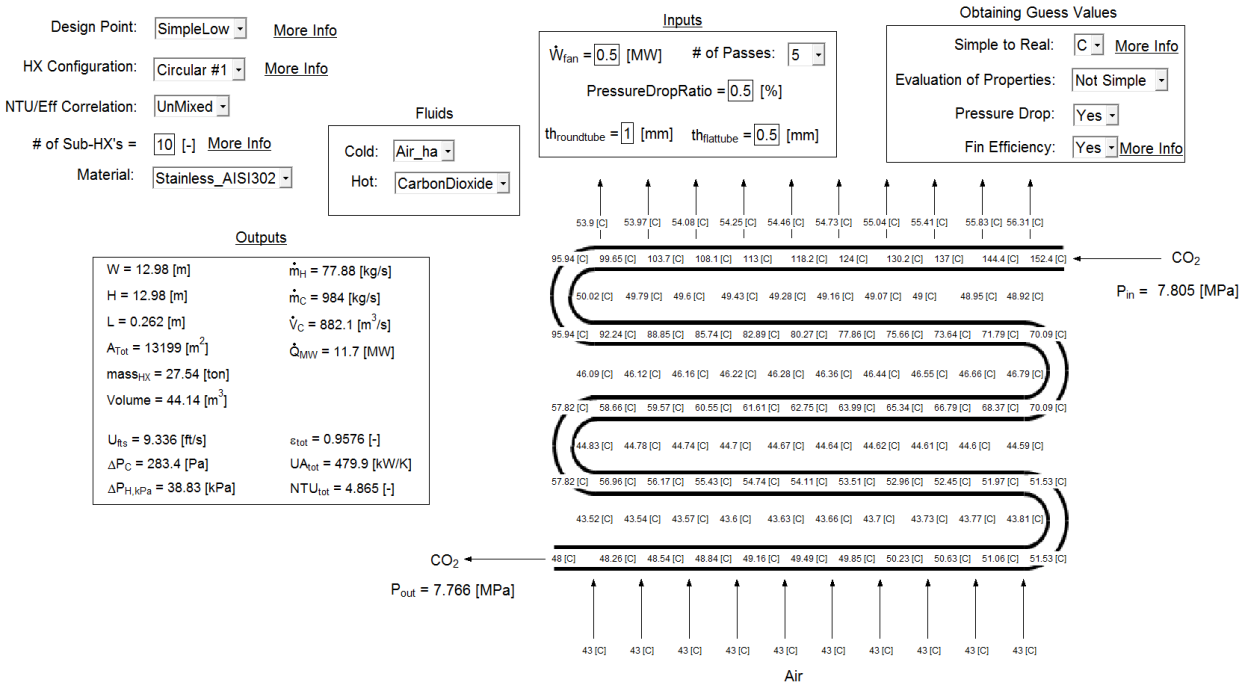

Figure 55: GUI for CO2-to-air cross-flow precooler heat exchanger

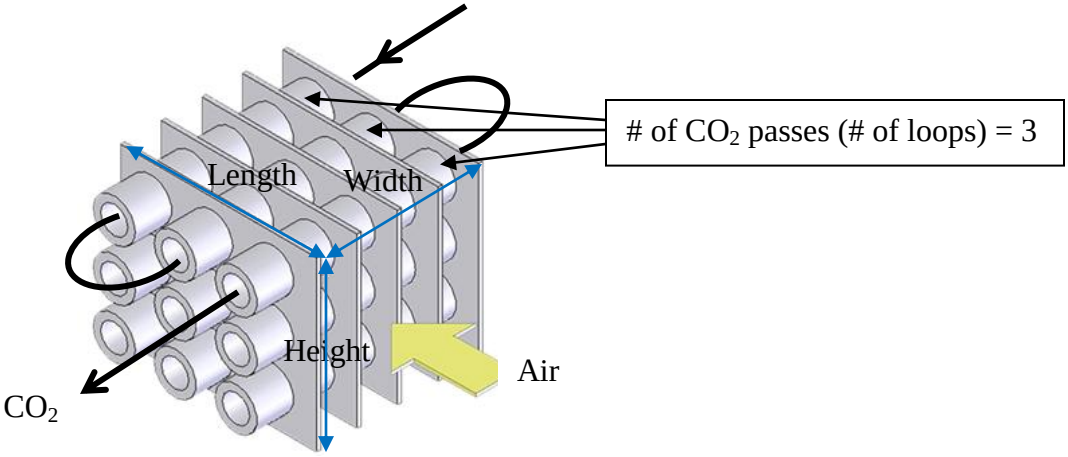

Figure 56: Schematic of CO¬2-to-air cross-flow heat exchanger

Table 18 provides the inputs, parameters, and performance constraints that are required by the CO_2-to-air model.

Inputs	Parameters	Performance Constraints
Air Outlet Pressure = 1 [atm]	**Pipe Wall Thickness** = 1 [mm] (Varied)	**Fan Power** = 0.5 [MW] (Varied)
Air Inlet Temperature = 43 [C]	**Configuration:** C #1-8 or F #1-5	**Heat Input Rate:** Based on Design Point
CO_2 Inlet Temperature: Based on Design Point	**Number of Tube Passes:** 1-10[-]	**Pressure Drop Ratio (CO_2)** = 0.5[%] (Varied)
CO_2 Outlet Pressure: Based on Design Point	**Number of Sub-HX's** = 10 [-]	
CO_2 Outlet Temperature = 48 [C]	**Material:** Steel or Aluminum	

Table 18: Tabular view of inputs, parameters, and performance constraints required by the model

The model requires the specification of the Brayton cycle design point, which establishes the CO_2 operating conditions for the heat exchanger. The design points that have been considered have been discussed earlier in Chapter 1 and are illustrated in Figure 2.

By selecting a design point, CO_2 inlet and outlet temperatures, outlet pressure, and either mass flow rate or heat input rate are established for the precooler. Selecting the design point completely prescribes the CO_2 flow and properties.

As each of the design points have different operating temperatures and pressures, it would be useful to see the state of carbon dioxide for each of the design points on a T-s diagram. For each design point, the CO_2 temperature is cooled from its specific inlet temperature down to 48°C at constant pressure. Figure 57 shows that the *recompression* and *simple low* points are super-critical, while the *simple high* points are super-heated at sub-critical pressure. In the super-critical state, carbon dioxide has higher density, specific heat, and thermal conductivity when compared to the super-heated state. These properties are illustrated in Figure 58 through Figure 60, which show the specific heat, thermal conductivity, and fluid density for carbon dioxide as a function of reduced temperature ($T/T_{critical}$) at the three design points. Again each design point curve is the CO_2 being cooled from each specific inlet temperature

to 48°C at constant pressure. High values of specific heat, thermal conductivity, and fluid density allows for smaller turbo machinery and heat exchangers, with the disadvantage of having to withstand high pressures.

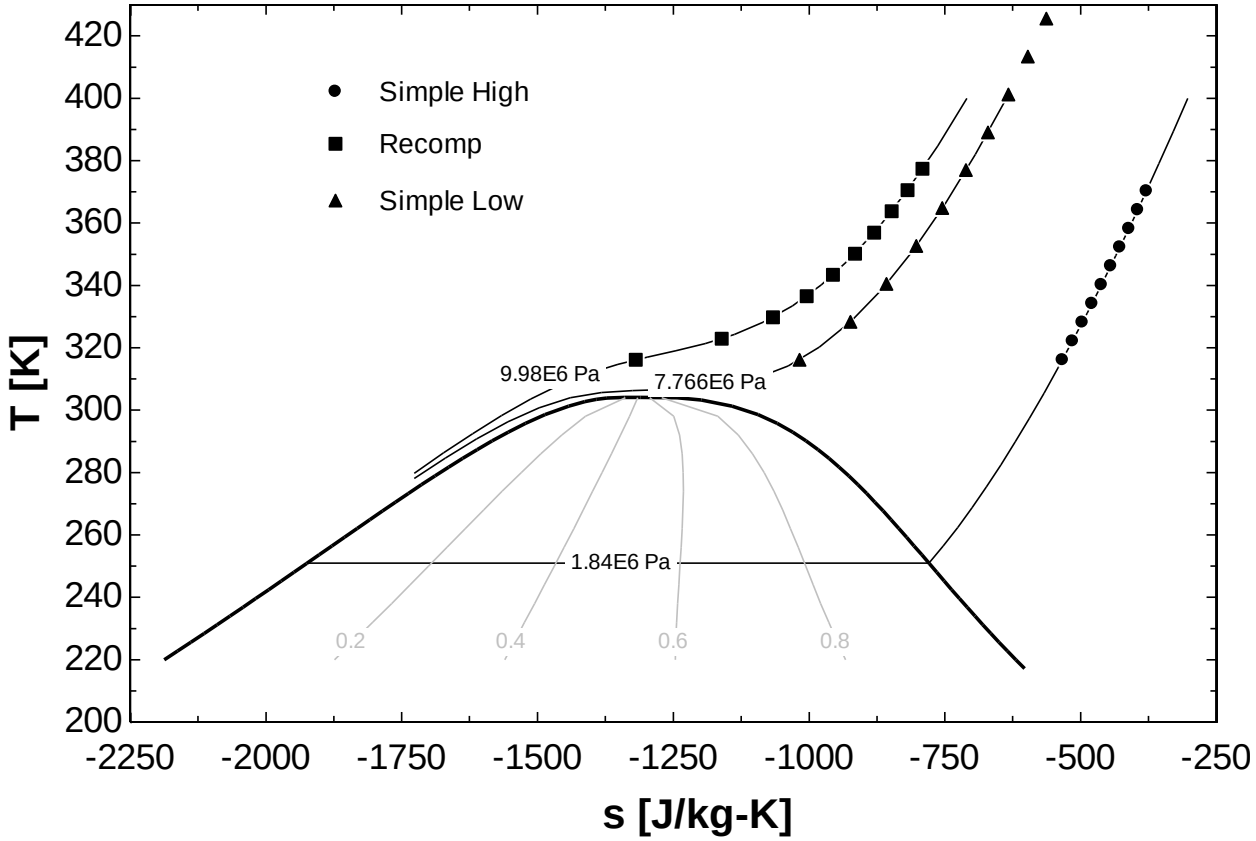

Figure 57: The three design point conditions overlaid on a T-s diagram of carbon dioxide

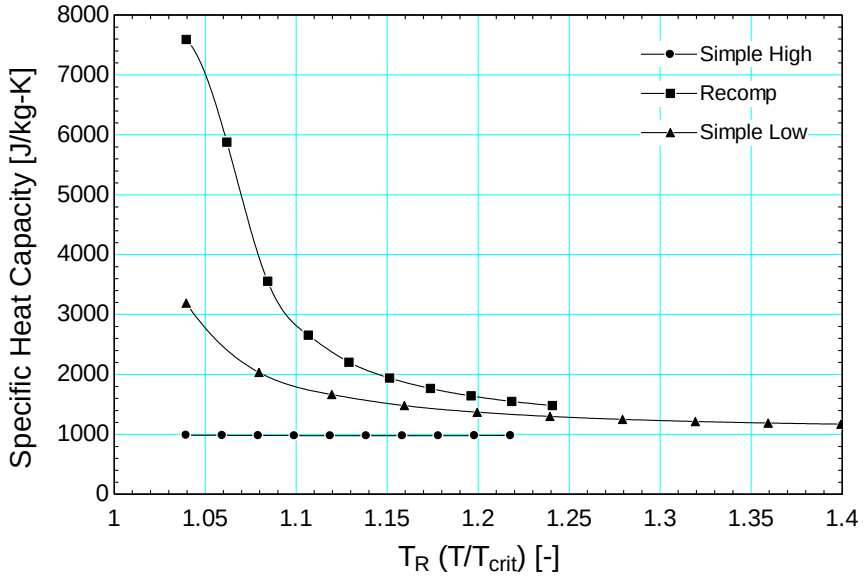

Figure 58: Specific heat capacity of carbon dioxide as a function of the reduced temperature at the three design conditions

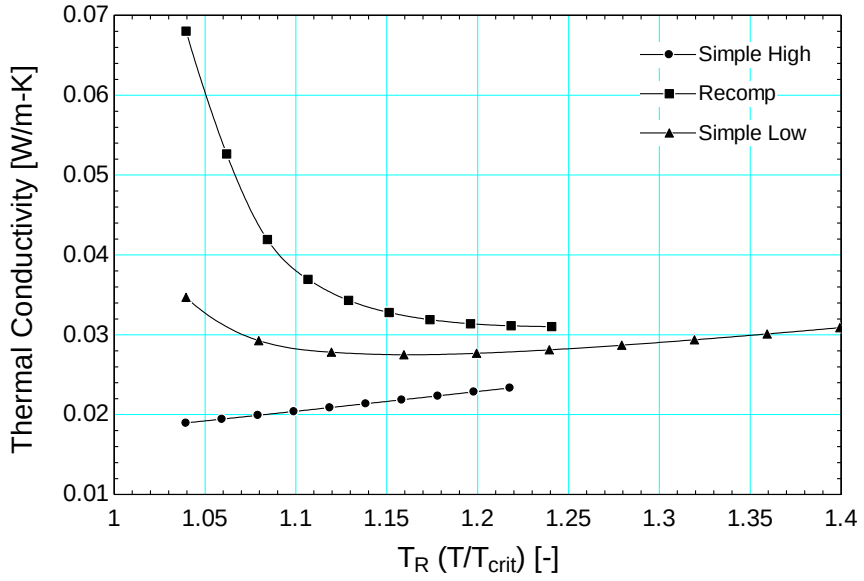

Figure 59: Thermal conductivity of carbon dioxide as a function of the reduced temperature at the three design conditions

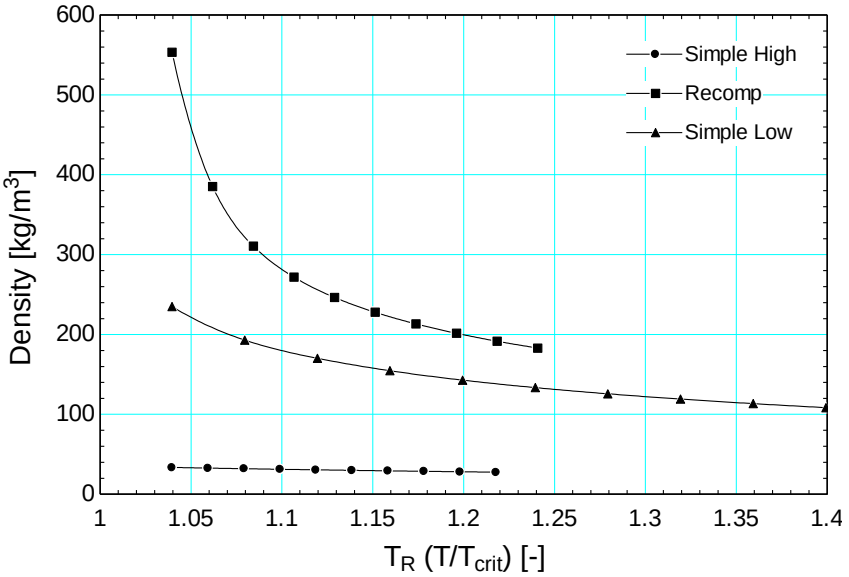

Figure 60: Density of carbon dioxide as a function of the reduced temperature at the three design conditions

To illustrate that the *simple high* design condition will require a much larger precooler, when compared to the *simple low* and *recompression* points, the model was run with constant performance constraints (Fan power = 0.5 MW, pressure drop ratio = 0.5%) and heat exchanger configuration, Circular #1, with a varied number of CO_2 passes/loops. The heat exchanger volume (Length x Width x Height) is presented in Figure 61 which shows that the *simple high* point requires the largest heat exchanger volume while the other two points are about half the size. The studies of John Dyreby have also shown that while the simple high point has high efficiency it requires not only large heat exchangers but also large turbo-machinery; therefore it is the least likely candidate for further studies (Dyreby, 2012).

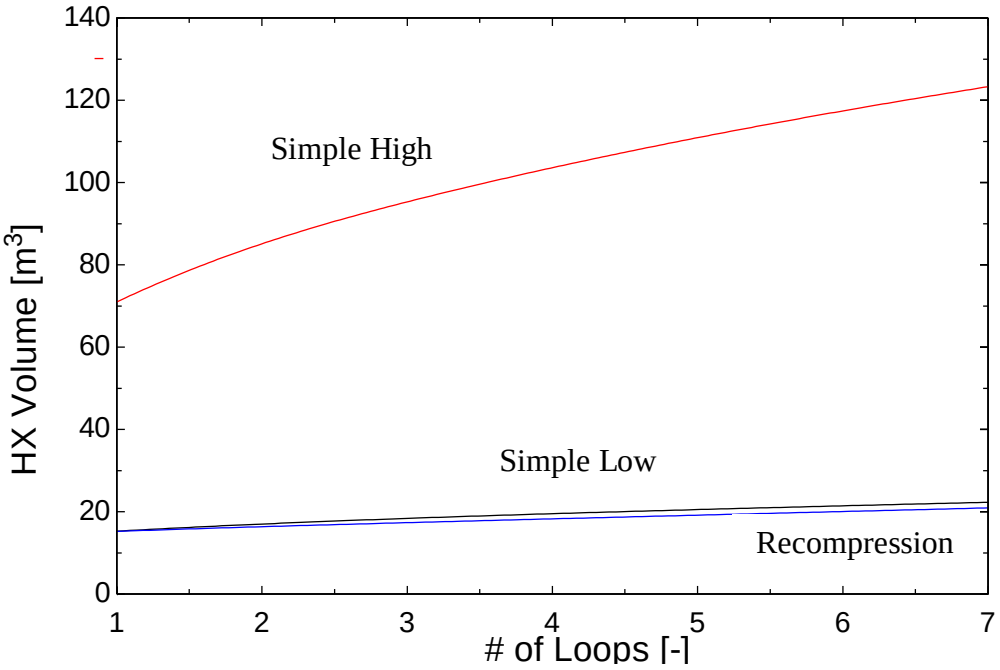

Figure 61: HX volume vs. the number loops specified by the user for the three design points

Once the design point is determined, the model requires the selection of one of the heat exchanger configurations included in the compact heat exchanger library in EES. The compact heat exchanger library is based on experimental results from Kays and London (Kays & London, 1984), which was discussed previously in Chapter 5. Figure 62 and Figure 63 show 13 different configurations, which are either finned circular-tube or flat-tube surfaces for which performance information is provided in EES. The configurations differ in terms of their dimensions, as well as the specific tube and fin geometry, as shown in Table 19 and Table 20. The number, which is located at the top middle of each schematic, and type of configuration (circular or flat) distinguish the different configurations in the model GUI.

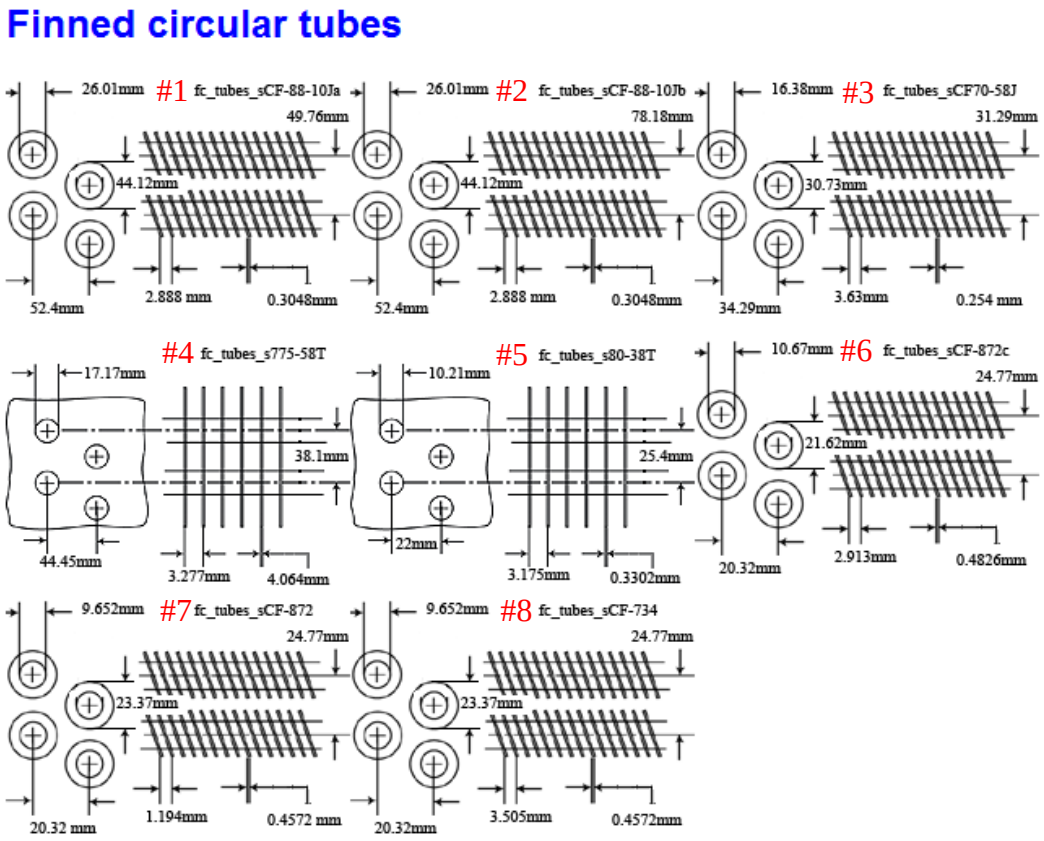

Figure 62: Eight different finned circular tube heat exchanger configurations with corresponding identifying number

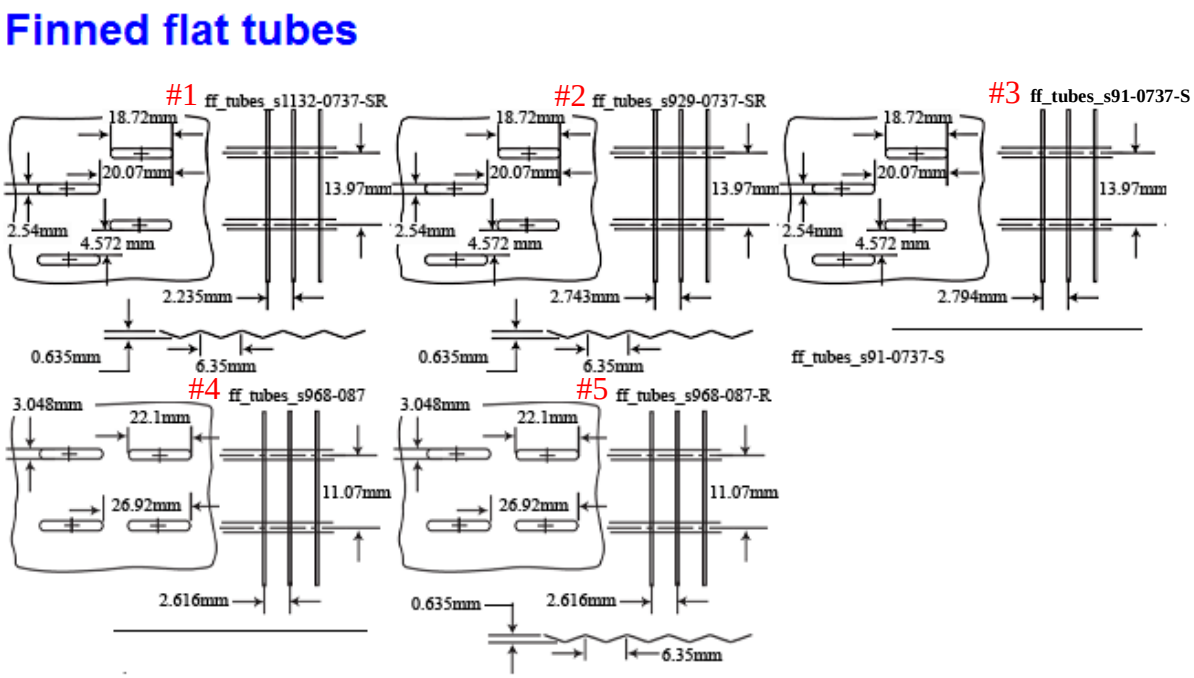

Figure 63: Five different finned flat tube heat exchanger configurations corresponding identifying number

Type/ Number	Alpha [m^2/m^3]	Tube Diameter [mm]	Fin Diameter [mm]	S_v [mm]	S_h [mm]	Pitch [mm]	Fin Thickness [mm]
Circular #1	299	26.01	44.12	49.76	52.4	2.888	0.3048
Circular #2	191	26.01	44.12	78.18	52.4	2.888	0.3048
Circular #3	269	16.38	30.73	31.29	34.29	3.63	0.254
Circular #4	554	17.17	Plate	38.1	44.45	3.277	0.4064
Circular #5	587	10.21	Plate	25.4	22	3.175	0.3302
Circular #6	446	10.67	21.62	24.77	20.32	2.913	0.4826
Circular #7	535	9.652	23.37	24.77	20.32	1.194	0.4572
Circular #8	459	9.652	23.37	24.77	20.32	3.505	0.4572

Table 19: Tabular view of the geometric differences between each of the circular tube configurations

Type/Number	Alpha [m^2/m^3]	Channel Width [mm]	Channel Height [mm]	S_v [mm]	S_h [mm]	Surface [mm]	Alignment [mm]	Pitch [mm]
Flat #1	886	18.72	2.54	13.97	20.07	0.635	4.572	2.235
Flat #2	748	18.72	2.54	13.97	20.07	0.635	4.572	2.743
Flat #3	735	18.72	2.54	13.97	20.07	0	4.572	2.794
Flat #4	751	22.1	3.048	11.07	26.92	0	0	2.616
Flat #5	751	22.1	3.048	11.07	26.92	0.635	0	2.616

Table 20: Tabular view of the geometric differences between each of the flat tube configurations

The important parameter to note when comparing the different heat exchanger configurations is the alpha value, which represents the total heat exchanger surface area to the total heat exchanger volume. Higher values of alpha correspond to high surface area per unit volume and lower air-side convection resistances. For air-coolers, the air-side resistance usually dominates the thermal performance of the heat exchanger. If the air-side convection coefficient can be increased, the required size of the air-cooled heat exchanger can be reduced.

Both finned circular and flat tubes are analyzed in this section. The finned flat tubes were analyzed to see the effect the flat tubes would have on reducing the air-side pressure drop. A simple model was run to test if there is any potential advantage to using finned flat tubes. The compact heat exchanger library procedure CHX_DELTAp_finned_tube will output air-side pressure drop given: heat exchanger configuration, air mass flow rate, heat exchanger frontal

area, length in the air direction, air inlet and outlet temperatures, and pressure. The heat exchanger configuration was varied at constant input parameters and displayed with a bar plot in Figure 64.

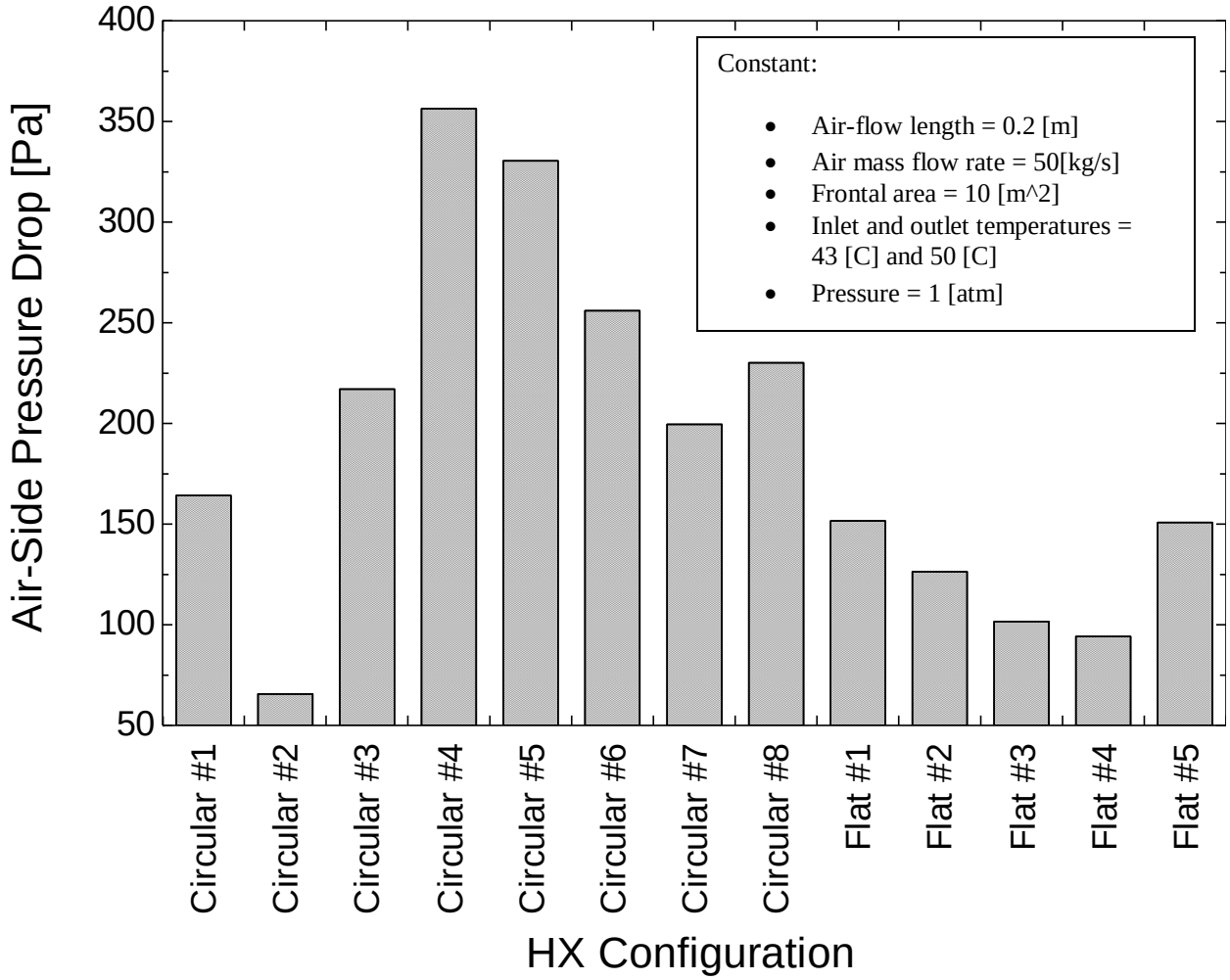

Figure 64: Overall air-side pressure drop vs. configuration with constant parameters and conditions

The bar plot shows that the air-side pressure drop, in general, is smaller for the flat tube when compared to the circular tubes. The very low Circular #2 pressure drop can be explained by looking at Table 19. It shows that the Circular #2 configuration has the largest spacing between its tubes, referring to values of s_v and s_h. However, this means it is less compact and less surface area per unit volume, corresponding to the low value of alpha. Overall, it looks like the flat tubes not only produce a lower air-side pressure drop; they also have very high

values of alpha. The disadvantage to flat tube heat exchangers is the limitation of withstanding high pressure fluids when compared to round tube. Stresses are larger in the flat tube walls when compared to the round tube, so more material is required.

5.1.1 Cross-flow/counter-flow configuration

The model requires the user to specify which compact heat exchanger configuration should be used. There is a drop-down menu with the thirteen different configurations that the model can support. The names used to distinguish the different configurations are located at the top right of each schematic.

Once the configuration has been selected, the CHX_geom_finned_tube procedure determines the outer tube diameter (D_O), fin pitch, hydraulic diameter ($D_{h,C}$), thickness of each fin (fin_{thk}), ratio of free-flow to frontal area (σ), ratio of gas-side heat transfer area to core volume (α), and finally the ratio of finned to total surface area on the gas-side ($A_{fin}\backslash A$). Refer to Figure 56 for a general 3 dimensional view of a cross-flow heat exchanger to give a sense of what the schematics in Figure 62 and Figure 63 are trying to show.

```
"Geometry"
Call CHX_geom_finned_tube(Config$: D_o, fin_pitch, D_h_C, fin_thk, sigma, alpha, A_fin\A)
```

The model requires some addition geometric parameters that the compact heat exchanger procedures do not provide. In the current implementation, these additional parameters are entered with directives that comment in or out code depending on the configuration selected. The additional parameters include the vertical and horizontal separation distance between tubes and fin diameter. The directives also allow for calculation of fin efficiency, CO_2 hydraulic diameter, tube wall thickness, tube inner diameter, cross-sectional area and perimeter of CO_2 flow. One of the thirteen directive code sections is shown below.

```
"Different Configurations"
$if Config$='fc_tubes_sCF-88-10Ja'
s_v=49.76[mm]*convert(mm,m)                    "Vertical separation distance between tubes"
s_h=52.4[mm]*convert(mm,m)                     "Horizontal separation distance between tubes"
```

```
D_fin=44.12[mm]*convert(mm,m)                                    "Fin diameter"
duplicate j=1,N_loops
duplicate i=1,N
"Fin efficiency"
eta_fin[i,j]=eta_fin_annular_rect(th_fin, D_out/2, D_fin/2, h_C[i,j], k_m_tube)
end
end
D_out=D_o                                                        "Tube outer diameter"
D_h_H=D_in                                                       "Hydraulic diameter for CO2-side"
th_tube=th_roundtube*convert(mm,m)                               "Tube thickness"
A_c_H=(PI/4)*D_in^2                                              "Cross sectional area of CO2 flow"
per_H=PI*D_in                                                    "Perimeter for CO2 flow"
D_in=D_out-2*th_tube                                             "Tube inner diameter"
$endif
```

The heat exchanger operating conditions are set by selecting one of three design points.

These design points were discussed in Chapter 1 with Figure 2 and Table 1.

```
"Operating Conditions"
$if DesignPoint$='SimpleLow'
T_H_inlet=152.4[C]                                               "CO2 inlet temp, C"
T_H_outlet=48[C]                                                 "CO2 outlet temp, C"
P_H_outlet=7.766[MPa]                                            "CO2 outlet press, MPa"
T_C_inlet=43[C]                                                  "Air inlet temp, C"
P_C_inlet=1 [atm]                                                "Air inlet press, atm"
Q_dot_MW=11.7[MW]                                                "Heat input rate, MW"
$endif
$if DesignPoint$='Recomp'
T_H_inlet=104.2[C]                                               "CO2 inlet temp, C"
T_H_outlet=48[C]                                                 "CO2 outlet temp, C"
P_H_outlet=9.98[MPa]                                             "CO2 outlet press, MPa"
T_C_inlet=43[C]                                                  "Air inlet temp, C"
P_C_inlet=1 [atm]                                                "Air inlet press, atm"
Q_dot_MW=8.87[MW]                                                "Heat input rate, MW"
$endif
$if DesignPoint$='SimpleHigh'
T_H_inlet=97.2[C]                                                "CO2 inlet temp, C"
T_H_outlet=48[C]                                                 "CO2 outlet temp, C"
P_H_outlet=1.84[MPa]                                             "CO2 outlet press, MPa"
T_C_inlet=43[C]                                                  "Air inlet temp, C"
P_C_inlet=1 [atm]                                                "Air inlet press, atm"
Q_dot_MW=8.7[MW]                                                 "Heat input rate, MW"
$endif
```

The operating conditions are then converted to standard SI units.

```
"Conversions"
T_H_in=converttemp(C,K,T_H_inlet)                                "CO2 inlet temp, K"
T_H_out=converttemp(C,K,T_H_outlet)                              "CO2 outlet temp, K"
T_C_in=converttemp(C,K,T_C_inlet)                                "Air  inlet temp, K"
P_C_in=P_C_inlet*convert(atm,Pa)                                 "Air inlet press, Pa"
Q_dot=Q_dot_MW*convert(MW,W)                                     "Heat input rate, W"
```

```
P_H_in=P_H_inlet*convert(MPa,Pa)          "CO2 inlet press, Pa"
P_H_out=P_H_outlet*convert(MPa,Pa)        "CO2 inlet press, Pa"
```

5.1.2 Discretization into sub heat exchangers

The difference between the water-to-air cross-flow heat exchanger model described in Chapter 4 and this model is a result of the major property variation on the CO_2 side. When the specific heat of a fluid varies significantly with temperature, the *ε-NTU* method becomes invalid. Therefore, the heat exchanger is divided into small "sub-heat exchangers," and properties are determined for each sub-heat exchanger. The size of each sub-heat exchanger is chosen to limit the property variations so the *ε-NTU* method becomes valid. The required number of sub-heat exchangers is found by plotting a significant output parameter as a function of the number of sub-heat exchangers. The plot should asymptotically approach a constant value, determining the number of sub-heat exchangers needed to obtain an accurate result. Figure 65 shows this plot and illustrates that ten sub-HX's is sufficient for accuracy purposes.

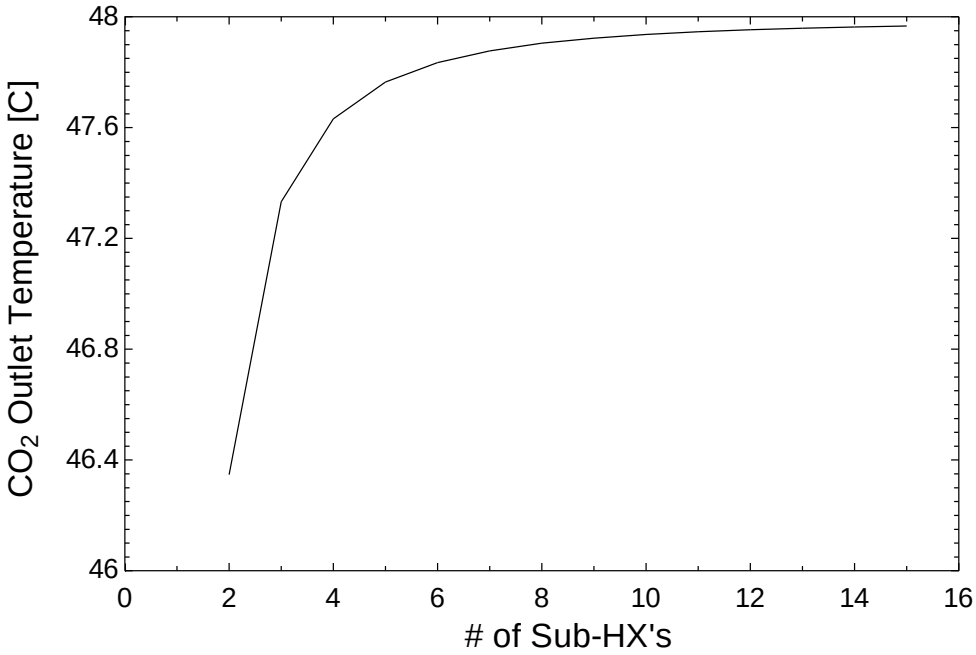

Figure 65: Plot showing the relationship between the number of sub-HX's and outlet CO2 temperature

A detailed schematic of the cross-flow heat exchanger is shown in Figure 66.

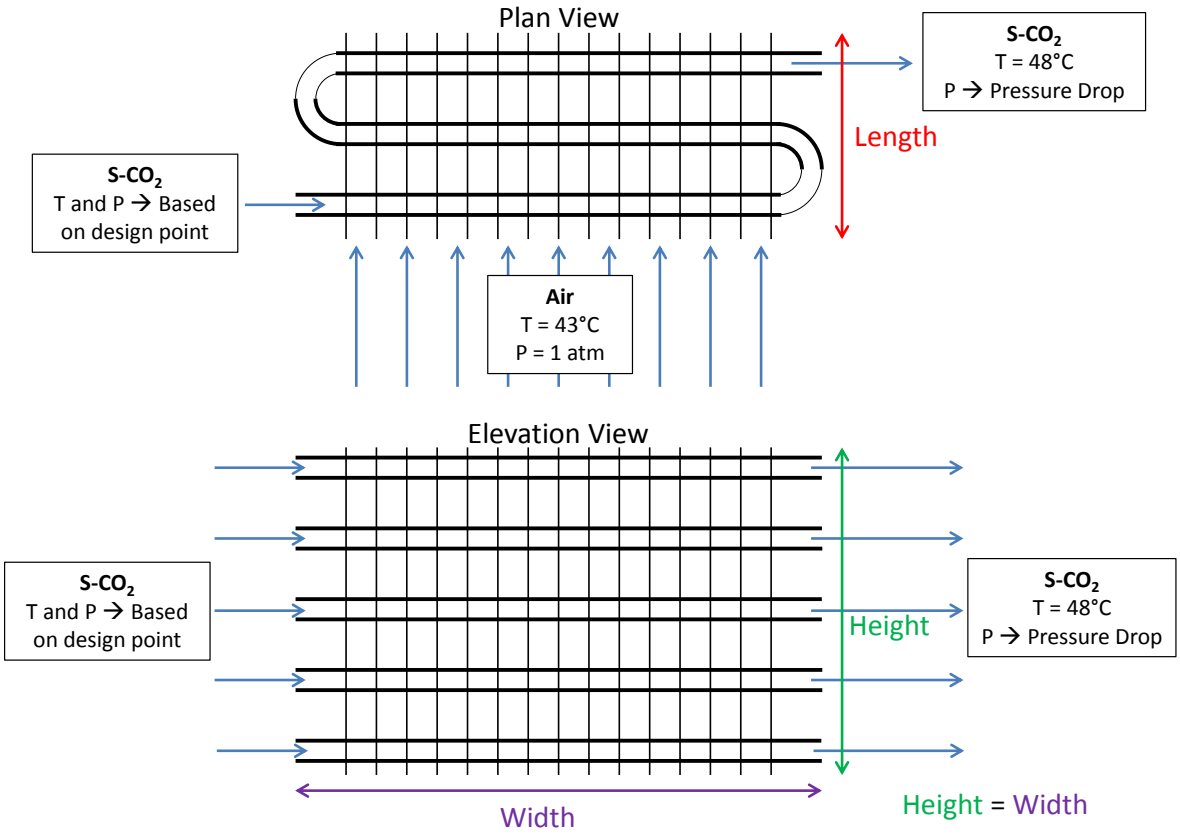

Figure 66: Schematic showing the plan view and elevation view of the cross-flow heat exchanger

Figure 66 shows that there is symmetry that can be utilized when modeling this heat exchanger with sub-HX's. Looking at an elevation view, each tube will experience the same CO_2 conditions. The inlet air temperature is assumed to be uniform across the entire frontal area of the heat exchanger. In addition, the inlet CO_2 temperature will be uniform for each tube along the height of the heat exchanger. Knowing that each tube along the height experiences the same effects, the plan view illustrates the important section for analysis. It shows the heat exchanger in the width and length view, where all the property changes will occur.

Figure 67 shows the heat exchanger broken up into sub-HX's with an arbitrary value of the number of loops (N_{loops}) and the number of sub-HX's (N) set to be 3 and 5, respectively. These values are required inputs for the model.

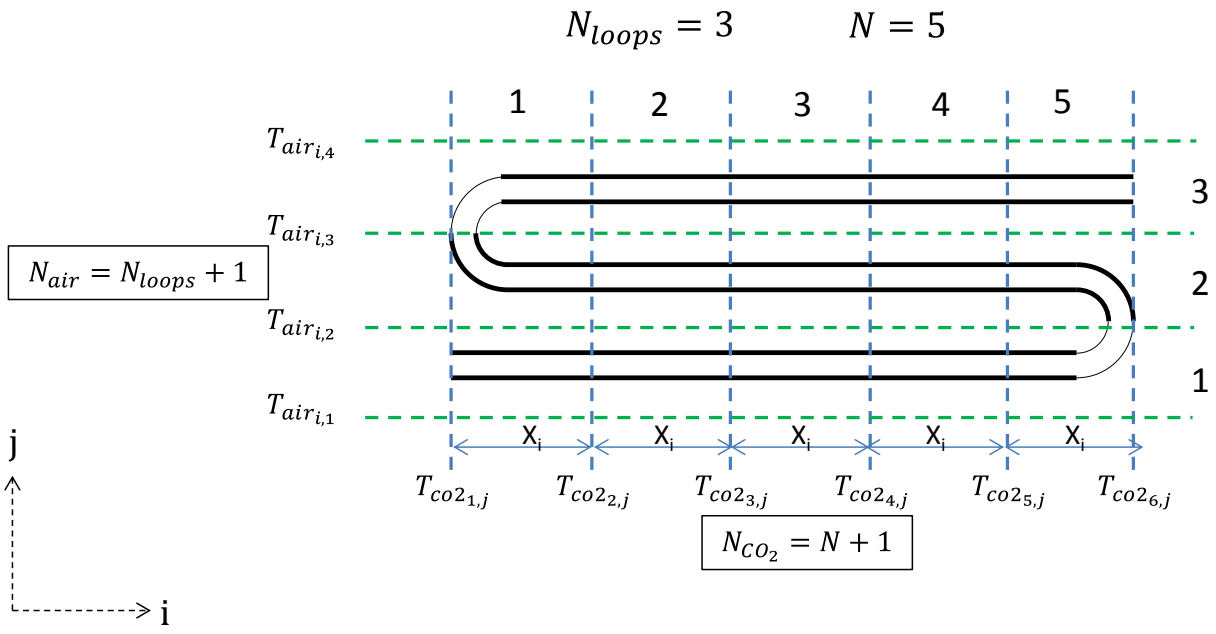

Figure 67: Top view illustrating the break-up into sub-HX's

As shown in Figure 67, the sub-HX's are defined with equal lengths along the width (i.e., along the i-axis) and divided equally along the length (i.e., along the j-axis). Earlier in Chapter 2, the counter-flow heat exchanger was analyzed using equal heat rates versus equal lengths, allowing the length of each sub-heat exchanger to vary. With properties varying in the i and j axes, dividing into equal lengths and letting the heat rate vary within each sub-heat exchanger made dividing the heat exchanger up more simple. The number of air and CO_2 temperatures are defined as:

$$N_{air} = N_{loops} + 1 \tag{5.1}$$

$$N_{CO2} = N + 1 \tag{5.2}$$

```
N_CO2=N+1                    "Number of co2 temperatures"
N_Air=N_loops+1              "Number of air temperatures"
```

The length of each sub-HX (X_i) is defined as:

$$X_i = \frac{Width}{N} \tag{5.3}$$

```
X_i=W/N                                   "Length of each sub-HX"
```

With the sub-HX setup, the model starts to distribute the known operating conditions.

$$T_{C[i,1]} = T_{C_{in}} \; for \; i = 1, N \tag{5.4}$$

$$P_{C[i,1]} = P_{C_{in}} \; for \; i = 1, N \tag{5.5}$$

```
duplicate i=1,N
T_C[i,1]=T_C_in                           "Entering air temperature at first tube"
P_C[i,1]=P_C_in                           "Entering air pressure at first tube"
end
```

$$T_{H[1,1]} = T_{H_{in}} \tag{5.6}$$

$$P_{H[1,1]} = P_{H_{in}} \tag{5.7}$$

```
T_H[1,1]=T_H_in                           "Entering CO2 temperature"
P_H[1,1]=P_H_in                           "Entering CO2 pressure"
```

$$T_{H[N_{co2},N_{loops}]} = T_{H_{out}} \; for \; odd \; number \; of \; loops \tag{5.8}$$

$$T_{H[1,N_{loops}]} = T_{H_{out}} \; for \; even \; number \; of \; loops \tag{5.9}$$

```
T_H[N_CO2,N_loops]=T_H_out                "Outlet co2 temperature for odd tubes"
T_H[1,N_loops]=T_H_out                    "Outlet co2 temperature for even tubes"
```

The overall heat input rate is known; therefore, the sum of the sub-HX heat input rates has to equal the overall heat input rate.

```
duplicate t=1,N_loops
Q_dot_tot[t]=SUM(Q_dot[i,t],i=1,N)        "Sum of sub-HX heat rates"
end
Q_dot=SUM(Q_dot_tot[t],t=1,N_loops)       "Setting sum equal to required overall heat rate"
```

Table 21 illustrates all of the inputs required by the model and possible values for each input.

Inputs	Parameters	Performance Constraints
Air Inlet Pressure = 1 [atm]	**Pipe Wall Thickness** = 1 [mm]	**Fan Power** = 0.5 [MW]
Air Inlet Temperature = 43 [C]	**Configuration:** CF-872c	**Heat Input Rate**: Based on Design Point
CO_2 Inlet Temperature: Based on Design Point	**Number of Tube Loops** = 3 [-]	
CO_2 Inlet Pressure: Based on Design Point	**Number of Sub-HX's** = 10 [-]	
CO_2 Outlet Temperature = 48 [C]		

Table 21: Inputs to model with possible values

Instead of specifying a volumetric flow rate of the air, the amount of fan power is set, and then used to solve for the volumetric flow rate. The value for maximum fan power is more relevant than the amount of volumetric flow rate. The mass flow rate on the CO_2 side is iteratively solved for by knowing the inlet and outlet temperatures, as well as the required heat input rate.

$$\dot{W}_{fan} = \frac{\Delta P_{CF} \dot{V}_{CF}}{\eta_{fan}} \qquad 5.10$$

```
"Fan power"
W_dot_fan=((DELTAP_C*V_dot_C)/eta_fan)*convert(W,MW)
eta_fan=0.5[-]                                          "Fan efficiency"
```

Once the operating conditions have been set, the model runs through each sub-HX determining outlet temperatures and pressures. It starts with the first sub-HX, which has specified values of the inlet temperatures and pressures, mass flow rates, and heat input rates, and determines the outlet conditions. Those outlet conditions are now the inlet conditions for the next sub-HX. This is repeated for all of the sub-HX's.

The properties for each sub-HX are determined by using the average of the inlet and outlet temperatures and the inlet pressure.

```
duplicate j=1,N_loops
duplicate i=1,N
"Air"
rho_C[i,j]=Density(C$,T=(T_C[i,j]+T_C[i,j+1])/2,P=P_C[i,j])          "Density"
Pr_C[i,j]=Prandtl(C$,T=(T_C[i,j]+T_C[i,j+1])/2,P=P_C[i,j])           "Prandtl number"
cp_C[i,j]=Cp(C$,T=(T_C[i,j]+T_C[i,j+1])/2,P=P_C[i,j])                "Specific Heat"
mu_C[i,j]=Viscosity(C$,T=(T_C[i,j]+T_C[i,j+1])/2,P=P_C[i,j])         "Viscosity"
k_C[i,j]=Conductivity(C$,T=(T_C[i,j]+T_C[i,j+1])/2,P=P_C[i,j])       "Thermal conductivity"

"Carbon Dioxide"
cp_H[i,j]=Cp(H$,T=(T_H[i,j]+T_H[i+1,j])/2,P=P_H[i,j])                "Specific Heat"
mu_H[i,j]=Viscosity(H$, T=(T_H[i,j]+T_H[i+1,j])/2,P=P_H[i,j])        "Viscosity"
k_H[i,j]=Conductivity(H$, T=(T_H[i,j]+T_H[i+1,j])/2,P=P_H[i,j])      "Thermal conductivity"
rho_H[i,j]=Density(H$, T=(T_H[i,j]+T_H[i+1,j])/2,P=P_H[i,j])         "Density"
Pr_H[i,j]=Prandtl(H$, T=(T_H[i,j]+T_H[i+1,j])/2,P=P_H[i,j])          "Prandtl number"
end
end
```

Mass flow rates for each sub-HX are determined as follows:

$$\dot{m}_{H,sub} = \dot{m}_H \tag{5.11}$$

$$\dot{m}_{C,sub} = \frac{\dot{m}_C}{N} \tag{5.12}$$

```
m_dot_C_sub=m_dot_C/N                "Mass flow rate of air experienced by sub-HX"
m_dot_H_sub=m_dot_H                  "Mass flow rate of CO2 experienced by sub-HX"
```

The *ε-NTU* method solves for the outlet conditions:

$$\dot{C}_H[i,j] = \dot{m}_{H,sub} cp_H[i,j] \quad for\ i = 1,N\ \&\ j = 1,N_{loops} \tag{5.13}$$

$$\dot{C}_C[i,j] = \dot{m}_{C,sub} cp_C[i,j] \quad for\ i = 1,N\ \&\ j = 1,N_{loops} \tag{5.14}$$

$$\dot{C}_{min}[i,j] = MIN\left(\dot{C}_C[i,j], \dot{C}_H[i,j]\right)\ for\ i = 1,N\ \&\ j = 1,N_{loops} \tag{5.15}$$

$$\dot{Q}_{max}[i,j] = \dot{C}_{min}[i,j](T_H[i,j] - T_C[i,j])$$
$$for\ i = 1,N\ \&\ j = 1,N_{loops}\ (Odd\ tube) \tag{5.16}$$

$$\dot{Q}_{max}[i,j] = \dot{C}_{min}[i,j](T_H[i+1,j] - T_C[i,j]) \quad for\ i = 1,N\ \&\ j = 1,N_{loops}\ (Even\ tube) \tag{5.17}$$

Note that the inlet and outlet CO_2 temperatures switch positions when going from one loop to the next, due to the mass flow rate direction alternating in each loop. Therefore, some equations change depending on if the model is analyzing an odd or even tube. This is done using multiple *if* directives built into EES, that comment in or comment out code depending on if an odd or even tube is being analyzed.

$$\varepsilon[i,j] = \dot{Q}[i,j]/\dot{Q}_{max}[i,j] \quad for\ i = 1,N\ \&\ j = 1,N_{loops} \tag{5.18}$$

```
duplicate j=1,N_loops
duplicate i=1,N
"Effectiveness-NTU method"
C_dot_H[i,j]=m_dot_H_sub*cp_H[i,j]                    "Capacitance rate CO2 side"
C_dot_C[i,j]=m_dot_C_sub*cp_C[i,j]                    "Capacitance rate air side"
C_dot_min[i,j]=MIN(C_dot_C[i,j],C_dot_H[i,j])         "Minimum capacitance rate"
Q_dot_max[i,j]=C_dot_min[i,j]*(T_H[i,j]-T_C[i,j])     "Max heat rate"
Q_dot_max[i,j]=C_dot_min[i,j]*(T_H[i+1,j]-T_C[i,j])   "Max heat rate"
Epsilon[i,j]=Q_dot[i,j]/Q_dot_max[i,j]                "Heat rate"
end
end
```

The number of transfer units is determined using the HX function in EES which implements the *ε-NTU* solutions. Depending on if the user would like the air temperatures modeled as mixed or unmixed, the function calls the 'crossflow_one_unmixed' or 'crossflow_both_unmixed', respectively. In the results to follow, the 'crossflow_both_unmixed' correlation was used based that it's performance in Chapter 4 and it being the more conservative solution. The real solution will likely lie somewhere in-between the two correlations.

```
"Finding NTU"
$if Corr$='UnMixed'
NTU[i,j]=HX('crossflow_both_unmixed', epsilon[i,j], C_dot_H[i,j], C_dot_C[i,j], 'NTU')
$endif
$if Corr$='Mixed'
NTU[i,j]=HX('crossflow_one_unmixed', epsilon[i,j], C_dot_H[i,j], C_dot_C[i,j], 'NTU')
$endif
```

With the effectiveness and the number of transfer units, the conductance is found:

$$NTU[i,j] = UA[i,j]/\dot{C}_{min}[i,j] \quad for\ i = 1,N\ \&\ j = 1,N_{loops} \tag{5.19}$$

Energy balances on the air and CO_2 sides, give the outlet temperatures of the heat exchanger.

$$\dot{C}_H[i,j]T_H[i+1,j] + \dot{Q}[i,j] = \dot{C}_H[i,j]T_H[i,j] \quad for\ i = 1,N\ \&\ j = 1,N_{loops}\ (Odd\ tube) \tag{5.20}$$

$$\dot{C}_H[i,j]T_H[i,j] + \dot{Q}[i,j] = \dot{C}_H[i,j]T_H[i+1,j] \quad for\ i = 1,N\ \&\ j = 1,N_{loops}\ (Even\ tube) \tag{5.21}$$

$$\dot{C}_C[i,j]T_C[i,j+1] = \dot{Q}[i,j] + \dot{C}_C[i,j]T_C[i,j] \quad for\ i = 1,N\ \&\ j = 1,N_{loops} \tag{5.22}$$

Note that the air temperatures can be modeled as mixed by replacing Equation 5.22 with Equations 5.23 and 5.24. This is done using directives that the user defines as mixed or unmixed.

$$\dot{C}_C[i,j]T_{C,test}[i,j+1] = \dot{Q}[i,j] + \dot{C}_C[i,j]T_C[i,j] \quad for\ i = 1,N\ \&\ j = 1,N_{loops} \tag{5.23}$$

$$T_C[i,j+1] = \frac{sum\left(\dot{m}_{C,sub}Cp_C[m,j]T_{C,test}[m,j+1], m = 1,N\right)}{sum\left(\dot{m}_{C,sub}Cp_C[m,j], m = 1,N\right)} \quad for\ i = 1,N\ \&\ j = 1,N_{loops} \tag{5.24}$$

```
duplicate j=1,N_loops
duplicate i=1,N
"Finding overall conductance"
NTU[i,j]=UA[i,j]/C_dot_min[i,j]
"Energy balance on CO2 side, odd tube"
C_dot_H[i,j]*T_H[i+1,j]+Q_dot[i,j]=C_dot_H[i,j]*T_H[i,j]
```

```
"Energy balance on CO2 side, even tube"
C_dot_H[i,j]*T_H[i,j]+Q_dot[i,j]=C_dot_H[i,j]*T_H[i+1,j]

 $if Corr$='Mixed'
"Energy balance on air-side"
C_dot_C[i,j]*T_C[i,j]+Q_dot[i,j]=C_dot_C[i,j]*T_C_test[i,j+1]
T_C[i,j+1]=sum((m_dot_C_sub*cp_C[m,j]*T_C_test[m,j+1]),m=1,N)/SUM((m_dot_C_sub*cp_C[m,j]),
m=1,N)
$endif
$if Corr$='unmixed'
"Energy balance on air-side"
C_dot_C[i,j]*T_C[i,j]+Q_dot[i,j]=C_dot_C[i,j]*T_C[i,j+1]
$endif
end
end
```

Pressure drop on the air-side for each sub-HX is determined using the CHX_DELTAp_finned_tube procedure. The procedure requires the HX configuration, sub-HX mass flow rate and frontal area, length in the air direction, fluid, inlet and outlet temperature, and inlet pressure.

```
"Pressure drop on the air side"
duplicate j=1,N_loops
duplicate i=1,N
Call CHX_DELTAp_finned_tube(Config$, m_dot_C_sub, A_fr/N,L/N_loops,C$, T_C[i,j],
T_C[i,j+1],P_C[i,j]: DELTAP_C[i,j])
end
end
```

The resistance network is included in the model to put geometric constraints into the calculation of the overall conductance. Figure 68 shows the resistance network for the heat exchanger.

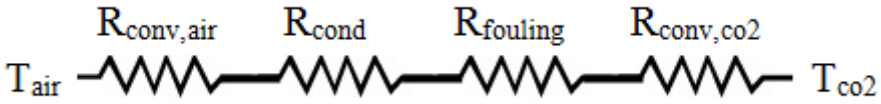

Figure 68: Resistance network for cross-flow heat exchanger

The number of tubes along the length ($N_{t,col}$) and along the height ($N_{t,row}$) can be determined by:

$$N_{t,col} = \frac{L}{s_h} \quad 5.25$$

$$N_{t,row} = \frac{H}{s_v} \quad 5.26$$

```
N_t_col=L/s_h                                   "Number of tube columns"
N_t_row=H/s_v                                   "Number of tube rows"
```

The number of loops is defined by the user. The number of loops defined by the user corresponds to the number of tubes along the length. By setting these two variables equal, the length in the air-flow direction is determined.

```
N_loops=N_t_col                                 "Setting the user defined number of loops to programs"
```

The air-side heat transfer coefficient for each sub-HX is determined using the CHX_DELTAp_finned_tube procedure. The procedure takes in HX configuration, sub-HX mass flow rate and frontal area, fluid, the average of the inlet and outlet temperatures, and inlet pressure.

```
"Air side heat transfer coefficient"
duplicate j=1,N_loops
duplicate i=1,N
Call CHX_h_finned_tube(Config$, m_dot_C/N, A_fr/N, C$,(T_C[i,j]+T_C[i,j+1])/2, P_C[i,j]:h_C[i,j])
end
end
```

The total air-side surface area of each sub-HX is found by multiplying α (ratio of total air side surface area to core volume) by the overall volume of each sub-HX.

```
A_s_out_tot=alpha*((L/N_loops)*L_sub*H)         "Total outside surface area"
```

The fin efficiency is found using the EES fin efficiency procedure, eta_fin_annular_rect, which needs the fin thickness, outer tube diameter, diameter of the fin, air-side heat transfer coefficient, and thermal conductivity of the metal for each sub-HX.

```
duplicate j=1,N_loops
duplicate i=1,N
"Fin efficiency"
eta_fin[i,j]=eta_fin_annular_rect(th_fin, D_out/2, D_fin/2, h_C[i,j], k_m_tube)
end
end
```

The overall surface efficiency is found using equation 1-252 (Nellis & Klein, 2009), which uses the ratio of fin area to total area and fin efficiency.

$$\eta_o[i,j] = 1 - \left(\frac{A_{fin}}{A_{tot}}\left(1 - \eta_{fin}[i,j]\right)\right) \quad for\ i = 1,N\ \&\ j = 1,N\_loops \tag{5.27}$$

```
duplicate j=1,N_loops
duplicate i=1,N
eta_o[i,j]=1-(A_fin\A*(1-eta_fin[i,j]))                    "Overall surface efficiency"
end
end
```

Finally, the outer surface resistance is found using the heat transfer coefficient, overall surface efficiency, and total air-side surface area.

$$R_{out}[i,j] = \frac{1}{\eta_o[i,j]h_{CF}[i,j]A_{s,out,tot}} \quad for\ i = 1,N\ \&\ j = 1,N\_loops \tag{5.28}$$

```
duplicate j=1,N_loops
duplicate i=1,N
R_out[i,j]=1/(eta_o[i,j]*h_C[i,j]*A_s_out_tot)              "Outer surface resistance"
end
end
```

The CO_2 flow is constrained by setting a pressure drop ratio which is defined as:

$$PressureDropRatio = \frac{\Delta P_H}{P_{H,in}} \tag{5.29}$$

```
DELTAP_H=PressureDropRatio*P_H_in                          "Pressure drop ratio"
```

By setting the pressure drop with the pressure drop ratio, the CO_2 fluid velocity, friction factor, Nusselt number, heat transfer coefficient, and Reynolds number are iteratively solved for in Equations 5.30 through 5.32, and the PipeFlow_N procedure for turbulent flow through a pipe.

$$f_H[i,j] = \frac{2\Delta P_H[i,j] D_{h,H}}{1.5 L_{sub} \rho_H[i,j] U_H^2} \quad for\ i = 1, N\ \&\ j = 1, N_{loops} \qquad 5.30$$

Note that the 1.5 constant in the denominator is used to account for header pressures.

$$Re_H[i,j] = \frac{\rho_H[i,j] U_H D_{h,H}}{\mu_H[i,j]} for\ i = 1, N\ \&\ j = 1, N_{loops} \qquad 5.31$$

$$Nusselt_H[i,j] = \frac{h_H[i,j] D_{h,H}}{k_H[i,j]} for\ i = 1, N\ \&\ j = 1, N_{loops} \qquad 5.32$$

The CO_2-side resistance is then found using the following equation:

$$R_{in}[i,j] = \frac{1}{h_H[i,j] per_H N_{t,row} L_{sub}} for\ i = 1, N\ \&\ j = 1, N_{loops} \qquad 5.33$$

```
"Determine heat transfer coefficient, pressure drop, and pump power"
duplicate j=1,N_loops
duplicate i=1,N
"Pressure drop"
f_H[i,j]=(2*DELTAP_H[i,j]*D_h_H)/(1.5*L_sub*rho_H[i,j]*U_H^2)
"Reynolds number"
Re_H[i,j]=rho_H[i,j]*U_H*D_h_H/mu_H[i,j]
"Pipe flow correlation"
call PipeFlow_N(Re_H[i,j],Pr_H[i,j],99999,(.0000015[m]/D_in):
Nusselt_T_H[i,j],Nusselt_H_H[i,j],f_H[i,j])
"Heat transfer coefficient"
Nusselt_T_H[i,j]=(h_H[i,j]*D_h_H)/k_H[i,j]
"CO2-side resistance"
R_in[i,j]=1/(h_H[i,j]*per_H*N_t_row*L_sub)
end
end
```

The fouling resistance is calculated by finding the fouling factor, which is found using the FoulingFactor procedure in EES using 'CO2 liquid'. Using ‘CO2 liquid’ or ‘CO2 vapor’, EES gives the same value for the fouling factor.

```
R``_f_in=FoulingFactor('CO2 liquid')                    "Fouling factor on inner surface of tube"
```

The fouling resistance is calculated using the following equation:

$$R_{f,in}[i,j] = \frac{R''_{f,in}}{per_H N_{t,row} L_{sub}} for\ i = 1,N\ \&\ j = 1,N_{loops} \qquad 5.34$$

```
duplicate j=1,N_loops
duplicate i=1,N
R_f_in[i,j]=R``_f_in/(per_H*N_t_row*L_sub)              "Fouling resistance on inner surface of tube"
end
end
```

Lastly, the conduction resistance through the tube wall is found using the cylinder conduction resistance definition (Nellis and Klein, 2009):

$$R_{cond}[i,j] = \frac{\ln\left(\frac{D_{out}}{D_{in}}\right)}{2k_{m,tube}[i,j]\pi N_{t,row} L_{sub}} \qquad 5.35$$
$$for\ i = 1,N\ \&\ j = 1,N_{loops}$$

```
duplicate j=1,N_loops
duplicate i=1,N
k_m_tube[i,j]=k_ (Metal$,(T_H[i,j]+T_C[i,j])/2)          "Thermal conductivity of material"
"Conduction resistance"
R_cond[i,j]=ln(D_out/D_in)/(2*k_m_tube[i,j]*PI*N_t_row*L_sub)
end
end
```

The total resistance is the sum of the four resistances, which is the inverse of the total conductance.

$$R_{tot}[i,j] = R_{out}[i,j] + R_{in}[i,j] + R_{f,in}[i,j] + R_{cond}[i,j] \qquad 5.36$$
$$for\ i = 1,N\ \&\ j = 1,N_{loops}$$

$$UA[i,j] = \frac{1}{R_{tot}[i,j]} for\ i = 1, N\ \&\ j = 1, N_{loops} \quad 5.37$$

```
duplicate j=1,N_loops
duplicate i=1,N
R_tot[i,j]=R_out[i,j]+R_in[i,j]+R_f_in[i,j]+R_cond[i,j]        "Total resistance"
UA[i,j]=1/ R_tot[i,j]                                          "Total heat exchanger conductance"
end
end
```

By setting the UA calculated using the ε-*NTU* method equal to the UA calculated using the resistance network, the final geometric parameter, width and height, is determined.

5.2 Graphical user interface (GUI)

The GUI, shown in Figure 69, allows for a user to easily and intuitively run the program for multiple configurations, conditions, and materials. The parameters with boxes around the numbers represent inputs to the model, while texts with no boxes represent outputs. These inputs and outputs can be easily interchanged and solved simultaneously.

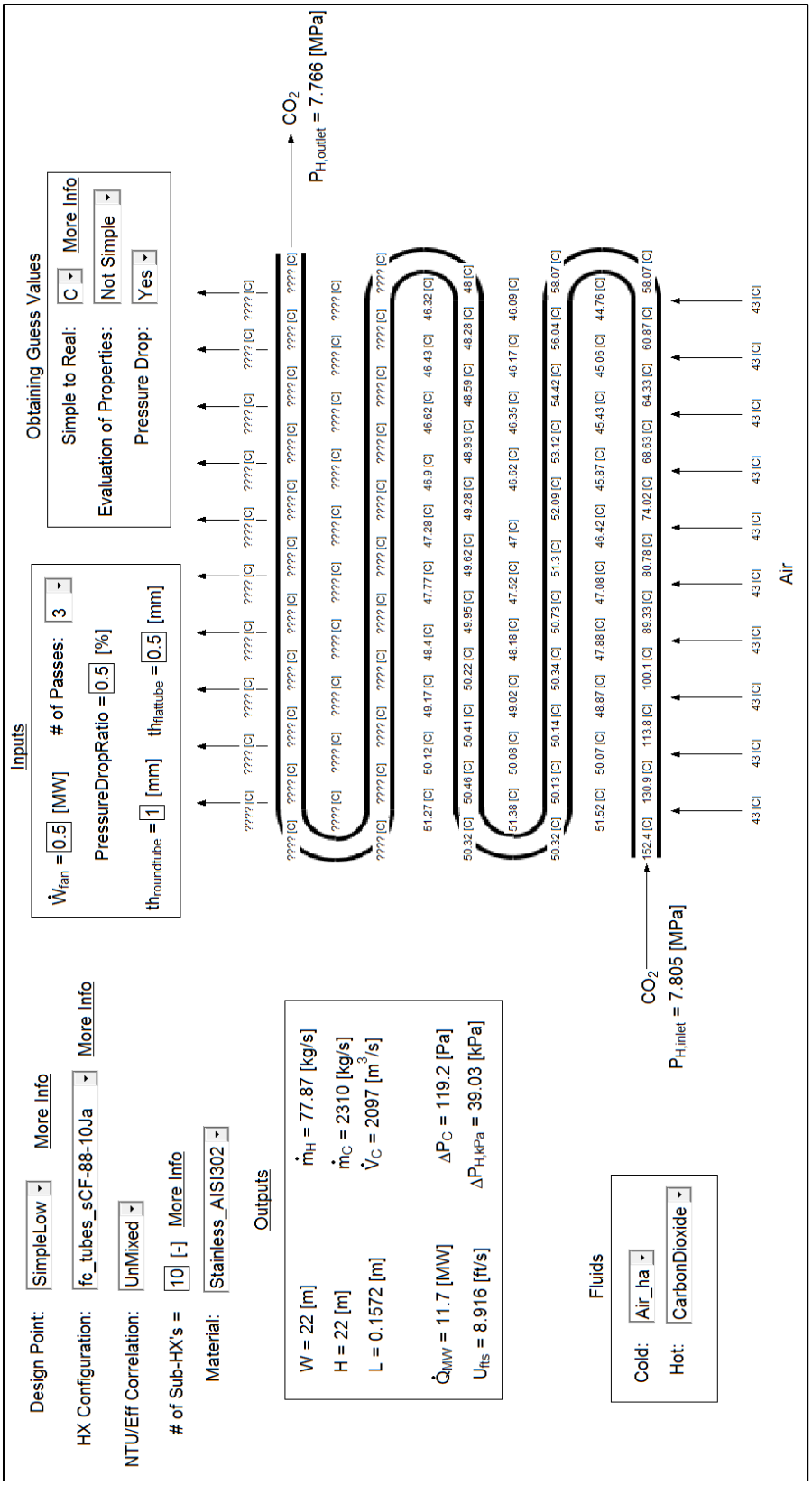

Figure 69: GUI for the Cross-Flow CO2-to-Air Heat Exchanger

First the user selects one of three design points they would like to run. Each design point has specific operating conditions that distinguish it from the others. By clicking “more info”, a plot and table appear, summarizing the three design points. Next the user will select one of thirteen HX configurations. Again by clicking “more info”, a page will pop up showing schematics of the thirteen available configurations. The user then can select what material the HX is made of, if the air temperatures are modeled as mixed or unmixed, the number of sub-HX’s and so on. There are also five value inputs required for the model to run, they include maximum fan power, number of loops in the air-flow direction, the pressure drop ratio for the CO_2 and the tube wall thicknesses for the round and/or flat tube.

There are times that switching between different conditions will cause the model not converge, due to improper guess values. The user can switch to evaluating the properties with just inlet conditions, instead of inlet and outlet, by switching from “Not Simple” to “Simple.” This speeds up calculation as well as it makes it easier for the program to converge. Another way of facilitating convergence is to neglect pressure drop on the CO_2 side. Finally, there is a three stage drop-down menu that goes from A to C. A is simplest, B is next and C is where the program should be run at for accurate results. By clicking “more info”, it will go into detail on what is occurring with each stage.

Having a sophisticated GUI aids in doing studies on multiple different conditions, configurations, and materials. Below are some examples of preliminary studies to show the versatility of the model.

Table 22 shows the results of the model when varying the type of HX configuration. Looking at the alpha values, which are the ratios of the total surface area per unit volume, the results make intuitive sense. The configurations with the larger alpha values, tend to have smaller overall dimensions.

Configuration	Height/Width [m]	Length [m]	Alpha [m^2/m^3]
fc_tubes_sCF-88-10Ja	21.99	0.1572	299
fc_tubes_sCF-88-10Jb	23.6	0.1572	191
fc_tubes_sCF-70-58J	22.79	0.1029	269
fc_tubes_sCF-872c	23.32	0.06096	446
fc_tubes_sCF-872	23.93	0.06096	535
fc_tubes_sCF-734	24.62	0.06096	459
fc_tubes_sCF-775-58T	20.52	0.1334	554
fc_tubes_s80-38T	21.06	0.066	587

Table 22: Varying HX configuration and results

Another interesting parameter is the material used for the heat exchanger. The results of this study listed in Table 23 show that copper leads to the smallest overall dimensions, while stainless steel leads to the largest. Knowing that copper has a high conductivity when compared to the rest, it makes sense that less surface area is needed for heat exchange. Inversely, stainless has the lowest conductivity when compared to the other materials.

Material	Height/Width [m]	Length [m]
Stainless	22	0.1572
Aluminum	20.24	0.1572
Copper	20.16	0.1572
Titanium	21.71	0.1572

Table 23: Varying HX material and results

Analyzing the previous two tables seems to show that the model is running as predicted and proves the versatility of the model for design studies in Section 5.3.

5.3 Performance plots

Given a set of input conditions, the model can be run for different scenarios in order to track how the heat exchanger performs. The first analysis was varying the heat exchanger configurations in order to see how each performs for a set of conditions. Table 24 specifies the set of inlet conditions that were modeled for the results in Figure 70 through Figure 81.

Input	Simple Low	Recompression	Simple High
Air Outlet Pressure [atm]	1.0	1.0	1.0
Air Inlet Temperature [C]	43	43	43
CO_2 Inlet Temperature [C]	152.4	104.2	97.2
CO_2 Outlet Pressure [Mpa]	7.766	9.98	1.84
CO_2 Outlet Temperature [C]	48	48	48
Tube Wall Thickness [mm]	1.0	1.0	1.0
Material	Aluminum	Aluminum	Aluminum
Fan Power [MW]	0.5	0.5	0.5
Heat Input Rate [MW]	11.7	8.87	8.7
Pressure Drop Ratio [%]	0.5	0.5	0.5

Table 24: Set of inlet conditions for results in Figures 11-22

Figure 70 through Figure 78 represent the heat exchanger volume, air-side pressure drop, and volumetric flow rate, respectively, as a function of the CO_2 passes for all thirteen configurations. Each figure represents the recompression, simple high, and simple low design points to see how they compare to one another. Each design point is split into two plots, left and right, corresponding to circular tube and flat tube, respectively.

Heat Exchanger Volume

Recompression:

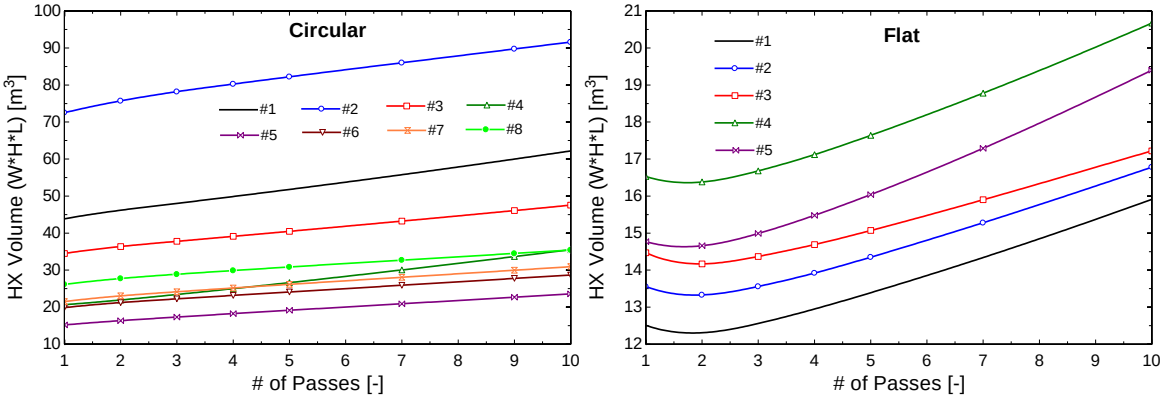

Figure 70: Heat exchanger volume as a function of CO2 passes for the thirteen heat exchanger configurations at the recompression condition

Simple Cycle, High Efficiency:

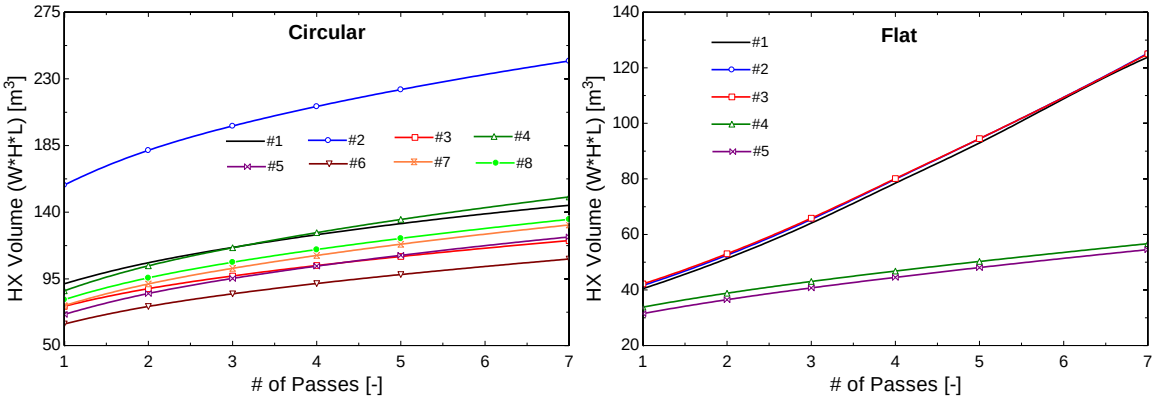

Figure 71: Heat exchanger volume as a function of CO2 passes for the thirteen heat exchanger configurations at the simple cycle, high efficiency condition

Simple Cycle, Low Efficiency:

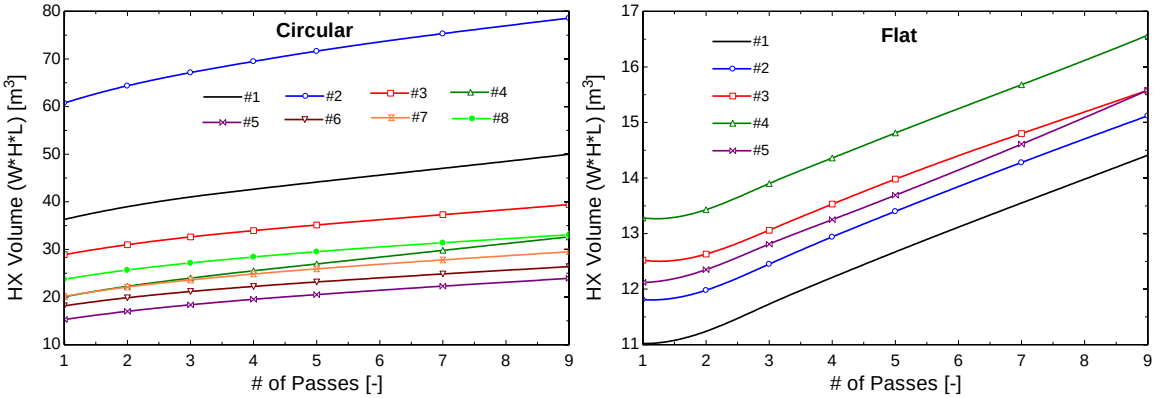

Figure 72: Heat exchanger volume as a function of CO2 passes for the thirteen heat exchanger configurations at the simple cycle, low efficiency condition

Looking at Figure 70 through Figure 72, it can be seen that the heat exchanger required by the *simple high* cycle is more than double the size required by the *simple low* or *recompression* cycle. Further, there is a large spread between the flat and circular configurations, with the flat tube configurations requiring less heat exchanger size. Recalling from the previous section, the alpha values for the flat tube configurations are much larger when compared to the circular tube configurations. Referring back to Table 19 and Table 20, the alpha values closely correlate to the size of the heat exchanger. Configurations with large alpha values tend to have smaller heat exchanger volume and vice versa.

Air-Side Pressure Drop

Recompression:

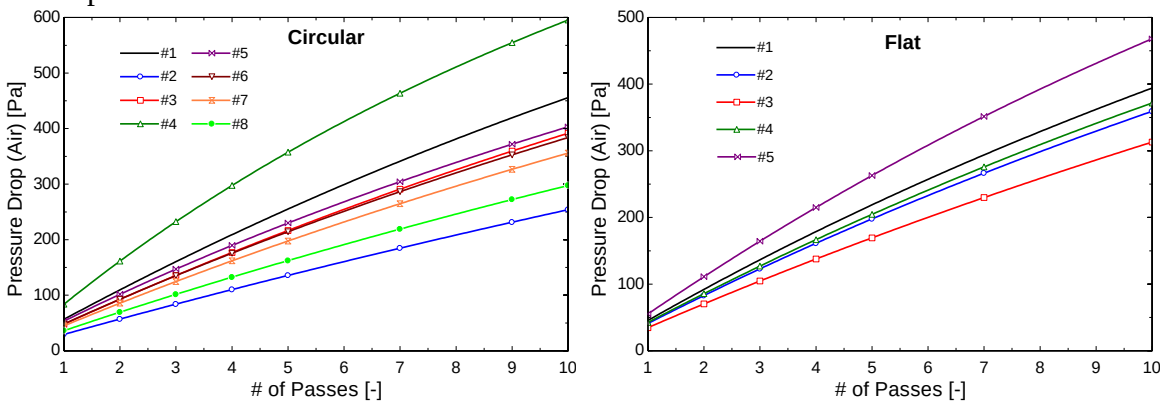

Figure 73: Air-side pressure drop as a function of CO2 passes for the thirteen heat exchanger configurations at the recompression condition

Simple Cycle, High Efficiency:

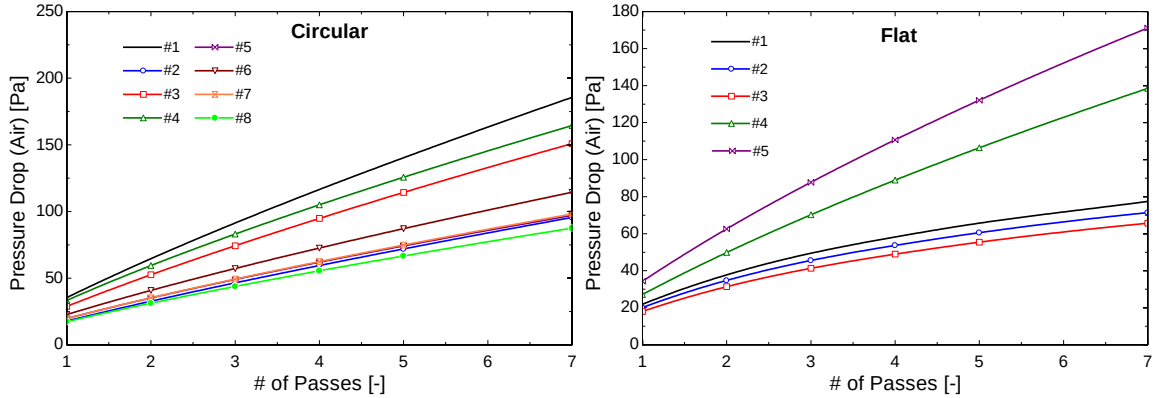

Figure 74: Air-side pressure drop as a function of CO2 passes for the thirteen heat exchanger configurations at the simple cycle, high efficiency condition

Simple Cycle, Low Efficiency:

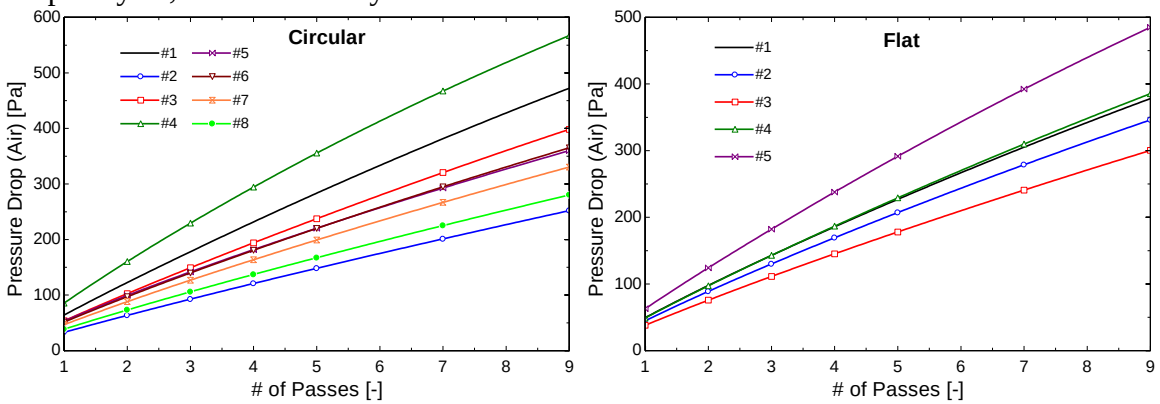

Figure 75: Air-side pressure drop as a function of CO2 passes for the thirteen heat exchanger configurations at the simple cycle, low efficiency condition

Air-side pressure drop is found to be smaller in the *simple high* design point than compared to the *simple low* and *recompression*. The *simple high* condition requires a larger heat exchanger size which in turn causes the flow rate to be larger. With constant fan power, the higher flow rate allows for a smaller overall air-side pressure drop.

Air-side pressure drop is relatively uniform across all configurations. This is explained by the length in the air direction not being uniform for each of the configurations. Air-coolers are limited by the amount of air-side pressure drop allowed, forcing there to be relatively small lengths in the air direction. Usually air-coolers take on the "pancake" shape, where they are much wider and taller than they are deep.

Volumetric Flow Rate

Recompression:

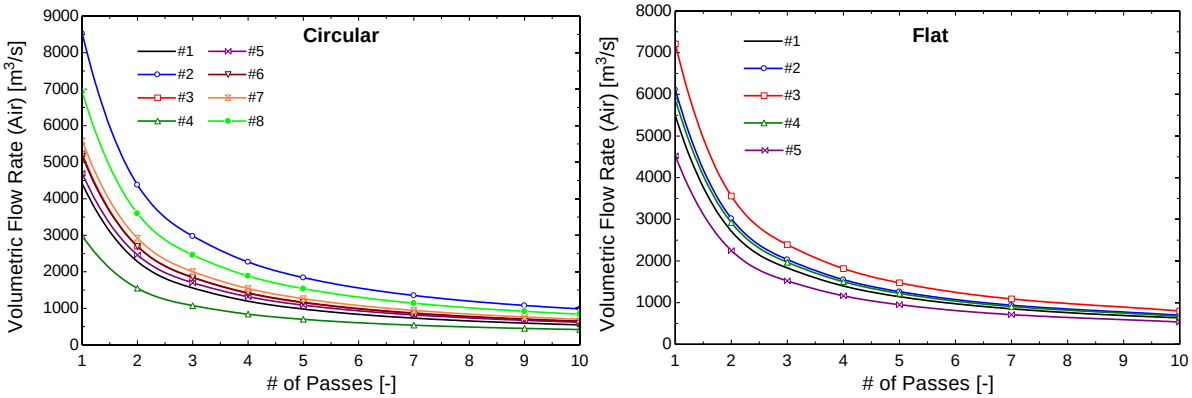

Figure 76: Air volumetric flow rate as a function of CO2 passes for the thirteen heat exchanger configurations at the recompression condition

Simple Cycle, High Efficiency:

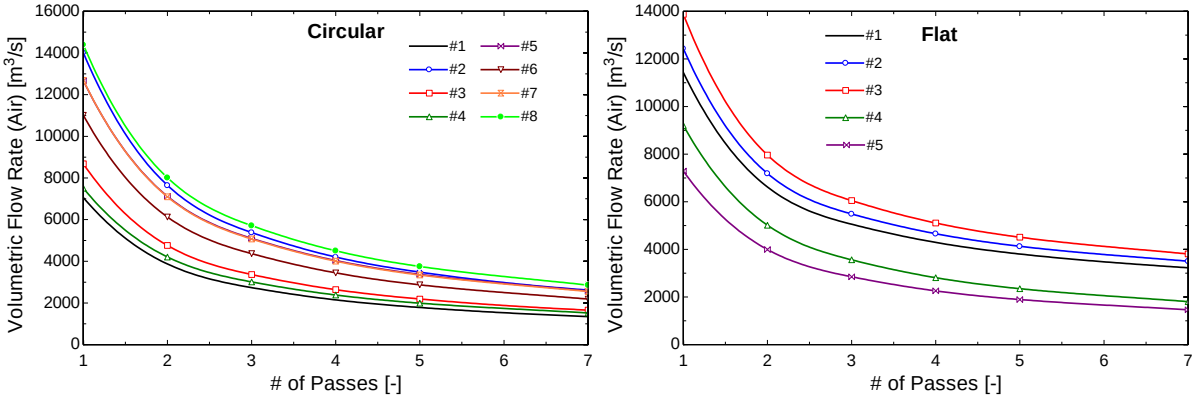

Figure 77: Air volumetric flow rate as a function of CO2 passes for the thirteen heat exchanger configurations at the simple cycle, high efficiency condition

Simple Cycle, Low Efficiency:

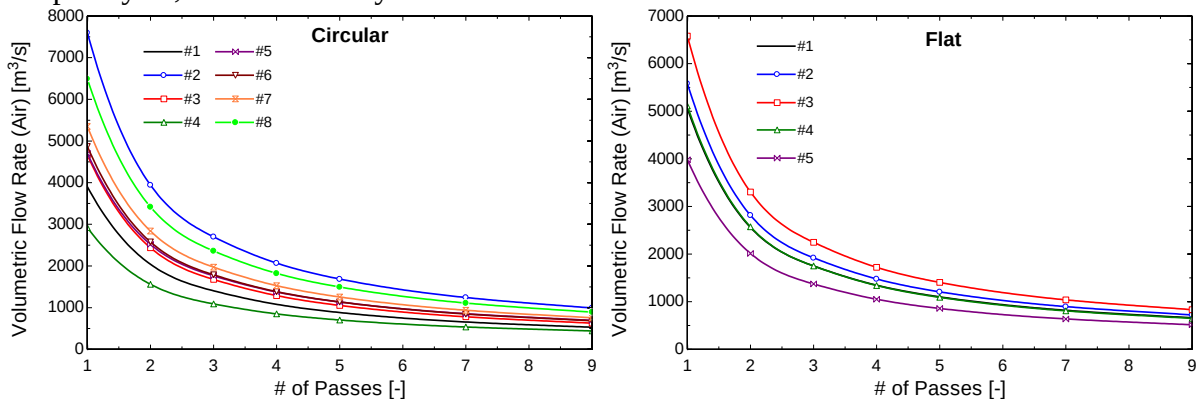

Figure 78: Air volumetric flow rate as a function of CO2 passes for the thirteen heat exchanger configurations at the simple cycle, low efficiency condition

The volumetric flow rate, as previously stated, is much higher for the *simple high* compared to the *simple low* and *recompression*. For all of the configurations, the volumetric flow rates have relatively similar values. All of the plots show that the volumetric flow rate will eventually level off and not be affected by the number of CO_2 passes/loops. The volumetric flow rate decreases with increased air-direction length because of increased air-side pressure drop. The level off effect is due to the fact that as more passes are added, more surface area is also being added, allowing for flow rate to decrease at the expensive of increased pressure drop.

Referring to Figure 79 through Figure 81, the total precooler conductance is evaluated for all design points and configurations as a function of CO_2 passes/loops. Each design point has a left and right plot, differing only in the y-axis as a zoomed in or out view, respectively. Looking at the plots to the right for all design points, it is interesting to note that the total conductance remains relatively unchanged due to stacking (increasing more loops). This is useful when running thermal cycle analyses where any one of the heat exchangers could be applied given a specific conductance value.

Total Precooler Conductance

Recompression:

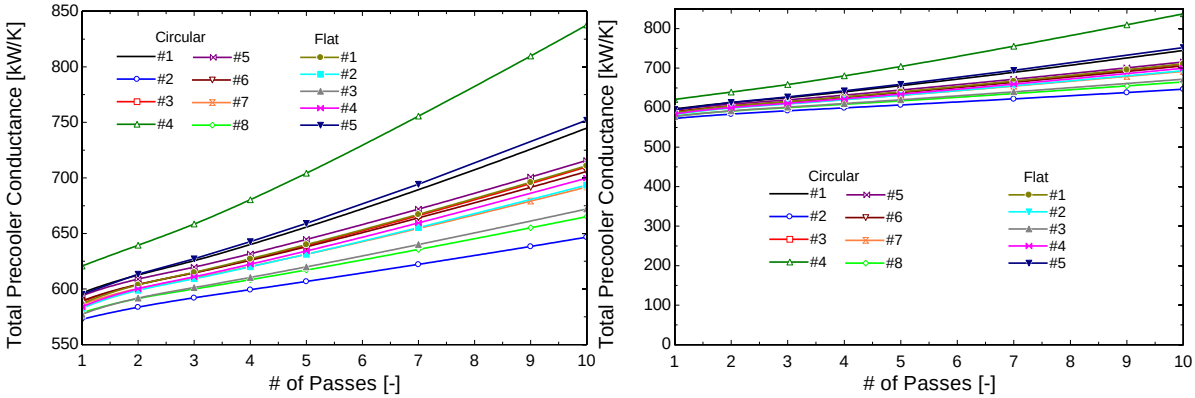

Figure 79: Total precooler conductance as a function of CO2 passes for the thirteen heat exchanger configurations at the recompression condition

Simple Cycle, High Efficiency:

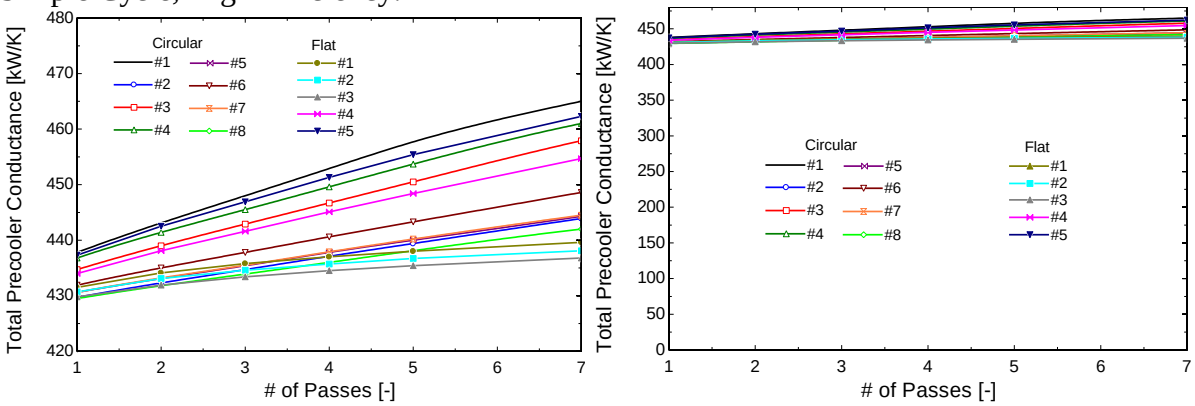

Figure 80: Total precooler conductance as a function of CO2 passes for the thirteen heat exchanger configurations at the simple cycle, high efficiency condition

Simple Cycle, Low Efficiency:

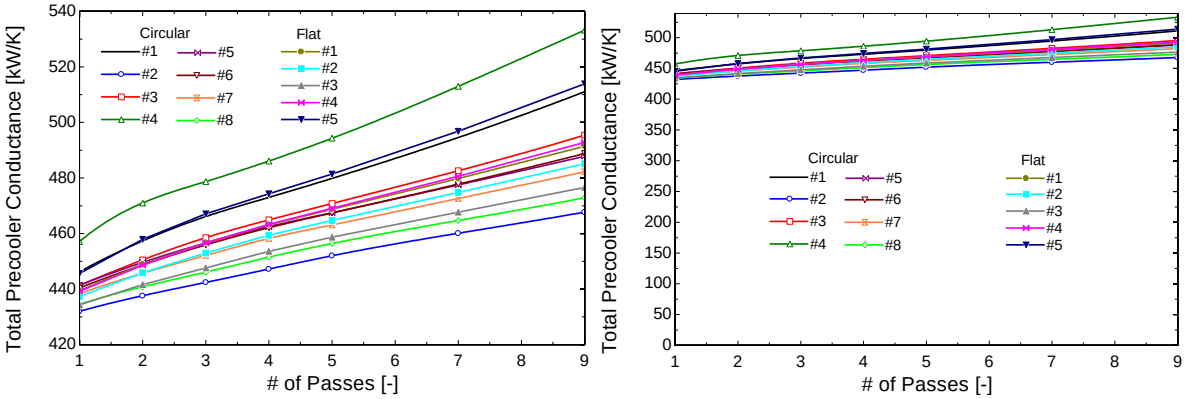

Figure 81: Total precooler conductance as a function of CO2 passes for the thirteen heat exchanger configurations at the simple cycle, low efficiency condition

To get a sense of the model's sensitivity, some of more important inputs were varied, including the fan power, pressure drop ratio on the CO_2 side, and approach temperature difference. The model was set to run the recompression design point as well as configuration C#5, which produced the smallest overall heat exchanger volume. It should be noted that if the test were run on other configurations or design points, it would produce similar results.

Fan Power

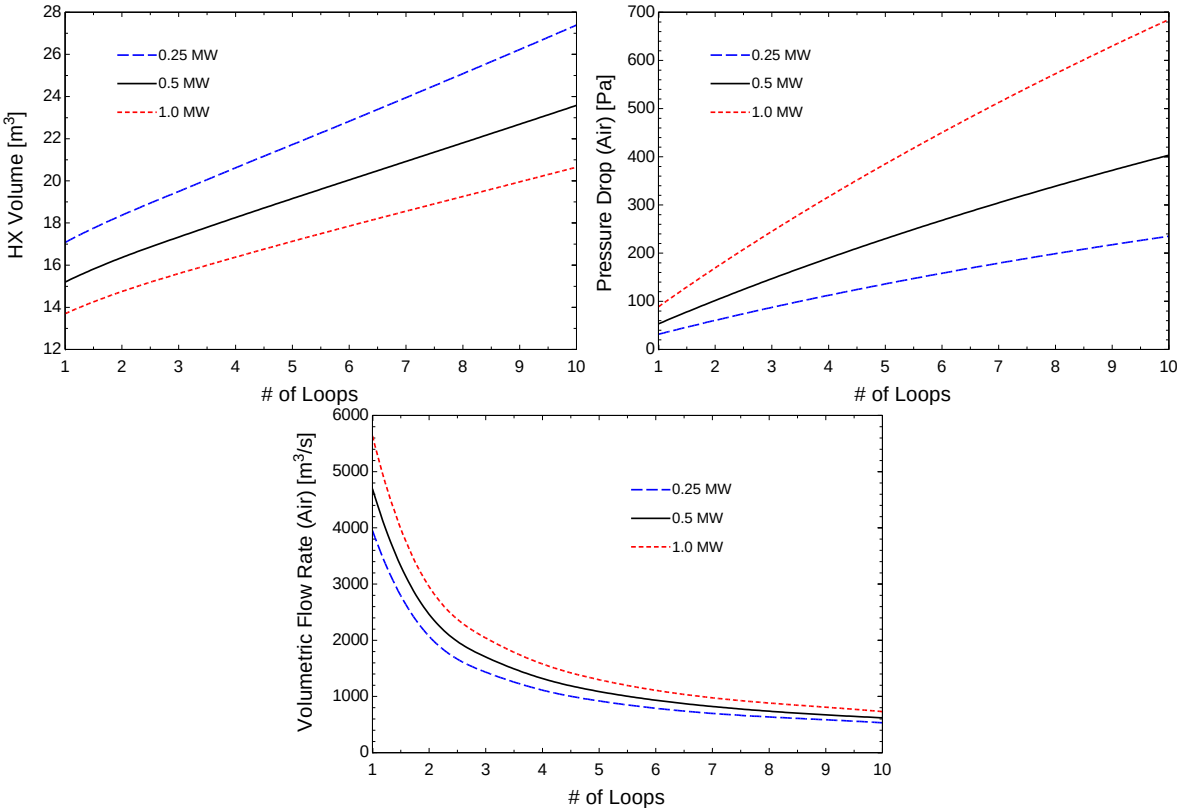

Figure 82: Heat exchanger volume, air-side pressure drop, and volumetric flow rate as a function of CO2 passes at various values of fan power

Increasing fan power increased pressure drop and volumetric flow rate which resulted in a decrease in the overall size of the heat exchanger. The opposite occurred with a decrease in fan power and were results to be expected.

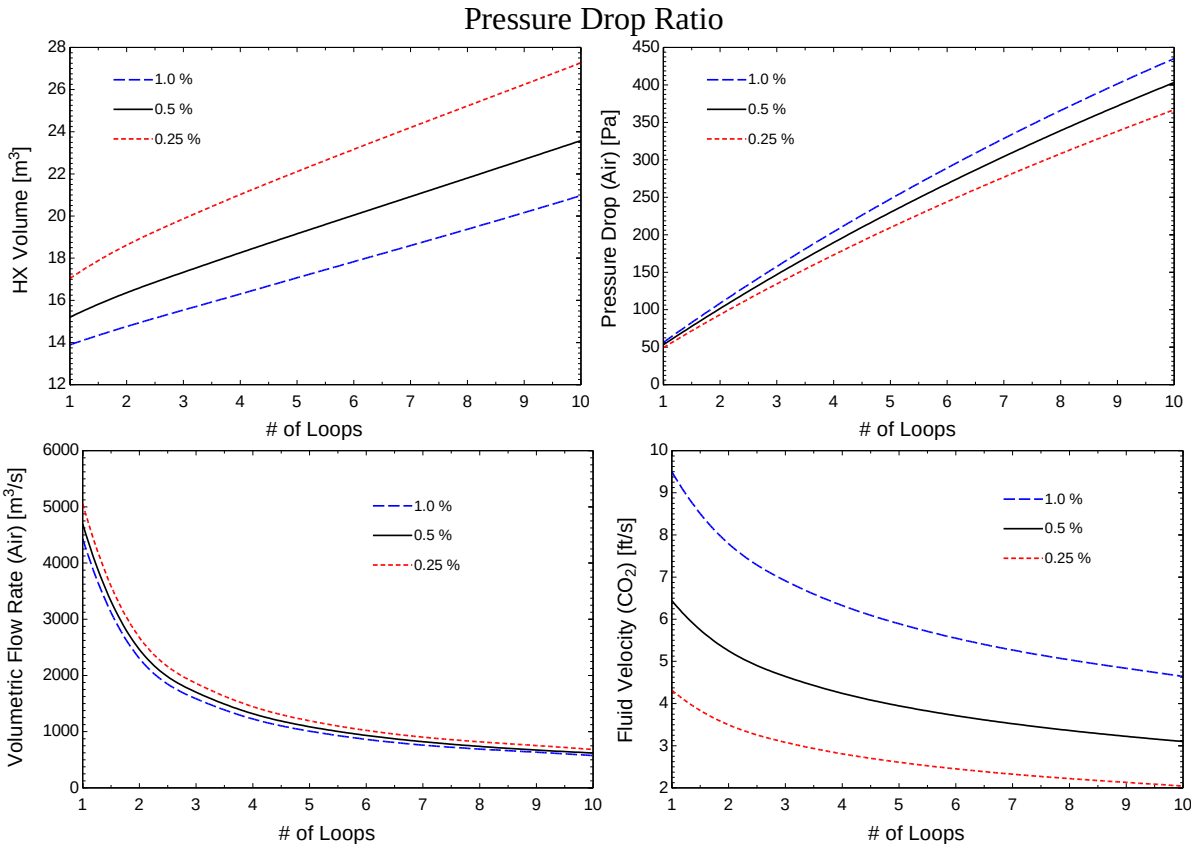

Figure 83: Heat exchanger volume, air-side pressure drop, volumetric flow rate, and fluid velocity as a function of CO2 passes at various values of pressure drop ratio

Increasing pressure drop ratio of the CO_2, had little effect on the air-side pressure drop and volumetric flow rate, as would be expected. It did, however, significantly affect the CO_2 fluid velocity. An increase in fluid velocity results in larger Reynolds number and increased heat transfer coefficient. With increased convection on the CO_2 side, less required surface area and heat exchanger volume would be expected.

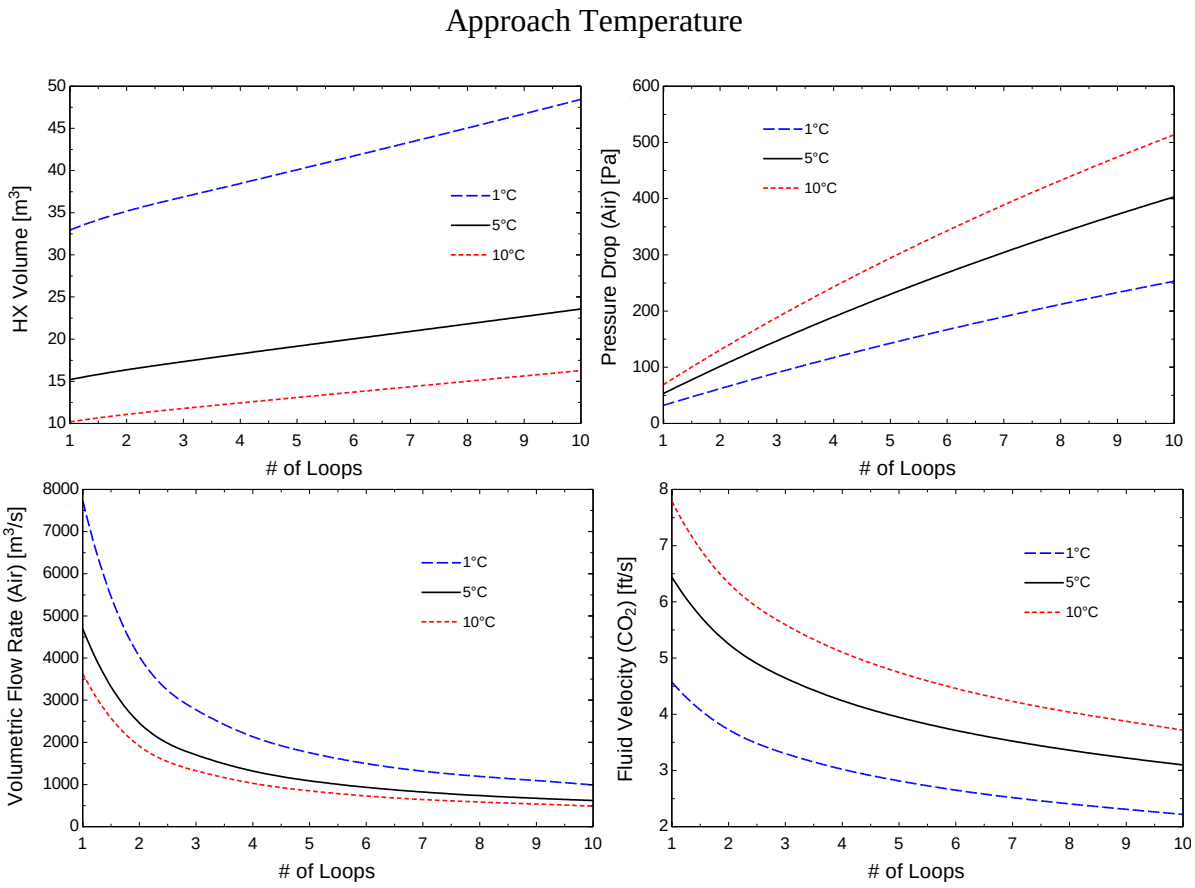

Figure 84: Heat exchanger volume, air-side pressure drop, volumetric flow rate, and fluid velocity as a function of CO2 passes at various values of approach temperature

The approach temperature difference is an important parameter. Basic heat exchanger knowledge says that as the "approach temperature" difference, defined as the difference between hot outlet and cold inlet temperatures, goes to zero, the size of the heat exchanger will increase toward infinity. The plots show that at 1 C approach the heat exchanger becomes massive and with a 10 C approach, the heat exchanger becomes smaller. This is also seen in Figure 85, where the number of CO_2 passes is held constant at 5 and the only input varied is the outlet CO_2 temperature.

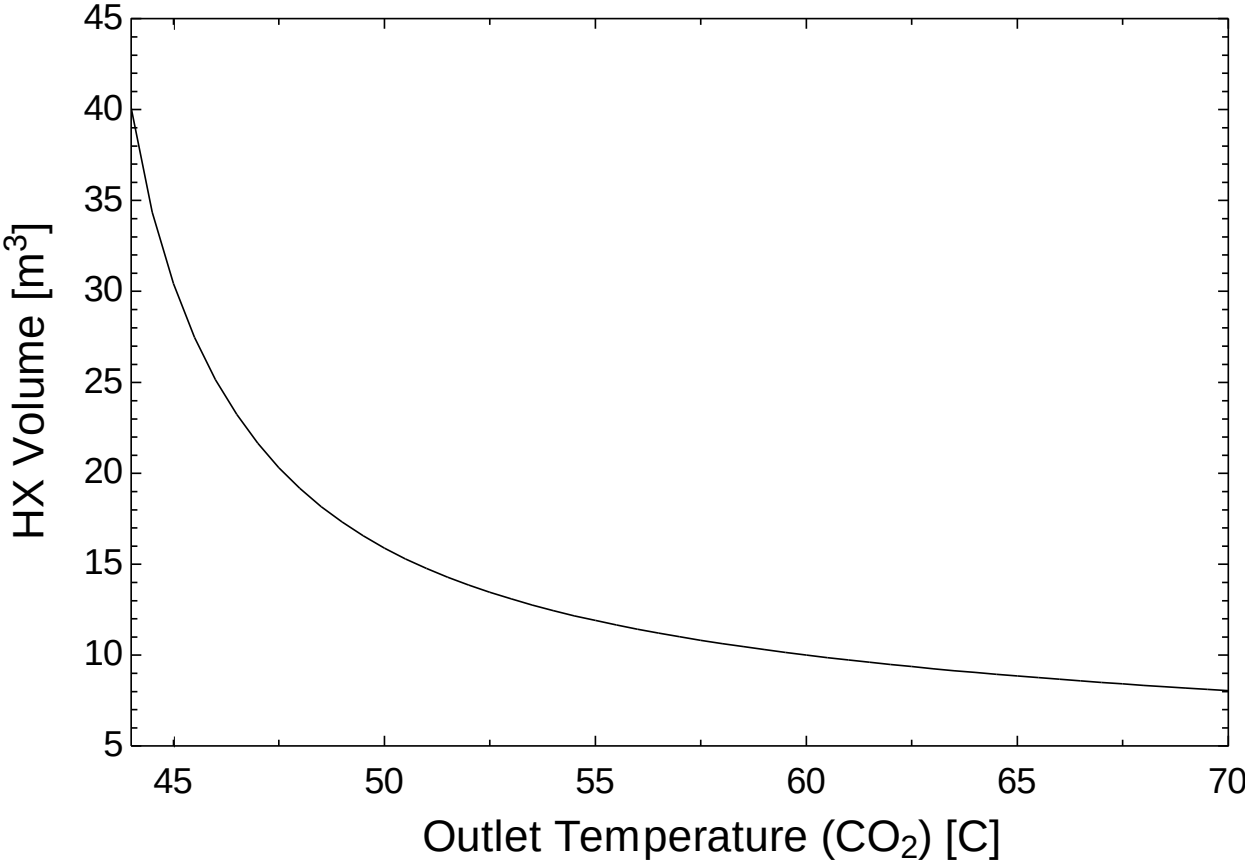

Figure 85: Heat exchanger volume as a function of outlet CO_2 temperature

A hybrid configuration might be very beneficial where a compact and more efficient water-cooler could be used to split the heat load between an air-cooler and water-cooler in series. If the air-cooler is set first in the series, the "approach temperature" difference is significantly increased allowing for a much smaller air-cooler. The rest of the cooling would then be finished by the more efficient water cooler. The hybrid configuration potentially reduces capital costs and water usage, while mitigating the disadvantages of having a less efficient air-cooler.

6 HYBRID CONFIGURATION

The Brayton cycle rejects heat to the ambient environment using air, water, or a hybrid arrangement that employs both fluids. Cooling with water, from a cooling tower, provides higher and more consistent Brayton cycle thermal efficiencies year-round, while also leading to lower capital costs for the heat exchanger equipment when compared to air-cooling. However, a major concern with water-cooling, especially for solar thermal applications, is the large amount of water required for the heat rejection coincident in plant locations where there is limited availability of water.

The alternative to direct water-cooling is a hybrid configuration that combines both water and air-cooling processes, with the main goal of reducing water usage. A hybrid configuration can take advantage of the variation in ambient conditions that occur year round. On hot days, the performance of the system can be enhanced by reducing the heat load in the air-cooler and increasing the heat load in the water-cooler. The hybrid configuration would require a smaller water cooler than a wet-cooled plant and a smaller air cooler than an air-cooled plant. Although the hybrid configuration is typically more expensive than a water-cooled plant, it should be less expensive than an entirely air-cooled plant (US Department of Energy, 2007).

In the Brayton cycle using carbon dioxide, the precooler can be configured to take advantage of the high CO_2 temperatures by arranging the heat rejection system into two heat exchangers, a water and air-cooler, each set in series. The advantage of the hybrid configuration for the Brayton cycle lies with the air-cooler being set first in the series followed by the water-cooler, resulting in higher cycle efficiencies, reduced water use, and potentially lower equipment cost. Figure 86 illustrates the components required for a hybrid configuration and how it is setup.

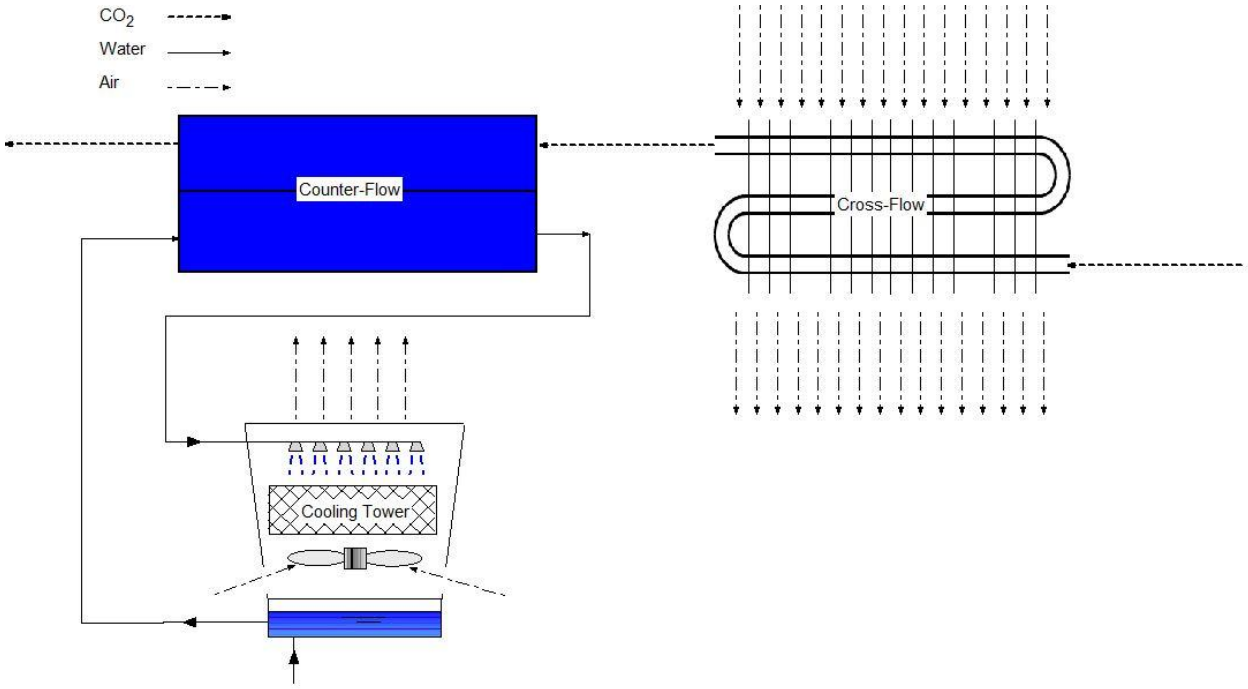

Figure 86: Schematic of hybrid configuration w/ cooling tower

The size of the air-cooler can be significantly reduced by increasing the approach temperature. The size of the air-cooler has been found to be more sensitive to the approach temperature, when compared to the more physically compact water-cooler. The water-cooler operates at a lower heat sink temperature (i.e., the wet bulb temperature) and completes the heat rejection from CO_2. It is sized and operated to reduce the CO_2 temperature to the desired condition for the compressor inlet.

6.1 Model coupling

The models for the air cooler, water cooler, and cooling tower have previously been developed as three separate models. By coupling the three models into one, it allows for analysis on the hybrid configuration as a solution for Brayton cycle cooling. The model will also have the ability to test either all water-cooling or air-cooling, which provides a powerful tool for analysis of different cooling scenarios. Figure 87 shows the main GUI that illustrates the entire schematic of the hybrid configuration process and indicates the linkage between models.

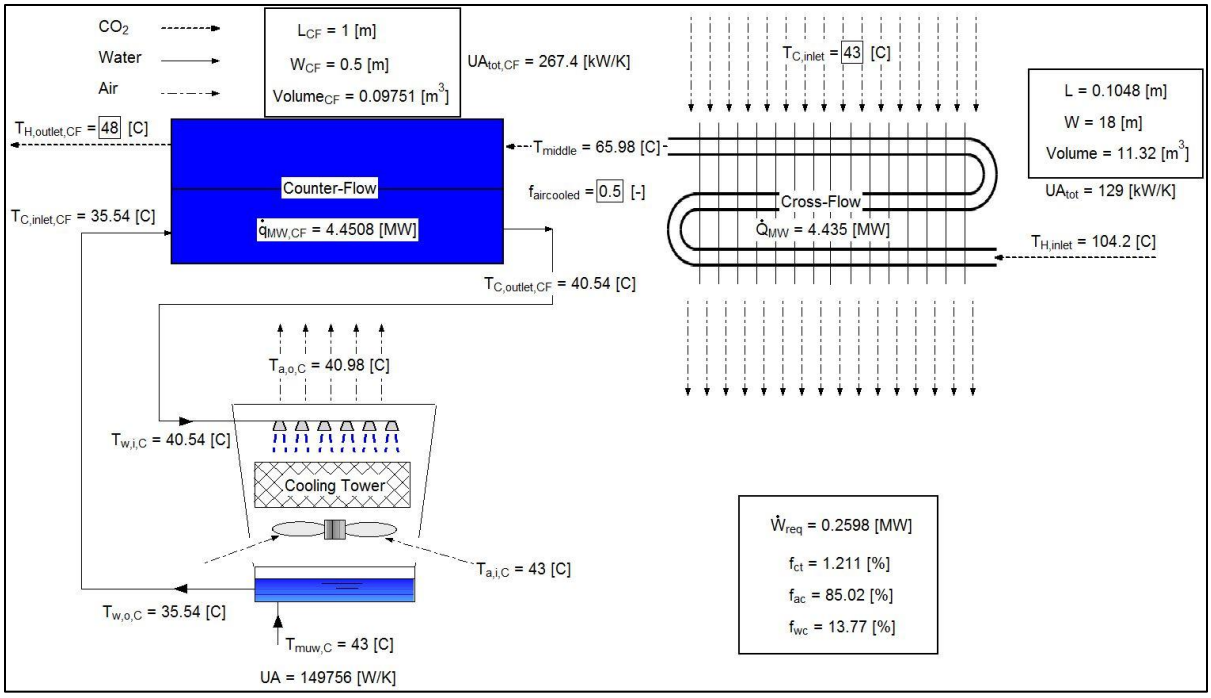

Figure 87: Main GUI for the hybrid configuration model

The addition of seven equations is required to link the three models, Equations 6.1 to 6.7:

Air cooler to water cooler:

$$\dot{m}_{CO2,AC} = \dot{m}_{CO2,WC} \quad 6.1$$

$$T_{CO2,out,AC} = T_{CO2,in,WC} \quad 6.2$$

$$P_{CO2,out,AC} = P_{CO2,in,WC} \quad 6.3$$

Water cooler to cooling tower:

$$\dot{m}_{water,WC} = \dot{m}_{water,CT} \quad 6.4$$

$$T_{water,in,WC} = T_{water,out,CT} \quad 6.5$$

$$T_{water,out,WC} = T_{water,in,CT} \quad 6.6$$

Air cooler to cooling tower:

$$T_{air,in,AC} = T_{air,in,CT} \quad 6.7$$

The addition of the seven equations allows for the three models to run simultaneously and track the performance of each component. Figure 88, Figure 89, and Figure 90 represent the GUI's for the water cooler, air cooler, and cooling tower, respectively. Each GUI window can be accessed from the main GUI by clicking on the respective component.

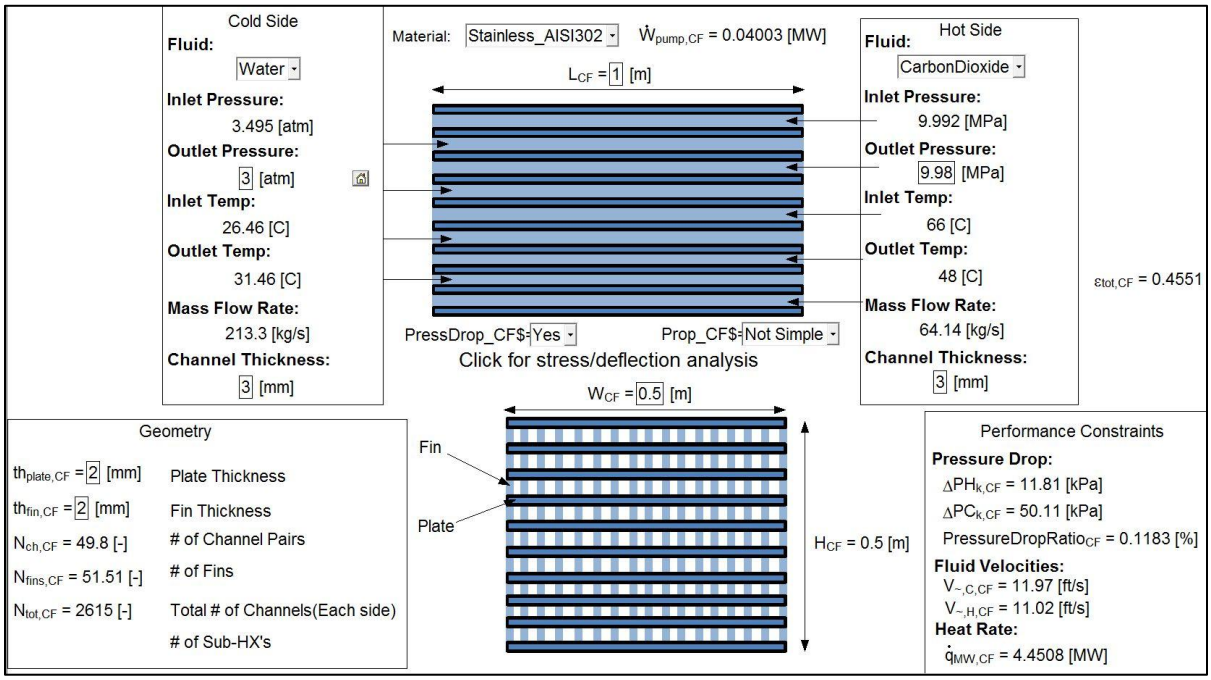

Figure 88: GUI for the water cooler component for the hybrid configuration model

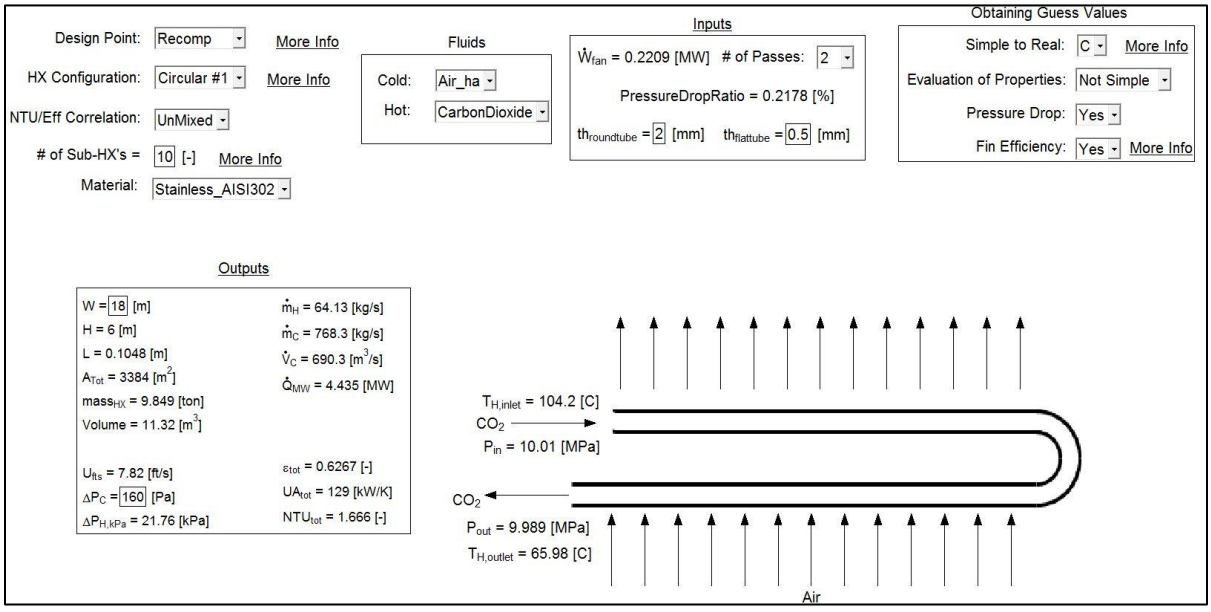

Figure 89: GUI for the air cooler component for the hybrid configuration model

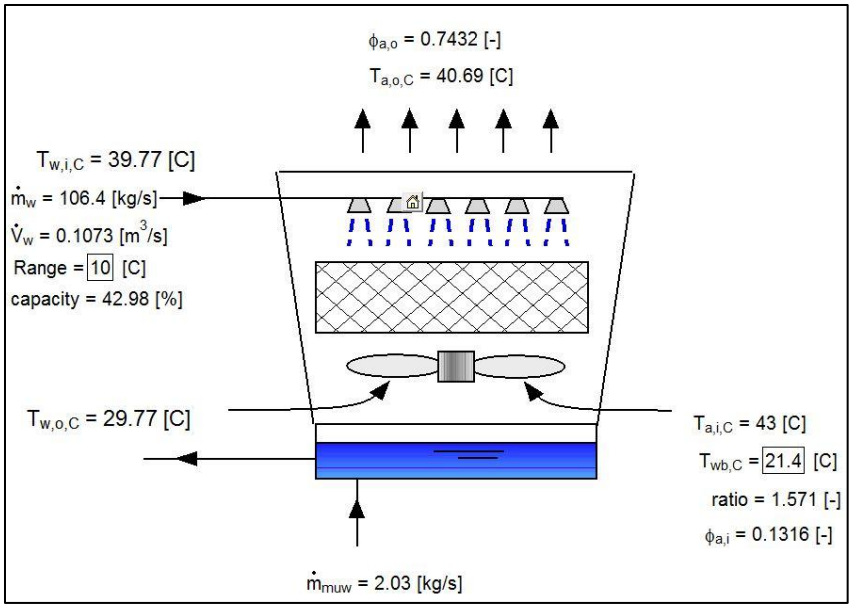

Figure 90: GUI for the cooling tower component for the hybrid configuration model

6.2 Model inputs and performance constraints

The model was first run with on-design conditions in mind. The on-design conditions meant that the model would run under certain inputs and performance constraints that would allow the size of the heat exchangers to float. Depending on certain conditions such as varying ambient temperature or varying the heat load imparted on each component, the model will output the size and power input required for each component.

The major performance constraint that was held constant for all of the simulations to follow was the use of the recompression design point, which was one of three design points discussed earlier in Chapter 1. The recompression design point not only produced the best results from earlier tests on the air cooler heat exchanger, but it is also the point of interest for the work being done by John Dyreby, who provided the three design points (Dyreby, 2012). Refer to Figure 2 and Table 1 from Chapter 1 for a summary of the recompression design point. By selecting a design point, it establishes the carbon dioxide mass flow rate by knowing the total heat load, outlet pressure, and inlet and outlet temperatures.

The advantage of the hybrid configuration is related to the fact that the size of the air cooler can be reduced by increasing the approach temperature. For cooling, the approach temperature is defined as the difference between the temperature of the hot fluid exiting the heat exchanger and the temperature of the cold fluid entering the heat exchanger.

The approach temperature can be varied two ways, in the case of the hybrid configuration. Either the fluid temperature between the two heat exchangers is set or the fraction of heat load for each heat exchanger is set. In the tests to follow, a variable representing the fraction of air cooling (f_{AC}) was established as the control knob for the approach temperature. The fraction of air cooling establishes the fraction of the total constrained heat load applied to the air cooler and the rest is applied to the water cooler/cooling tower. If the fraction of air cooling increases, the approach temperature for the air cooler decreases, and vice versa. Knowing the total heat load to be shared by the water cooler and air cooler, setting a fraction of air cooling allowed for the calculation of the heat load to be applied to each component. Setting the fraction of air cooling also means that the model now can represent three different cooling scenarios: all water cooling ($f_{AC} = 0$), all air cooling ($f_{AC} = 1$), and hybrid cooling ($0 < f_{AC} < 1$). This will be the method of comparing the different cooling scenarios later in the thesis.

6.2.1 Water cooler

The water cooler model requires several parameters and performance constraints in addition to the design point and fraction of heat load applied at a system level. Table 25 summarizes the values of these additional inputs that were used in the on-design simulations.

Parameters	Performance Constraints
Channel Heights = 3 [mm]	Outlet CO_2 Pressure = 9.98 [MPa]
Plate thickness = 2 [mm]	Outlet CO_2 Temperature = 48 [C]
	Inlet Water Temperature = 30 C
	Pressure Drop Ratio of CO_2 (Total for both air-cooler and water-cooler) = 0.5 %

Table 25: On-design water cooler inputs

For the water cooler, there are geometry constraints found through a design study that minimized the mass of the heat exchanger. In the design study, it was found that channel heights and plate thickness were driven to as small as possible to minimize mass. The channel heights are driven to as small as possible because the heat transfer coefficient increases inversely with channel cross-sectional area (Kirby & Rumbold, 2009). Plate thickness was driven to low values because of its proportionality to conduction resistance and its reduction in material. A simple stress/deflection analysis found that a 1 mm plate thickness would hold the required pressures.

Typical micro-channel heat exchangers currently being developed have ranges of 0.2 mm to 5 mm for width and height of channels and 0.5 mm to 5 mm for plate thickness (Kirby & Rumbold, 2009). These same micro-channel heat exchangers were rated up to 55 MPa of pressure.

The outlet CO_2 pressure and temperature are set according to the recompression design point. The last constraint was the pressure drop ratio of the CO_2, which is defined as the pressure drop over the inlet pressure of the CO_2. This constraint was selected to keep the fluid velocities in a reasonable range between 5 and 15 ft/s (i.e., 1.5 and 4.6 m/s). The inlet water temperature and pressure drop ratio constraints are removed when the heat exchanger sizes are set in the later off-design simulations.

6.2.2 Air cooler

The air cooler also requires several parameters and performance constraints that are summarized in Table 26.

Parameters	Performance Constraints
HX Configuration: Circular #1	Inlet Air Temperature = 43 [C]
# of tube passes = 2	Inlet CO_2 Temperature = 104.2 [C]
Tube wall thickness = 2 [mm]	Pressure Drop of Air = 160 [Pa]
Width (parallel to CO_2 flow) = 3 times Height (perpendicular to CO_2 flow)	Pressure Drop Ratio of CO_2 (Total for both air-cooler and water-cooler) = 0.5 %

Table 26: On-design air cooler inputs

The first parameter is the HX configuration type from the compact heat exchanger library, which was previously discussed in Chapters 4 and 5. Configuration "Circular #1" was selected due to its performance in the design study performed in Chapter 5 as well as it being one of the only configuration with a tube diameter of approximately 25 mm (i.e., approximately 1.0"). According to a review by API, by far the most common tube diameter used by air-cooled heat exchanger venders (ACHE) is 25 mm (i.e., approximately 1.0") (API, 2006). API 661 also says that stainless steel tube walls must be at least 1.6 mm thick.

The number of tube passes (in the direction of air flow) was set to 2, which is typical in air cooler designs (API, 2006). The last parameter was constraining the height of the ACHE to 3 times smaller than the width. This aspect ratio is common practice for ACHE to help reduce the header size, which is typically the most expensive part of the air cooler (GEA, 2011).

The inlet air temperature is set at 43 C which is one of the higher ambient temperatures seen throughout the year in Daggett, CA. This temperature is varied to see its effect on performance in Section 6.7. The inlet CO_2 temperature is set according to the recompression design point. The pressure drop was constrained to 160 Pa which was found to be a typical pressure drop for a 2 pass ACHE (GEA, 2011). The pressure drop ratio constraint for the CO_2 was discussed earlier about controlling the fluid velocities in Chapter 6.2.1. The pressure drop ratio constraint is replaced by specifying the heat exchanger dimensions in the later off-design simulations.

6.2.3 Cooling tower

The additional performance constraints required by the cooling tower are summarized in Table 27. For a detailed look at how the cooling tower model was developed, refer to Chapter 3 in the thesis.

Performance Constraints
Range (water) = 10 [C]
Inlet wet bulb temperature = 21.4 [C]
Inlet dry bulb temperature = 43 [C]
Outlet Water Temperature = 30 [C]

Table 27: On-design inputs to the cooling tower

The range for the cooling tower, which is defined as the difference between the inlet and outlet water temperatures, was set to 10 C. This has been found to be a typical value for the temperature difference across a water cooler (GEA, 2011). The mean coincident value for the wet bulb temperature at dry bulb of 43 C was found to be 21.4 C from the TMY2 data in Daggett, CA. The outlet water temperature was set at 30 C to establish a minimum approach temperature for the cooling tower of around 8 C, which is slightly greater than the minimum recommended approach according to GEA Heat Exchangers (GEA, 2011). The inlet air temperature was set equal to the air cooler inlet air temperature and will also be varied to see its effect on performance.

6.3 On-design performance curves

Given the previous set of input conditions, the model can be run for multiple fractions of air cooling in order to track how the hybrid configuration and each component performs. By selecting a fraction of air cooling the heat load for each heat exchanger is set. The model then solves for the heat exchanger sizes, water and air mass flow rates, and power required by the water pump and fans in the cooling tower and air cooler.

Figure 91 shows the total required power as a function of the fraction of air cooling. The total required power includes the fan power for the air cooler and cooling tower, as well as the total water pump power from the cooling tower and water cooler. As seen by Figure 91, the total required power is significantly higher for the air cooler when compared to the water cooler, due to the size of the fan required by the air cooler. This can also be seen with the percent of total required power for the air cooler, cooling tower, and water cooler. Percent of total required power is defined as:

Total required power:

$$\dot{W}_{tot,req} = \dot{W}_{AC,fan} + \dot{W}_{WC,pump} + \dot{W}_{CT,fan} + \dot{W}_{CT,pump} \quad 6.8$$

Air cooler:

$$F_{AC} = \frac{\dot{W}_{AC,fan}}{\dot{W}_{tot,req}} \quad 6.9$$

Water cooler:

$$F_{WC} = \frac{\dot{W}_{WC,pump}}{\dot{W}_{tot,req}} \quad 6.10$$

Cooling tower:

$$F_{CT} = \frac{\dot{W}_{CT,fan} + \dot{W}_{CT,pump}}{\dot{W}_{tot,req}} \quad 6.11$$

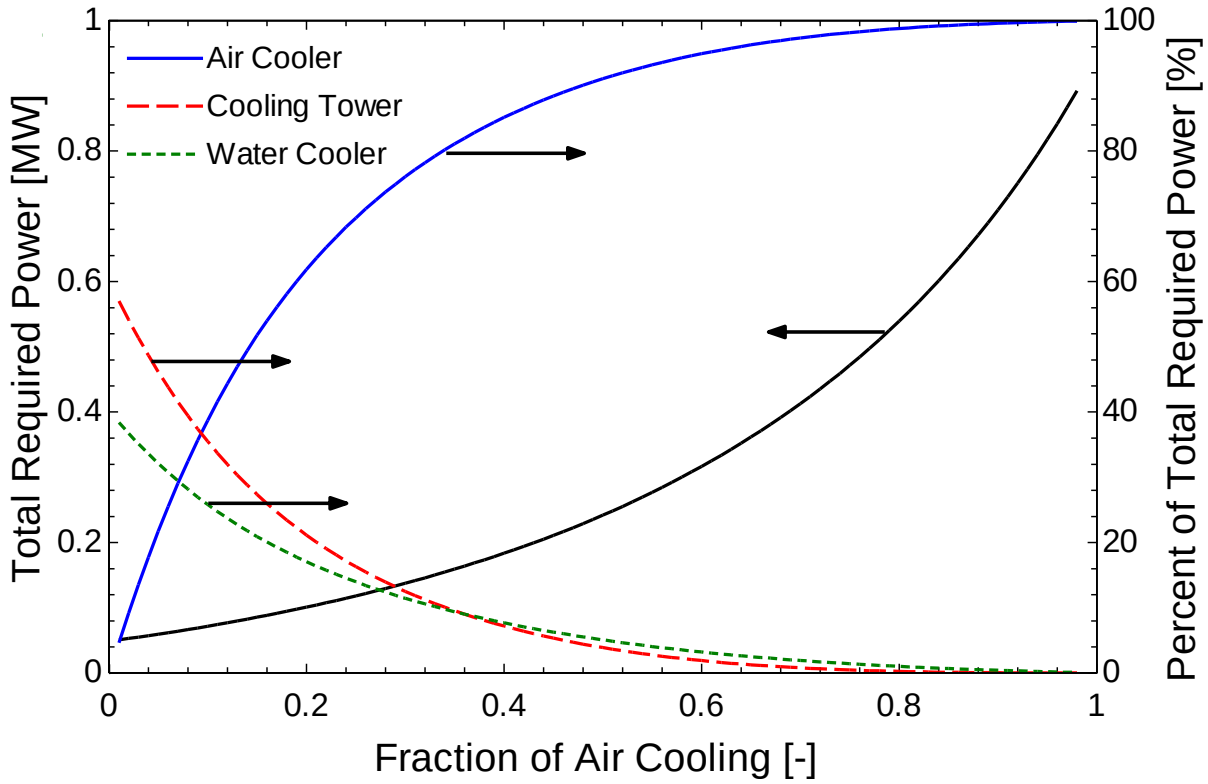

Figure 91: Total required power and percent of total required power for the air cooler, cooling tower and water cooler as a function of the fraction of air cooling

The cost of water that is being lost through the cooling tower must be considered. Figure 92 shows both the total required power and the cooling tower makeup water as a function of the fraction of air cooling. The plot shows that there is the tradeoff between the water use and required power input.

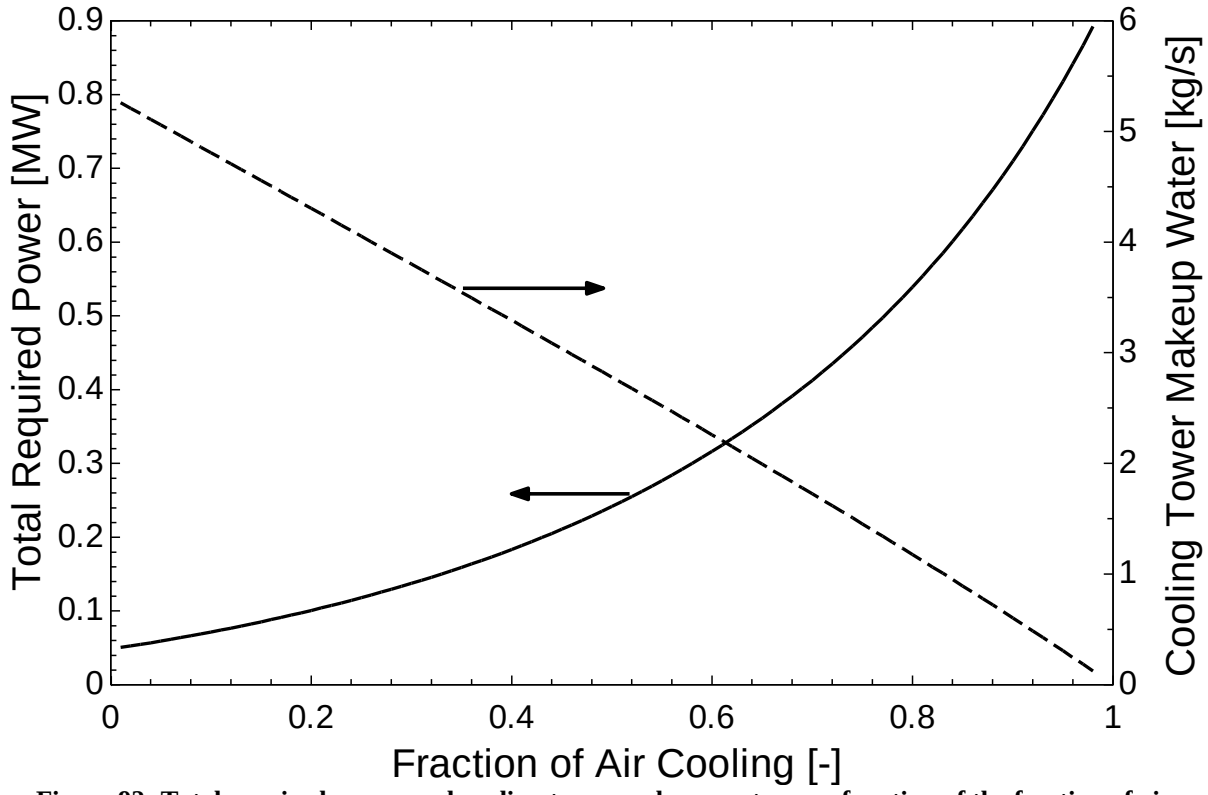

Figure 92: Total required power and cooling tower makeup water as a function of the fraction of air cooling

The total cost of the required power and make up water can be examined in order to see if there is an optimal point for operating the hybrid configuration.

The cost of electricity is usually presented as dollars per kilowatt-hour. The price of electricity can vary depending on where it is being purchased from, as can be seen by Figure 93. The U.S. average cost for electricity is around $0.1 per kW-hr (U.S. Energy Information Administration, 2010). The following tests will use a range of electricity cost from $0.05 to $0.25 per kW-hr.

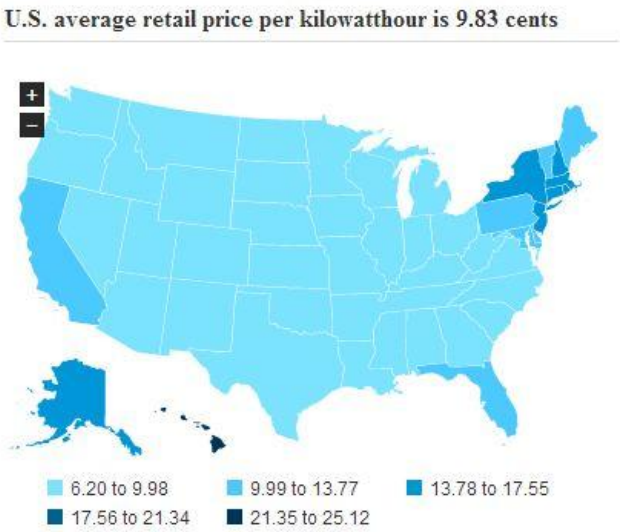

Figure 93: Cost of electricity across the United States (U.S. Energy Information Administration, 2010)

The cost of water is harder to define. The California Energy Commission (CEC) estimates water cost at $1.00 to $2.50 per 1,000 gallons (California Energy Commission, 2006). This estimate is based solely on the value of the water and the range is given depending on where the water is being purchased. The CEC also gives an "equivalent cost" of water at $3.00 to $5.00 per 1,000 gallons (California Energy Commission, 2006). This equivalent cost includes the value of water as well as other elements like the cost of water delivery, piping installation, well maintenance, etc. Given this information, a reasonable range of water cost to be tested is $1.50 to $4.00 per 1,000 gallons.

The initial investigation uses electrical and water costs of $0.1 per kW-hr and $3 per 1,000 gal, respectively. The ambient air temperature was also varied to see its effect on the performance. Figure 94 shows that there is an optimal value for the fraction of air cooling, which for the 43 C ambient dry bulb case is around 0.37. It also shows that as the ambient temperature is decreased the fraction of air cooling matters less and less. As the cooling fluid (i.e., air) temperature decreases, both systems (air cooling and water cooling) become more efficient. At 43 C, the approach temperature is small and the cost to run the precooler is almost double at some conditions when compared to 30 C or 20 C.

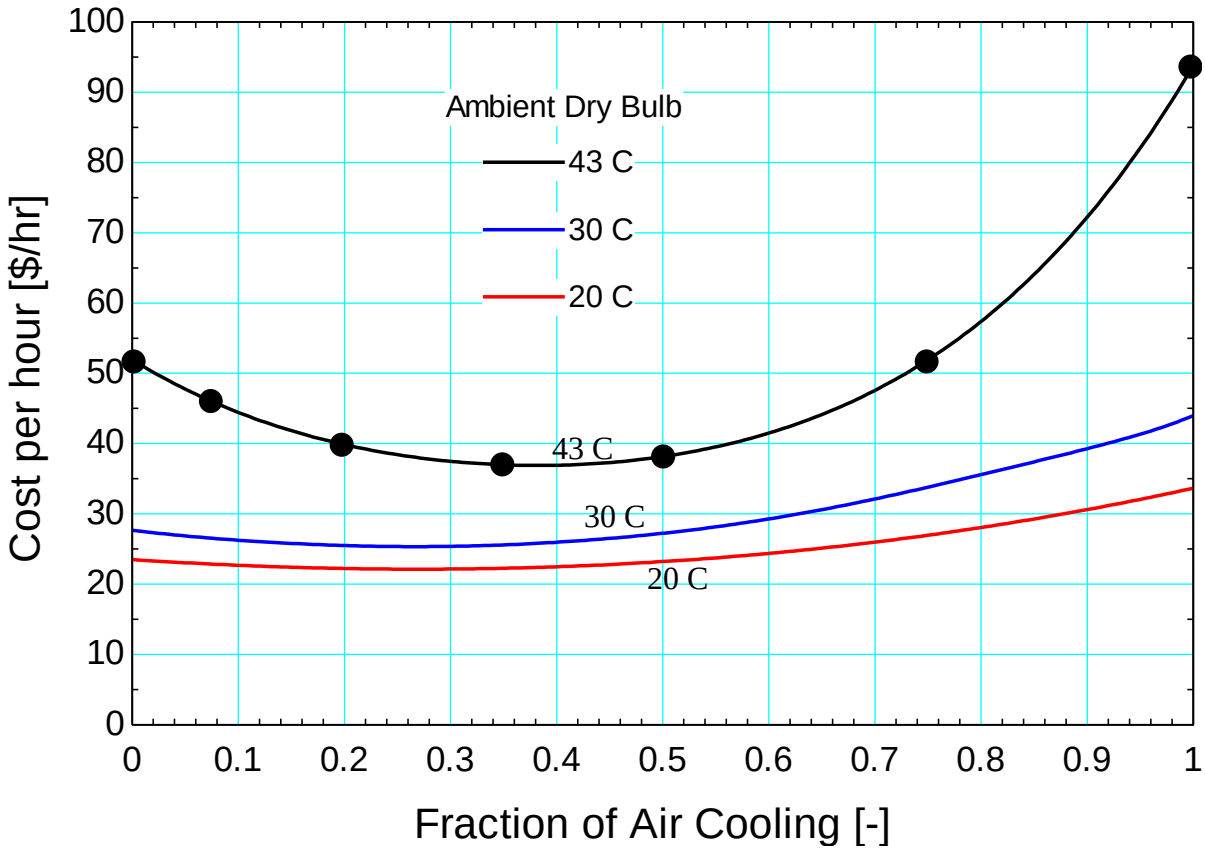

Figure 94: Operating cost per hour as a function of the fraction of air cooling at various ambient dry bulb temperatures

These results show that there is an advantage to using the hybrid configuration. This investigation allowed the size of the heat exchangers to vary in size to meet the performance requirements constrained in the inputs. Also, this result is only for one set of costs for electricity and water.

The hybrid configuration can take advantage of the varying ambient conditions seen year-round. On the hottest days it can use the more efficient water cooler, while on colder days it can reduce its water usage by using the air cooler. On a system level, the size of the heat exchangers would be established and remain fixed throughout the year. Operating conditions would be set at the optimal fraction of air cooling where the minimum cost per hour occurs for that ambient condition.

Selecting a point on one of the curves in Figure 94 establishes the size of the heat exchangers required to meet that load at the specific design point. The 43 C curve was selected as it would guarantee that the total required load would be met by the specified sized heat exchangers. Seven points were selected, as shown in Figure 94, corresponding to fractions of air cooling of 0.0 (no air cooling), 0.075, 0.2, 0.35, 0.5, 0.75, and 1.0 (no water cooling). Off-design simulations can be run to see how each design performs on a yearly basis. Using weather data for Daggett, CA, the model varies the fraction of air cooling, at each ambient condition in order to find the minimum value of cost per hour.

6.4 Capital investment analysis

For large scale power production, the heat exchangers represent a major portion of the total cost to run and purchase the facility. It is important to have a valid and relatively simple way to estimate the cost of the three components in the hybrid configuration in order to be able to do a cost analysis on the system.

In 2002, the DOE did an analysis to assist engineers and scientists in performing rapid cost estimates on typical components for system studies done on new processes (DOE/NETL, 2002). The DOE prepared a report with generic cost curves that provide purchased equipment cost as a function of a capacity variable. In the report they include cost curves for typical air coolers, water coolers, and cooling towers. The purchased cost given by the curves is in 1998 dollars, so a conversion factor is used, called the Chemical Engineering Plant Cost Index, *Equipment Index,* to escalate the cost to 2011 (DOE/NETL, 2002). The *Equipment Index*, for 1998 to 2011 is:

$$Dollars_{2011} = Dollars_{1998} * \left(\frac{724}{436}\right) \qquad 6.12$$

The curves were used to estimate the cost of the three components at the seven designated design points selected from Figure 94. The curves for the air cooler, water cooler, and cooling tower can be found in Figure 95, Figure 96, and Figure 97, respectively. In each of the figures, the image on the top represents the actual cost curve produced by DOE and the

image on the bottom is a curve fit to the actual curves. This curve fit allowed for fast and easy calculation of the purchased cost given the certain capacity variable.

The air cooler cost curve, Figure 95, requires the bare tube area, which is the surface area of just the tubes on the air cooler, excluding the area of the fins.

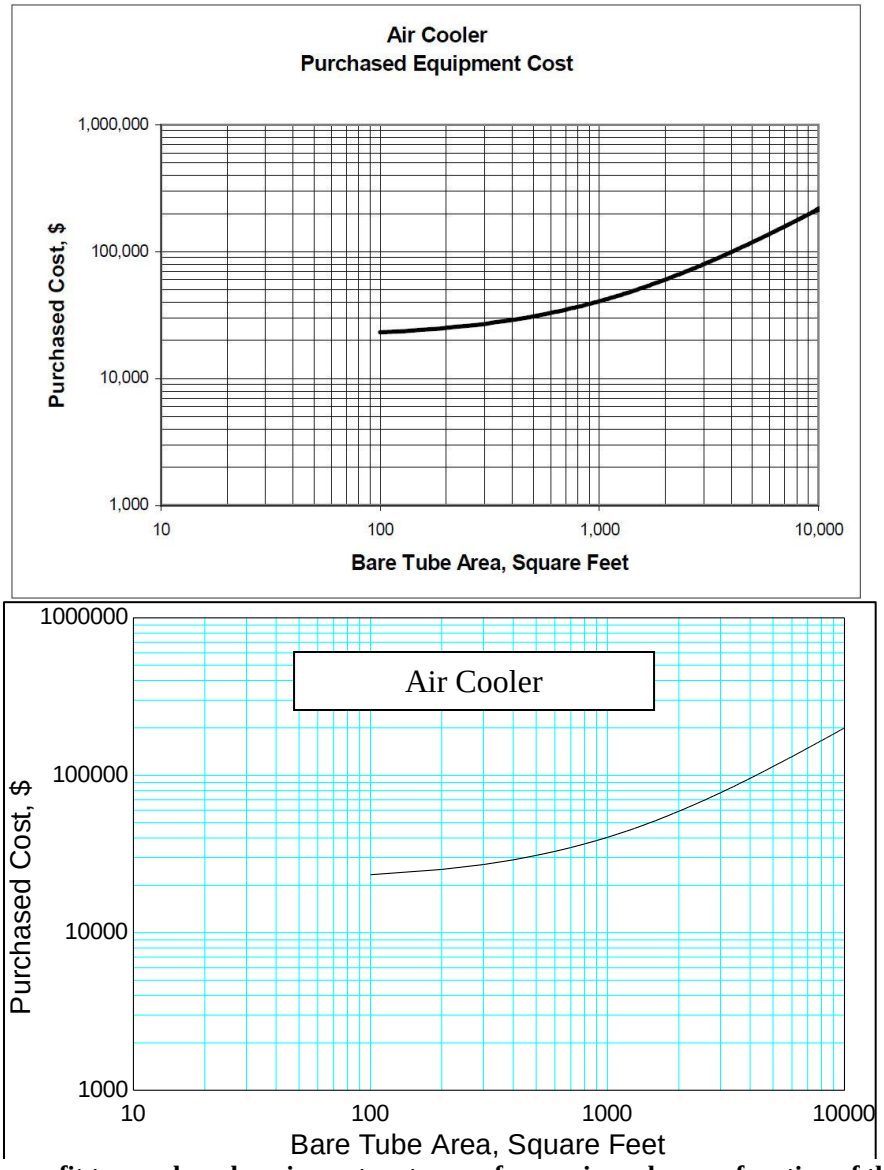

Figure 95: Curve fit to purchased equipment cost curve for an air cooler as a function of the bare tube area (DOE/NETL, 2002)

The total area of the heat exchanger can easily be found using the compact heat exchanger library in EES (Klein, 2011) as a function of the heat exchanger volume (L*W*H) and α (the ratio of the total surface area to heat exchanger volume). The total surface area is then equal to:

$$A_{total} = (L * W * H) * \alpha \qquad 6.13$$

The compact heat exchanger library also provides the ratio of fin area to total surface area, A_{fin}/A_{total}. So the bare tube area can be found using:

$$A_{bare\ tubes} = A_{total} * \left(1 - \frac{A_{fin}}{A_{total}}\right) \qquad 6.14$$

The water cooler cost curve is actually an estimate for a shell and tube heat exchanger, as there was no curve for compact heat exchangers. It was felt that the cost curve for a shell and tube heat exchanger would be similar to the heat exchanger being evaluated in the model. With that in mind, the cost curve required the total surface area of the heat exchanger as the capacity variable. This variable is very simple as it is an output of water cooler model because it is necessary in fundamental calculations within the model.

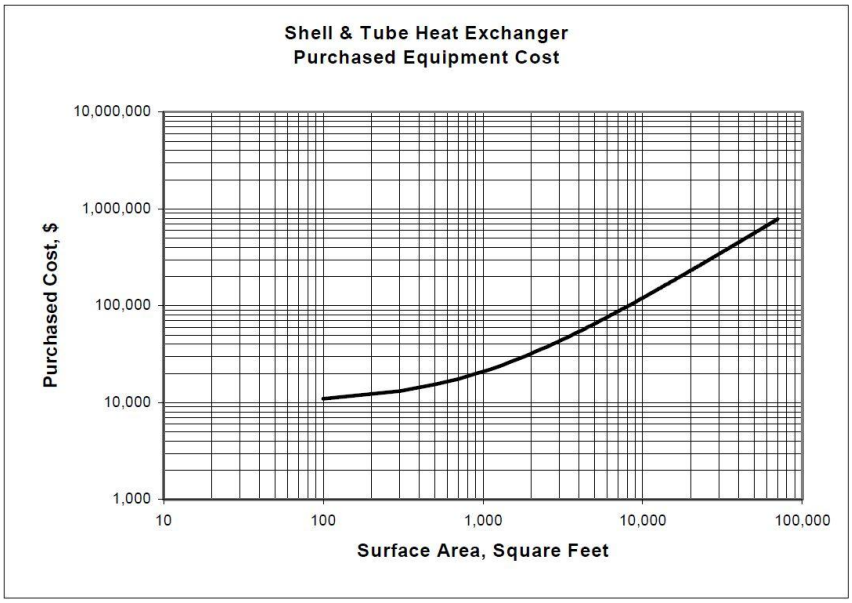

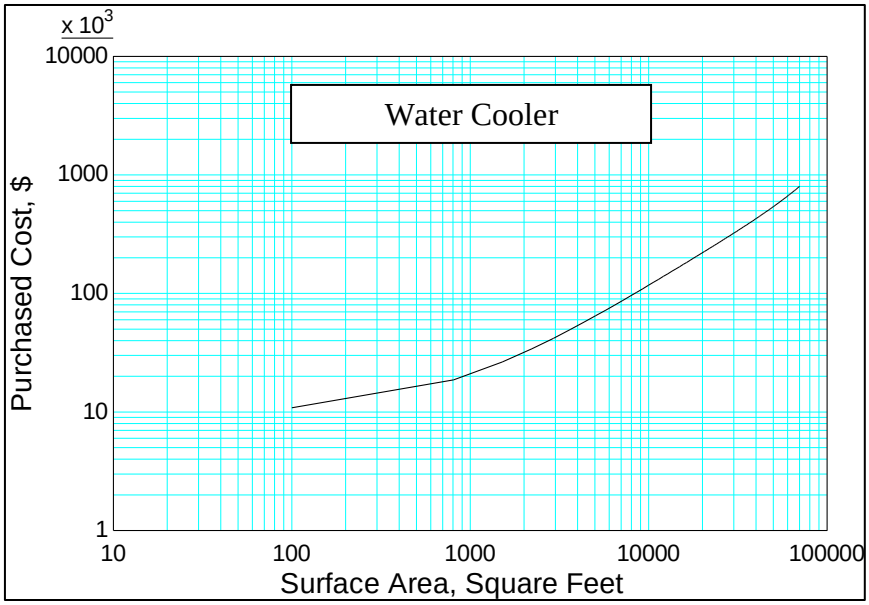

Figure 96: Purchased equipment cost curve for a water cooler as a function of the total heat exchanger surface area (DOE/NETL, 2002)

Looking at the cost curves, the water cooler is the least expensive component of the three as well as being the least affected when it comes to the size required to meet the load. The analysis assumes one sized water cooler that would meet the required load no matter what fraction of air cooling the analysis was running at. This assumption was made based on the results from the on-design tests which showed that the precooler size varied only slightly, for a wide range of conditions.

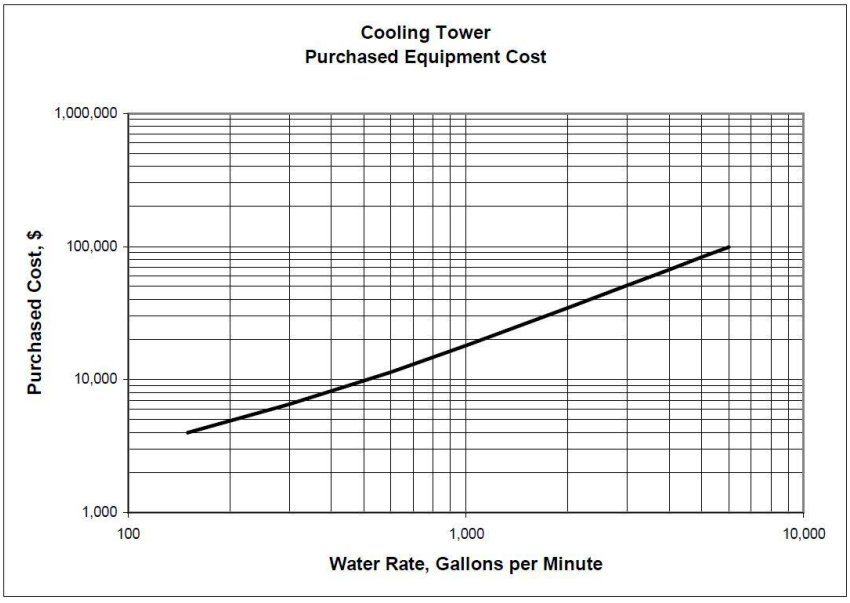

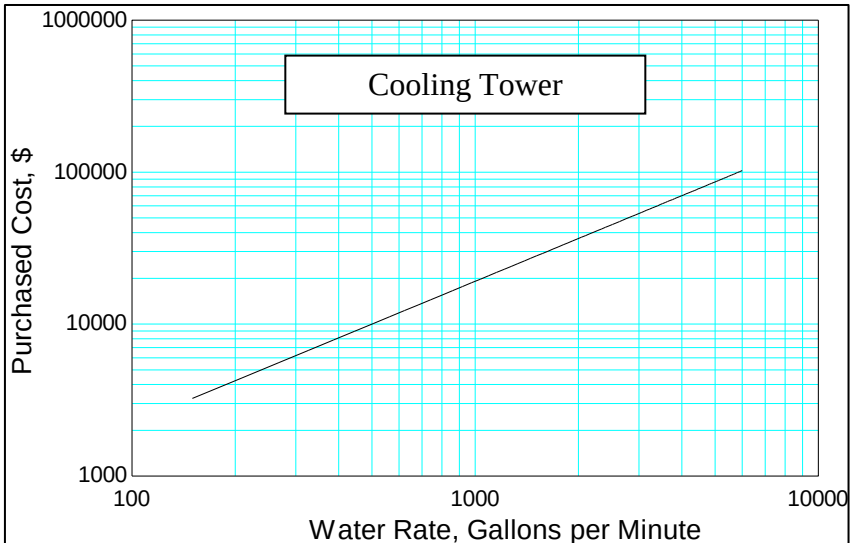

Figure 97: Purchased equipment cost curve for a cooling tower as a function of the water flow rate (DOE/NETL, 2002)

The cooling tower cost curve requires only the water flow rate, which is required for calculation of cooling tower performance. The cooling tower model uses data from actual performance data from a Baltimore Aircoil Company tower, model 31301C (Baltimore Aircoil Company, 2011). The assumption in the following analysis is that the model representing this specific tower scales so that the performance estimates are provided for other cooling tower sizes. From Figure 94, each design point is assuming a different sized cooling tower based solely on the capital purchase cost curve which is a function of water flow rate. As the value of the fraction of air cooling increases, the cooling tower size (cost) decreases.

With good estimates of the purchase cost for each heat exchanger at each of the seven design points, a bar plot was produced to show the spread from 0 to 1 fraction of air cooling. This can be seen in Figure 98.

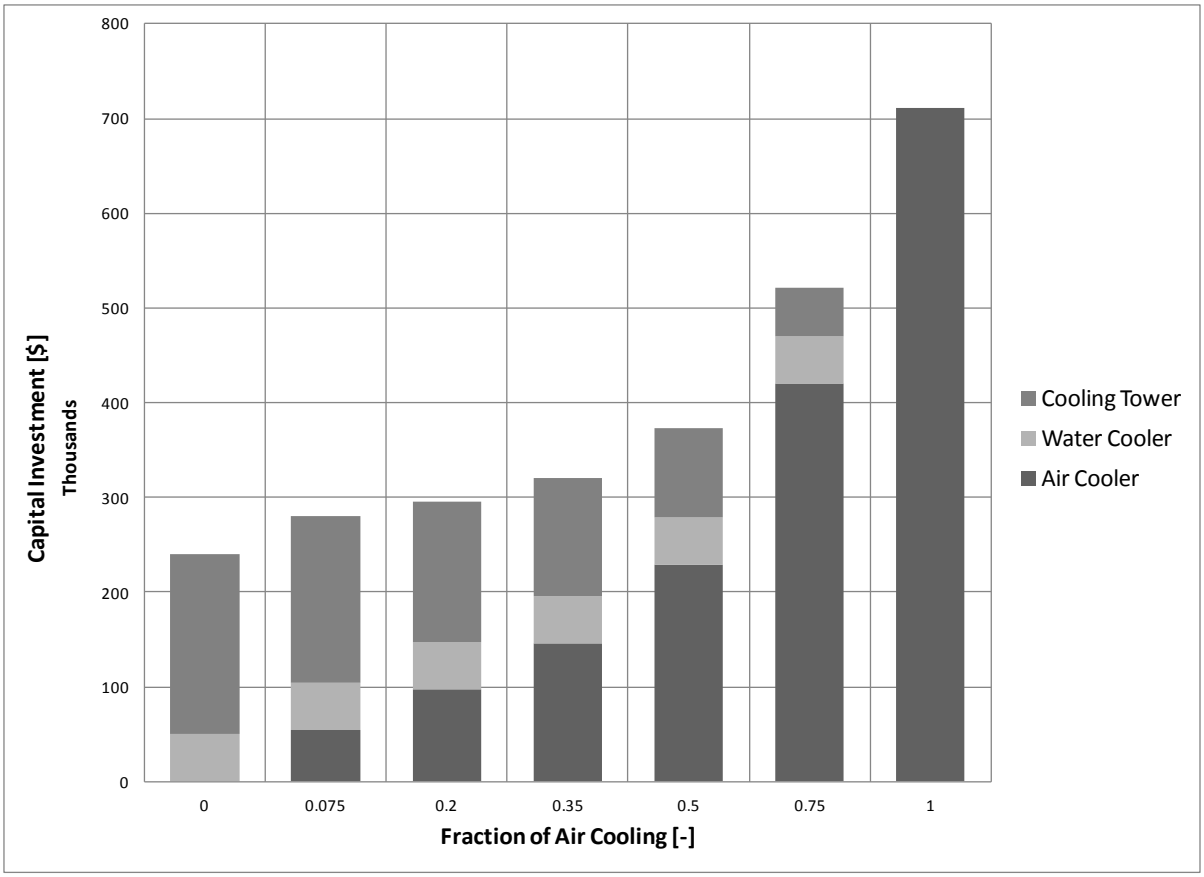

Figure 98: Capital investment for the air cooler, water cooler, and cooling tower as a function of fraction of air cooling

The water cooler was the least expensive component among the three components. The air cooler was the most expensive component of the three heat exchangers. Figure 98 also shows that at zero fraction of air cooling, an air cooler does not exist and at unity fraction of air cooling, a water cooler and cooling tower do not exist. Also, looking at the cost of the cooling tower for the fraction of air cooling equal to zero, shows that it is approximately equal to $200,000. This estimation agrees with the quoted unit price of the cooling tower modeled (i.e. $98,000), discussed in Chapter 3, which would require two cooling towers to satisfy the entire load for an all water cooling system. Everywhere in between has some sort of cost for all three heat exchangers.

With the capital investment for the heat exchangers figured out for each of the design point the next step is figuring out how to analyze hourly weather data over the course of a year.

6.5 Weather data

The hybrid cooling configuration can take advantage of the varying weather conditions during a year; therefore it is necessary to do a simulation using hourly weather data for a year. The only required information from weather data for a certain area is the ambient dry bulb and wet bulb temperatures. The area of interest is Daggett, CA; TMY2 weather data are appropriate for this analysis.

In a TMY2 data file, ambient dry bulb and wet bulb temperatures, as well as other information, are given for every hour of the year. Figure 99 shows dry and wet bulb temperatures from a TMY2 data file for Daggett, CA over the span of a year.

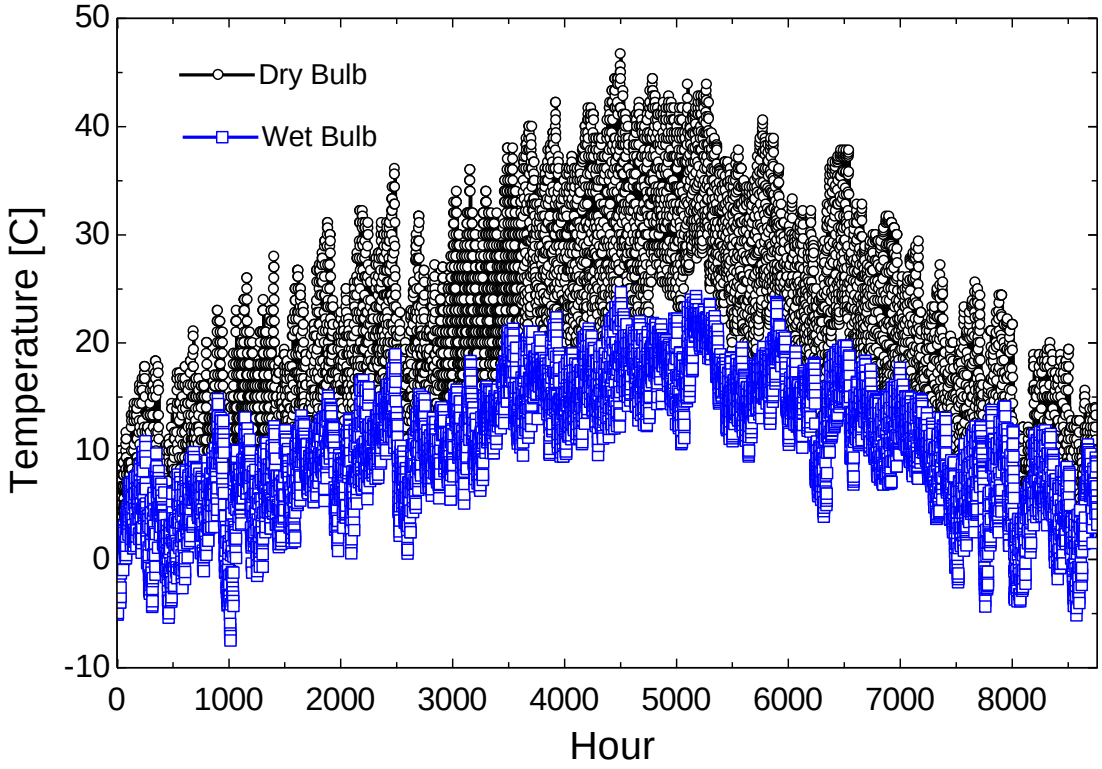

Figure 99: TMY2 weather data for Daggett, CA showing dry and wet bulb temperatures at specific hours during the year

The issue with having data for 8760 hours of the year is that running any sort of analysis that optimizes for each ambient condition requires significant computational effort. The model takes approximately three seconds to converge on a solution at each ambient condition, so

with 8760 runs it would take approximately eight hours to do one yearly analysis. The way to resolve this issue is to bin the data, by taking ranges of dry bulb temperatures and finding the mean coincident wet bulb temperature associated with this range. The amount of hours that the specific range of dry bulb temperatures is seen throughout the year will also be given.

6.6 Binned data

There are many methods of binning weather data, but in this case BinMaker™ (BinMaker, 1995), is used to convert hourly data to bin data. The program's main screen asks for the location of interest for the weather data, shown in Figure 100.

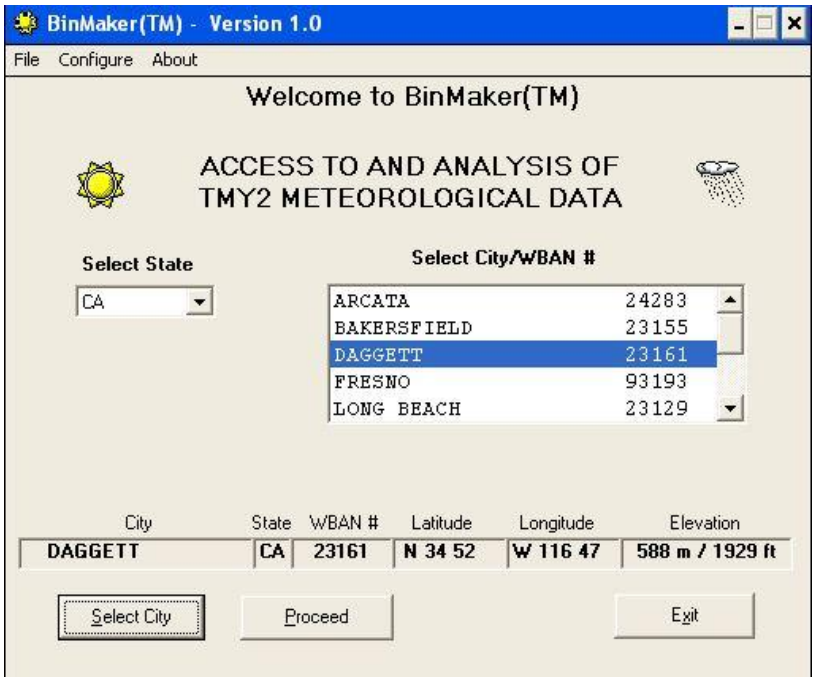

Figure 100: BinMaker™ main screen

From there, times of interest can be specified for the selected location. The GUI allows the user to select specific months as well as specific times during the day. For the analysis that follows, the hours from 9 A.M. to 3 P.M. were used as the hours of interest throughout the entire year. These are the hours that typically see the most amount of solar irradiance and when solar power plants would likely be running. This GUI can be seen in Figure 101.

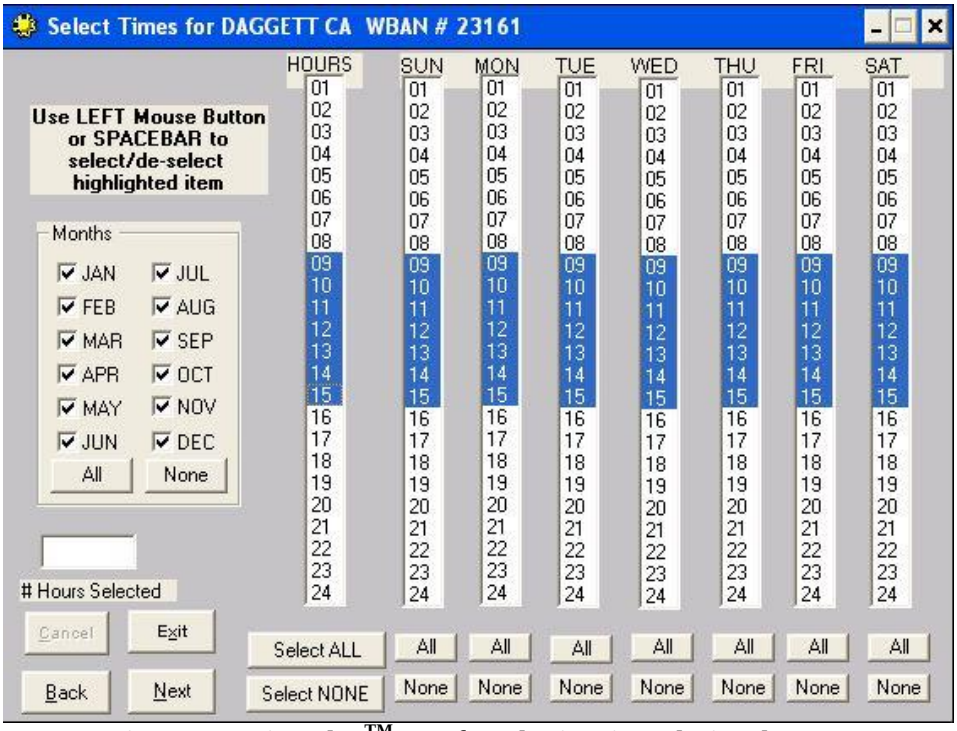

Figure 101: BinMaker™ GUI for selecting times during the year

In the case of the analysis to follow, the weather was binned by dry bulb temperature in 2ºC intervals, displaying the mean coincident wet bulb in that range as well as the amount of hours for each interval. This can be seen in Figure 102.

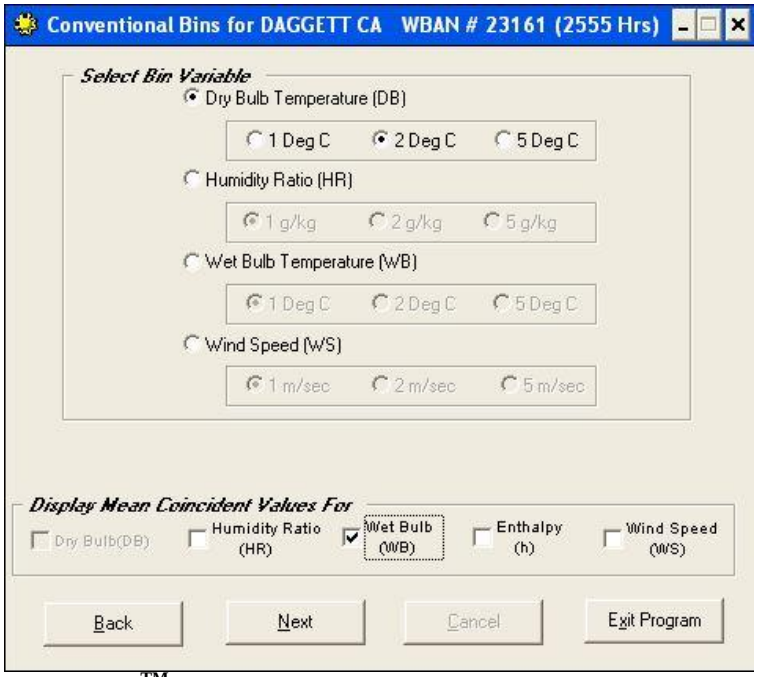

Figure 102: BinMaker™ GUI giving users the option for variable to bin and bin range

Finally, the program outputs a text file that can be imported to an excel file. The excel file can be seen in Figure 103, which shows the dry bulb range, mean coincident wet bulb, and hours.

Mid-pts	DB (C)	Hrs	WB (C)
45	44 to 46	1	21.3
43	42 to 44	10	21.4
41	40 to 42	50	20.5
39	38 to 40	86	19.6
37	36 to 38	136	18.9
35	34 to 36	136	18
33	32 to 34	153	17.2
31	30 to 32	190	15.9
29	28 to 30	173	15
27	26 to 28	167	14.1
25	24 to 26	157	12.6
23	22 to 24	175	11.4
21	20 to 22	195	10.7
19	18 to 20	140	9.5
17	16 to 18	187	8.1
15	14 to 16	180	7.2
13	12 to 14	163	6.5
11	10 to 12	120	5.1
9	8 to 10	64	3.2
7	6 to 8	48	2.1
5	4 to 6	17	0.5
3	2 to 4	6	-1.2
1	0 to 2	1	-2.9

Figure 103: Binned weather data showing dry bulb range, mean coincident wet bulb, and hours

By binning the weather data, the number of runs that the model has been reduced from 8760 to 23 runs. The model is run for each ambient condition varying the fraction of air cooling in order to minimize the operating cost per hour.

6.7 Off-design performance curves

The off-design analysis allows a larger and more realistic picture of the performance of a specifically designed system of heat exchangers. To make this analysis cover a wide range of possibilities, five tests were created that varied the cost of water and electricity. The control test was the average values of $3 per 1,000 Gal and $0.10 per kW-hr. There were four other tests also run in which both costs were halved (Test #1), doubled (Test #2), water-doubled and electricity-halved (Test #3), and water-halved and electricity-doubled (Test #4). These tests are summarized in Table 28.

Test	Cost of Water [$/1,000 Gal]	Cost of Electricity [$/kW-hr]	Water to Electricity Cost Ratio [kW-hr/1,000 Gal]
Control	3.0	0.10	30
#1	1.5	0.05	30
#2	6.0	0.20	30
#3	6.0	0.05	120
#4	1.5	0.20	7.5

Table 28: Five tests run varying the cost of water and electricity

Table 28 also includes a column of the cost of water to cost of electricity ratios in kW-hr/1,000 Gal. This ratio is reported in order to test the dependence of the results on individual costs as opposed to the ratio of the costs. As seen from Table 28, the control, #1, and #2 tests all have the same water to electricity cost ratio, while #3 and #4 have two different values.

With the established testing matrix, the model was run at the each of the seven different design points selected from Figure 94. As stated before, using the equipment associated with each design point the model minimized the cost per hour by varying the fraction of air cooling at each binned ambient condition. The cost per hour, which includes the power from the water pump for the cooling tower and water cooler, and fan power from the cooling tower and air cooler, was multiplied by the number of hours each binned ambient condition saw

throughout the year. These values were summed to produce the yearly operating cost at each design point. The seven design points were plotted with the yearly operating cost as a function of the fraction of air cooling. Figure 104 shows the curves for same water to electricity cost ratios and Figure 105 shows the curves for different ratios.

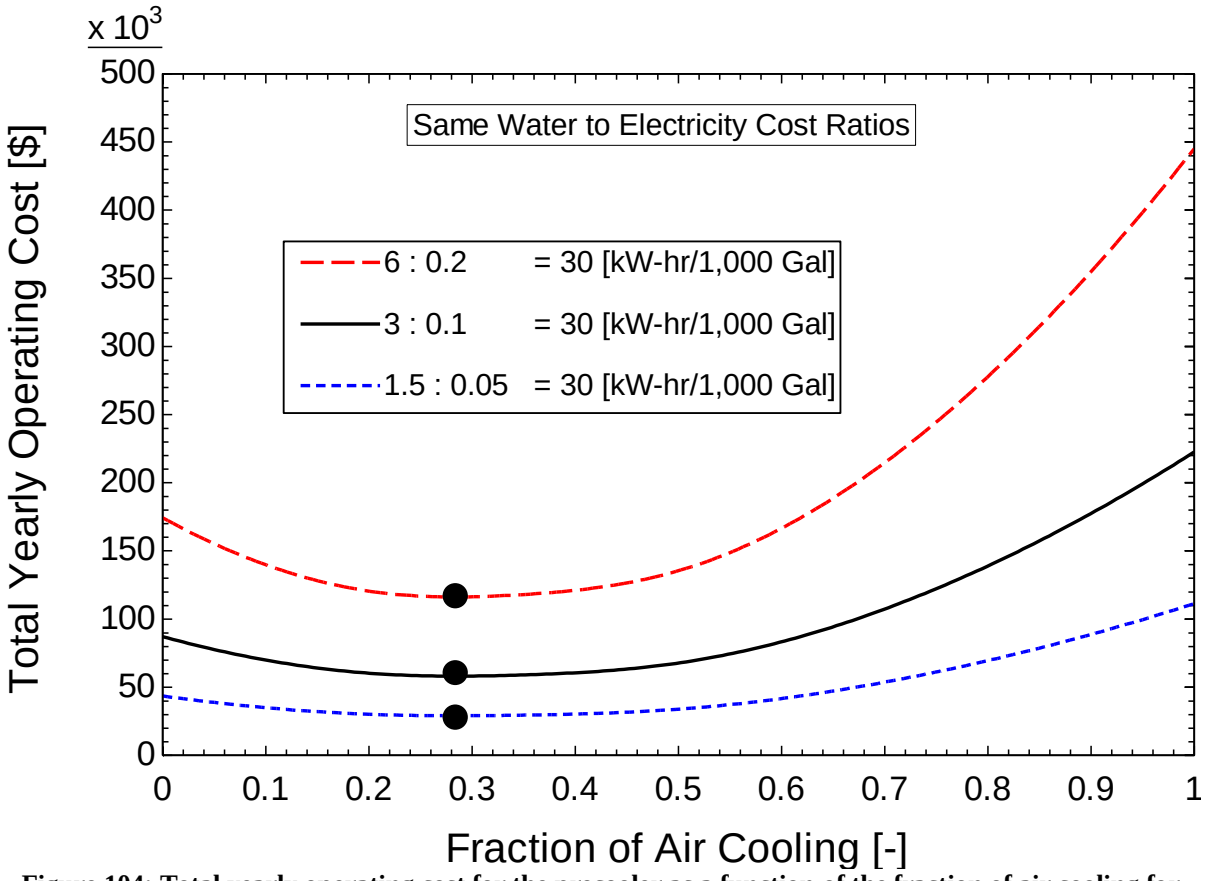

Figure 104: Total yearly operating cost for the precooler as a function of the fraction of air cooling for same water to electricity cost ratios

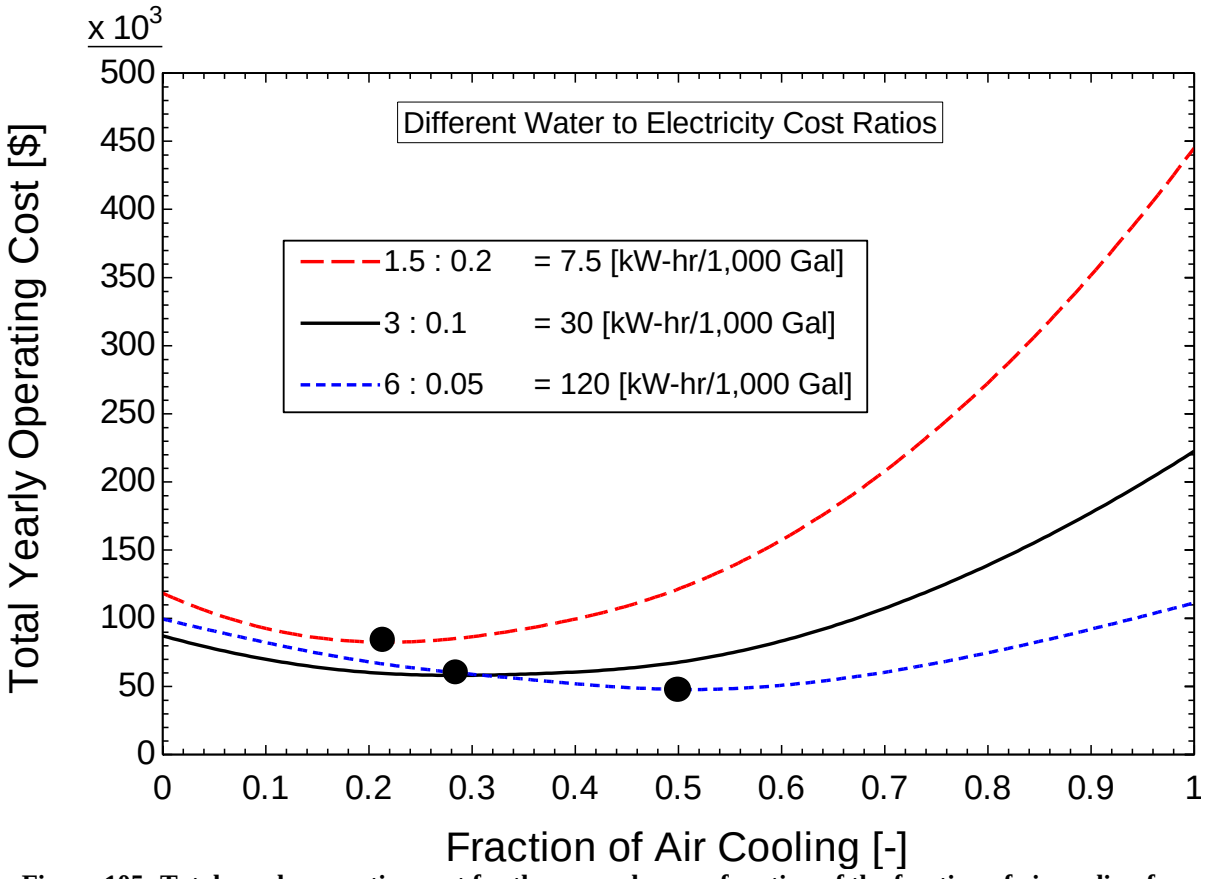

Figure 105: Total yearly operating cost for the precooler as a function of the fraction of air cooling for different water to electricity cost ratios

These plots show where a cooling system should be designed based on one year's operating costs. In each of the curves, the minimum occurs between 0 and 1 indicating that on an operating cost basis there is a benefit to running a hybrid configuration. Looking at the difference between Figure 104 and Figure 105, it shows that there is a major dependence on the cost ratio but no dependence on the individual costs. Figure 104, where the curves represent the same cost ratios, shows that the minimums occur at the same fraction of air cooling. On the other hand, Figure 105, where the curves represent different cost ratios, shows that the minimums occur at different fractions of air cooling. In Figure 105, the curve representing a cost ratio of 120 has a minimum occurring around 0.5. This occurs because a high value of the cost ratio means water is expensive compared to electricity, so the minimum will likely occur by favoring more air cooling. The opposite is true about the cost ratio of 7.5. This curve represents a case where the cost of electricity is expensive when

compared to the cost of water, so the minimum occurs closer to water cooling. This cost ratio has a minimum limit of zero (i.e. free water) and no maximum limit (i.e. free electricity). Figure 106 illustrates the optimal fraction of air cooling as a function of the cost ratio.

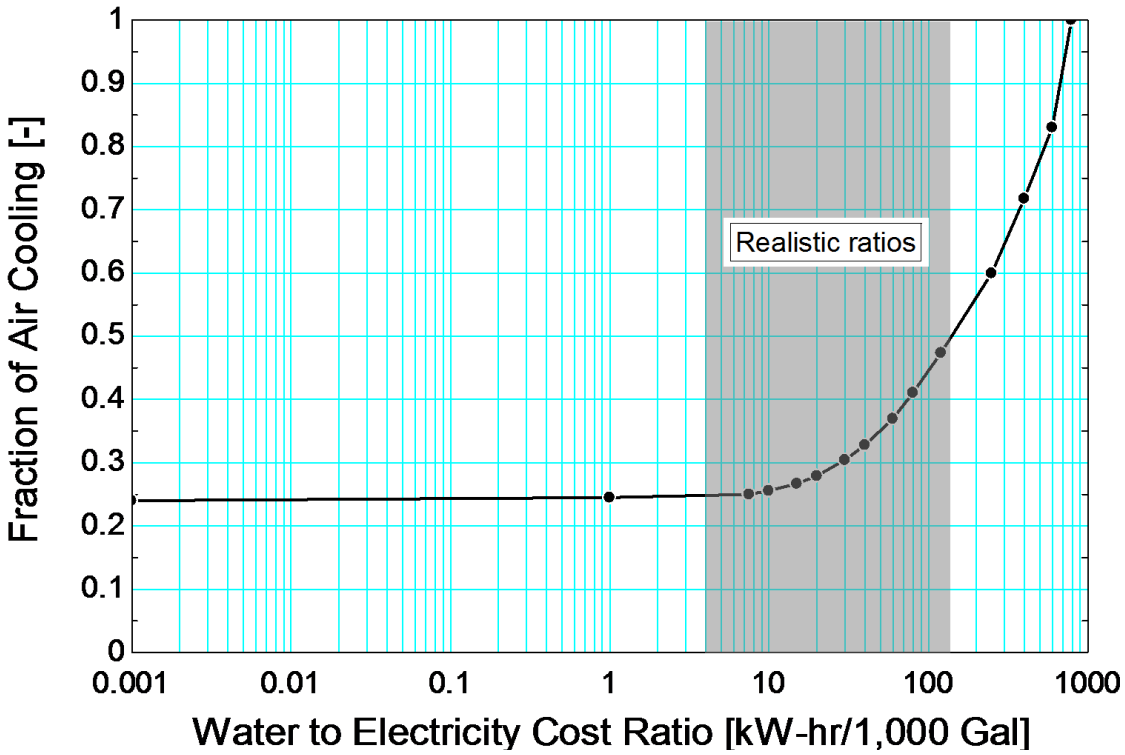

Figure 106: The fraction of air cooling as a function of the water to electricity cost ratio

The gray shaded region represents the realistic range of cost ratios, as electricity and water will never be free. It is interesting to see that on a purely operating cost basis, as water becomes free compared to electricity there is still a benefit to having some air cooling to share the load with the water cooler. On the opposite end, as electricity becomes free compared to water, there is a point where the system should be designed for all air cooling.

A purely operating cost analysis leaves out the impact of capital investment costs. Capital investments are usually large compared to the operating costs especially near the beginning of the life cycle of the process. It is important that operating and investment costs are analyzed over a period of time to make a decision on the most sensible solution.

7 RESULTS & DISCUSSION

A simple but effective method for cost analysis on a process over a period of time is a life cycle cost (LCC) analysis. Typically, a LCC analysis includes the cost of capital investment, operating cost, maintenance cost, taxes, as well as the cost of financing, replacement, and renovation over the entire analysis period. For large scale operations, the maintenance costs, taxes, and costs of financing, replacement, and renovation are generally negligible when compared to the operating costs (i.e., water and energy) and capital costs. This LCC analysis will only consider the effects of operating costs and capital investments cost. The results of this analysis will provide a basis for comparison among the three configurations of cycle heat rejection (i.e., water cooling, air cooling, or hybrid cooling).

One method of determining the LCC is by using the P1 and P2 method (Duffie & Beckman, 2006). The LCC is defined as the sum of two terms; the first is proportional to the first year operating cost (F) and the second term is proportional to the first costs of the system (E).

$$LCC = P_1 F + P_2 E \tag{6.15}$$

The P_1 constant is the present worth factor (PWF) which depends primarily on the number of years the equipment will be operated (N), as well as the inflation rate for expenses of operation (i) and the market discount rate (d).

$$P_1 = PWF(N, i, d) \tag{6.16}$$

The P_2 constant depends on many economic parameters. Assuming that all initial investment costs are paid in full at the time of purchase and the economic factors such as maintenance costs, taxes, and costs of financing, replacement, and renovation are negligible, the P_2 constant is equal to unity. The P_1 constant is calculated using the PWF external function in EES. For the following simulations, the inflation rate and market discount rate were assumed constant at 3.0 % (Bureau of Labor Statistics, 2012) and 7.0 % (Federal Reserve System,

2012), respectively. These values are estimates based on current and previous years data. Table 29 shows the P_1 constant values with the corresponding years that are used in this analysis.

Years (N)	P_1 Constant
0	0
1	0.9346
2	1.834
5	4.336
10	7.921
20	13.33

Table 29: P_1 constant values at corresponding years

The first year operating cost curves presented in the previous section are multiplied by the P_1 values and summed with the investment cost. These LCC curves will show that the optimal design fraction of air cooling depends on the system's life cycle timeline. Figure 107 through Figure 111 illustrate the results to the analysis for the five tests summarized in Table 28 from the previous section.

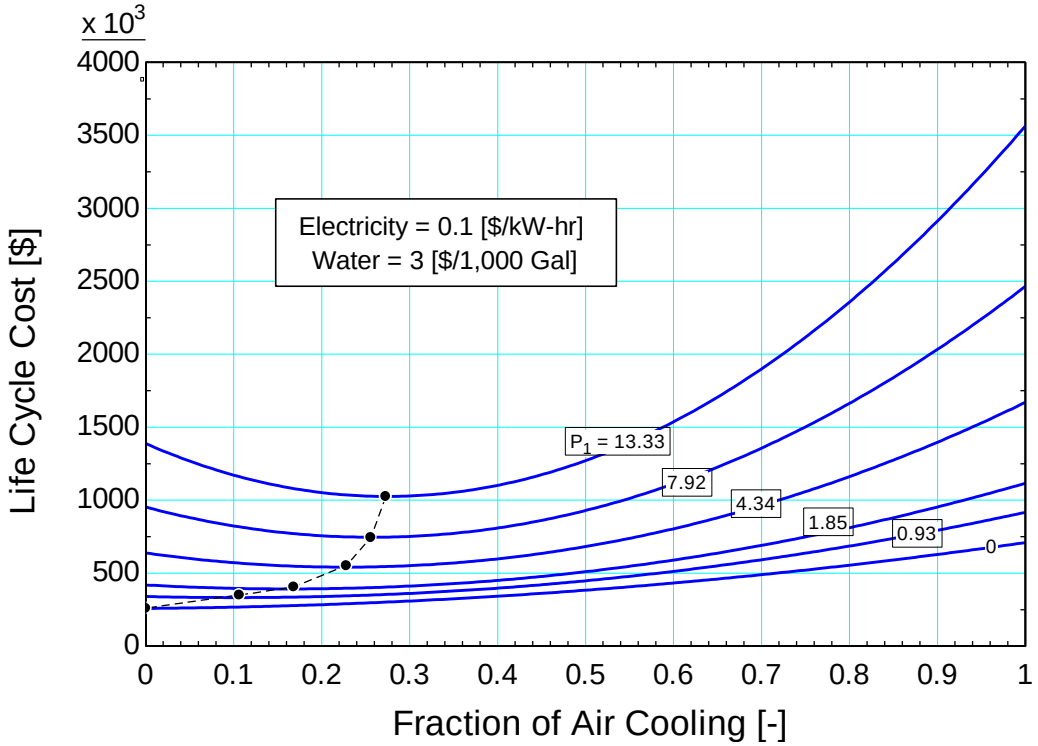

Figure 107: LCC as a function of the fraction of air cooling for the control test, refer to Table 28. The amount of years of operation varies from 0-20 years

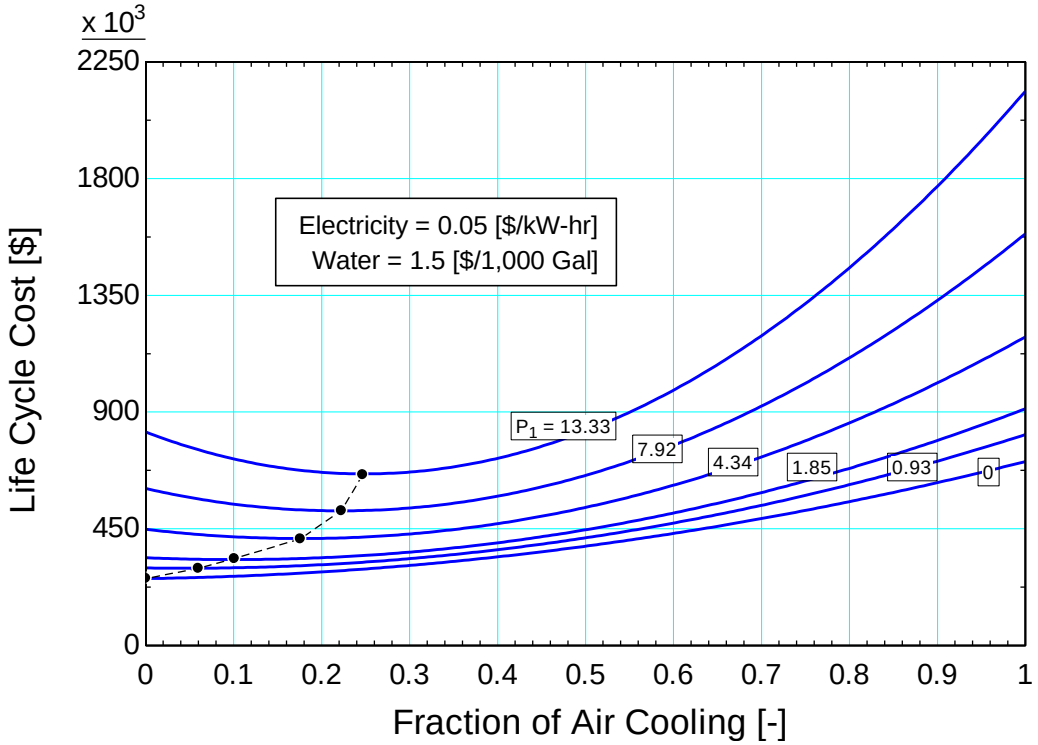

Figure 108: LCC as a function of the fraction of air cooling for test #1, refer to Table 28. The amount of years of operation varies from 0-20 years

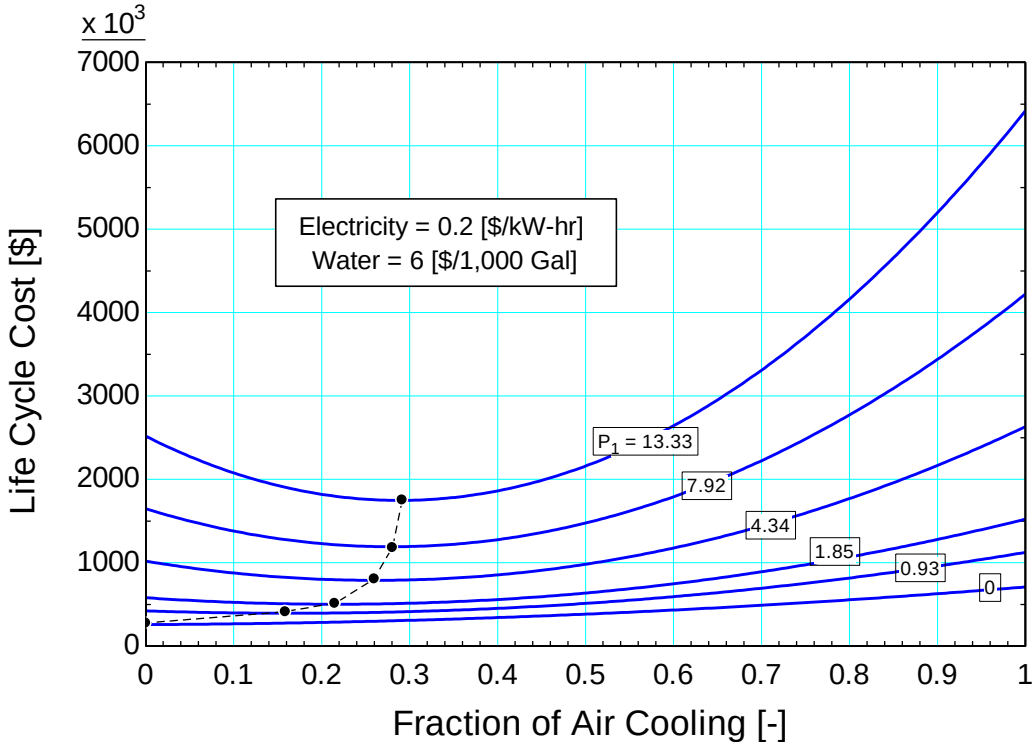

Figure 109: LCC as a function of the fraction of air cooling for test #2, refer to Table 28. The amount of years of operation varies from 0-20 years

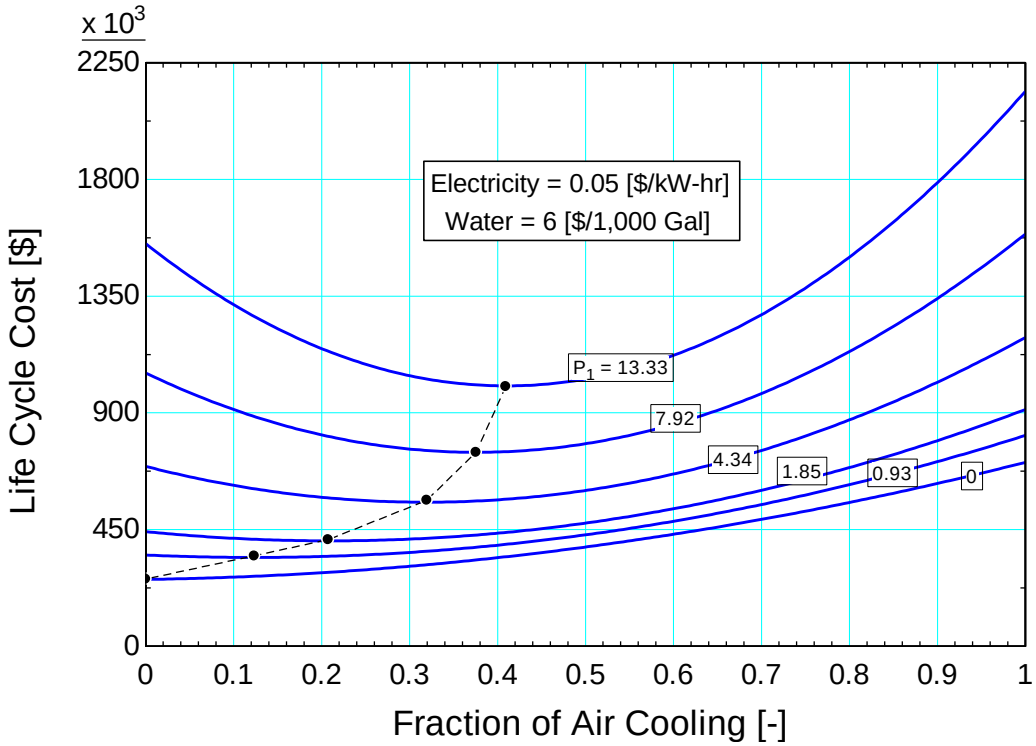

Figure 110: LCC as a function of the fraction of air cooling for test #3, refer to Table 28. The amount of years of operation varies from 0-20 years

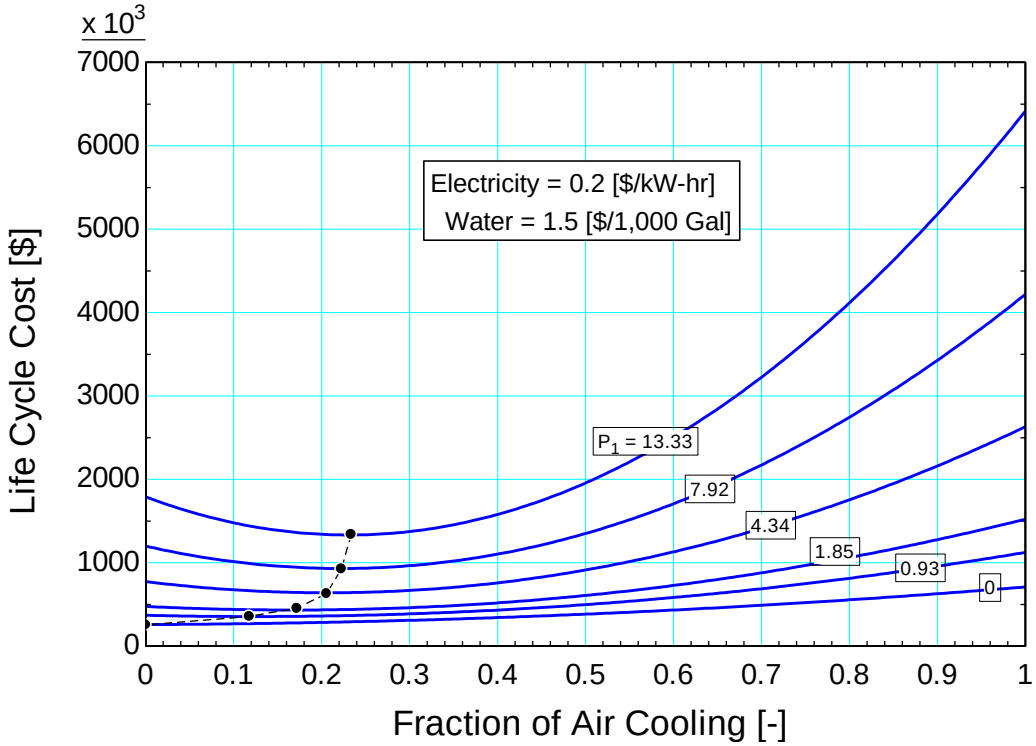

Figure 111: LCC as a function of the fraction of air cooling for test #4, refer to Table 28. The amount of years of operation varies from 0-20 years

The five plots above show various LCC curves at various P_1 constants. At P_1 of zero, there are no operating costs and all plots show that the optimal fraction of air cooling is zero (i.e. all water cooling). This is because the overall investment costs of water cooling are lower than hybrid or air cooling. As the number of years is increased the optimal value of the fraction of air cooling is increased due to the impact of the operating costs on the system. For all plots, as the P_1 value increases the optimal value begins to approach a fraction of air cooling predicted by an operating cost analysis.

The effect of the water and electricity costs can be shown by plotting only the optimal points for all tests at various values of P_1 on one plot, shown in Figure 112.

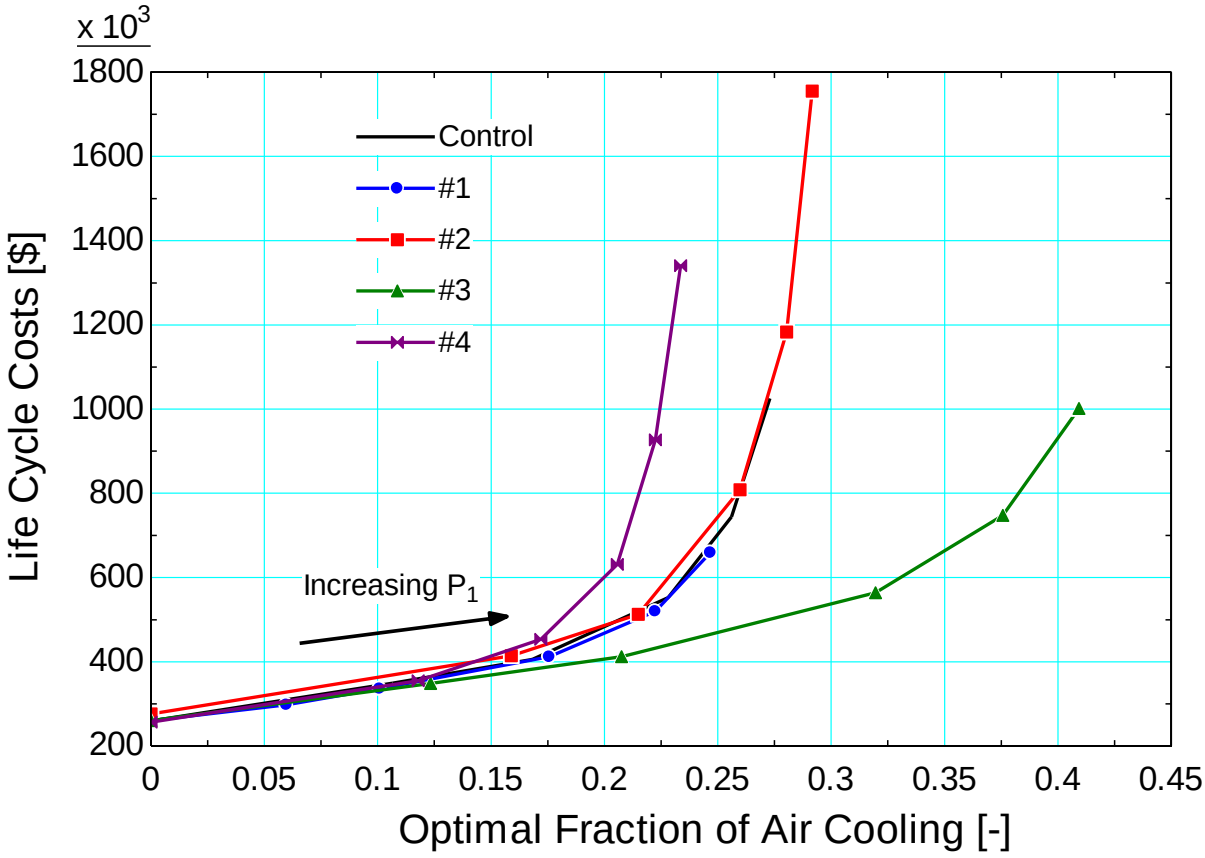

Figure 112: LCC as a function of the optimal fraction of air cooling for various water to electricity cost ratios

It shows that for same cost ratios the LCC predicts the same optimal fraction of air cooling. The simulations also show that for the tests run with a low water to electricity cost ratio (i.e., cheap water compared to electricity, test #4) the optimal values are pushed towards water cooling. The opposite happens with a high water to electricity cost ratios (i.e., test #3) where the optimal values favor higher air cooling fractions.

Figure 113 and Figure 114 show the optimal values from the previous curve on plots of fraction of air cooling and LCC as a function of P_1 constant values. These curves will show the effect of the water to electricity cost ratio on the analysis based on the number of years (i.e., P_1).

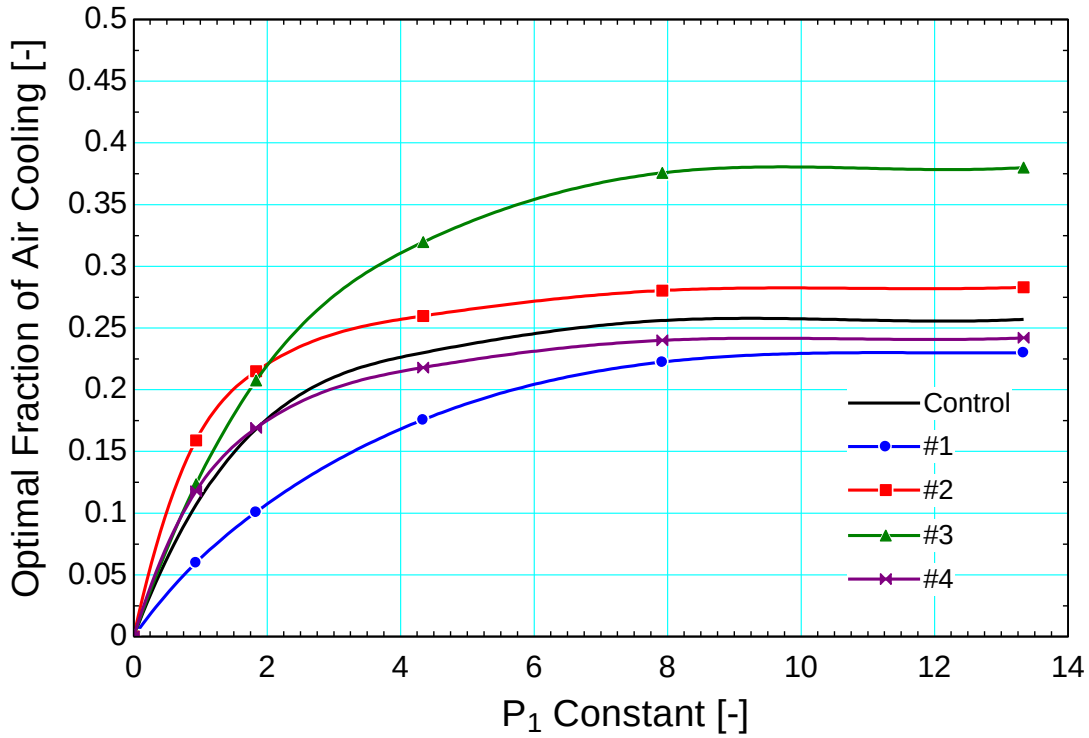

Figure 113: 5 curves associated with the minimum LCC value taken from the five figures above showing the optimal fraction of air cooling as a function of P_1

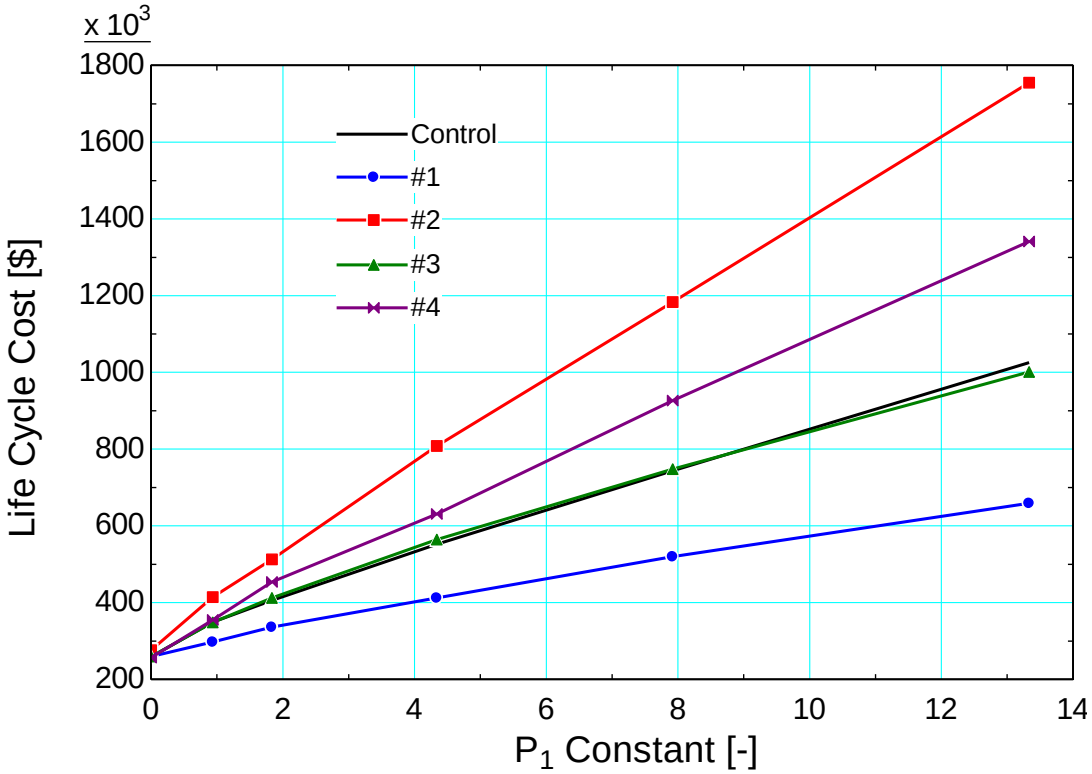

Figure 114: Life cycle costs as a function of P_1

Notice that the optimal fraction of air cooling is not the same for the same water to electricity cost ratios when plotted as a function of P_1. The control, #1, and #2 tests have the same water to electricity cost ratios and yet test #1 (i.e., halved costs) favors water cooling and test #2 (i.e., doubled costs) favors air cooling.

As discussed in Section 6.6, the analysis only uses ambient conditions at the hours between 9 A.M. and 3 P.M. each day throughout the year. This was done to simulate the hours of most solar irradiance when a solar plant would be operating. A comparison between the current analysis and an analysis of a solar plant operating 24 hours a day (e.g., thermal storage) will give a full picture of what can be expected, shown in Figure 115. Note both analyses represent a water to electricity cost ratio of 30.

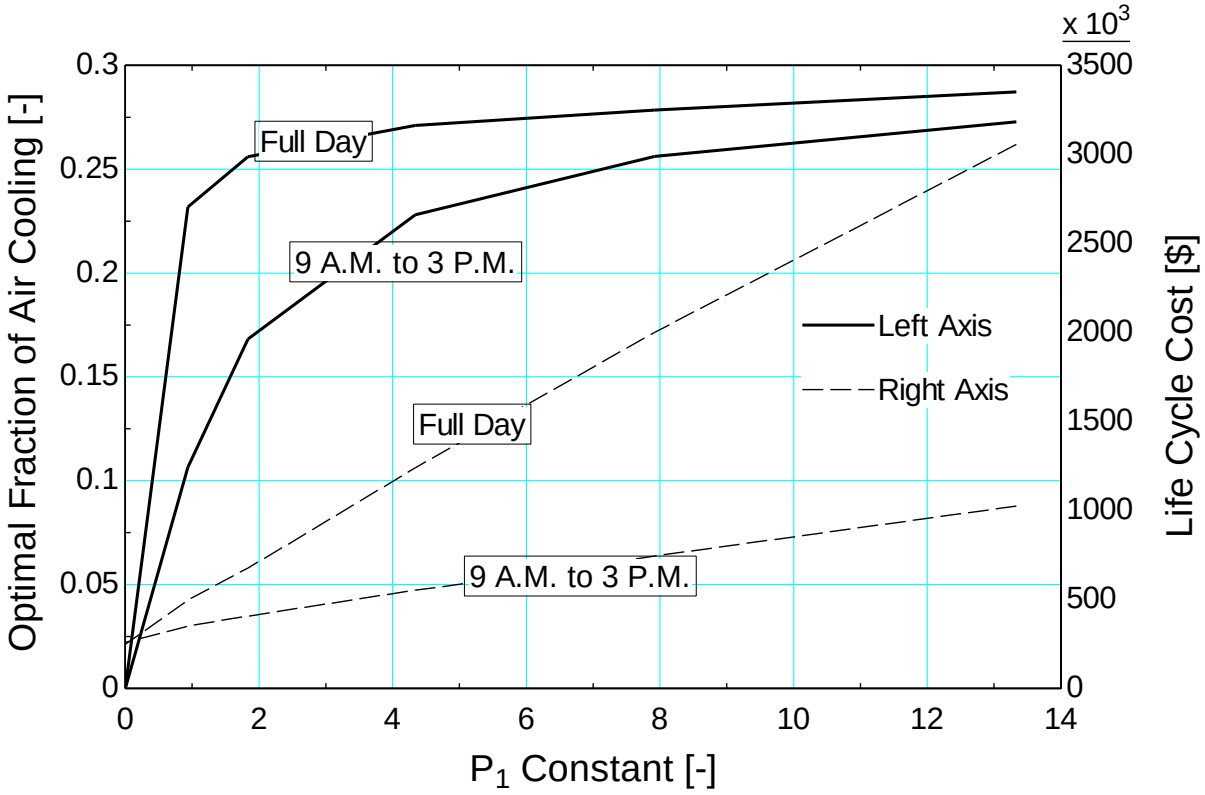

Figure 115: Comparison of an analysis done for a full day and sunlight hours of weather data. It shows the total cost as a function of the fraction of air cooling

The dark solid lines (i.e., optimal fraction of air cooling) show that operating for an analysis representing operating 24 hours a day, the optimal values favor more air cooling. This is due

to the ambient temperature dropping during the hours without sunlight and causing the efficiency of the air cooler to increase. Also, the dry bulb temperature experiences a greater daily range (difference between the high temperature and the low temperature during a given 24 hour period). The daily range in the wet bulb temperature is on the order of half the daily range in dry bulb. In other words, a cycle with air cooling would experience a greater capacity increase at night compared to a water-cooled option. The actual operating point will likely lie somewhere in between the two lines depending on the number of hours the plant will be running.

This analysis showed that depending on the number of years of operation, the design point will differ due to the effect of the investment costs. It also showed that while there is a difference between analyzing for full day operation and for a sunlight-only operation, it is not very significant on where the design point will lie. Depending on how many years of operation and number of hours during the year the plant will operate, there is a minimum LCC that occurs in between air cooling and water cooling. This suggests that there is an advantage to hybrid cooling based on an LCC alone.

The LCC analysis represents the optimal fraction of air cooling when reducing costs and does not represent optimal fraction when reducing water or energy is more important than reducing costs. Figure 116 shows the total amount of water and energy consumed within a year as a function of the fraction of air cooling. Notice that approximately 13 million gallons of water per year are used for an all-water cooling process, while no water is consumed for the all air-cooling process. Approximately half a million kW-hr of energy is consumed yearly for the water cooling case while air cooling consumes around 2.3 million kW-hr.

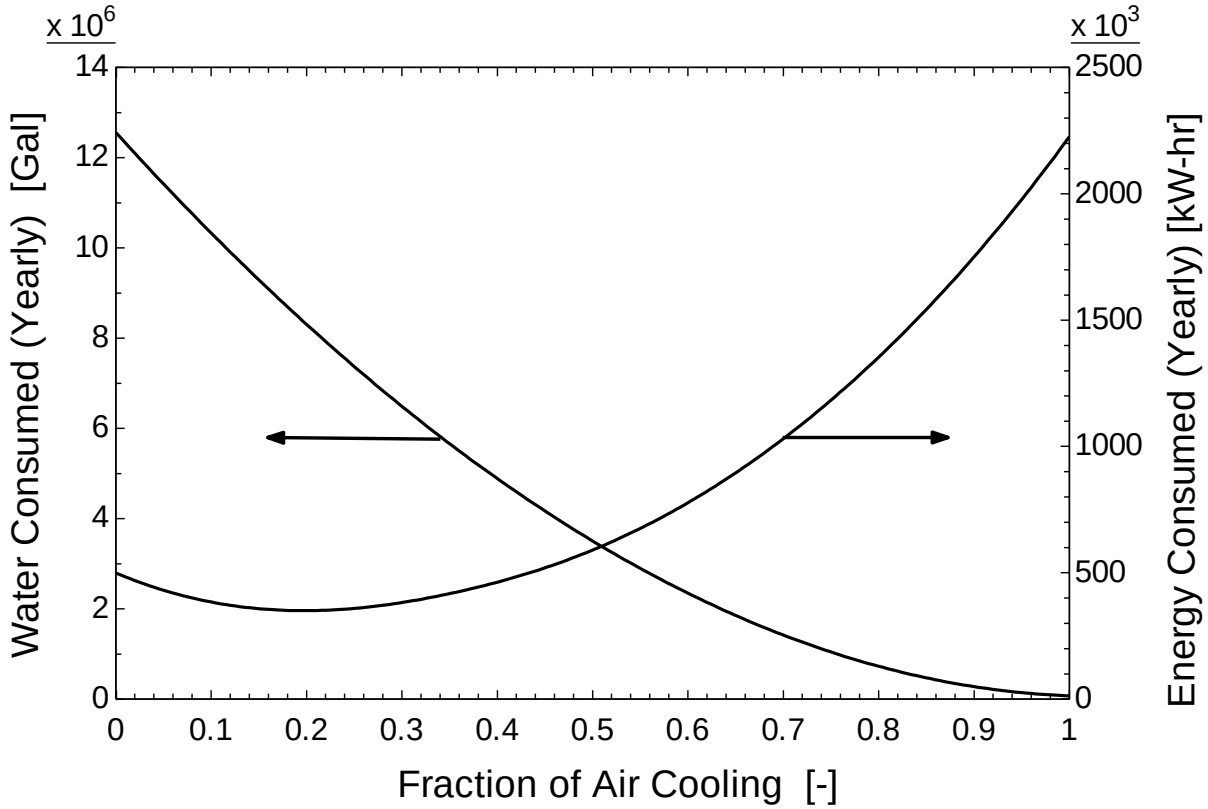

Figure 116: Water and energy consumed by the precooler on a yearly basis as a function of the fraction of air cooling

It is important to decide if reducing water, energy or overall costs is the most important concern because it will change where a cooling process should be designed at. NREL's interest in the "precooler" heat exchanger is finding a heat rejection method using ambient air or some combination of air and water, wherein water consumption is minimized (Turchi, 2012).

In comparing the three different configurations, it was found that there is an advantage to the hybrid configuration as a cooling solution for the Brayton cycle. The hybrid configuration advantage lies with the ability to design the system at the optimal point and constantly operate at a fraction of air cooling that minimizes cost per hour, provided that sufficient air cooling equipment is available. On a cost stand point, hybrid cooling makes sense because of the flexibility of the system. It also creates a best of both worlds situation where capital costs and energy use are reduced when compared to air cooling and water use is reduced when compared to water cooling.

8 CONCLUSIONS & RECOMMENDATIONS

The Brayton cycle rejects heat to the ambient environment using air, water, or a hybrid arrangement that employs both fluids. Cooling with water, from a cooling tower, provides higher and more consistent Brayton cycle thermal efficiencies year-round, while also having lower capital costs for the heat exchanger equipment when compared to air-cooling. However, a major concern with water-cooling, especially for solar thermal applications, is the large amount of water required for the heat rejection coincident in plant locations where there is limited availability of water.

To address water limitations, air-cooling has become a major topic among researchers in the field of CSP technologies. It has been found that while air-cooling will eliminate the majority of the water usage, it causes reduced thermal efficiencies year-round and higher capital costs due to the substantial size of the air-coolers.

The alternative to direct water-cooling or direct air-cooling is a hybrid configuration that combines both water and air-cooling processes. The hybrid configuration strives to maintain the advantages of each process, but can also potentially mitigate the disadvantages. In the Brayton cycle using carbon dioxide, the precooler can be configured to take advantage of the high CO_2 temperatures by arranging the heat rejection system into two heat exchangers, a water and air-cooler, each set in series.

The size of the air-cooler can be significantly reduced by increasing the approach temperature. The size of the air-cooler has been found to be more sensitive to the approach temperature, when compared to the more physically compact water-cooler. The water-cooler operates at a lower heat sink temperature (i.e. wet bulb temperature) and completes the heat rejection from CO_2. It is sized and operated to reduce the CO_2 temperature to the desired condition for the compressor inlet.

In comparing the three different configurations using an LCC analysis, it was found that there is an advantage to the hybrid configuration as a cooling solution for the Brayton cycle. The hybrid configuration advantage lies with the ability to design the system at the optimal point and constantly operate at a fraction of air cooling that minimizes cost per hour. On a cost stand point, hybrid cooling makes sense because of the flexibility of the system.

NREL's interest in the "precooler" heat exchanger is to reduce water use by using air or a combination of air and water. The LCC is a good representation of the design concern for NREL. It shows that on a LCC basis, there is an advantage to designing for a hybrid configuration. Using the hybrid configuration with air cooling as the primary means of cooling allows for reduced water usage. The water cooling is used when the load cannot be met by the air cooling alone. This means that the cooling process is very flexible and can be optimized to reduce water use and cost. Hybrid cooling should be considered a viable cooling solution for NREL's 10 MW CSP plant.

This analysis is part of the future continuation of heat exchanger design for the Brayton cycle. This analysis considered a relatively high compressor inlet temperature at 48 C. This temperature is an important constraint because it determines the maximum temperature of the inlet cooling fluid temperature (e.g., wet bulb or dry bulb). A recommendation would be to analyze the effect on the overall cycle as well as effect on heat exchangers performance and size by allowing lower compressor inlet temperatures.

Another recommendation would be to incorporate maintenance costs and other economic parameters into the LCC analysis. This analysis showed what the effect of operating costs and investment costs, which typically outweigh most other costs, had on the designing of a cooling solution. It would be interesting to see the effect maintenance costs, taxes, and costs of financing, replacement, and renovation, etc. have on the applicability of the hybrid configuration.

9 REFERENCES

API Standard 661 (2002). *Air Cooled Heat Exchangers for General Refinery Service.* Fifth Edition.

Baltimore Aircoil Company (2011). *Product Selection Program.* <http://www.baltimoreaircoil.com/english/product-selection-software-public>.

BinMaker (1995). License provided by Doug Reindl.

Braun (1989). *Methodologies for the Design and Control of Central Cooling Plants*. Master's thesis, University of Wisconsin-Madison.

Bureau of Labor Statistics. (2012). *Inflation Rate Data.* <http://www.bls.gov/>.

California Energy Commission (2006). *Cost and Value of Water Use at Combined Cycle Power Plants.* Public Interest Energy Research Program.

Campbell, Sylvester J. (1987). *Solid-State AC Motor Controls.* New York: Marcel Dekker, Inc.. pp. 79–189.

Cooling Technology Institute (2012). *Cooling Towers Certified by CTI Under STD-201.* <http://www.cti.org/certification.shtml>.

Duffie J. & Beckman W. (2006). *Solar Engineering of Thermal Processes.* 3rd ed. Godfrey Boyle.

Dyreby, J., S. Klein, G. Nellis, and D. Reindl. (2012). *Development of Advanced Models for Supercritical Carbon Dioxide Power Cycles for use in Concentrating Solar Power Systems.* National Renewable Energy Laboratory.

DOE / NETL (2002). *Process Equipment Cost Estimation.* National Energy Technology Center, Pittsburgh, PA.

Federal Reserve System. (2012). *The Discount Rate.* <http://www.federalreserve.gov/monetarypolicy/discountrate.htm>.

GEA Heat Exchangers (2011). *Air-Cooled Heat Exchangers*. <www.gearainey.com>

Kays, W.M., & London, A.L. (1984). *Compact Heat Exchangers.* 3rd ed., McGraw Hill, New York.

Kirby, M. & Rumbold, S. (2009). *Microchannel Heat Exchangers and Reactors.* Microchemical Engineering in Practice. John Wiley & Sons, Inc.

Klein, S.A. (2011). *Engineering Equation Solver (EES),* F-Chart software.

Juvinall, R. C., & Marshek, K. M. (2006). *Fundamentals of Machine Component Design.* (4th ed). John Wiley & Sons.

Nellis, G., & Klein, S. (2009). *Heat Transfer.* New York, NY: Cambridge University Press.

Seidel, W. (2010). *Model development and annual simulation of the supercritical carbon dioxide Brayton cycle for concentrating solar power applications.* Master's thesis, University of Wisconsin-Madison.

Southall, David. (2009). *Diffusion Bonding in Compact Heat Exchangers.* Supercritical Carbon Dioxide Power Cycle Symposium.

Turchi, Craig. (2012). FY12 Milestone complete-Analysis of S-CO_2 heat exchangers. National Renewable Energy Laboratory.

U.S. Department of Energy. (2007). *Concentrating Solar Power Commercial Application Study: Reducing Water Consumption of Concentrating Solar Power Electricity Generation.*

U.S. Energy Information Administration. (2010). *Many Factors Impact Electricity Prices.* <www.eia.gov>

U.S. Environmental Protection Agency. (2010). *Flowcharts and Ventilation Systems – Fans – Operating Principles.* <http://www.epa.gov/apti/bces/module5/fans/principle/principle.htm>.

Van Abel, E. N. (2011). *Computational studies on the fluid flow and heat transfer of supercritical carbon dioxide in printed circuit heat exchangers.* Master's thesis, University of Wisconsin-Madison.

Appendix

All EES codes have been attached with the electronic version of this thesis.